Bret P. Nelson
Eric Topol
Anjali Bhagra
Sharon L. Mulvagh
Jagat Narula
Editors

Atlas of Handheld Ultrasound

Springer

EXTRAS ONLINE

Atlas of Handheld Ultrasound

Bret P. Nelson • Eric Topol
Anjali Bhagra • Sharon L. Mulvagh
Jagat Narula
Editors

Atlas of Handheld Ultrasound

Springer

Editors
Bret P. Nelson
Department of Emergency Medicine
Icahn School of Medicine at Mount Sinai
New York, New York
USA

Anjali Bhagra
Department of Medicine
Mayo Clinic School of Medicine
Rochester, Minnesota
USA

Jagat Narula
Department of Cardiology
Icahn School of Medicine at Mount Sinai
New York, New York
USA

Eric Topol
Scripps Translational Science Institute
Scripps Research Institute
La Jolla, California
USA

Sharon L. Mulvagh
Department of Medicine
Dalhousie University Department of Medicine
Halifax, Nova Scotia
Canada

Additional material to this book can be downloaded from http://extras.springer.com.

ISBN 978-3-319-73853-6 ISBN 978-3-319-73855-0 (eBook)
https://doi.org/10.1007/978-3-319-73855-0

Library of Congress Control Number: 2018939184

Printed on acid-free paper

This Springer imprint is published by the registered company Springer International Publishing AG part of Springer Nature.
The registered company address is: Gewerbestrasse 11, 6330 Cham, Switzerland

Dedicated to the stethoscope on its retirement after 200 years of excellent service to the bedside cardiovascular examination

Preface

Tremendous strides in noninvasive diagnostic imaging have been made over decades in radiology, obstetrics, and cardiology. More recently, a revolution in bedside diagnosis has begun with the advent of point-of-care ultrasound. Now, clinicians can apply imaging to their own patients, in real time, to answer focused questions that will immediately impact their care.

The most recent generation of inexpensive, handheld ultrasound devices has taken this a step further—we are now firmly within the era of ultrasound availability for providers of all specialties. Thus, we have created this *Atlas of Handheld Ultrasound* to demonstrate the power of even basic organ assessments across the entire body.

Ultrasound is a force multiplier for the clinical assessment of patients, adding vital information to the history, physical examination, and other diagnostic testing available at the bedside. We hope the basic scan techniques and recognition of normal and pathologic states described here will inspire deliberate practice in improving the skill set of image acquisition and interpretation for an ever-growing number of providers.

We believe that it is time to add ultrasound imaging as a fifth vital pillar to the bedside examination. From now on it must be Inspection, Palpation, Percussion, Auscultation and INSONATION.

Contents

Contributors

Stephen Alerhand, M.D. Department of Emergency Medicine, Icahn School of Medicine at Mount Sinai, New York, NY, USA

Tara L. Anderson, M.D. Department of Radiology, Mayo Clinic Health System, Austin, MN, USA

Phillip Andrus, M.D. Department of Emergency Medicine, Icahn School of Medicine at Mount Sinai, New York, NY, USA

Edgar Argulian, M.D., M.P.H. Mount Sinai St. Luke's Hospital, Icahn School of Medicine at Mount Sinai, New York, NY, USA

Marko Balan, M.D., F.R.C.P.C. Department of Critical Care, Dalhousie University, Halifax, NS, Canada

Anjali Bhagra, M.D. Department of General Internal Medicine, Mayo Clinic, Rochester, MN, USA

Crystal R. Bonnichsen, M.D. Department of Cardiovascular Diseases, Mayo Clinic, Rochester, MN, USA

Carlo Canepa, M.D. Department of Emergency Medicine, Harvard Medical School, Massachusetts General Hospital, Boston, MA, USA

Oana Dickinson, M.D. Department of Medicine, University of Minnesota Medical School, Minneapolis, MN, USA

Department of Hospital Medicine, HealthPartners, St. Paul, MN, USA

Renee K. Dversdal, M.D. Division of Hospital Medicine, Oregon Health and Science University, Portland, OR, USA

Matthew Egan, M.D. Department of Emergency Medicine, Icahn School of Medicine at Mount Sinai, New York, NY, USA

Catherine Erickson, M.D. Department of Emergency Medicine, OHSU, Portland, OR, USA

Lauren Ferrara, M.D. Icahn School of Medicine at Mount Sinai, New York, NY, USA

Eugene M. Fine, M.D. Department of Urology, Icahn School of Medicine at Mount Sinai, New York, NY, USA

Christopher Gelabert, M.D. Department of Emergency Medicine, UT Health San Antonio, San Antonio, TX, USA

Bruce R. Gilbert, M.D., Ph.D. The Smith Institute for Urology, Zucker School of Medicine at Hofstra/Northwell, New Hyde Park, NY, USA

Laura S. Greenlund, M.D., Ph.D. Department of Medicine, Division of Primary Care Internal Medicine, Mayo Clinic, Rochester, MN, USA

Stella S. Hahn, M.D. Donald and Barbara Zucker School of Medicine at Hofstra/Northwell, New Hyde Park, NY, USA

Babar Haroon, M.D., F.R.C.P.C., Dip.(Clin Epi) Department of Critical Care, Dalhousie University, Halifax, NS, Canada

Kevin Hu, M.D. Department of Emergency Medicine, Icahn School of Medicine at Mount Sinai, New York, NY, USA

Jennifer V. Huang, D.O. Department of Emergency Medicine, Icahn School of Medicine at Mount Sinai, New York, NY, USA

Amer M. Johri, M.D., M.Sc., F.R.C.P.C. Department of Medicine, Division of Cardiology, Kingston General Hospital, Kingston, ON, Canada

Kevin Ka-Ho Kam, M.B., Ch.B. Department of Medicine and Therapeutics, Prince of Wales Hospital, The Chinese University of Hong Kong, Hong Kong, China

Huidong Kang, M.D., Ph.D. Department of Emergency Medicine, University of Ulsan, College of Medicine, Gangneung Asan Hospital, Gangneung, Gangwon, South Korea

Errel Khordipour, D.O. Emergency Department, Maimonides Medical Center, Brooklyn, NY, USA

Kyle W. Klarich, M.D. Department of Cardiovascular Medicine, Mayo Clinic, Rochester, MN, USA

Tobias Kummer, M.D. Department of Emergency Medicine, Mayo Clinic, Rochester, MN, USA

Pimpa Limphan-udom, M.D. Emergency Medicine Department, Icahn School of Medicine at Mount Sinai, New York, NY, USA

Benji K. Mathews, M.D. Department of Medicine, University of Minnesota Medical School, Minneapolis, MN, USA

Department of Hospital Medicine, HealthPartners, St. Paul, MN, USA

Brendan H. A. Milliner, M.D. Division of Emergency Medicine, University of Utah Hospital, Salt Lake City, UT, USA

William R. Miranda, M.D. Department of Cardiovascular Diseases, Mayo Clinic, Rochester, MN, USA

Apichaya Monsomboon, M.D. Department of Emergency Medicine, Icahn School of Medicine at Mount Sinai, New York, NY, USA

Sharon L. Mulvagh, M.D., F.R.C.P.C. Department of Medicine, Division of Cardiology, Dalhousie University, Halifax, NS, Canada

Naveen S. Murthy, M.D. Department of Radiology, Mayo Clinic, Rochester, MN, USA

Mangala Narasimhan, D.O. Donald and Barbara Zucker School of Medicine at Hofstra/Northwell, New Hyde Park, NY, USA

Gopal Narayanswami, M.D. Division of Pulmonary and Critical Care Unit, Mount Sinai St. Luke's Hospital, New York, NY, USA

Jagat Narula, M.D., Ph.D. Mount Sinai Hospital, Icahn School of Medicine at Mount Sinai, New York, NY, USA

Alaa M. Omar, M.D., M.Sc., Ph.D. Department of Cardiology, Icahn School of Medicine at Mount Sinai, New York, NY, USA

Department of Internal Medicine, Bronx Lebanon Hospital Center, Bronx, NY, USA

Department of Internal Medicine, National Research Center, Cairo, Egypt

Kevin M. Piro, M.D. Division of Hospital Medicine, Oregon Health and Science University, Portland, OR, USA

Division of General Internal Medicine, Oregon Health and Science University, Portland, OR, USA

Terry K. Rosborough, M.D. Department of Medical Education, Abbott Northwestern Hospital, Minneapolis, MN, USA

Daniel J. Schnobrich, M.D. Department of Medicine, Division of General Internal Medicine, University of Minnesota, Minneapolis, MN, USA

Hiroshi Sekiguchi, M.D. Division of Pulmonary and Critical Care Medicine, Mayo Clinic, Rochester, MN, USA

David Spinner, D.O. Department of Rehabilitation Medicine, Mount Sinai Hospital, New York, NY, USA

Peter C. Spittell, M.D. Department of Cardiovascular Medicine, Mayo Clinic, Rochester, MN, USA

Ee Tay, M.D. Department of Emergency Medicine, Icahn School of Medicine at Mount Sinai, New York, NY, USA

David M. Tierney, M.D. Department of Medical Education, Abbott Northwestern Hospital, Minneapolis, MN, USA

James W. Tsung, M.D., M.P.H. Department of Emergency Medicine, Mount Sinai Health System, Icahn School of Medicine at Mount Sinai, New York, NY, USA

Jacob E. Voelkel, M.D. Department of Emergency Medicine, Mayo Clinic, Rochester, MN, USA

Steve J. Wisniewski, M.D. Departments of Sports Medicine and Physical Medicine and Rehabilitation, Mayo Clinic, Rochester, MN, USA

Soft-Tissue Complaints

1

Errel Khordipour and Ee Tay

Soft-tissue complaints are common presentations in acute care environments. Ultrasound may assist in the diagnosis of soft-tissue findings, such as identifying cellulitis [1, 2], abscesses [3, 4], and foreign bodies [5, 6]. Most soft-tissue structures are readily visible on ultrasound, as they conduct sound waves well and are superficial. Ultrasound may guide procedures involving the skin and joints, such as incision and drainage, foreign body removals, and joint aspirations [7, 8]. While the use of bedside ultrasound for soft tissue is operator-dependent [9], it is easy to learn, readily available, affordable, and decreases overall time to diagnosis. In many cases it is an excellent alternative to X-ray, CT scan, or MRI (Figs. 1.1, 1.2, 1.3, 1.4, 1.5, 1.6, 1.7, 1.8, 1.9, and 1.10; Videos 1.1, 1.2, and 1.3).

Electronic Supplementary Material The online version of this chapter (https://doi.org/10.1007/978-3-319-73855-0_1) contains supplementary material, which is available to authorized users.

E. Khordipour, D.O. (✉)
Emergency Department, Maimonides Medical Center,
Brooklyn, NY, USA

E. Tay, M.D.
Department of Emergency Medicine,
Icahn School of Medicine at Mount Sinai, New York, NY, USA

B. P. Nelson et al. (eds.), *Atlas of Handheld Ultrasound*, https://doi.org/10.1007/978-3-319-73855-0_1

Fig. 1.1 Select a high frequency (linear) probe for the evaluation of skin, subcutaneous tissue, fascia, muscle, and bone. Image courtesy of Errel Khordipour

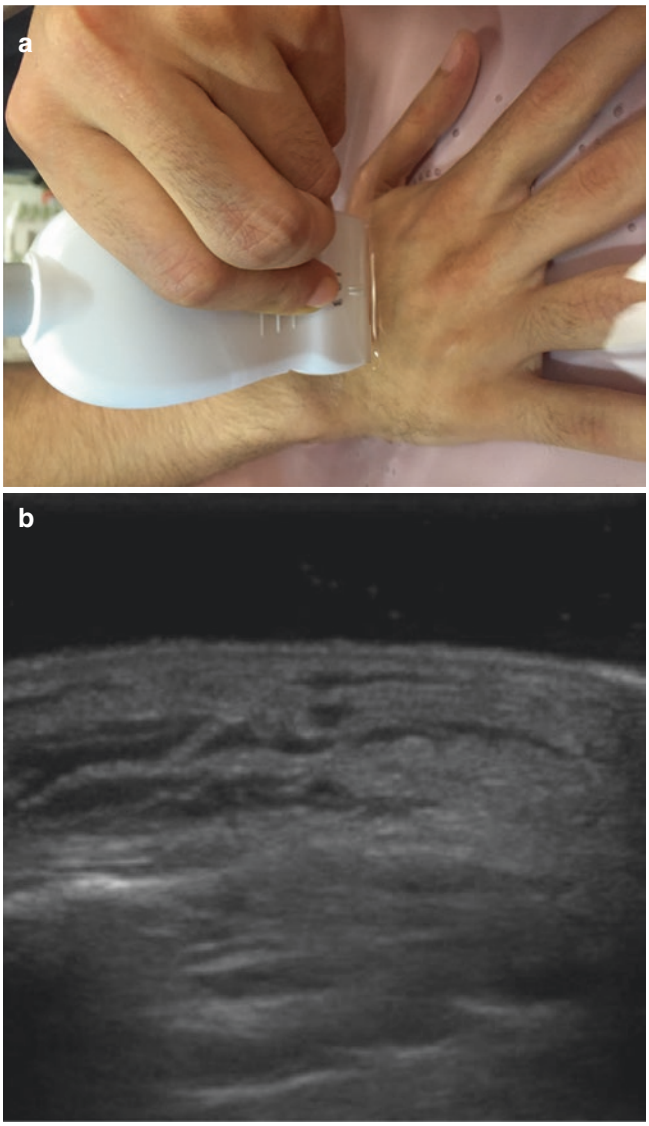

Fig. 1.2 (**a**, **b**) The water bath technique uses water as a medium to conduct sounds waves, similar to using gel during an examination. This is performed by immersing the extremity to be ultrasound under water. Consider using a water bath particularly when looking at hands and feet for abscess, cellulitis, foreign body, fracture, and evaluation of muscles and tendons. (**a**) Image courtesy of Errel Khordipour, (**b**) Image courtesy of Ee Tay

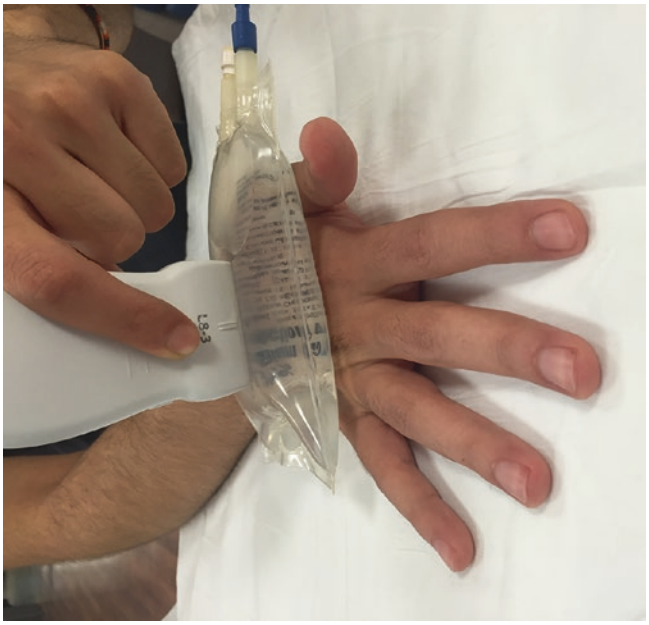

Fig. 1.3 A 100 mL saline bag may also be placed on top of the hand with gel on stop to be used an aqueous medium. Image courtesy of Errel Khordipour

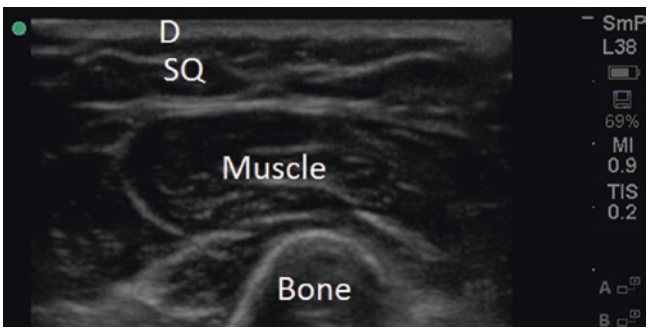

Fig. 1.4 The skin (D), both epidermis and dermis, will appear as a hyperechoic thin layer. The subcutaneous (SQ) layer has hypoechoic fat interspersed with hyperechoic linear echoes running parallel to the skin, which represent connective tissue septa. Veins and nerves may also be seen within this layer. Image courtesy of Errel Khordipour

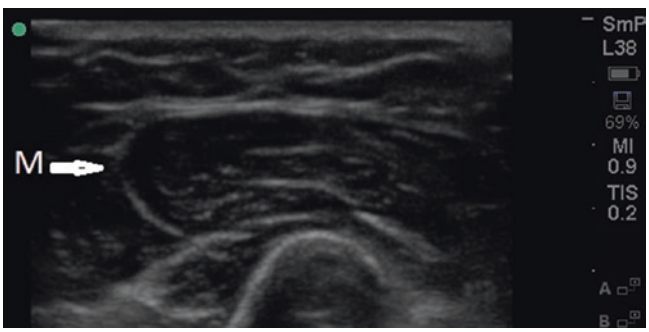

Fig. 1.5 Muscle fascicles can be visualized as hypoechoic cylindrical structures with hyperechoic connective tissue surrounding them. Image courtesy of Errel Khordipour

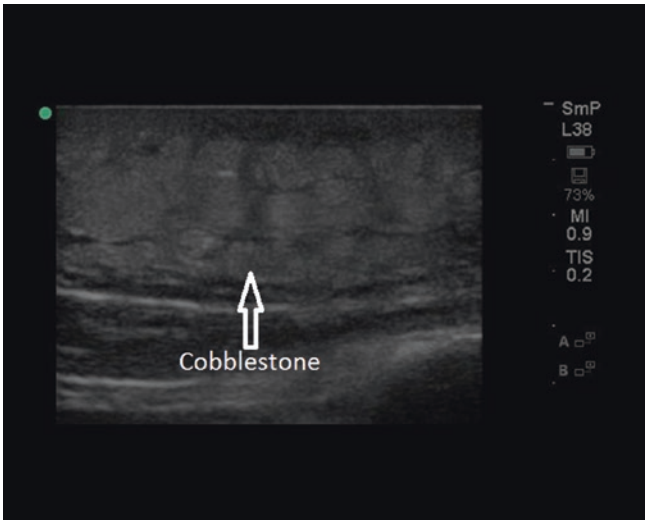

Fig. 1.6 Cellulitis can be differentiated form abscess by soft tissue ultrasound. Interstitial edema surrounding subcutaneous adipose is a hallmark of this disease and it is referred to as "cobblestoning." Although cobblestone appearance is common in cellulitis, it is advanced finding. Early cellulitis may appear as generalized swelling with increased echogenicity of the skin and subcutaneous tissues. Image courtesy of Ee Tay

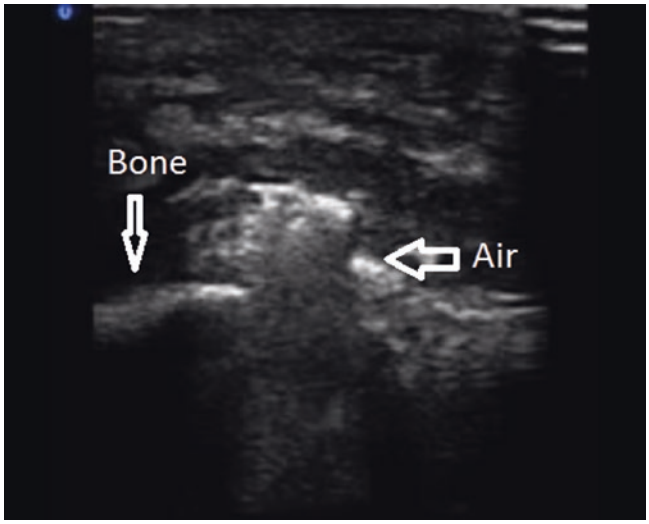

Fig. 1.8 Necrotizing fasciitis will appear as a thickened and distorted fascia with adjacent hypoechoic fluid colleting along the subcutaneous tissues of muscle. Small foci of gas can appear as well. A mixture of abscess, cellulitis and gas should strongly suggest this disease. Image courtesy of Jim Tsung (YouTube.com/Pocus4Geri)

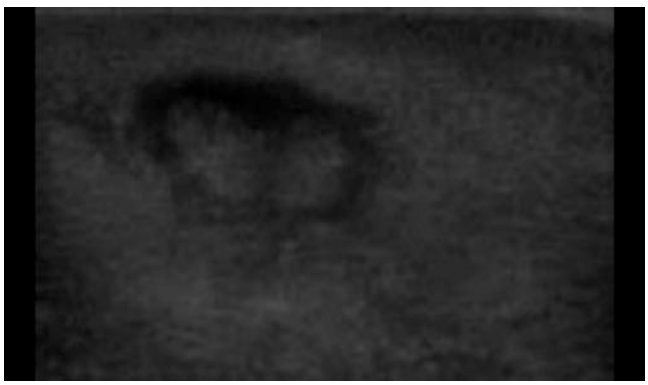

Fig. 1.7 Abscess has a characteristic spherical or elliptical shape with loosely defined margins. Within the abscess cavity, there may be a mixture of anechoic, hypoechoic and/or hyperechoic ultrasound findings. The abscess cavity can be compressed with the probe which may produce a swirling of the contents. It should be noted that absence of swirling does not rule out abscess (*see* Video 1.1). Images courtesy of Ee Tay

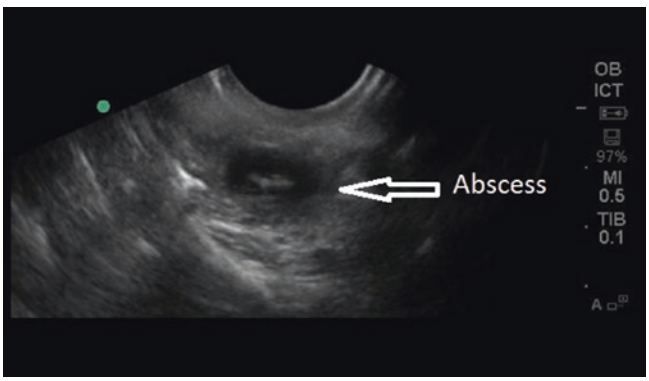

Fig. 1.9 For the evaluation of peritonsillar abscess you may decide to use the endocavitary probe. Place the probe inside the patient's mouth on top of the enlarged tonsil and fan toward the patient's head or cephalad with the head rotated to the opposite side. A linear probe may also be used to detect peritonsillar abscess in patients who have trismus and are unable to tolerate the probe inside the mouth. Look for similar findings as described above to distinguish abscess from cellulitis. Image courtesy of Ee Tay

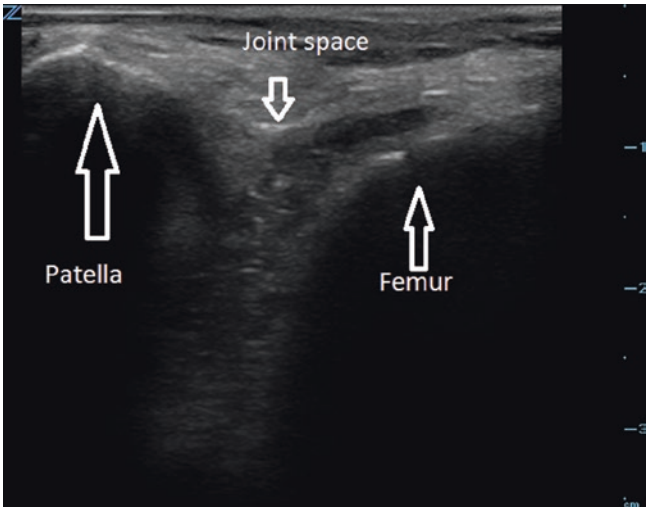

Fig. 1.10 In evaluating a knee or joint effusion, place the linear probe over the area of fluctuance. Ultrasound the contralateral side of the same area for comparison. Image courtesy of Errel Khordipour

References

1. Adhikari S, Blaivas M. Sonography first for subcutaneous abscess and cellulitis evaluation. J Ultrasound Med. 2012;31(10):1509–12.
2. Chao HC, Lin SJ, Huang YC, Lin TY. Sonographic evaluation of cellulitis in children. J Ultrasound Med. 2000;19(11):743–9.
3. Chau CL, Griffith JF. Musculoskeletal infections: ultrasound appearances. Clin Radiol. 2005;60(2):149–59.
4. Gaspari R, Dayno M, Briones J, Blehar D. Comparison of computerized tomography and ultrasound for diagnosing soft tissue abscess. Crit Ultrasound J. 2012;4(1):5.
5. Crawford R, Matheson AB. Clinical value of ultrasonography in the detection and removal of radiolucent foreign bodies. Injury. 1989;20:341–3.
6. Crystal CS, Masneri DA, Hellums JS, Kaylor DW, Young SE, Miller MA, et al. Bedside ultrasound for the detection of soft tissue foreign bodies: a cadaveric study. J Emerg Med. 2009;36(4):377–80.
7. Adhikari S, Blaivas M. Utility of bedside sonography to distinguish soft tissue abnormalities from joint effusions in the emergency department. J Ultrasound Med. 2010;29(4):519–26.
8. Wiler JL, Costantino TG, Filippone L, Satz W. Comparison of ultrasound-guided and standard landmark techniques for knee arthrocentesis. J Emerg Med. 2010;39(1):76–82.
9. Ohrndorf S, Naumann L, Grundey J, Scheel T, Scheel AK, Werner C, et al. Is musculoskeletal ultrasonography an operator-dependent method or a fast and reliably teachable diagnostic tool? Interreader agreements of three ultrasonographers with different training levels. Int J Rheumatol. 2010;2010:164518.

Shoulder

2

Laura S. Greenlund

The shoulder is a common site of pain, and point-of-care ultrasound is a very useful tool for examining the soft tissues surrounding the shoulder to determine its cause. Used along with physical examination, it compares well with more expensive and resource-intensive imaging [1, 2]. Typically, a linear mid-frequency (3–16 Hz) probe or curvilinear (1–7 Hz) probe is used. Depending on the site of pain and the mechanism of injury, different scanning techniques may be utilized. Ultrasound examination of the anterior, lateral, superior, or posterior shoulder will be used to visualize specific structures that are suspected to be injured, torn, arthritic, or inflamed (Figs. 2.1, 2.2, 2.3, 2.4, 2.5, 2.6, 2.7, 2.8, 2.9, 2.10, 2.11, and 2.12; Videos 2.1 and 2.2).

Electronic Supplementary Material The online version of this chapter (https://doi.org/10.1007/978-3-319-73855-0_2) contains supplementary material, which is available to authorized users.

L. S. Greenlund, M.D., Ph.D.
Department of Medicine, Division of Primary Care
Internal Medicine, Mayo Clinic, Rochester, MN, USA
e-mail: Greenlund.Laura@Mayo.edu

B. P. Nelson et al. (eds.), *Atlas of Handheld Ultrasound*, https://doi.org/10.1007/978-3-319-73855-0_2

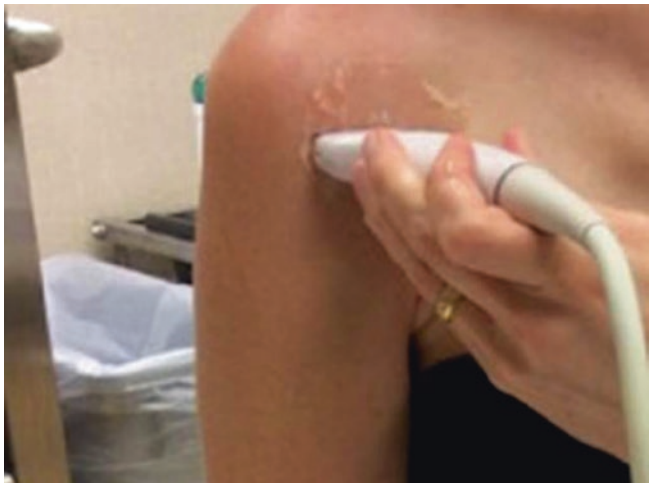

Fig. 2.1 An anterior shoulder examination is performed using a linear probe with the patient in a seated position. The patient's hand is placed palm up in his or her lap, on the lateral thigh. The probe marker is directed toward the patient's body and the probe is moved from a position on the proximal shoulder at the top of the humeral head downward toward the biceps muscle while imaging

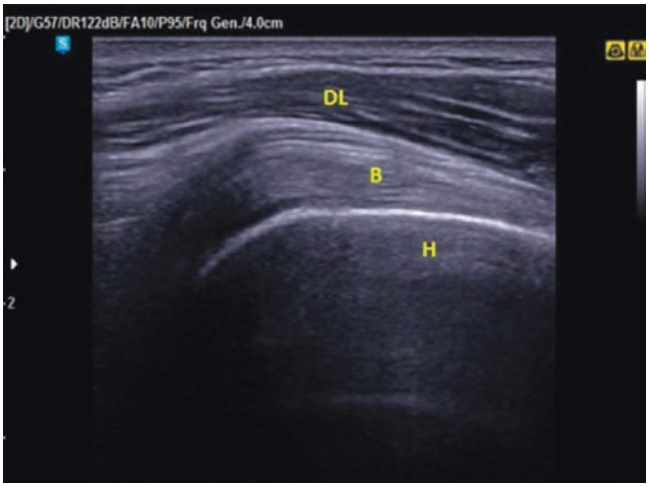

Fig. 2.3 The long head of the biceps tendon (B) is then examined in the longitudinal view with the probe marker pointing upward, moving the probe from a superior to inferior position. The deltoid muscle (DL) is seen overlying the biceps tendon, and the humerus (H) is seen below

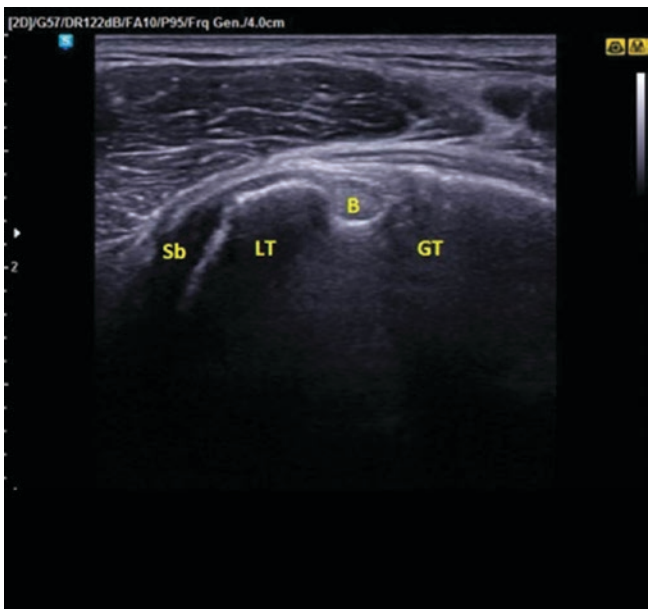

Fig. 2.2 Structures that are frequently painful or injured include the long head of the biceps tendon (B), which is visualized in the biceps groove between the greater tuberosity (GT) and lesser tuberosity (LT) of the humerus, and the subscapularis (Sb) tendon of the rotator cuff, which can be seen to the medial side. These are first examined in transverse view

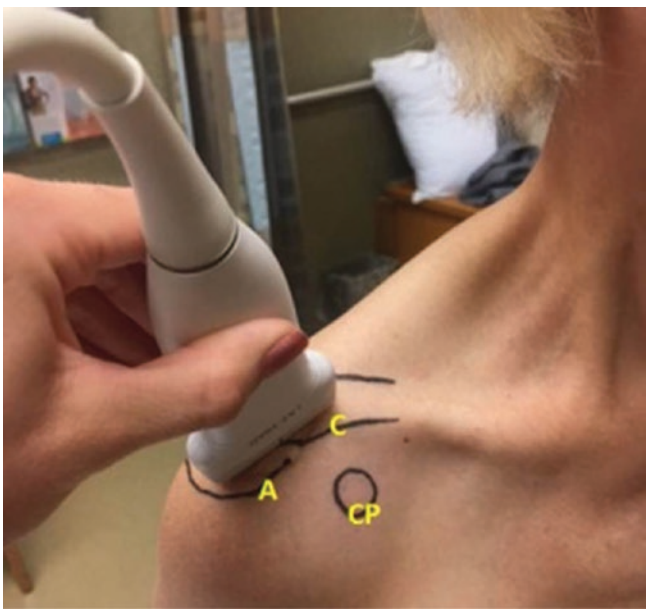

Fig. 2.4 A superior scan of the shoulder is performed if injury or arthritis of the acromioclavicular joint is suspected as the cause of pain. The linear probe is placed over the joint with the probe marker medial toward the clavicle (C) and the acromion (A) toward the lateral portion of the image. The coracoid process (CP) is palpable just below

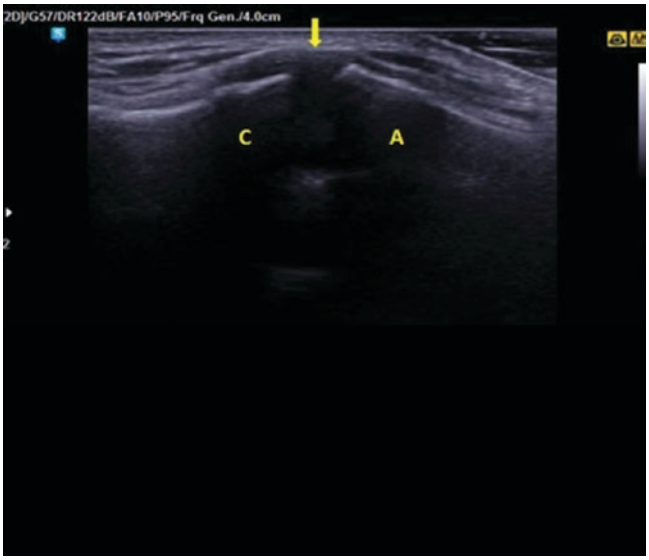

Fig. 2.5 The acromioclavicular joint capsule and overlying acromioclavicular ligament are indicated by the *arrow*. A tear of the ligament can result in shoulder separation and displacement or hypermobility of the clavicle (C) relative to the acromion (A)

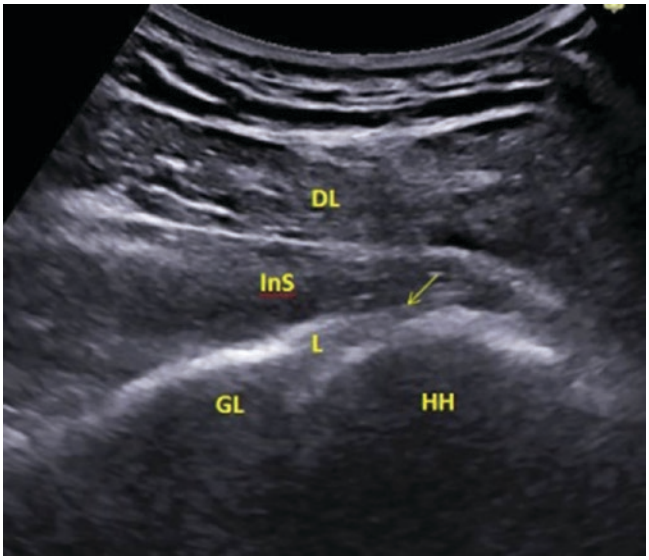

Fig. 2.7 The glenoid (GL), humeral head (HH), and glenoid labrum (L) are visualized deep to the infraspinatus muscle (InS). The deltoid muscle (DL) overlies the infraspinatus. The joint capsule is indicated by the *arrow*

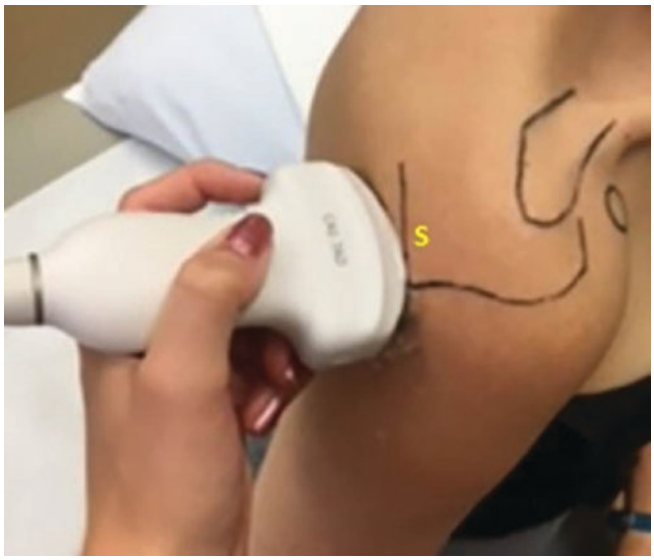

Fig. 2.6 The posterior shoulder is examined with a low- to mid-frequency curvilinear probe (1–7 Hz) to evaluate the posterior portion of the glenohumeral joint. The probe is placed just below the scapular spine (S), with the probe marker pointing toward the medial side

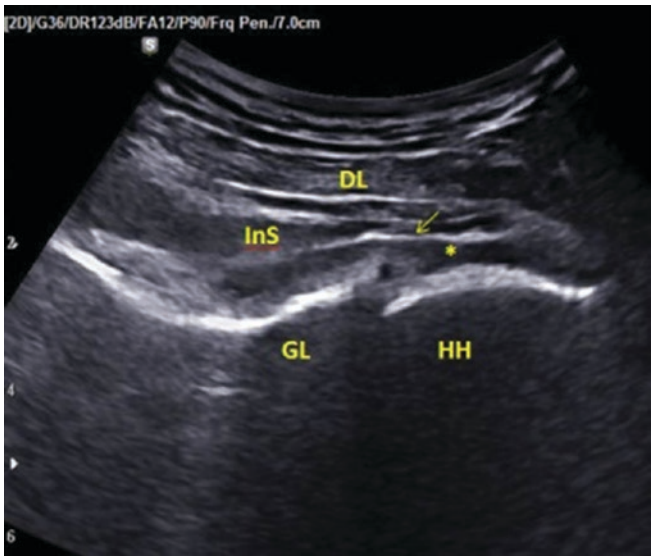

Fig. 2.8 A glenohumeral joint effusion is evidenced by hypoechoic fluid (*asterisk*) distending the joint capsule (*arrow*); it will lie beneath the infraspinatus muscle (InS) and above the glenoid (GL) and humeral head (HH). Movement of the glenohumeral joint can be assessed by ultrasound, as shown in Video 2.1

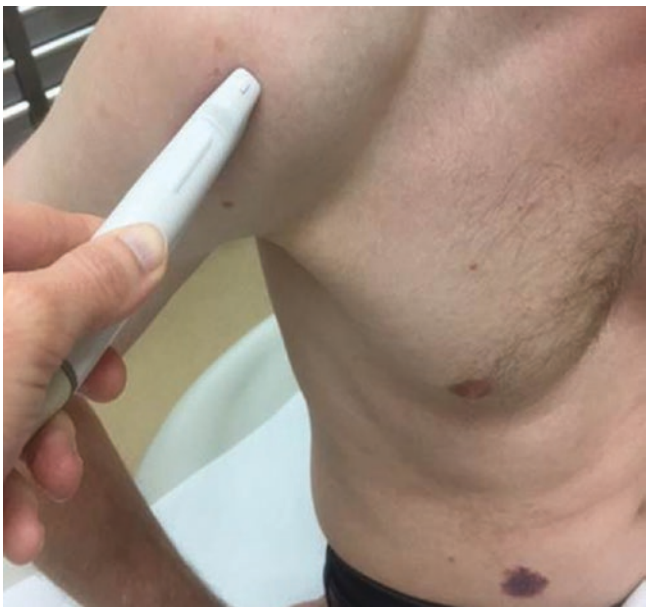

Fig. 2.9 The lateral shoulder is examined using a linear probe with the marker facing upward. The top of the probe is at the level of the acromion. The lateral shoulder exam is useful for visualizing the subacromial bursa and supraspinatus tendon. The patient's hand is in a position with the palm over the gluteus maximus as if placing it over a rear pants pocket. This view is in the long axis relative to the supraspinatus tendon

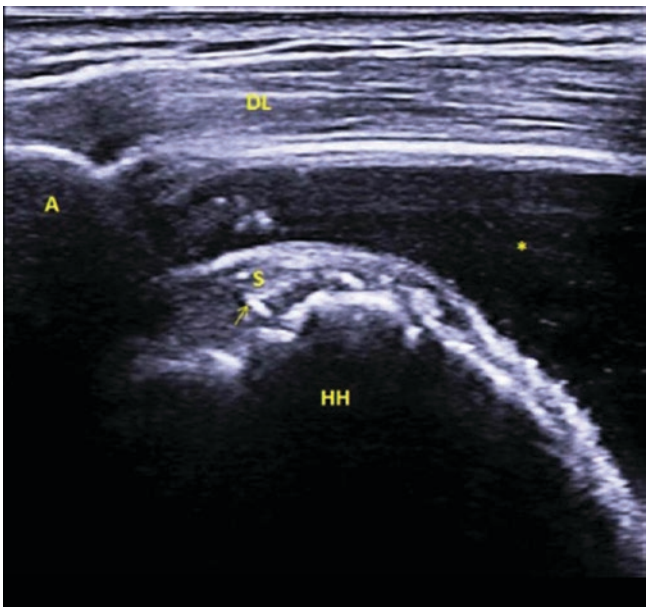

Fig. 2.11 In this patient with subacromial bursitis, fluid is visualized within the bursa. The acromion (A) is to the left, with the deltoid (DL) on top of the bursa and the supraspinatus tendon (S) below. Dark, hypoechoic fluid (*asterisk*) is seen within the subacromial bursa. The humeral head (HH) is deep to the overlying structures. Small, bright, hyperechoic calcifications are visible in the supraspinatus tendon (*arrow*)

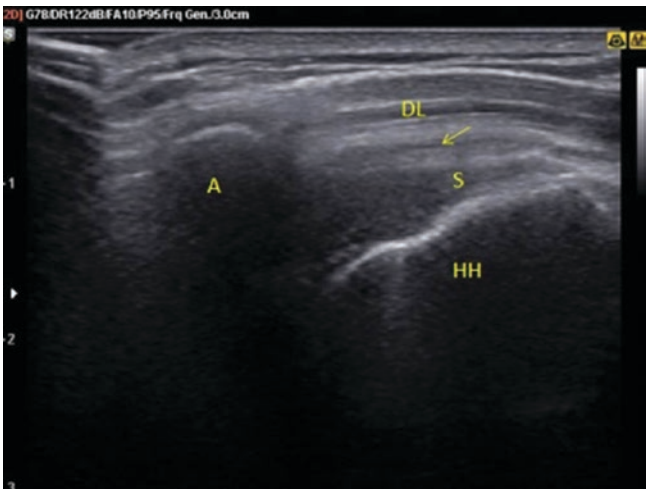

Fig. 2.10 With the probe in the long axis relative to the supraspinatus tendon (S), the acromion (A) is viewed on the left of the image. The deltoid muscle (DL) lies above the supraspinatus tendon, and the humeral head (HH) is deep to the tendon. The subacromial bursa is indicated by the *arrow*. In this normal patient, no fluid is visualized in the bursa, which appears very thin

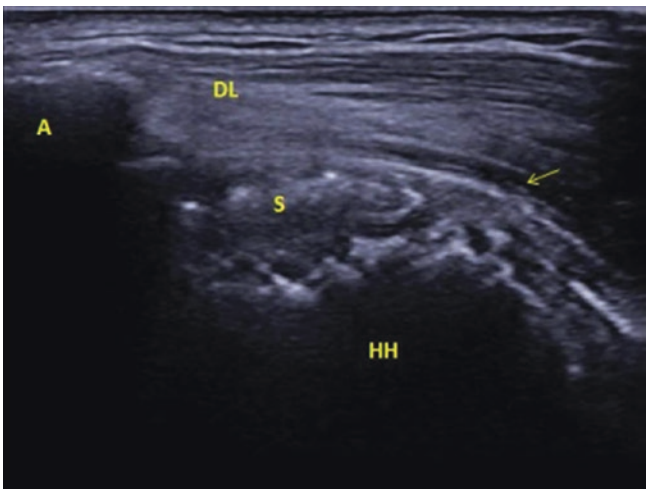

Fig. 2.12 If fluid is present within the bursa, it can be aspirated. This image shows the same patient as Fig. 2.11 after aspiration of the subacromial bursa fluid. The acromion (A) is to the left, with the deltoid (DL) on top of the bursa and the supraspinatus tendon (S) below. The *arrow* indicates the subacromial bursa. The humeral head (HH) is deep to the overlying structures. Video 2.2 shows dynamic ultrasound imaging used to assess for subacromial impingement of the supraspinatus tendon

References

1. Levine BD, Motamedi K, Seeger LL. Imaging of the shoulder: a comparison of MRI and ultrasound. Curr Sports Med Rep. 2012;11:239–43.
2. Sheehan SE, Coburn JA, Singh H, Vanness DJ, Sittig DF, Moberg DP, et al. Reducing unnecessary shoulder MRI examinations within a capitated health care system: a potential role for shoulder ultrasound. J Am Coll Radiol. 2016;13(7):780.

Elbow

3

Matthew Egan and David Spinner

The elbow has multiple bony and soft tissue structures that can be imaged superficially to aid in diagnosis of common pathology. For common overuse injuries such as "golf elbow" and "tennis elbow," ultrasound can evaluate the associated flexor and extensor tendons to identify acute conditions, compared with chronic symptoms of overuse. According to the American College of Radiology, ultrasound may be adequate as an initial evaluation for epicondylitis, allowing MRI to be used if ultrasound findings are normal [1, 2]. This evaluation can potentially decrease costs. For similar functional injuries, ultrasound may be performed to evaluate for ligamentous damage to the ulnar and radial collateral ligaments. According to the Appropriateness Criteria of the American College of Radiology, both ultrasound and MRI may be used to detect soft tissue abnormalities [1]. Confirming these diagnoses by point-of-care ultrasound ensures that patients move forward with the right plan of care and do not undertreat an undiagnosed pathology. In the setting of the nontraumatic, swollen elbow, point-of-care ultrasound can evaluate for joint effusion and bursitis, potentially helping to obviate the need for aspiration. Additionally, in patients who have muscular pain after lifting or heavy exertion, point-of-care ultrasound may be performed to evaluate for tears and rupture of the triceps and biceps brachii tendons, as well as to evaluate for muscle tears. For distal neuropathic pain or for invasive procedures, ultrasound also may be used to guide regional anesthesia in the ulnar, median, or radial nerves, all of which can be seen on point-of-care elbow ultrasound, as discussed further in Chap. 8, *Peripheral Nerves*. Figures 3.1, 3.2, 3.3, 3.4, 3.5, 3.6, 3.7 and 3.8 illustrate the various probe positions and the resulting views in the elbow area.

M. Egan, M.D. (✉)
Department of Emergency Medicine, Icahn School of Medicine at Mount Sinai, New York, NY, USA
e-mail: matthew.egan@mountsinai.org

D. Spinner, D.O.
Department of Rehabilitation Medicine, Mount Sinai Hospital, New York, NY, USA

B. P. Nelson et al. (eds.), *Atlas of Handheld Ultrasound*, https://doi.org/10.1007/978-3-319-73855-0_3

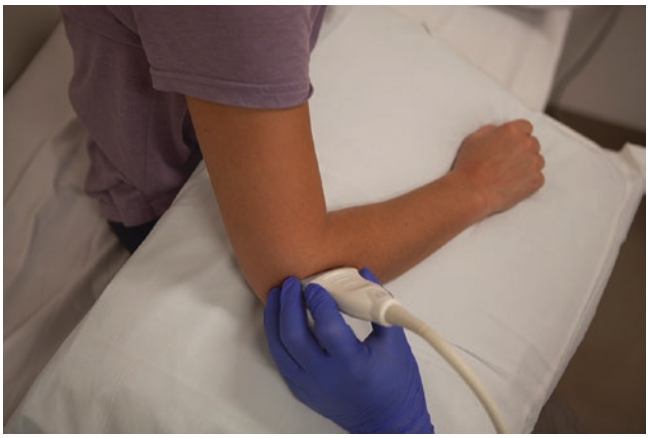

Fig. 3.1 A linear probe should be used for ultrasound evaluation of the elbow. Sagittal views should be obtained with the probe marker directed towards the patient's head. The probe is oriented with the proximal end at the lateral humeral epicondyle, extending distally along the midline in the anterior-posterior dimension

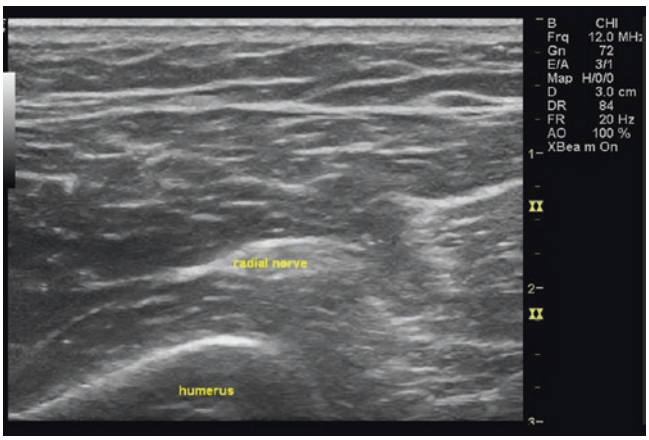

Fig. 3.4 This transverse-axis view demonstrates the radial nerve and humerus

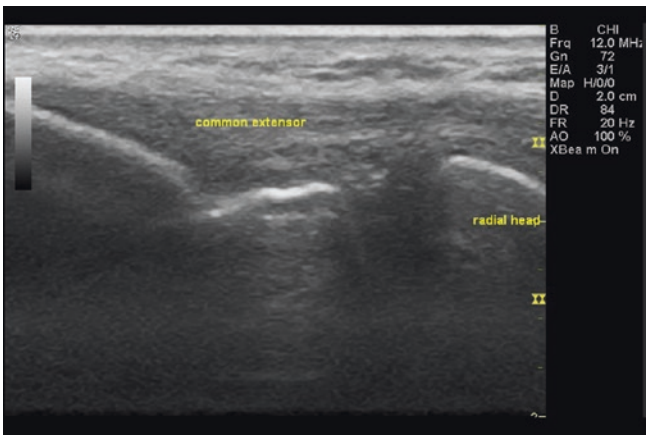

Fig. 3.2 This long-axis view demonstrates the common extensor tendon, radial head, and lateral humeral epicondyle

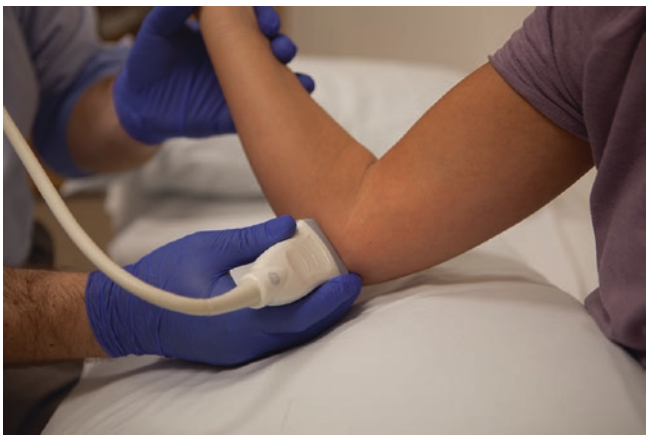

Fig. 3.5 With the linear probe oriented longitudinally with the probe marker toward the patient's head, the probe extends distally from the medial humeral epicondyle at approximately the midline in the anterior-posterior dimension

Fig. 3.3 With the linear probe oriented transversely with probe marker toward the patient's right, the probe is centered at the lateral margin of the anterior elbow fold

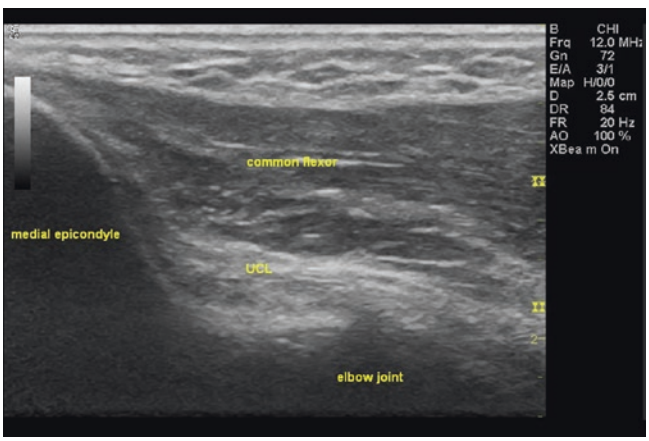

Fig. 3.6 This long-axis view demonstrates the medial (humeral) epicondyle, common flexor (tendon), ulnar collateral ligament (UCL), and the elbow joint

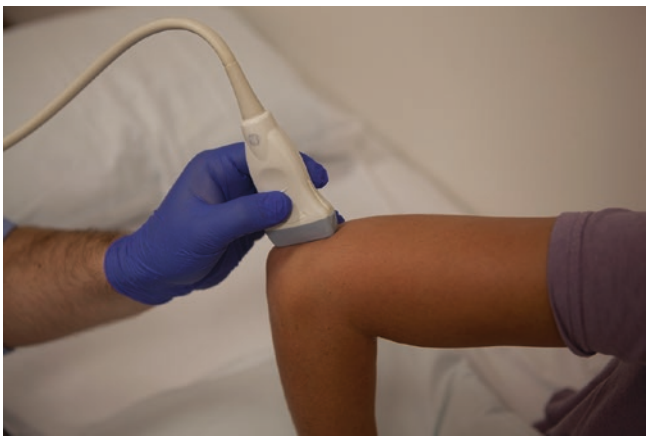

Fig. 3.7 With the linear probe oriented longitudinally with the probe marker toward the patient's feet, the probe extends proximally from the olecranon process on the posterior elbow

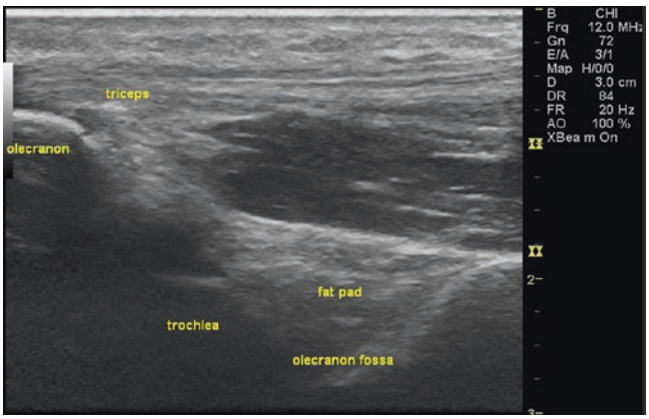

Fig. 3.8 This long-axis view demonstrates the triceps and triceps tendon insertion on the olecranon process. Also demonstrated are the olecranon fossa, fat pad, and trochlea

References

1. American College of Radiology. ACR appropriateness criteria®. https://acsearch.acr.org/docs/69423/Narrative/. Accessed 23 Oct 2017.
2. Miller TT, Shapiro MA, Schultz E, Kalish PE. Comparison of sonography and MRI for diagnosing epicondylitis. J Clin Ultrasound. 2002;30:193–202.

Hip

4

Steve J. Wisniewski and Naveen S. Murthy

The hip joint is visualized well in most adults with point-of-care ultrasound. Depending on body habitus, a mid-frequency linear or low-frequency curved transducer is required for ultrasound evaluation of this area (Figs. 4.1 and 4.2). Presence of a hip joint effusion can be reliably identified with ultrasound (Fig. 4.3). A hip joint effusion is present in adults when the anterior joint recess (the distance between the neck of the femur and the overlying joint capsule) is measured at greater than 6 mm, or if there is a side-to-side difference of more than 1 mm [1, 2]. Hip joint effusions can be seen in patients with degenerative arthritis, inflammatory arthritis, and septic arthritis. Fluid aspiration is required for a definite diagnosis.

S. J. Wisniewski, M.D. (✉)
Departments of Sports Medicine
and Physical Medicine and Rehabilitation,
Mayo Clinic, Rochester, MN, USA
e-mail: wisniewski.stephen@mayo.edu

N. S. Murthy, M.D.
Department of Radiology, Mayo Clinic, Rochester, MN, USA

B. P. Nelson et al. (eds.), *Atlas of Handheld Ultrasound*, https://doi.org/10.1007/978-3-319-73855-0_4

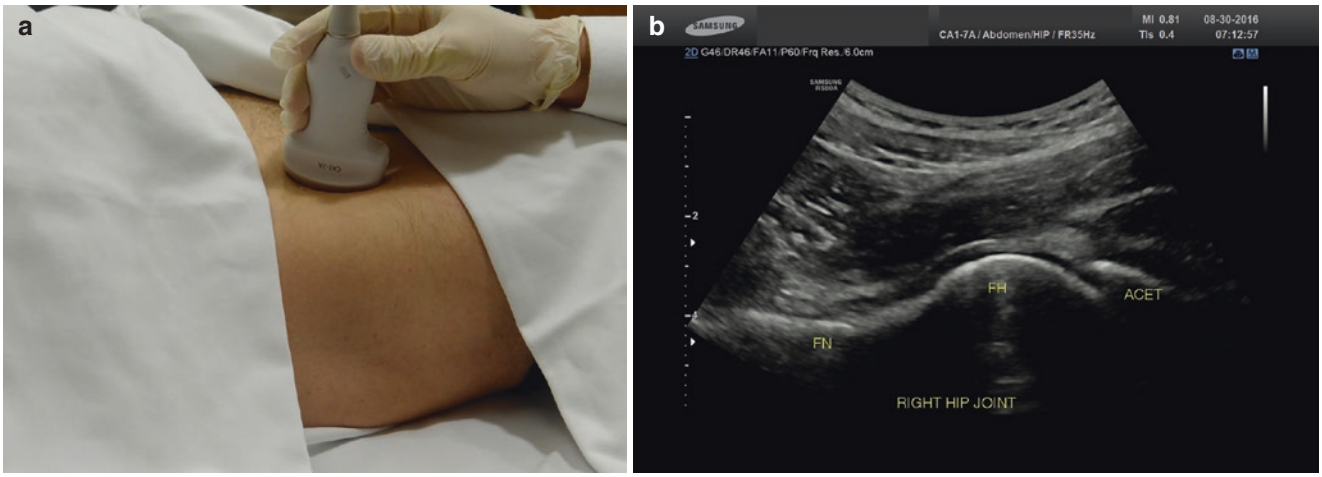

Fig. 4.1 (**a**) Use of a low-frequency curvilinear transducer to view the hip joint. (**b**) Oblique sagittal view of a normal hip joint using a low-frequency curvilinear transducer. *ACET* acetabulum, *FH* femoral head, *FN* femoral neck. (*Image courtesy of* Steve Wisniewski)

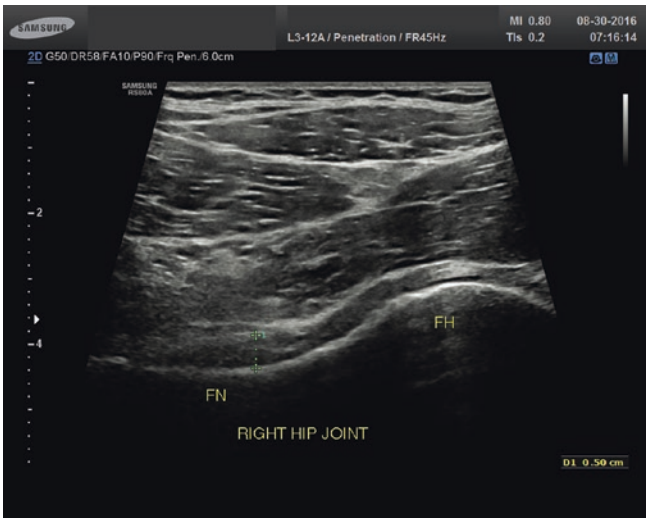

Fig. 4.2 Oblique sagittal view of a normal hip joint using a mid-frequency linear transducer. The anterior joint recess is normal, with no joint effusion. *FH* femoral head, *FN* femoral neck. (*Image courtesy of* Steve Wisniewski)

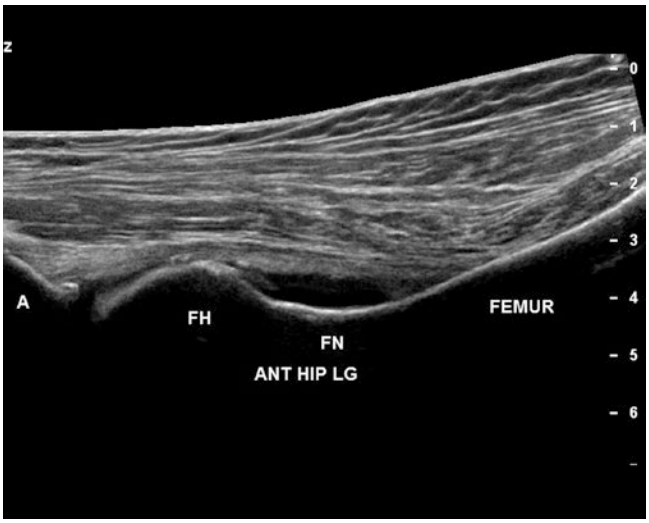

Fig. 4.3 Oblique sagittal image of a hip joint effusion. *A* acetabulum, *FH* femoral head, *FN* femoral neck. (*Image courtesy of* Jay Smith)

Soft tissue structures of the hip, such as a distended iliopsoas bursa, can also be readily identified with ultrasound (Figs. 4.4 and 4.5). The iliopsoas bursa communicates with the hip joint in approximately 15% of people [3]. When the bursa is distended, it is most commonly seen medial to the iliopsoas tendon (Fig. 4.6). The bursa has been shown to have a "U-shaped" configuration, with the bottom of the "U" situated against the acetabular rim/iliopectineal eminence [4]. The contents of a distended bursa should have a nearly anechoic appearance on ultrasound if simple joint fluid is present (Fig. 4.6), but when complex fluid such as blood, pus, or particle disease from a joint arthroplasty is present, the fluid may have a more echogenic appearance that can mimic a solid mass. Furthermore, not all structures in this location represent an iliopsoas bursa. Giant cell tumor of the tendon sheath can occur in a similar location and should raise suspicion, as it does not have all the typical features associated with an iliopsoas bursa (Fig. 4.7).

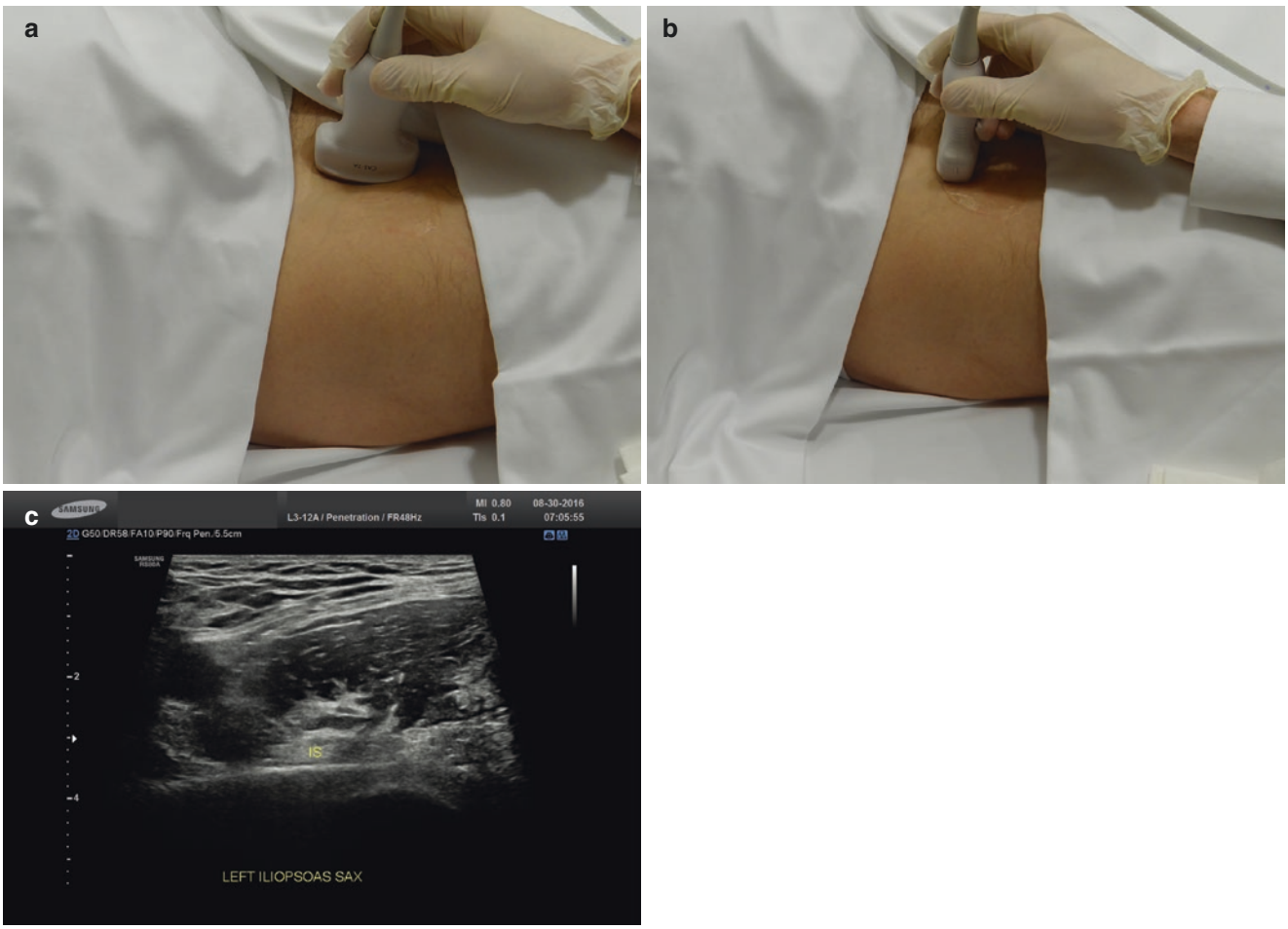

Fig. 4.4 (**a** and **b**) The transducer is placed slightly cephalad to the femoral head to view the iliopsoas tendon. (**c**) Transverse image of the iliopsoas tendon at the iliopectineal eminence. The iliopsoas bursa would be found deep to the tendon. Right side of the image is lateral. *IS* iliopsoas tendon. (*Image courtesy of* Steve Wisniewski)

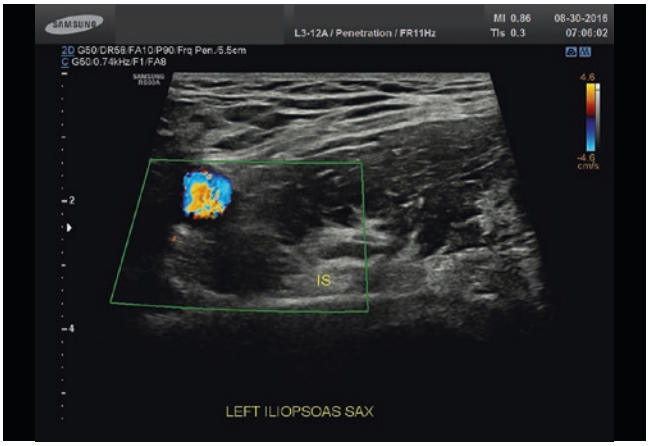

Fig. 4.5 Transverse image of the iliopsoas tendon at the iliopectineal eminence. Doppler shows the femoral vessels, which are located just medial to the tendon. Right side of the image is lateral. *IS* iliopsoas tendon. (*Image courtesy of* Steve Wisniewski)

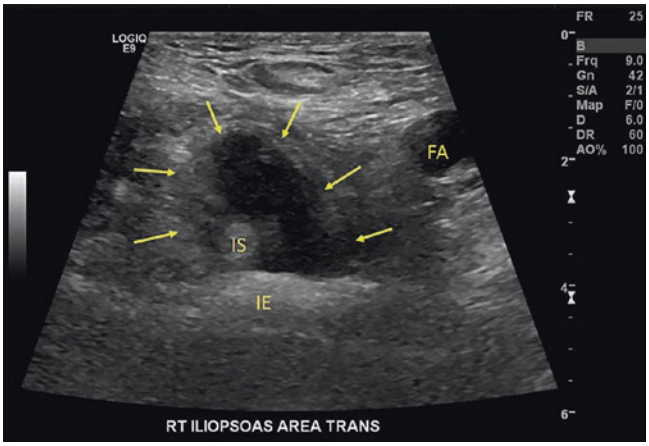

Fig. 4.6 Transverse image of a nearly anechoic right iliopsoas bursa at the iliopectineal eminence (IE) in a person with a total hip arthroplasty. The iliopsoas bursa (*outlined by arrows*) is medial to the iliopsoas tendon (IS). Left side of the image is lateral. *FA* femoral artery. (*Image courtesy of* Naveen Murthy)

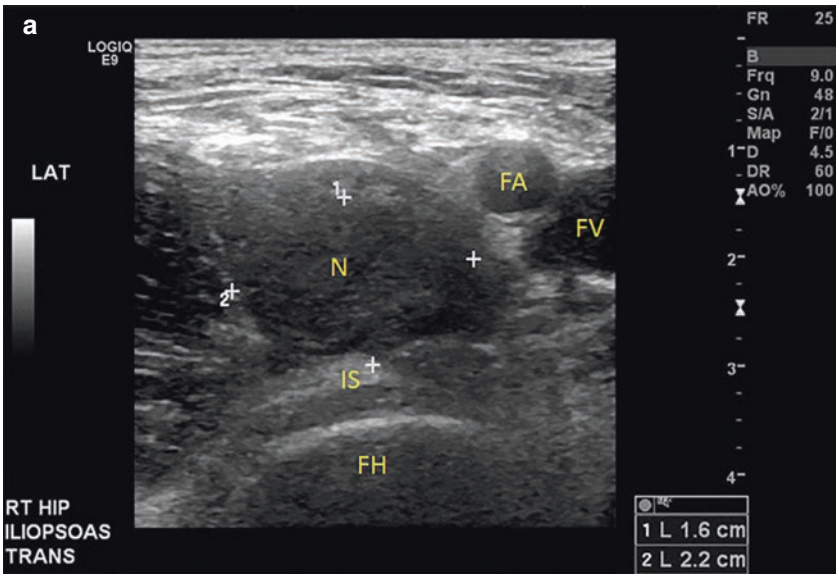

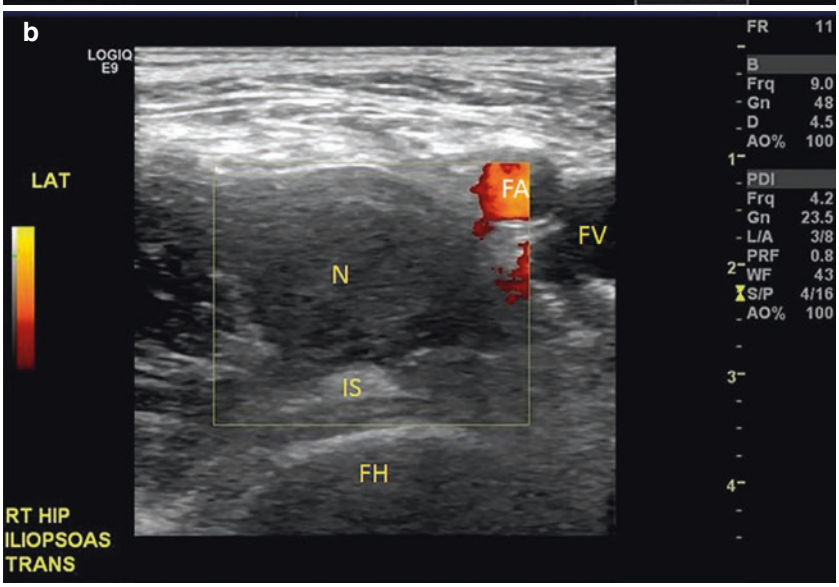

Fig. 4.7 (**a**) Transverse image of the right iliopsoas (IS) at the level of the femoral head (FH) just distal to the iliopectineal eminence. There is a hypoechoic nodule (N, delineated by measurement calipers) intimately associated with the anterior margin of the iliopsoas tendon (IS); the nodule was pathologically proven to be a giant cell tumor of the tendon sheath. Left side of image is lateral. (**b**) The same image with power Doppler showing no discernible blood flow in the nodule, compared with the blood flow within the femoral vessels. *FA* femoral artery, *FV* femoral vein. (*Images courtesy of* Naveen Murthy)

References

1. Koski JM, Anttila PJ, Isomaki HA. Ultrasonography of the adult hip joint. Scand J Rheumatol. 1989;18:113–7.
2. Bierma-Zienstra SMA, Bohnen AM, Verhaar JAN, Prins A, Ginai-Karamat AZ, Lameria JS. Sonography for hip joint effusion in adults with hip pain. Ann Rheum Dis. 2000;59:178–82.
3. Ginesty E, Dromer C, Galy-Fourcade D, Bénazet JF, Marc V, Zabraniecki L, et al. Iliopsoas bursopathies. A review of twelve cases. Rev Rhum Engl Ed. 1998;65:181–6.
4. Dauffenbach J, Pingree MJ, Wisniewski SJ, Murthy N, Smith J. Distribution pattern of sonographically guided iliopsoas injections: cadaveric investigation using coned beam computed tomography. J Ultrasound Med. 2014;33:405–14.

Knee

5

Matthew Egan and David Spinner

Many of the vascular, bony, and soft tissue structures in the knee can be readily evaluated with point-of-care ultrasound. Point-of-care ultrasound can assist in initial diagnostic evaluation in the setting of direct or indirect traumatic injury to the knee or in undifferentiated knee effusion. The objective of knee ultrasound is to evaluate the normal muscular, ligamentous, cartilaginous, and bony structures of the knee, looking for irregularities in these structures. For atraumatic swollen knees, ultrasound can detect bursitis and can give information regarding the degree of joint effusion. For functional injuries (like those typically related to athletics) or traumatic injuries to the knee, ultrasound can detect a fractured patella or tears of the menisci, medial collateral ligament (MCL), lateral collateral ligament (LCL), patellar tendon, and muscles of the quadriceps. Ultrasound has been found to be more sensitive than radiographs in assessing for lipohemarthrosis, which can be evidence of occult intra-articular knee fracture [1, 2]. For individuals with lower extremity swelling, knee ultrasound can help determine the existence of a Baker's cyst or deep vein thrombosis. Determining the etiology of knee pain or dysfunction at the bedside may prevent unnecessary imaging, invasive procedures like arthrocentesis, and delay to care. If invasive procedures are needed, however, ultrasound may be used to guide aspiration or therapeutic injection of the knee joint. It is important to note that ultrasound has limited ability to evaluate the deeper ligamentous structures such as the cruciate ligaments, so any clinical suspicion that a patient has further underlying ligamentous damage will warrant further workup with other imaging modalities (Figs. 5.1, 5.2, 5.3, 5.4, 5.5, 5.6, 5.7, 5.8, 5.9, 5.10, 5.11, 5.12, 5.13, 5.14 and 5.15).

M. Egan, M.D. (✉)
Department of Emergency Medicine, Icahn School of Medicine at Mount Sinai, New York, NY, USA
e-mail: matthew.egan@mountsinai.org

D. Spinner, D.O.
Department of Rehabilitation Medicine, Mount Sinai Hospital, New York, NY, USA

B. P. Nelson et al. (eds.), *Atlas of Handheld Ultrasound*, https://doi.org/10.1007/978-3-319-73855-0_5

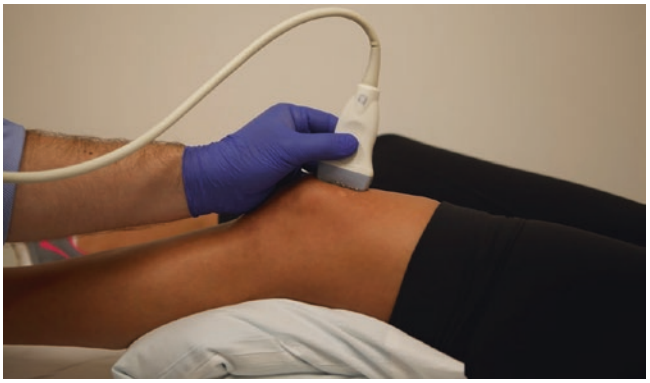

Fig. 5.1 A linear probe should be used to evaluate the suprapatellar knee. Sagittal views should be obtained with the probe marker facing the patient's head and the distal edge of the probe overlying the proximal aspect of patella in the midline of the knee. Transverse views should also be obtained with the probe marker to the patient's right and the probe placed slightly proximal to the patella with the middle of the probe at centered at the midline of the knee

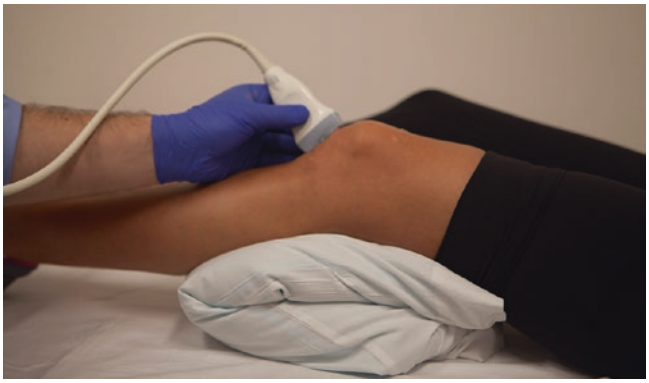

Fig. 5.4 A linear probe is again used to evaluate the infrapatellar knee. Sagittal views should be obtained with the probe marker facing towards the patient's head. The proximal edge of the probe should overlie the distal aspect of the patella in the midline of the knee. Scan distally, terminating with the distal edge of the probe overlying the tibial tuberosity

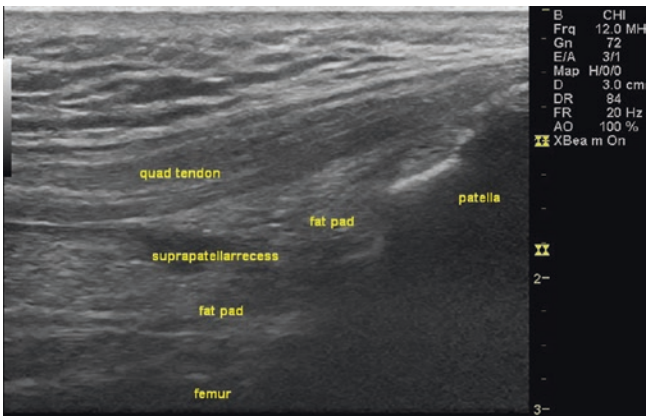

Fig. 5.2 A longitudinal view of the suprapatellar region should reveal the quadriceps tendon, proximal patella, suprapatellar recess or bursa, suprapatellar fat pad, and anterior portion of the femur

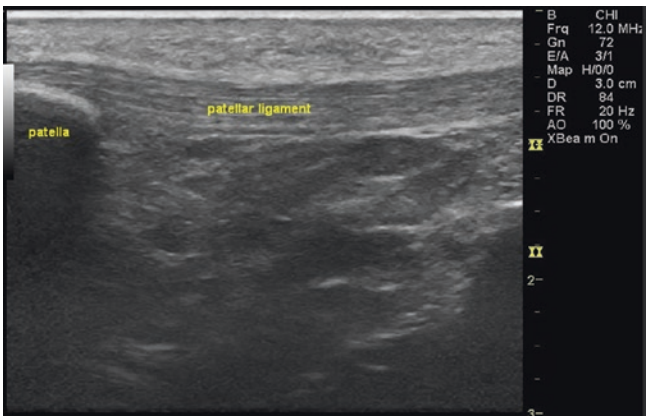

Fig. 5.5 A longitudinal view demonstrates the distal patella and the patellar ligament extending distally

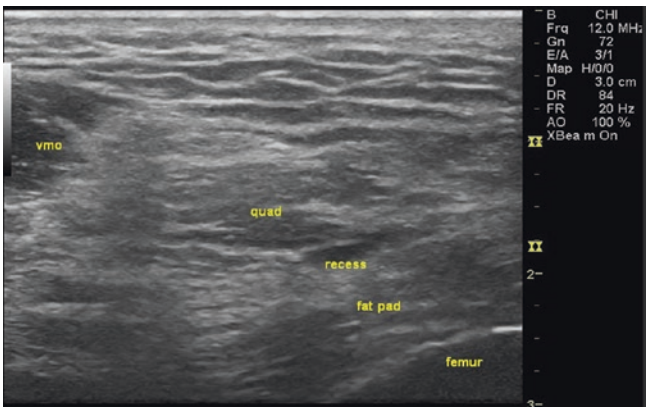

Fig. 5.3 A transverse view of the suprapatellar region demonstrates the vastus medialis oblique muscle (vmo), quadriceps muscle, suprapatellar recess or bursa, suprapatellar fat pad, and femur

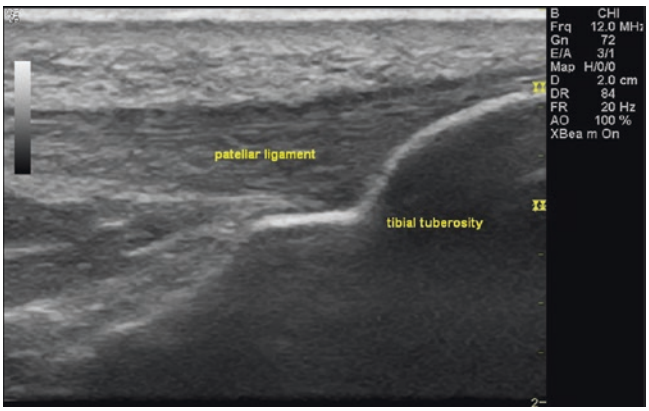

Fig. 5.6 A longitudinal view demonstrates the patellar ligament inserting into the tibial tuberosity

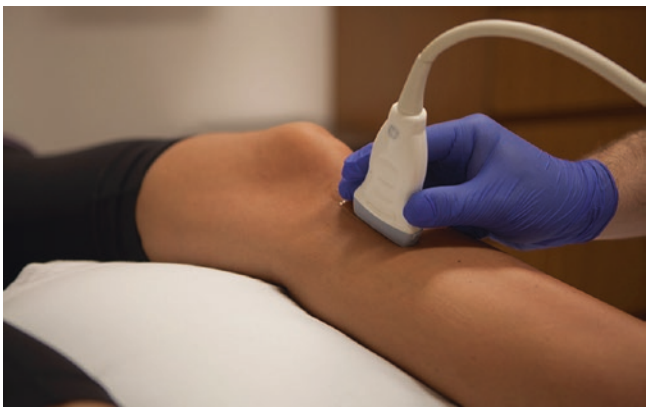

Fig. 5.7 A linear probe is again used to evaluate the pes anserine tendons and associated bursa. The probe marker is directed cephalad. The probe is angled obliquely, with the distal aspect of the probe directed laterally and the proximal portion of the probe directed medially, with the proximal aspect of the probe medial to the patella and beginning at the inferior line of the patella

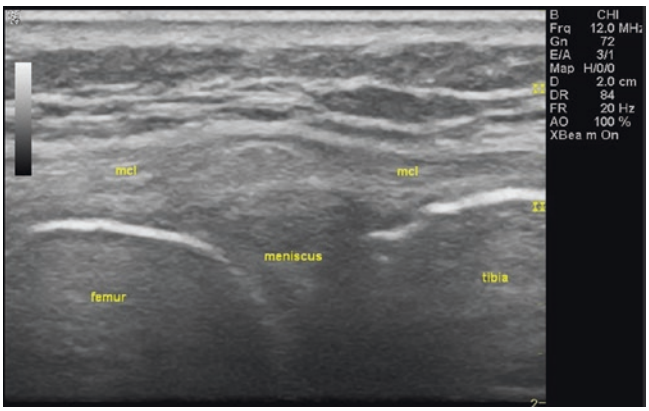

Fig. 5.10 This long-axis view demonstrates the medial collateral ligament (mcl), meniscus, femur, and tibia

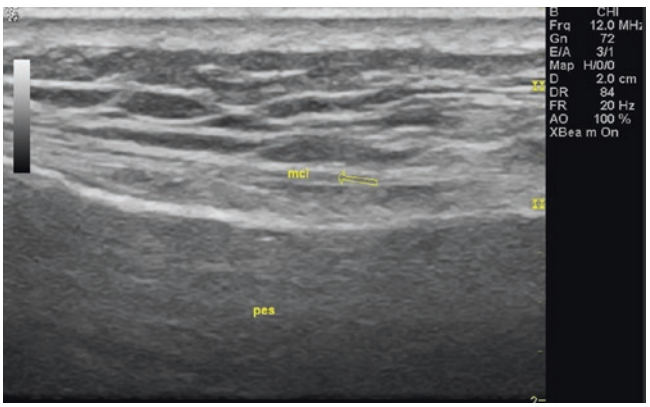

Fig. 5.8 A longitudinal view demonstrates the pes anserine tendons (pes) and medial collateral ligament (mcl)

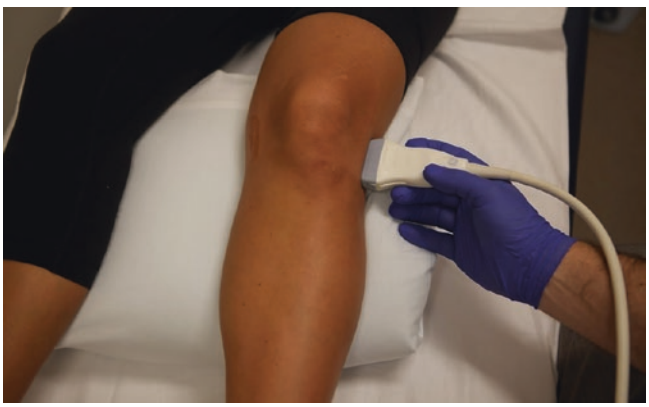

Fig. 5.11 A linear probe is again used to evaluate the lateral structures of the knee. Sagittal views should be obtained with the probe marker facing the patient's head. The probe is oriented at the lateral aspect of knee, approximately midline in the anterior-posterior dimension. The middle of the probe should overlie the joint space

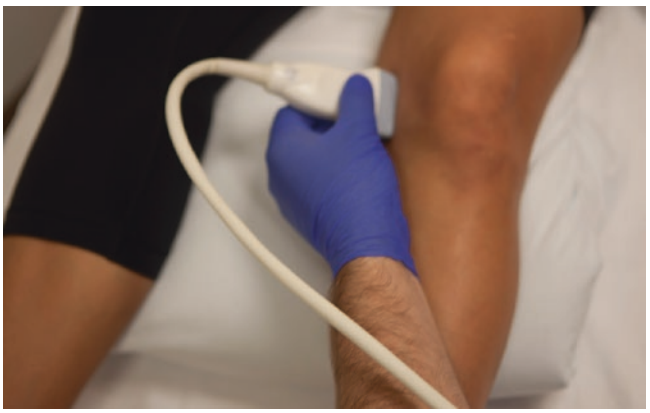

Fig. 5.9 A linear probe is again used to evaluate the medial structures of the knee. Sagittal views should be obtained with the probe marker facing the patient's head. The probe is oriented at the medial aspect of knee, approximately midline in the anterior-posterior dimension. The middle of the probe should overlie the joint space

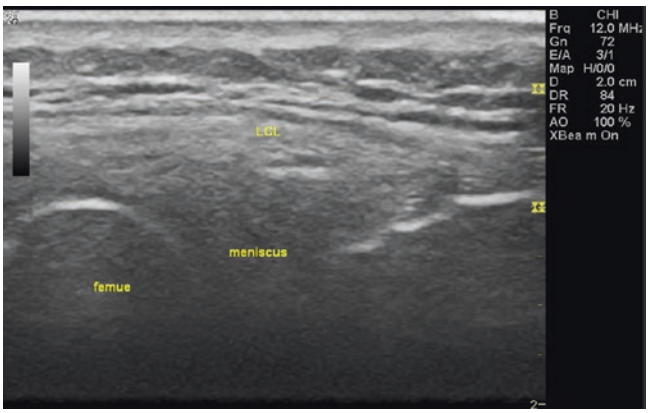

Fig. 5.12 This long-axis view demonstrates the femur, meniscus, lateral collateral ligament (LCL), and fibula

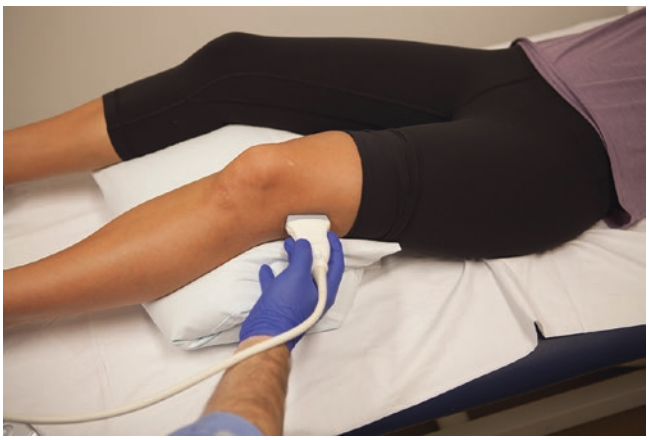

Fig. 5.13 A linear probe is used to evaluate the Iliotibial band. Sagittal views should be obtained with the probe marker facing the patient's head. The probe is oriented on lateral aspect of leg at about midline in the anterior-posterior dimension with the distal aspect of the probe terminating at proximal patellar line

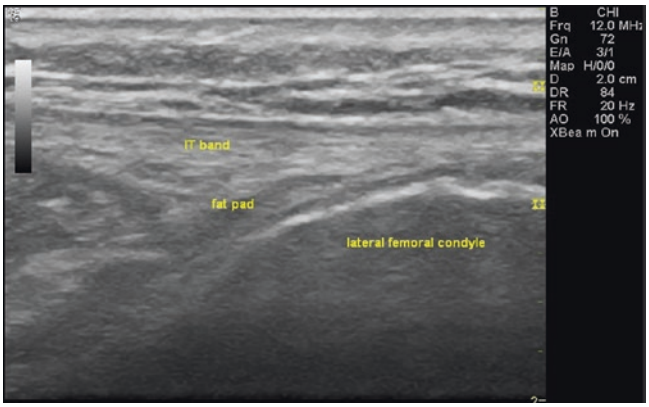

Fig. 5.14 This long-axis view demonstrates the iliotibial band (IT band), fat pad, and lateral femoral condyle

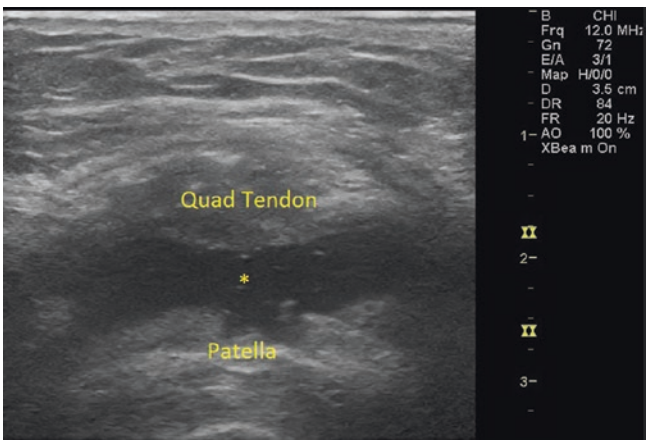

Fig. 5.15 A suprapatellar effusion is evident in this image, as indicated by the anechoic structure (*asterisk*) underneath the quad tendon and above the patella

References

1. Alves TI, Girish G, Kalume Brigido M, Jacobson JA. US of the knee: scanning techniques, pitfalls, and pathologic conditions. Radiographics. 2016;36:1759–75.
2. Bonnefoy O, Diris B, Moinard M, Aunoble S, Diard F, Hauger O. Acute knee trauma: role of ultrasound. Eur Radiol. 2006;16:2542–8.

Ankle and Foot

6

Jacob E. Voelkel and Tobias Kummer

Ultrasound can be used to identify a wide variety of pathologies common to the ankle joint, including ankle joint effusions, Achilles tendon rupture, and fractures.

The Achilles tendon is the most frequently injured ankle tendon. Early diagnosis of a complete tendon rupture is important to prevent a permanent functional deficit of the ankle joint. Although Achilles tendon injuries can be difficult to identify with physical examination alone, the tendon is easily visualized on ultrasound, given its superficial lie. Originating from the gastrocnemius and soleus muscles, the tendon runs just beneath the skin to its insertion at the calcaneus. Ultrasound can be used to diagnose complete or partial tendon injuries (Fig. 6.1) [1].

Ankle joint effusions can be easily identified by ultrasound, which is more sensitive than standard ankle radiograph films, especially in the setting of a small effusion (Fig. 6.2) [2].

Fractures are commonly diagnosed with radiographic films, but ultrasound is highly sensitive in diagnosing ankle fractures [3, 4]. Occult fractures, which require repeat imaging, might be identified on ultrasound, with the added benefit of being able to correlate imaging findings with pain sensitivity from the ultrasound probe (Fig. 6.3).

Ultrasound can also be used to evaluate common foot problems such as plantar fasciitis and podagra in gout. In plantar fasciitis, the plantar fascia is thickened more than 4 mm at the calcaneal insertion site, and the fascia can appear hypoechoic (Fig. 6.4) [5, 6]. The most commonly affected joint in a gout attack is the first metatarsophalangeal joint (Fig. 6.5). In addition to demonstrating an effusion and changes to the synovial lining and cartilage, ultrasound can be used to directly guide a joint aspiration [7].

J. E. Voelkel, M.D. (✉) • T. Kummer, M.D.
Department of Emergency Medicine, Mayo Clinic,
Rochester, MN, USA
e-mail: voelkel.jacob@mayo.edu

B. P. Nelson et al. (eds.), *Atlas of Handheld Ultrasound*, https://doi.org/10.1007/978-3-319-73855-0_6

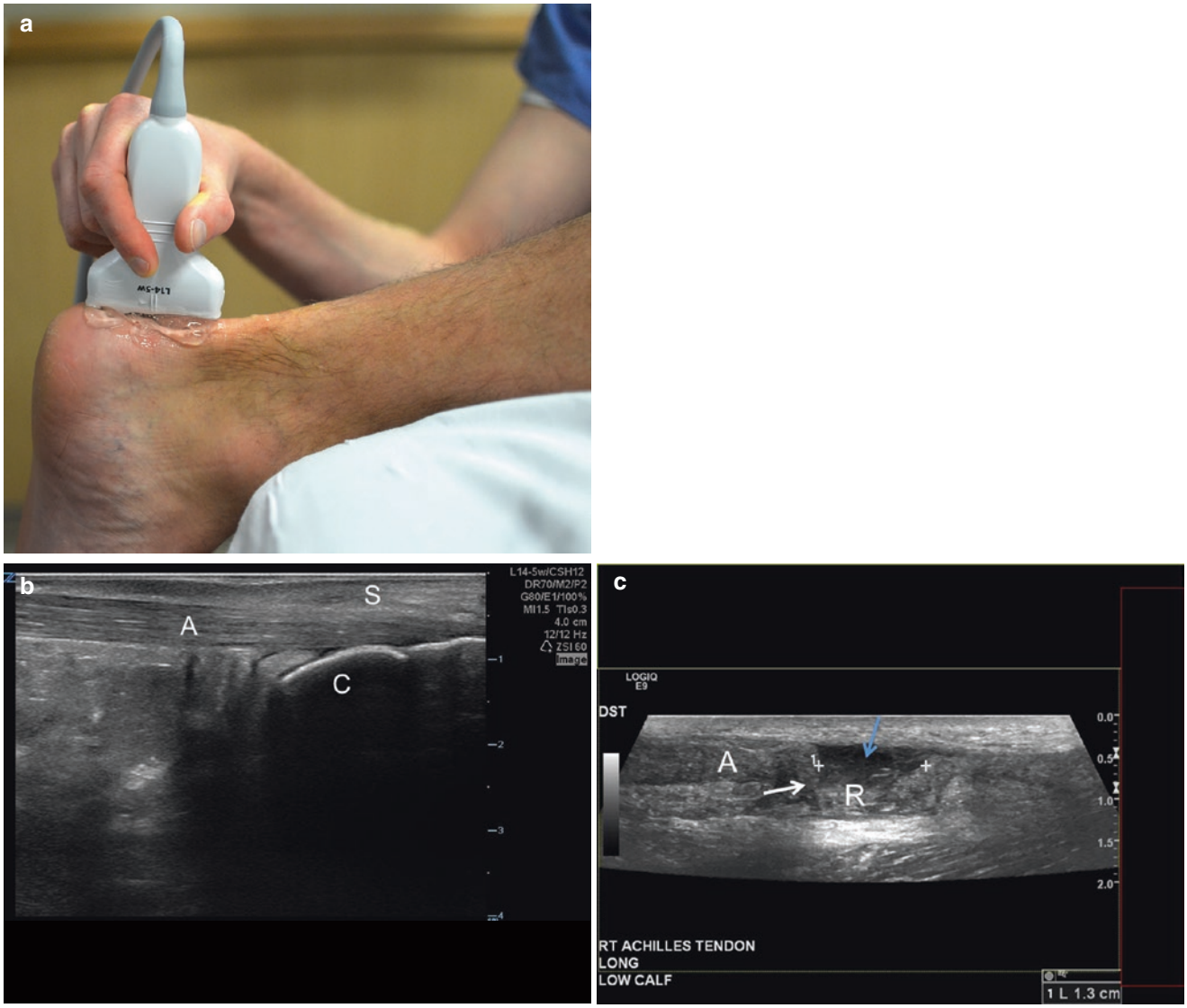

Fig. 6.1 (**a**) Sonographic images of the Achilles tendon can easily be obtained by using a linear transducer in the longitudinal and transverse planes. Place the patient in the prone position with the ankle in slight dorsiflexion. With the probe marker towards the patient's head, scan in the longitudinal plane from the Achilles tendon insertion at the calcaneus proximally until the tendon blends with the gastrocnemius muscle. The tendon should have uniform thickness and echogenicity without disruption or hypoechoic areas, which may indicate edema or blood. (**b**) In this longitudinal view, a normal Achilles tendon (A) is demonstrated just below the skin layer (S) by heterogenic fibers with uniform thickness at its insertion into the calcaneus (C). A hypoechoic or an anechoic area at the calcaneal insertion with disruption of the Achilles tendon fibers may demonstrate a partial tendon tear, or, if the Achilles tendon fibers show no disruption, a bursitis. (**c**) Longitudinal view of a full Achilles tendon rupture demonstrated by the area of heterogenicity (R). A disruption of the Achilles tendon (A) can be seen, as the tendon fibers are blunted and retracted (*white arrow*). A large hypoechoic area (*blue arrow*) indicates an effusion, which resulted from the injury. Passive plantar flexion of the ankle will highlight the defect, as the tendon fibers will fail to maintain uniform thickness with movement. The tendon most commonly ruptures a few centimeters proximal to the calcaneus insertion site

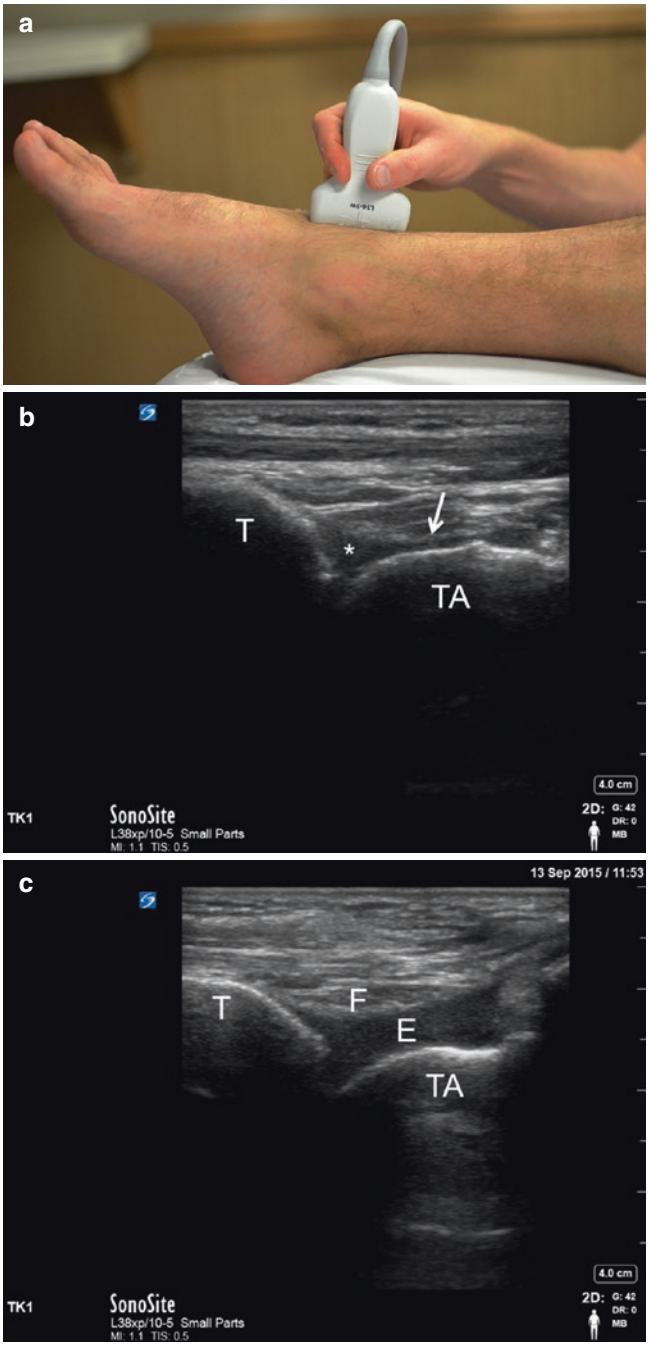

Fig. 6.2 (**a**) Ultrasound is highly sensitive for diagnosing ankle joint effusions, which are predominately visualized in the anterior recess. A linear probe should be used and placed longitudinally with the probe marker pointed cranially over the distal end of the tibia's articulation with the talar dome, while the patient's foot is in slight plantar flexion. (**b**) The talar dome (TA) articulates with the tibia (T) and is covered with hyaline cartilage (*arrow*), which should not be mistaken for an effusion. A normal amount of fluid can be seen within the joint space (*asterisk*); this should measure less than 1.8 mm in the anterior-posterior diameter. (**c**) More than 1.8 mm of anechoic fluid in the anterior-posterior diameter indicates joint effusion (E). Once the tibia (T) and talar dome (TA) are visualized, scanning medial and lateral will allow visualization of the entire joint space. Joint effusion in the anterior recess is also distinguished by displacement of the anterior fat pad (F), which becomes compressed by the anechoic fluid

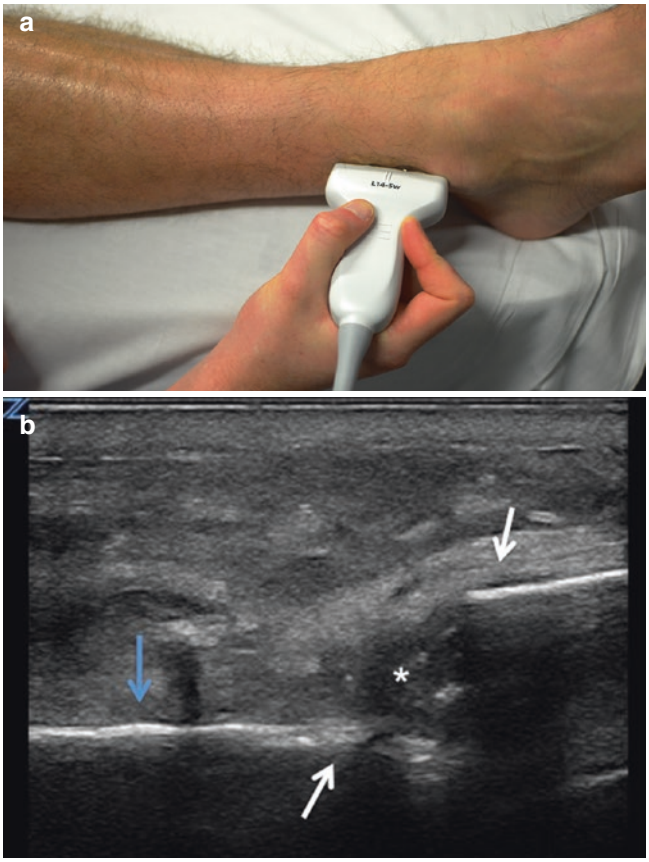

Fig. 6.3 (**a**) When looking for fractures, a linear array probe should be used in the standard fashion, with the probe marker towards the patient's head to obtain a longitudinal view. Scan proximal from the area of deformity distally while correlating physical exam findings with ultrasound images, noting any cortical step-offs or deformities of the normal, smooth echogenic cortex of the bone. (**b**) A longitudinal view of a lateral malleolus fracture denoted by an apparent step-off (*white arrows*) of the normal smooth, echogenic cortex (*blue arrow*). An isoechoic and hypoechoic traumatic hemorrhage adjacent to the cortical step-off (*asterisk*) can be an additional sign to identify an acute fracture

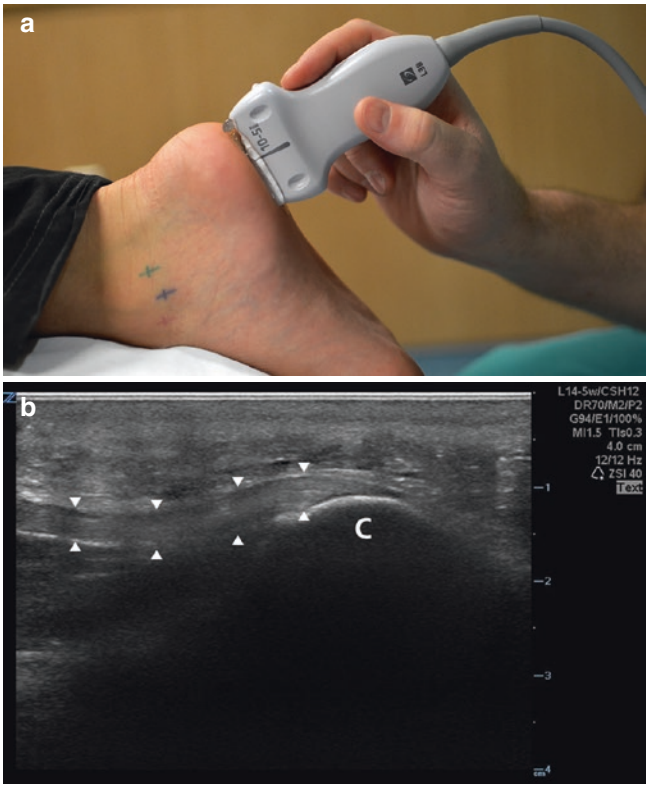

Fig. 6.4 (**a**) The plantar fascia is best imaged with the patient in a prone position and the foot hanging off the end of the exam Table. A linear-array transducer is placed over the heel and centered over the insertion site of the plantar fascia. (**b**) The plantar fascia (*between the arrowheads*) attaches proximally to the calcaneus (C). Thickening of the plantar fascia more than 4 mm at the insertion site and hypoechoic changes of the fibers are the most common findings in plantar fasciitis. Other findings can include perifascial fluid and the presence of calcifications or bony spurs

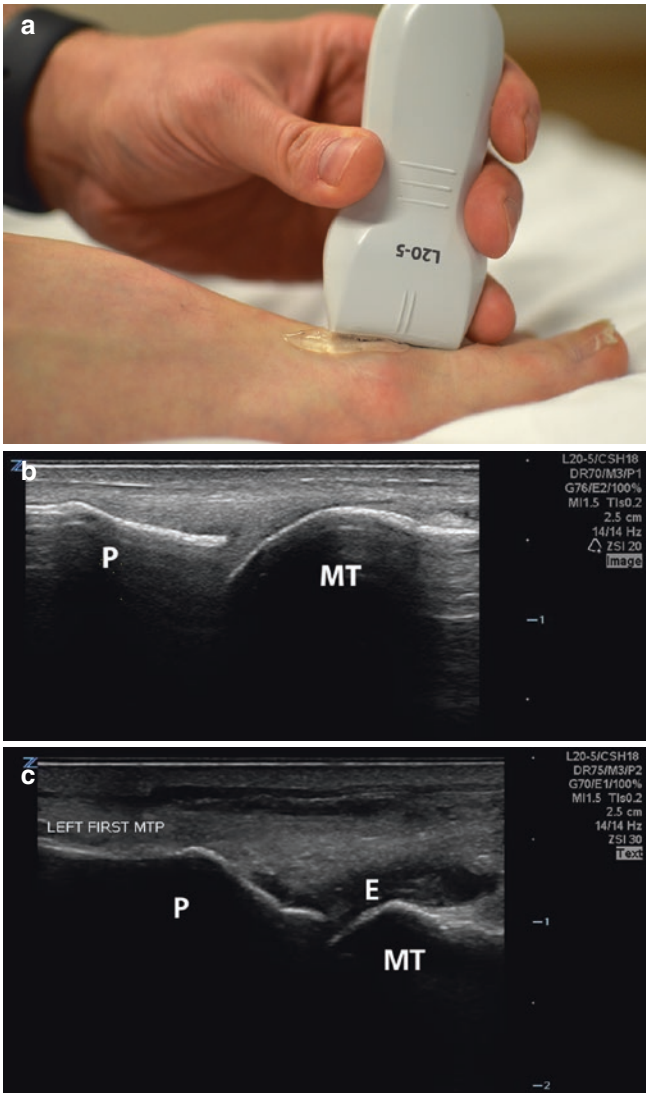

Fig. 6.5 (**a**) The first metatarsal joint is very superficial, and imaging requires a high-frequency linear-array transducer. The transducer is placed just over the joint line on the dorsum of the foot. (**b**) A normal metatarsophalangeal (MT-P) joint without effusion. (**c**) In this patient with gout, the joint capsule is distended due to an effusion (E) and slightly more echogenic, hypertrophic synovium. Other findings in gout can include a cloudy appearance of the fluid due to urate crystals, and linear crystal deposits along the cartilage surface of the joint

References

1. Hartgerink P, Fessell DP, Jacobson JA, van Holsbeeck MT. Full- versus partial-thickness Achilles tendon tears: sonographic accuracy and characterization in 26 cases with surgical correlation. Radiology. 2001;220:406–12.
2. Jacobson J, Andersen R, Jaovisidha S, De Maeseneer M, Foldes K, Trudell DR, et al. Detection of ankle effusions: comparison study in cadavers using radiography, sonography, and MR imaging. AJR Am J Roentgenol. 1998;170:1231–8.
3. Ekinci S, Polat O, Günalp M, Demirkan A, Koca A. The accuracy of ultrasound evaluation in foot and ankle trauma. Am J Emerg Med. 2013;31:1551–5.
4. Wang CL, Shieh JY, Wang TG, Hsieh FL. Sonographic detection of occult fractures in the foot and ankle. J Clin Ultrasound. 1999;27:421–5.
5. Cardinal E, Chhem RK, Beauregard CG, Aubin B, Pelletier M. Plantar fasciitis: sonographic evaluation. Radiology. 1996;201:257–9.
6. Radwan A, Wyland M, Applequist L, Bolowsky E, Klingensmith H, Virag I. Ultrasonography, an effective tool in diagnosing plantar fasciitis: a systematic review of diagnostic trials. Int J Sports Phys Ther. 2016;11:663–71.
7. Nazarian L, Rawool N, Martin C, Schweitzer ME. Synovial fluid in the hindfoot and ankle: detection of amount and distribution with US. Radiology. 1995;197:275–8.

Hand

7

Matthew Egan and David Spinner

The hand joint, though complex, has a variety of different identifiable pathologies that can be visualized by point-of-care ultrasound. In patients with blunt or penetrating trauma to the hand, it is important to evaluate for tendon laceration, as a complete laceration often requires a hand surgeon for further repair. Point-of-care ultrasound is able to evaluate both the extensor and flexor tendons of the hand to ensure their integrity. To that end, evaluation of these tendons can also provide diagnoses for nontraumatic pathologies such as "trigger finger" and can guide injection therapies for this pathology. While evaluating the same area, evaluation may be done for flexor tenosynovitis, joint effusions, phalangeal fractures, and tendonitis. Additionally, ultrasound can visualize a tear of the ulnar collateral ligament resulting in the condition called "gamekeepers thumb." Ultrasound has been found to be effective in reliably diagnosing both ulnar collateral ligament tears and associated Stener lesions, depending upon operator competency [1, 2]. Additionally, ultrasound can allow for evaluation of occult tears of the ulnar collateral ligament otherwise missed on radiography via dynamic abduction stress testing of the thumb [3]. Differentiating these diagnoses can have a huge impact on the patient's ultimate disposition and treatment plan, given the varied acuity of the possible diagnoses (Figs. 7.1, 7.2, 7.3, 7.4, 7.5, and 7.6).

M. Egan, M.D. (✉)
Department of Emergency Medicine,
Icahn School of Medicine at Mount Sinai, New York, NY, USA
e-mail: matthew.egan@mountsinai.org

D. Spinner, D.O.
Department of Rehabilitation Medicine,
Mount Sinai Hospital, New York, NY, USA

B. P. Nelson et al. (eds.), *Atlas of Handheld Ultrasound*, https://doi.org/10.1007/978-3-319-73855-0_7

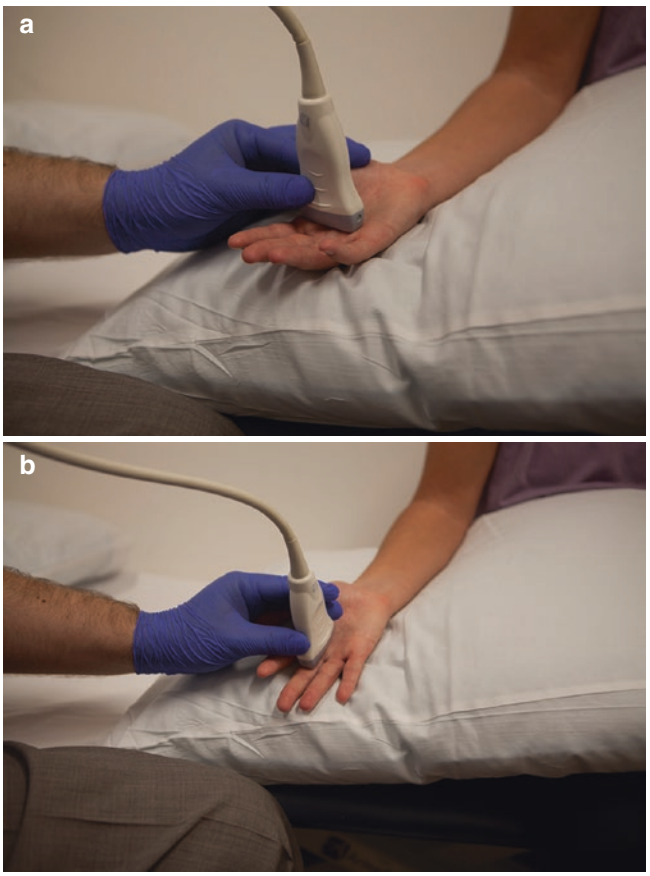

Fig. 7.1 When evaluating the hand, a linear probe should be used. (**a**) Sagittal views should be obtained with the probe marker towards the patient's wrist. (**b**) Transverse views should also be obtained. The probe is located on the palmar aspect of the hand at the metacarpophalangeal (MCP) joint. Views should be obtained in the same fashion for the first through fifth digits

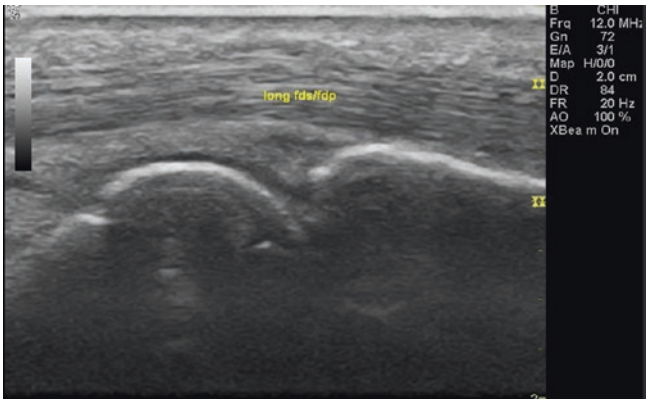

Fig. 7.3 This long-axis view demonstrates the fds superiorly and the fdp inferiorly

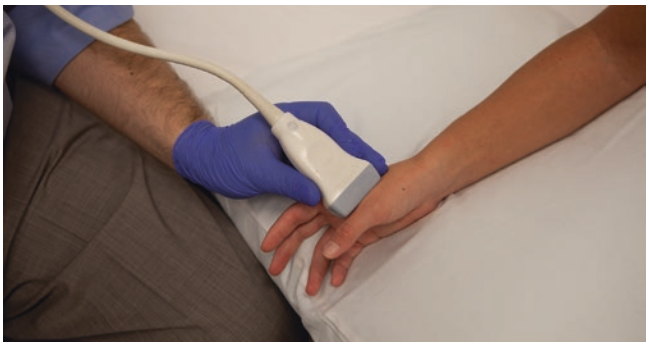

Fig. 7.4 Using the linear probe in the longitudinal axis with the probe marker pointing away from the patient's wrist, the ulnar collateral ligament (UCL) is evaluated. The probe is placed on the ulnar aspect of the thumb, with the proximal aspect of the probe over the MCP joint

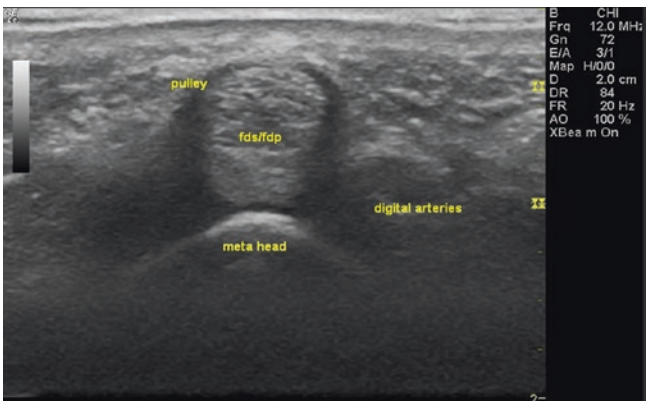

Fig. 7.2 This transverse view demonstrates the flexor digitorum superficialis (fds) tendon superiorly and the flexor digitorum profundus (fdp) tendon inferiorly, with the annular pulley surrounding and superior to the metacarpal head (meta head). Also demonstrated are the digital arteries

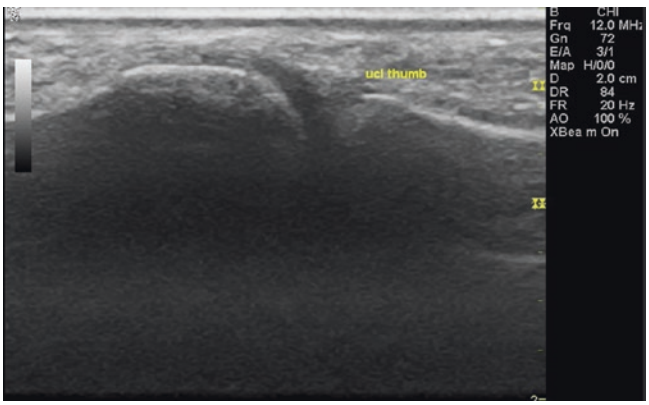

Fig. 7.5 This long-axis view demonstrates the UCL overlying the metacarpal head (meta head) and proximal phalanx (PPX)

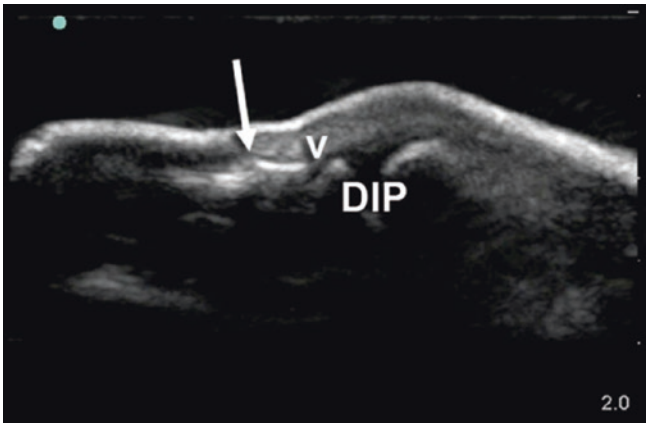

Fig. 7.6 This long-axis view demonstrates a fracture of the distal phalanx which was not evident on X-ray. Moving from image right (proximal) to image left (distal), bony cortex appears as a bright white horizontal line interrupted by the distal Interphalangeal (DIP) joint, growth plate (*down arrowhead*), and then the fracture (*arrow*)

References

1. O'Callaghan BI, Kohut G, Hoogewoud HM. Gamekeeper thumb: identification of the Stener lesion with US. Radiology. 1994;192:477–80.
2. American College of Radiology. ACR appropriateness criteria®. https://acsearch.acr.org/docs/69418/Narrative. Accessed 23 Oct 2017.
3. Koslowsky TC, Mader K, Gausepohl T, Heidemann J, Pennig D, Koebke J. Ultrasonographic stress test of the metacarpophalangeal joint of the thumb. Clin Orthop Relat Res. 2004;427:115–9.

Peripheral Nerves

8

Matthew Egan and David Spinner

The role of peripheral nerves in point-of-care ultrasound is mostly limited to their utility in providing quality regional anesthesia. Superior analgesia can be achieved in multiple painful pathologies by injecting local anesthetic around the nerve distribution producing pain. For instance, pain from a femur fracture can be well managed by injection of local anesthetic around the femoral nerve. A meta-analysis of patients with hip and femoral neck fractures found that, overall, regional anesthesia outperformed analgesia from opiates, acetaminophen, and non-steroidal anti-inflammatories [1]. When administering regional anesthesia, ultrasound guidance is used to track the injection needle and avoid surrounding vasculature as it advances toward the desired nerve. Similarly, regional anesthesia by ultrasound guided injection can be used to allow for otherwise painful, invasive procedures to be performed, such as fracture reduction or laceration repair.

Figs. 8.1, 8.2, 8.3, 8.4, 8.5, 8.6, 8.7, 8.8, 8.9, 8.10, 8.11, 8.12, and 8.13 and Videos 8.1, 8.2, and 8.3 focus on the nerves commonly used in regional anesthesia and the surrounding anatomy requiring identification as landmarks or as sites to avoid while performing the procedure.

Electronic Supplementary Material The online version of this chapter (https://doi.org/10.1007/978-3-319-73855-0_8) contains supplementary material, which is available to authorized users.

M. Egan, M.D. (✉)
Department of Emergency Medicine,
Icahn School of Medicine at Mount Sinai, New York, NY, USA
e-mail: matthew.egan@mountsinai.org

D. Spinner, D.O.
Department of Rehabilitation Medicine, Mount Sinai Hospital,
New York, NY, USA

B. P. Nelson et al. (eds.), *Atlas of Handheld Ultrasound*, https://doi.org/10.1007/978-3-319-73855-0_8

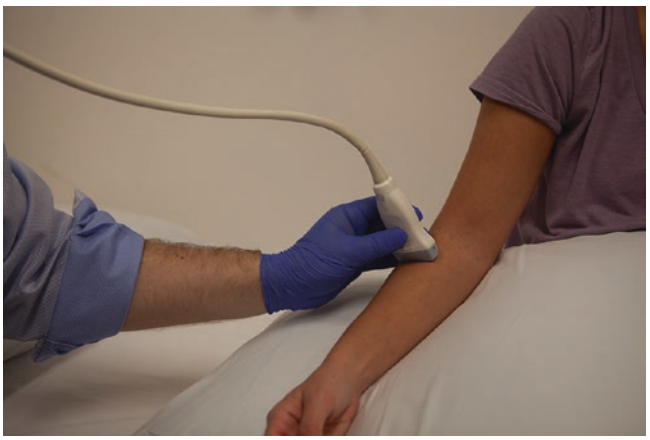

Fig. 8.1 A linear probe should be used. Transverse images should be obtained with the probe marker directed laterally toward the radius. The probe is placed distal to the elbow joint, slightly lateral to midline. Image courtesy of David Spinner

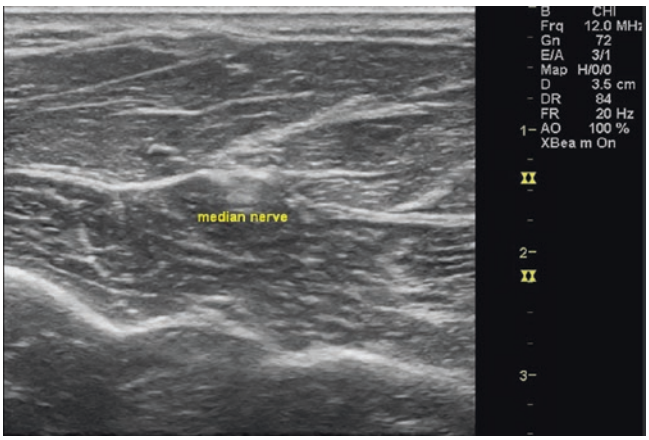

Fig. 8.4 This transverse view demonstrates the median nerve at the proximal forearm. Image courtesy of David Spinner

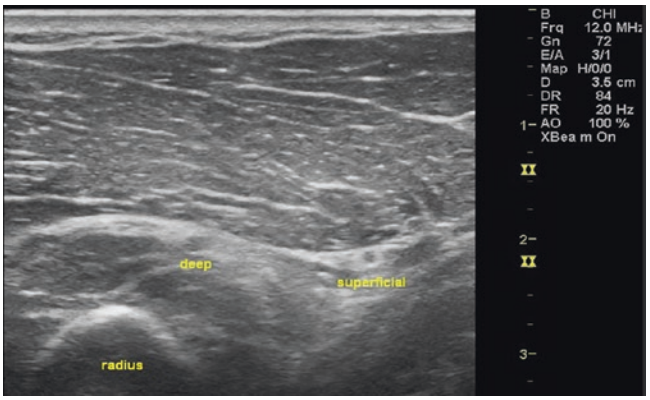

Fig. 8.2 This transverse view demonstrates the division of the deep and superficial radial nerves. Image courtesy of David Spinner

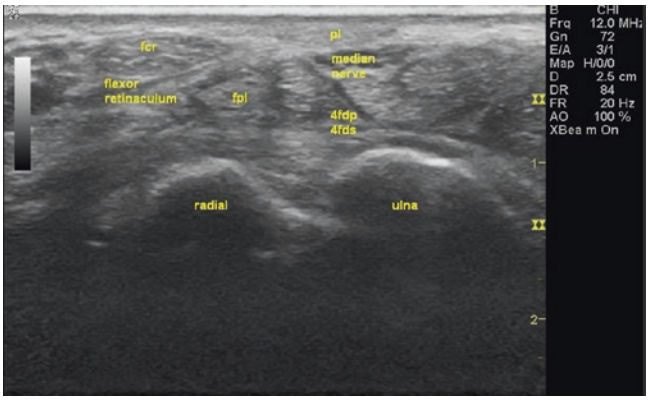

Fig. 8.5 This transverse view demonstrates the median nerve at the wrist. Pictured here are the flexor retinaculum, the flexor pollicis longus (FPL), the flexor digitorum profundus of the fourth metacarpal (4FDP), the flexor digitorum superficialis of the fourth metacarpal (4FDS), the flexor carpi radialis (FCR), the palmaris longus (PL), and the median nerve. Image courtesy of David Spinner

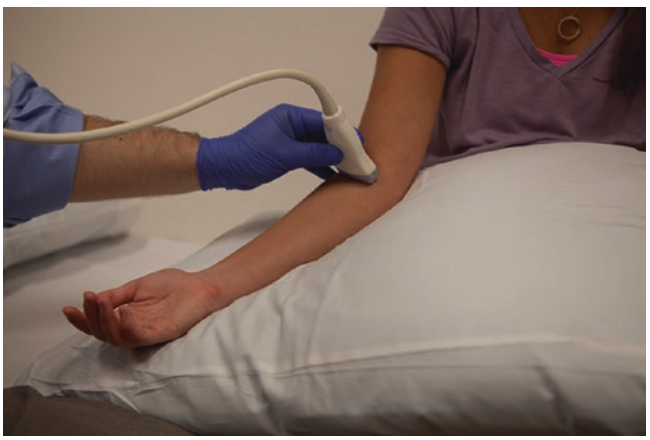

Fig. 8.3 Transverse images should be obtained with a linear probe to evaluate the median nerves as it traverses the forearm. The probe marker is facing laterally toward the radius with the probe placed at the midline of the forearm just distal to the elbow joint on the volar surface. The probe is then advanced distally down the midline of the forearm terminating at the wrist. Image courtesy of David Spinner

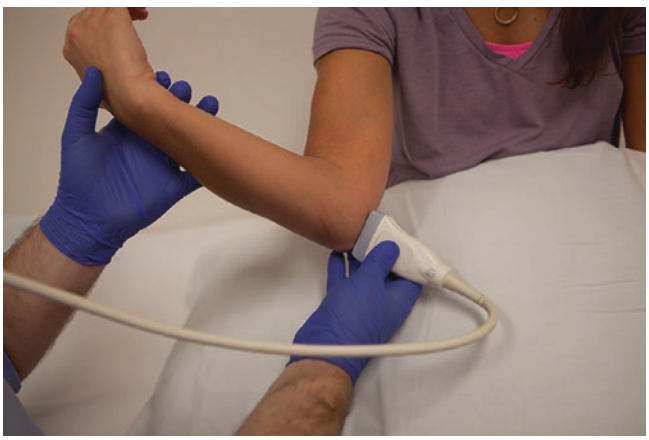

Fig. 8.6 Transverse views should be obtained with a linear probe to evaluate the ulnar nerve as it traverses the forearm. The probe marker is directed laterally toward the radius. The probe is placed on the medial aspect of the forearm beginning distal to the medial epicondyle on the volar surface. The probe is advance distally along the lateral aspect of the forearm on the volar surface following the ulnar nerve. Image courtesy of David Spinner

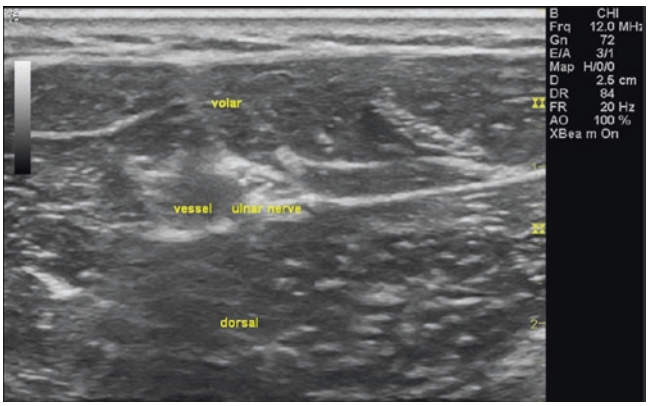

Fig. 8.7 This transverse view demonstrates the ulnar nerve at the proximal forearm. Image courtesy of David Spinner

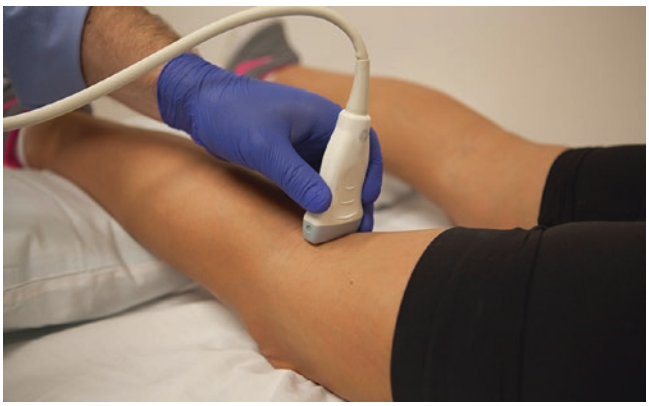

Fig. 8.10 With a linear probe, transverse views are used to visualize the tibial nerve. The probe marker faces medially and is placed just inferior to the popliteal fossa on the dorsum of the leg in the midline. Image courtesy of David Spinner

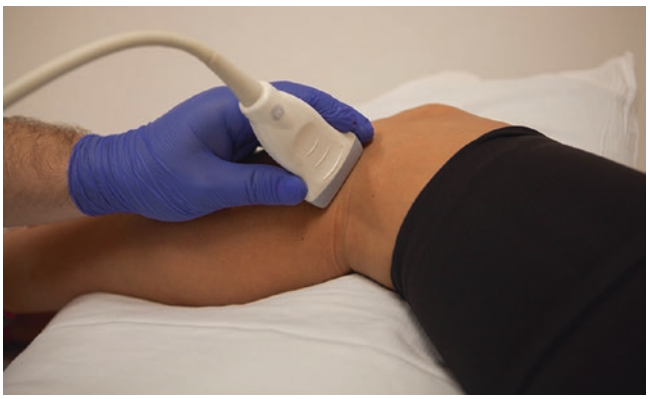

Fig. 8.8 Transverse views should be obtained with a linear probe to visualize the peroneal nerve as it wraps around the fibular head. The probe marker should face laterally and is positioned on the dorsal side of the leg and laterally over the fibular head. Image courtesy of David Spinner

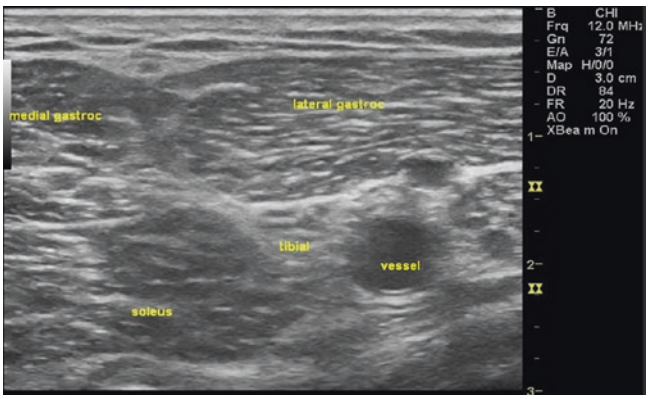

Fig. 8.11 This transverse view demonstrates the tibial nerve (tibial) located adjacent to the soleus, medial head of the gastrocnemius (medial gastroc), and lateral head of the gastrocnemius (lateral gastroc). Image courtesy of David Spinner

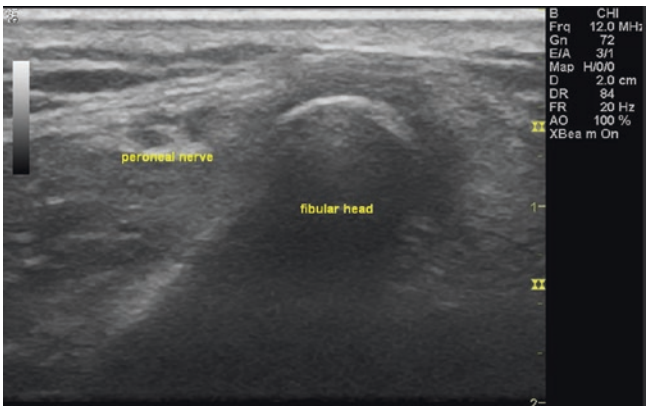

Fig. 8.9 This transverse view demonstrates the peroneal nerve and the fibular head. Image courtesy of David Spinner

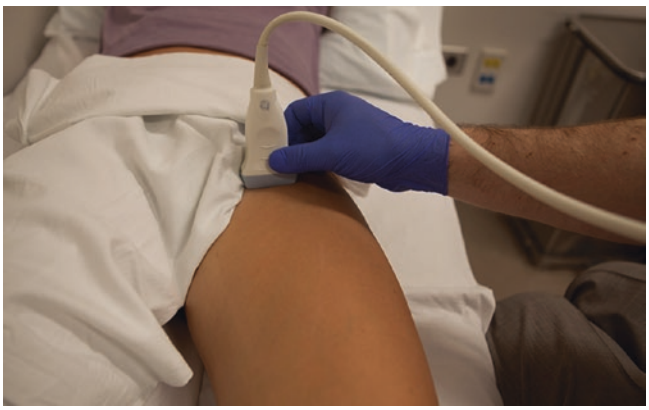

Fig. 8.12 With a linear probe, transverse views are used to visualize the femoral nerve. The probe marker faces medially. The probe is placed on the medial aspect of the anterior proximal thigh just distal to the inguinal crease. Image courtesy of David Spinner

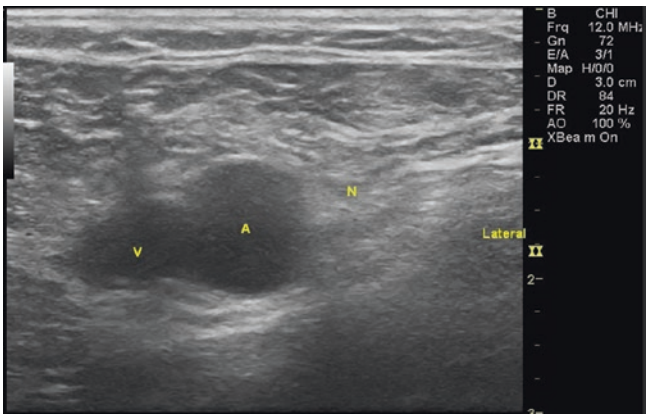

Fig. 8.13 This transverse view demonstrates the femoral nerve (N) located lateral to the femoral vein (V) and femoral artery (A). Image courtesy of David Spinner

Reference

1. Ritcey B, Pageau P, Woo MY, Perry JJ. Regional nerve blocks for hip and femoral neck fractures in the emergency department: a systematic review. CJEM. 2016;18(1):37–47.

Skull and Sinus

9

David M. Tierney, Terry K. Rosborough, and Catherine Erickson

9.1 Sinus

Traditional outpatient diagnosis of acute rhinosinusitis frequently results in overuse of antibiotics. Point-of-care ultrasound (POCUS) of the maxillary sinus is specific for clinically important fluid, but may miss subtle abnormalities that are rarely clinically important. The ethmoid and frontal sinuses are more challenging to image and are infrequently abnormal in isolation from the maxillary sinus. The absence of maxillary sinus fluid is a strong reason to avoid antibiotics in most patients, and helps reassure them. However, a patient with fever, severe symptoms suggestive of sinusitis, but no fluid with maxillary ultrasound, may need a computerized tomography (CT) scan to look for isolated ethmoid, frontal, or sphenoid sinusitis. A few clinical studies, and our clinic's experience, suggest that ultrasound can substantially reduce antibiotic use for sinusitis [1–3], although there are no large randomized trials to confirm this. Only 23% of patients suspected of sinusitis in our clinic had positive ultrasound [3]. The presence of fluid does not differentiate between viral and bacterial disease, so the final antibiotic decision requires integration of ultrasound with the rest of the patient findings.

The critical care patient who cannot be placed completely upright (ideal when possible) can be a greater diagnostic challenge, as fluid in a partially-filled sinus may be present but not visible when it layers dependently with a buffer of air between it and the probe. When visible, however, fluid in the maxillary sinus of a recumbent or semi-upright patient can be very helpful amongst febrile, intubated patients without a fever source, potentially avoiding CT scans, their associated cost, radiation, and risk of transportation [4, 5]. Figs. 9.1, 9.2, 9.3, 9.4, 9.5, 9.6 and 9.7.

D. M. Tierney, M.D. (✉) · T. K. Rosborough, M.D.
Department of Medical Education, Abbott Northwestern Hospital, Minneapolis, MN, USA
e-mail: david.tierney@allina.com

C. Erickson, M.D.
Department of Emergency Medicine, OHSU, Portland, OR, USA

B. P. Nelson et al. (eds.), *Atlas of Handheld Ultrasound*, https://doi.org/10.1007/978-3-319-73855-0_9

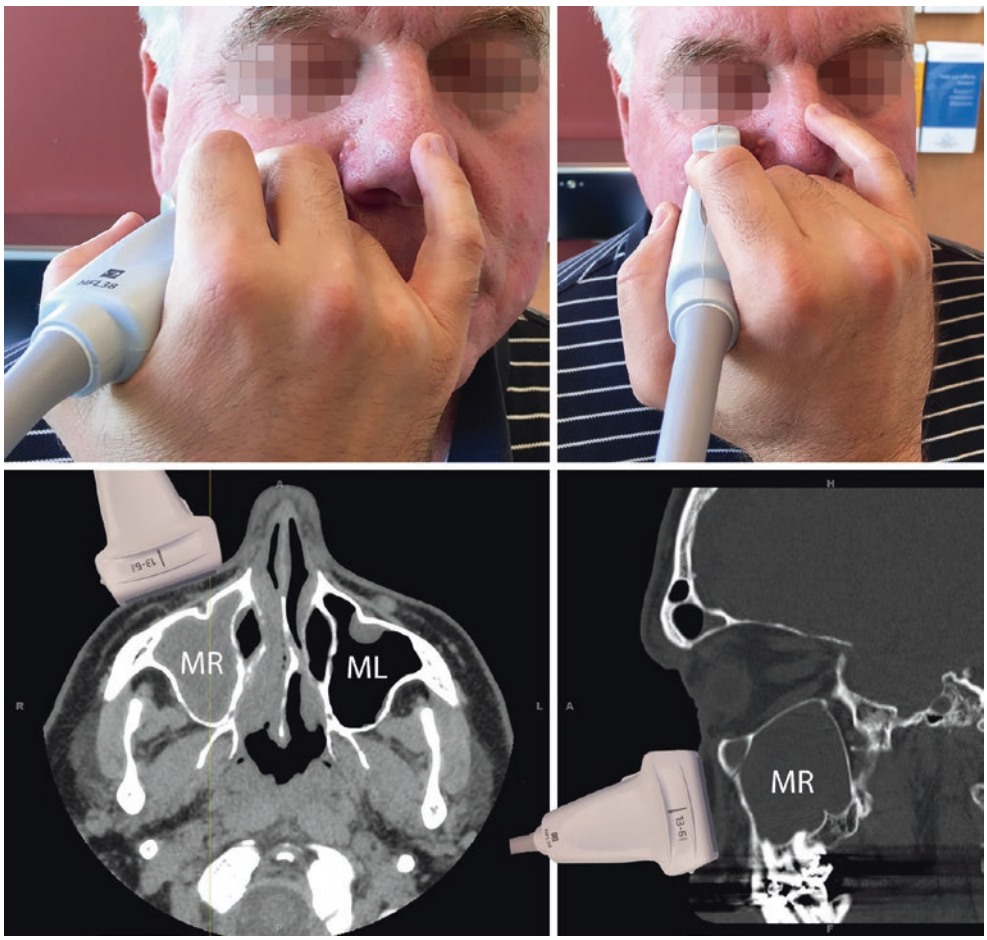

Fig. 9.1 Right maxillary transverse and parasagittal probe positions with CT correlates: a linear probe, musculoskeletal exam preset when available, is used with the indicator to the sitting patient's right for transverse imaging or cephalad for parasagittal imaging of the maxillary sinus. The depth setting is 6 cm. With the right hand, a top and bottom grip is used, anchoring the little finger on the patient's nose. Transverse view is begun at the bottom of the nose, rocking medially a modest amount (so the cord end of the probe moves toward the ear). The parasagittal view is just lateral to the nose, rocking the probe slightly cephalad (so the cord end of the probe moves toward the chest). Fluid always appears first at the caudal aspect of the sinus when the patient is sitting upright. *MR* maxillary sinus, right, *ML* maxillary sinus, left

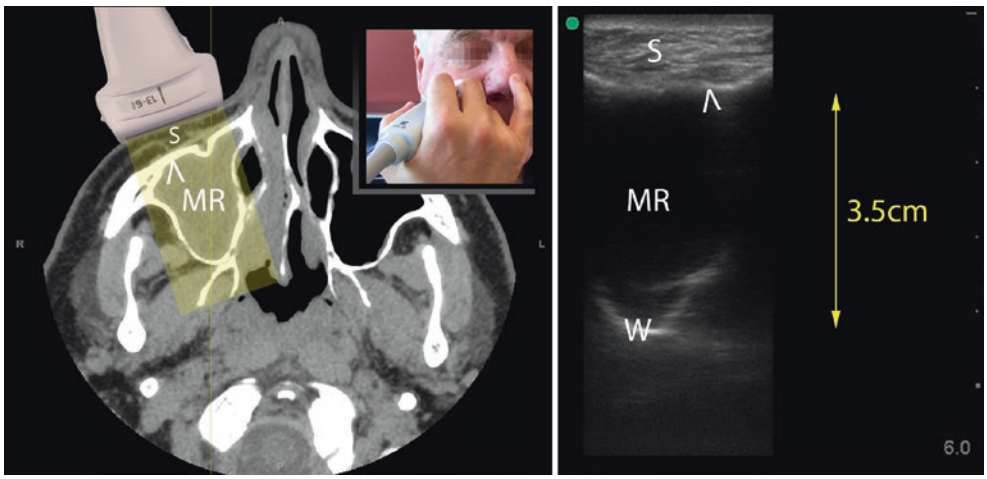

Fig. 9.2 Right maxillary sinus abnormal CT and transverse ultrasound: The right maxillary sinus (MR) is fully opacified. The "V" or "U" shaped back wall (W) is the distinctive appearance in the transverse view and is easily distinguished from reverberation artifact of the anterior sinus wall seen in a normal air-filled sinus. The back wall (W) is almost always at least 2.75 cm from the front wall in adults. ^ anterior maxillary sinus wall, *S* facial soft tissue

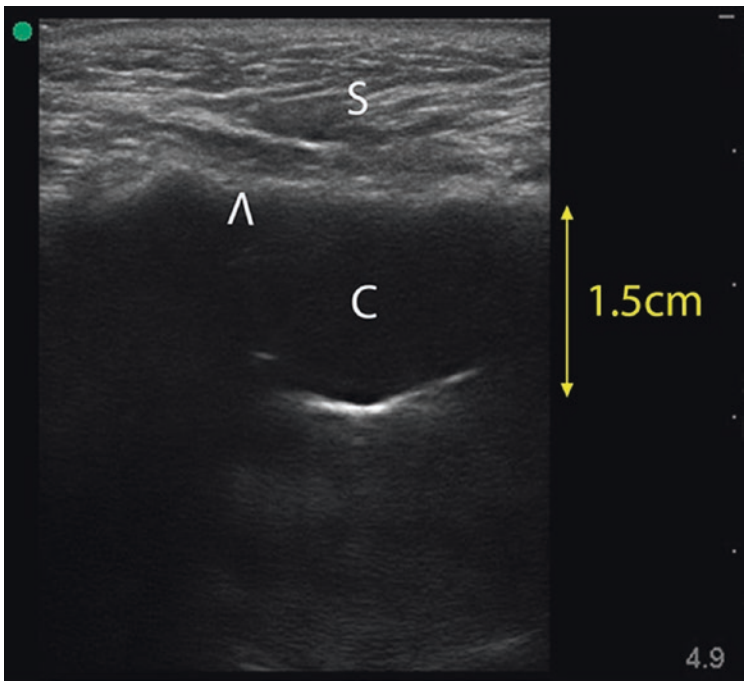

Fig. 9.3 Sinus retention cyst: Sinus retention cysts (C) occur and are distinguished from free fluid by being localized hyperechoic lines, and not usually having the typical V-shaped appearance or depth (only 1.5 cm from the front wall in this example) of the maxillary sinus back wall. They are differentiated from reverberation artifact seen in the air-filled sinus because their shape does not match that of the anterior sinus wall. ^ anterior maxillary sinus wall, *S* facial soft tissue

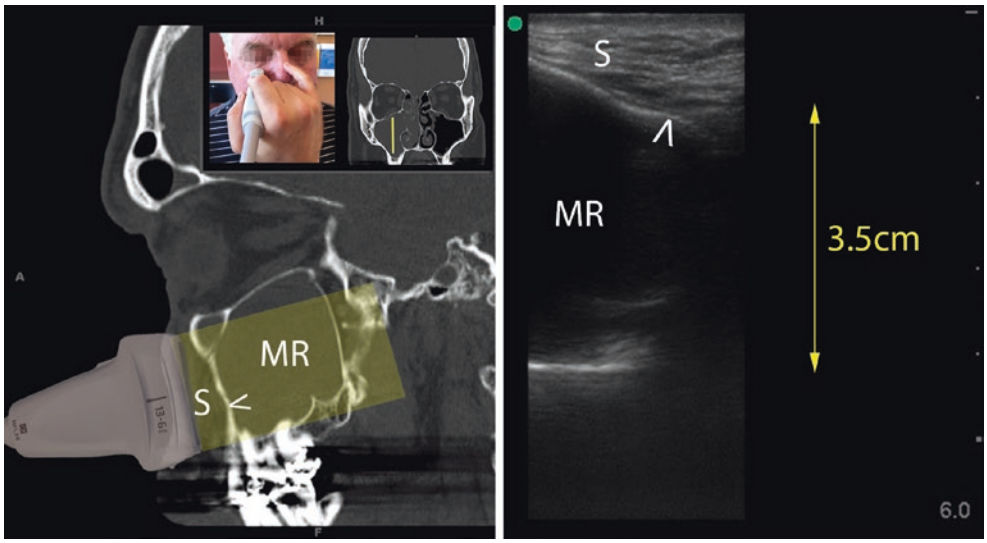

Fig. 9.4 Abnormal right maxillary sinus (MR) CT and parasagittal ultrasound: The back wall (W) in the parasagittal view is a horizontal line, and the length of this line corresponds with the height of the fluid level in the sinus. Note that the back wall (W) is not parallel to the anterior wall (^) of the sinus, helping differentiate it from reverberation artifact of the anterior sinus wall in a normal air-filled sinus. *S* facial soft tissue

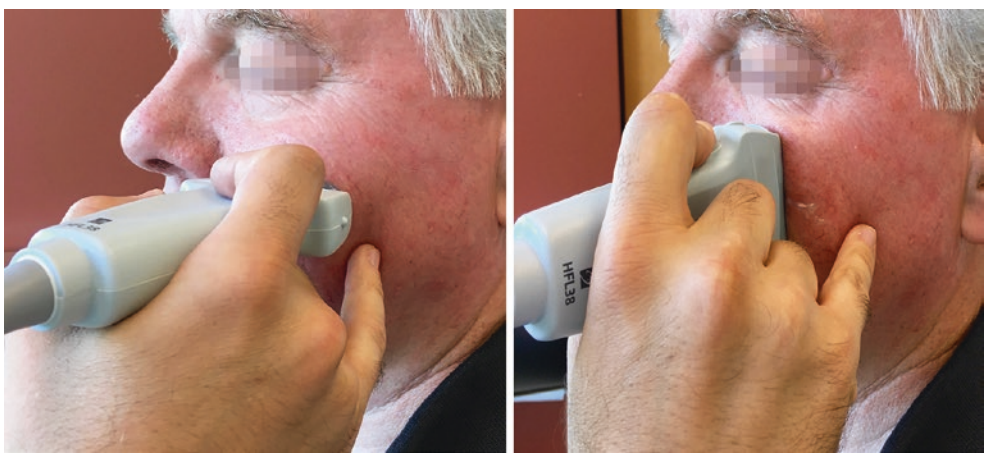

Fig. 9.5 Left maxillary sinus transverse and parasagittal probe positions: the right-hand grip on the probe changes to a medial/lateral grip with the little finger anchoring on the patient's cheek

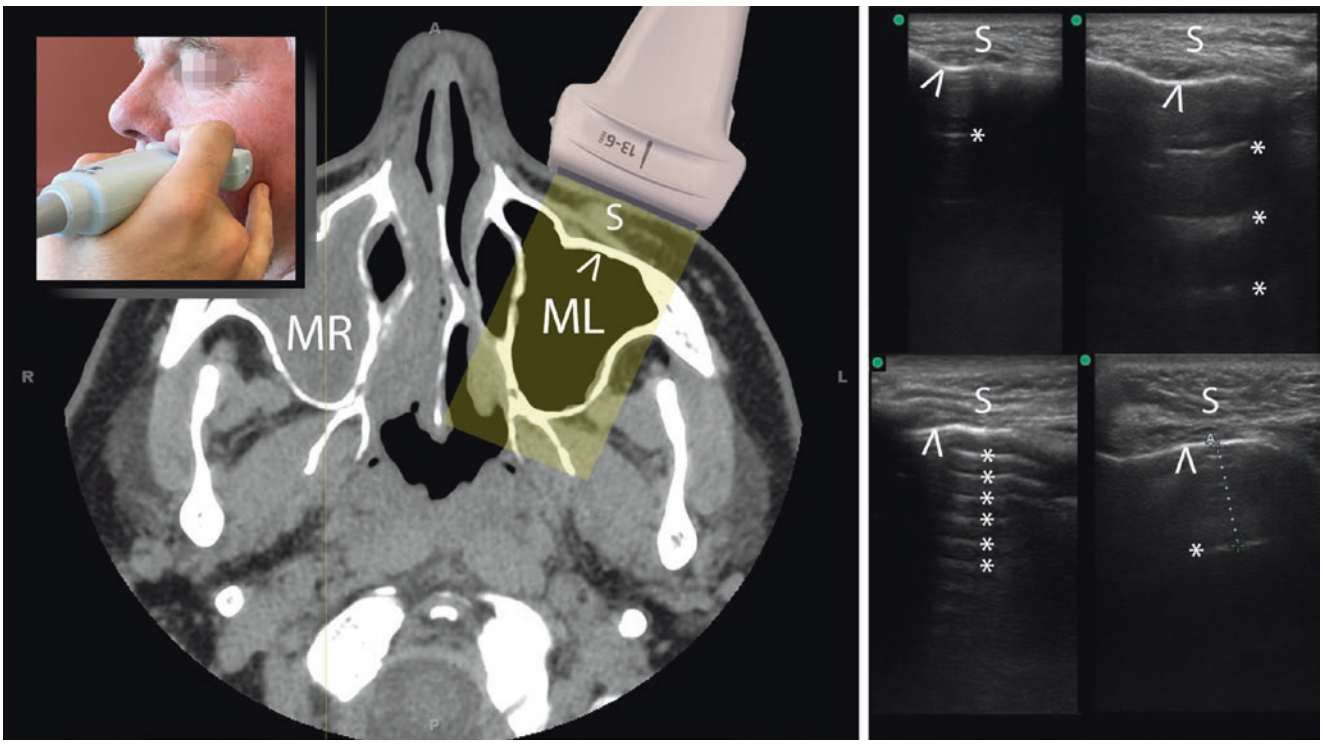

Fig. 9.6 Normal left maxillary sinus (ML) transverse ultrasound variation with CT reference: Only the anterior wall (^) resulting in partial acoustic shadowing with minimal reverberation artifact (*) may be seen (upper left ultrasound image), but reverberation artifact (similar to "A-lines" in normal lung) may be more prominent (upper right, lower left). A single visible reverberation artifact of the anterior sinus wall (lower right) may look like marked thickening of the mucosa or the posterior wall of the sinus; however, it is not deep enough (1.4 cm from front sinus wall) to be the posterior wall of the sinus and is parallel to the anterior wall. *S* facial soft tissue, *MR* maxillary sinus, right

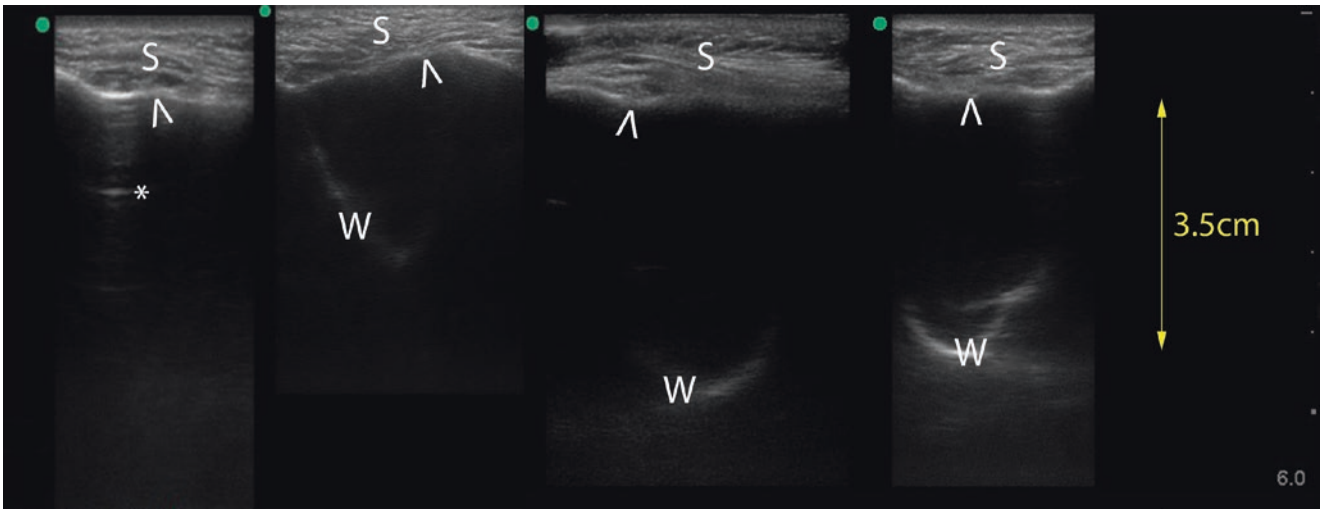

Fig. 9.7 Spectrum of transverse maxillary sinus ultrasound findings: Here is the spectrum of transverse maxillary sinus ultrasound findings with *normal*, air-filled sinus on the left and *strongly positive* fluid-filled sinus on the right. The middle two images are *weakly positive* results seen with smaller amounts of fluid. In these middle two images, the back wall (W) is fainter and only part of the wall may be visualized. This may lead to different treatment decisions than strongly positive results, depending on the rest of the clinical information. *S* facial soft tissue, ^ anterior maxillary sinus wall, *asterisk* reverberation artifact

9.1.1 Skull

Point-of-care ultrasound of the skull has largely been focused on diagnosing skull fractures indicating underlying traumatic brain injury (TBI), rather than other non-traumatic skull pathologic states. Brain injury in adults and children accounts for many visits to emergency departments and clinics annually. In pediatric patients, the presence of a skull fracture is of particular importance given its high association with TBI.

Currently, the standard for diagnosing skull fractures and evaluating for underlying pathology is CT imaging. Radiographs have proven to be of limited use in adults since the sensitivity is approximately five percent. Point-of-care ultrasound for skull fractures, as an indicator of clinically significant brain injury, has not yet been widely incorporated into clinical practice; however, studies suggest that this tool warrants further investigation. Skull ultrasound is thought of as more useful in pediatric than in adult patients. One widely used tool, the Pediatric Emergency Care Applied Research Network (PECARN) decision rule, helps guide whether to obtain CT brain imaging in children, and limit radiation exposure, while focusing CT imaging for clinically important TBIs. Given that ultrasound enables diagnosis of many types of fractures in children and young adults [6], many have looked at whether clinicians are able to use ultrasound for diagnosing skull fractures. Rabiner et al. found that point-of-care ultrasound in children and young adults less than 21 years old, with a median age of 6.4 years, was 88% sensitive and 97% specific in detecting skull fractures [7]. In the future, point-of-care ultrasound for skull fractures may be incorporated into important decision rules in order to decrease radiation exposure and increase the sensitivity of detecting TBI.

See Figs. 9.8 and 9.9 for additional details.

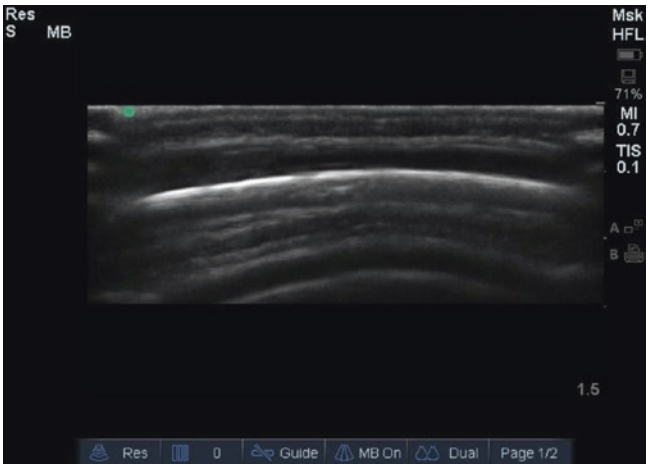

Fig. 9.8 Normal pediatric skull imaged with a linear transducer in a systematic fashion in both sagittal and transverse views. The probe indicator should be placed cephalad and the region of interest should be scanned. The probe should then be rotated 90° for the transverse views with the indicator pointing to the patient's right. Image courtesy of Stephanie Doniger

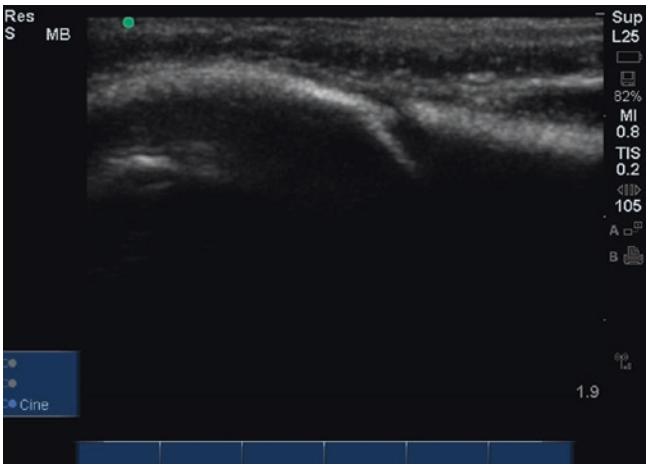

Fig. 9.9 The linear probe is placed over the region of interest, in this case a scalp hematoma, and scanned in two orientations to assess for skull fracture. As you can see, there is a skull fracture present. Image courtesy of Stephanie Doniger

References

1. Varonen H, Kunnamo I, Savolainen S, Mäkelä M, Revonta M, Ruotsalainen J, et al. Treatment of acute rhinosinusitis diagnosed by clinical criteria or ultrasound in primary care. A placebo-controlled randomized trial. Scand J Prim Health Care. 2003;21:121–6.
2. Varonen H, Savolainen S, Kunnamo I, Heikkinen R, Revonta M. Acute rhinosinusitis in primary care: a comparison of symptoms, signs, ultrasound, and radiography. Rhinology. 2003;41:37–43.
3. Rosborough TK. Verbal communication 8/6/2016.
4. Lichtenstein D, Biderman P, Meziere G, Gepner A. The "sinusogram", a real-time ultrasound sign of maxillary sinusitis. Intensive Care Med. 1998;24(10):1057–61.
5. Vargas F, Boyer A, Bui HN, Salmi LR, Gruson D, Hilbert G. A postural change test improves the prediction of a radiological maxillary sinusitis by ultrasonography in mechanically ventilated patients. Intensive Care Med. 2007;33(8):1474–8.
6. Weinberg ER, Tunik MG, Tsung JW. Accuracy of clinician-performed point-of-care ultrasound for the diagnosis of fractures in children and young adults. Injury. 2010;41(8):862.
7. Rabiner JE, Friedman LM, Khine H, Avner JR, Tsung JW. Accuracy of point-of-care ultrasound for diagnosis of skull fractures in children. Pediatrics. 2013;131:8,1757–64.

Eye

10

Jennifer V. Huang and Apichaya Monsomboon

Point-of-care ocular ultrasound can be used to rapidly identify potential vision-threatening ocular emergencies in the emergency department [1]. Because the globe is a fluid-filled structure, it provides a perfect medium for ultrasonography. Direct visualization of the anterior and posterior chambers of the globe, as well adjacent structures, are easily identified with ultrasonography, even when the eyelids are swollen shut. Ocular ultrasound is a safe, non-invasive and well-tolerated adjunct to the physical eye exam that can be performed quickly at the bedside. It is a valuable tool that can be used to evaluate various ocular emergencies including retinal detachment [2], vitreous hemorrhage, lens subluxation, globe rupture, intraocular foreign bodies [3], and elevated intracranial pressure [4].

See Figs. 10.1, 10.2, 10.3, 10.4, 10.5, 10.6, 10.7, 10.8, 10.9, 10.10, 10.11, 10.12, 10.13, and 10.14 and Videos 10.1, 10.2, 10.3, 10.4, 10.5, 10.6, 10.7, 10.8, and 10.9 for details.

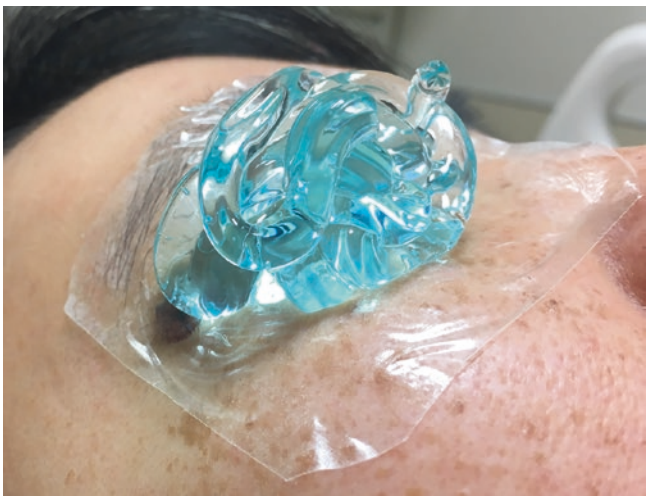

Fig. 10.1 Gel placement: place a Tegaderm (or other transparent film dressing) over a closed eye and place a large amount of ultrasound gel onto the eyelid so that when you place the probe onto the gel, pressure on the globe is minimized. The Tegaderm protects the eye from the gel and will not remove eyelashes or eyebrows when it is removed. Image courtesy of Jennifer Huang

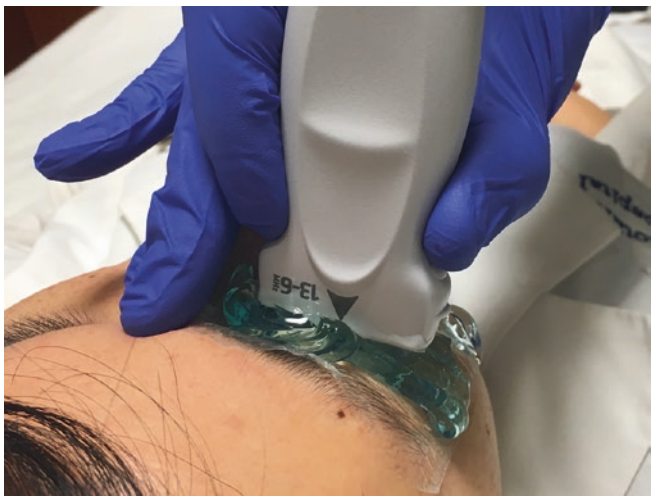

Fig. 10.2 Probe position: a high frequency (7.5–10 MHz or higher) linear probe should be used. Gently place the probe on the gel over the eyelid in a transverse position over the middle of the globe with the probe marker facing the patient's right. Stabilize your hand on the patient's forehead and take care not to place pressure directly on the globe

Electronic Supplementary Material The online version of this chapter (https://doi.org/10.1007/978-3-319-73855-0_10) contains supplementary material, which is available to authorized users.

J. V. Huang, D.O. (✉) · A. Monsomboon, M.D.
Department of Emergency Medicine, Icahn School of Medicine at Mount Sinai, New York, NY, USA

B. P. Nelson et al. (eds.), *Atlas of Handheld Ultrasound*, https://doi.org/10.1007/978-3-319-73855-0_10

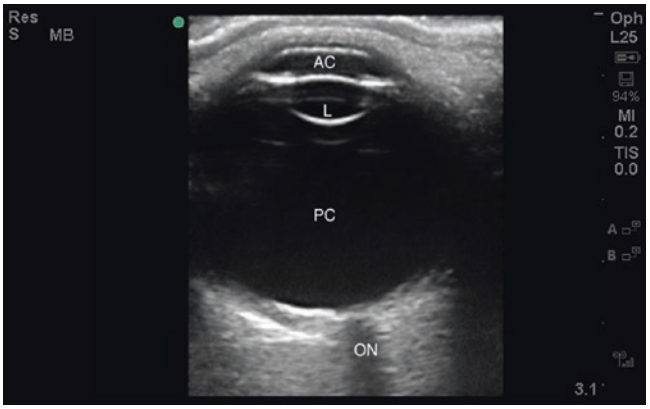

Fig. 10.3 Normal anatomy: a transverse view of the eye should demonstrate the anterior chamber (AC), lens (L), posterior chamber (PC), optic nerve (ON)

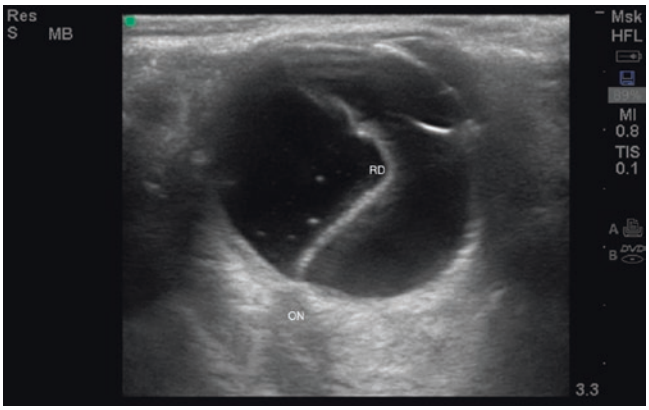

Fig. 10.6 Retinal detachment: this transverse view of the eye demonstrates another retinal detachment (RD). Note that the retina does not detach from the site of the optic nerve (ON). Retinal detachments are typically visible with normal gain settings. Image courtesy of Mikaela Baker

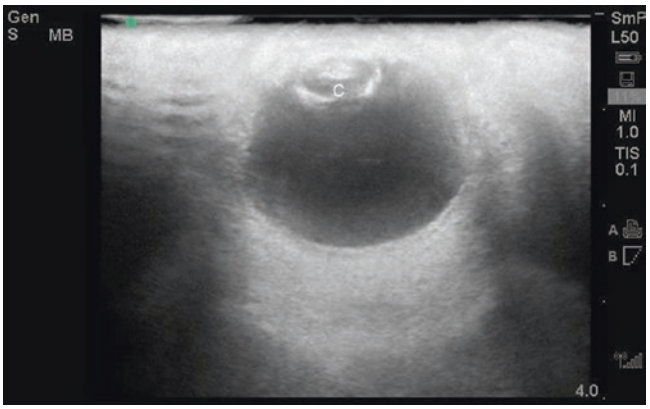

Fig. 10.4 Cataract: this transverse view of the eye demonstrates a cataract (C). Image courtesy of Mikaela Baker

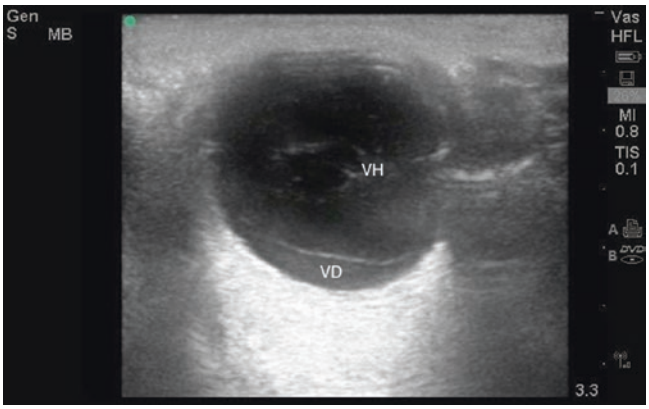

Fig. 10.7 Vitreous detachment and hemorrhage: This transverse view of the eye demonstrates echogenic material in the posterior chamber consistent with vitreous hemorrhage (VH) and a vitreous detachment (VD). To visualize the vitreous hemorrhage and detachments, the gain settings often need to be increased. Image courtesy of Mikaela Baker

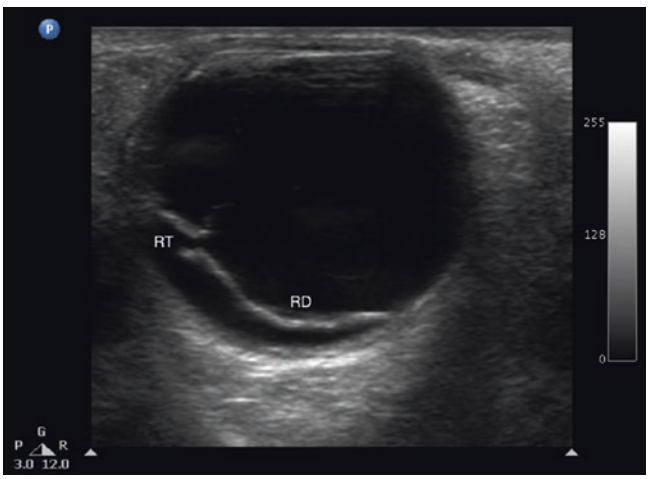

Fig. 10.5 Retinal detachment with a retinal tear: this transverse view of the eye demonstrates a retinal detachment (RD) with a retinal tear (RT)

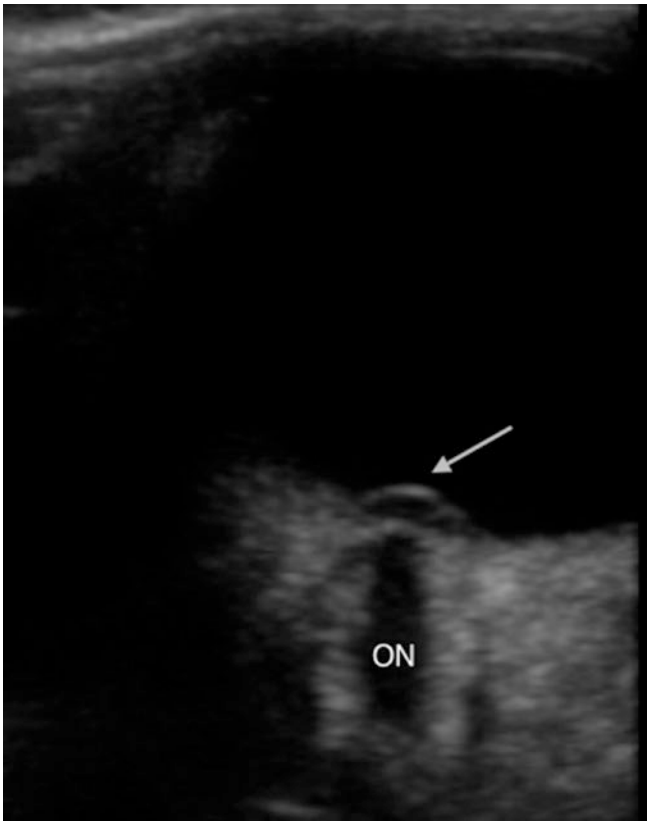

Fig. 10.8 Papilledema: this transverse view of the eye demonstrates papilledema (arrow) and hypo echoic fluid within the optic nerve sheath (ONS)

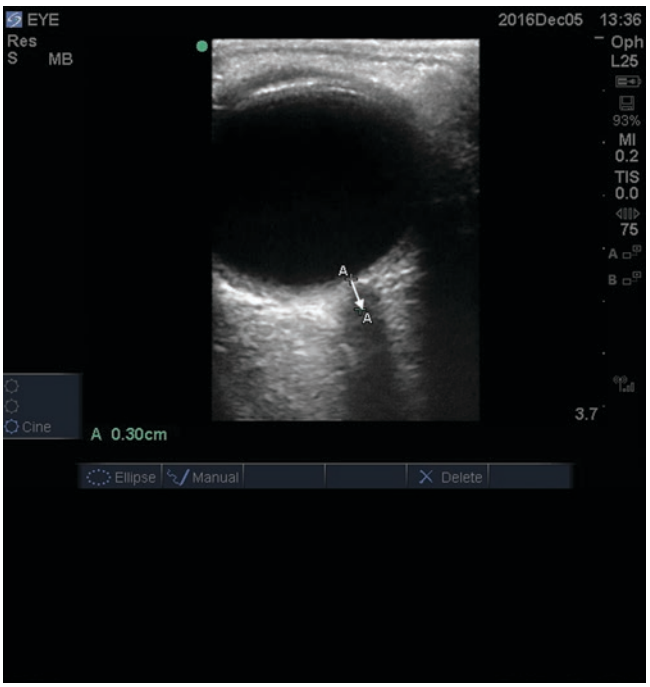

Fig. 10.9 ONSD normal: this transverse view of left eye demonstrates a normal optic nerve sheath diameter. The diameter of the optic nerve should be measured 3 mm posterior the retina (distance A marked, with an arrow)

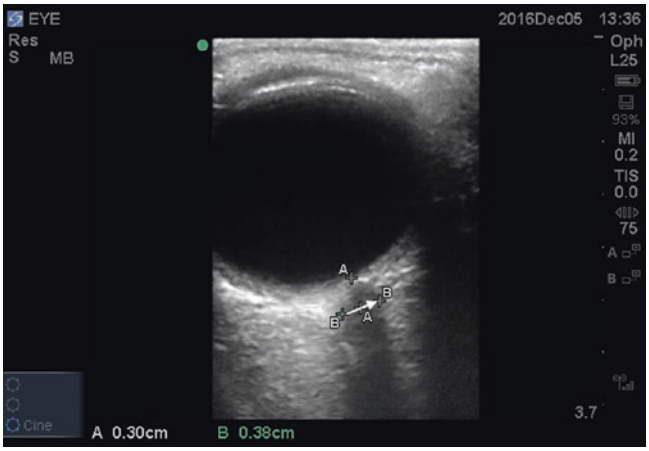

Fig. 10.10 ONSD normal: a normal optic nerve sheath diameter measures less than 5 mm in adults (distance B, marked with an arrow)

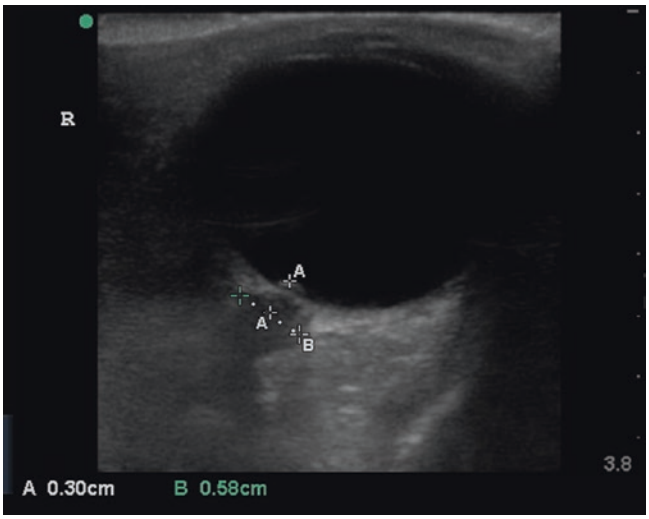

Fig. 10.11 ONSD enlarged: an optic nerve sheath diameter greater than 5 mm in adults indicates increased intracranial pressure

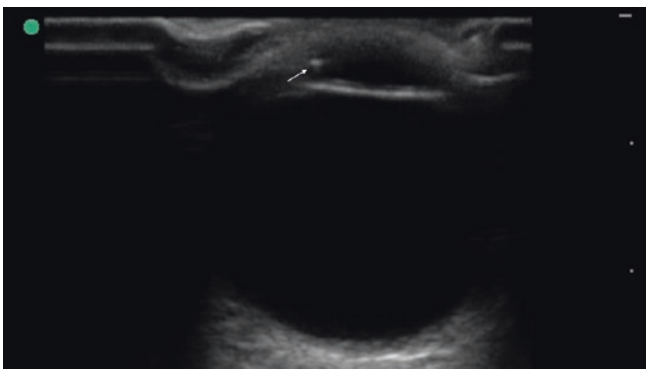

Fig. 10.12 Foreign body: this transverse view of the eye demonstrates a small metal foreign body (see arrow) on the surface of the cornea on the left side of the anterior chamber. Image courtesy of Errel Khordipour

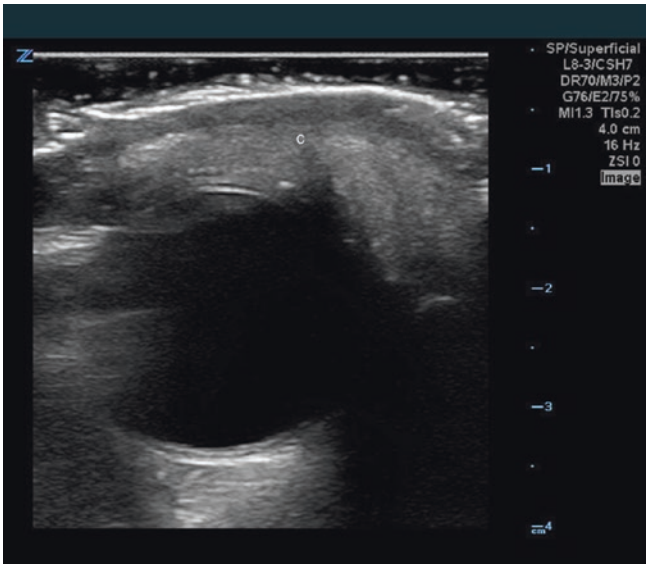

Fig. 10.13 Periorbital cellulitis: this transverse view of the eye demonstrates periorbital cellulitis (C). Note the soft tissue swelling of the eyelid anteriorly

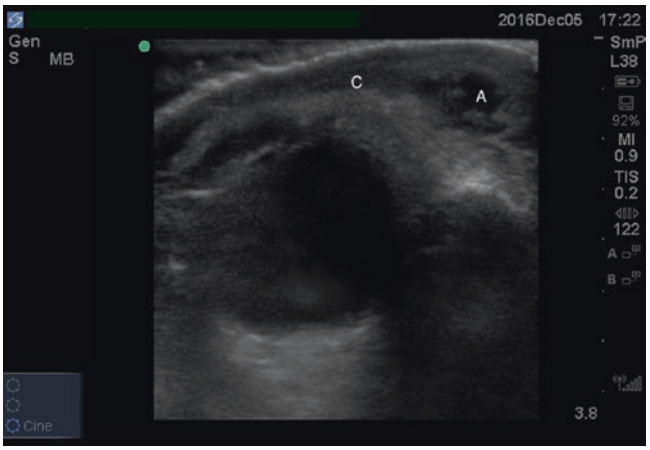

Fig. 10.14 Periorbital cellulitis and abscess: this transverse view of the eye demonstrates periorbital cellulitis (C) and an abscess (A)

References

1. Roque PJ, Hatch N, Barr L, Wu TS. Bedside ocular ultrasound. Crit Care Clin. 2014;30(2):227–41.
2. Blaivas M, Theodoro D, Sierzenski PR. A study of bedside ocular ultrasonography in the emergency department. Acad Emerg Med. 2002;9(8):791–9.
3. Vrablik ME, Snead GR, Minnigan HJ, Kirschner JM, Emmett TW, Seupaul RA. The diagnostic accuracy of bedside ocular ultrasonography for the diagnosis of retinal detachment: a systematic review and meta-analysis. Ann Emerg Med. 2015;65(2):199–203.e1.
4. Fielding JA. The assessment of ocular injury by ultrasound. Clin Radiol. 2004;59(4):301–12.

Neck

11

Benji K. Mathews and Oana Dickinson

Ultrasonography of the neck has been performed for decades, primarily by radiologists and interventional radiologists. Ongoing improvements in ultrasound technology, portability, and resolution have made bedside ultrasound much more accessible to clinicians. Handheld devices can now allow clinicians to perform and record real-time diagnostic evaluations tremendously speeding the diagnostic process. This ability makes POCUS an important aid in addition to the physical examination, enabling clinicians to rapidly diagnose and treat their patients [1].

The neck constitutes a complex anatomic region that includes parts of the respiratory and digestive tracts, salivary glands, nervous, lymphatic, endocrine, and vascular structures. Numerous pathologic conditions can affect the neck's organ systems. Since the majority of these anatomical structures are easily accessible by ultrasound imaging, POCUS becomes an indispensable tool for the medical provider at a patient's bedside. Both the American Institute of Ultrasound (AIUM) and the American Academy of Otolaryngology have published guidelines on the use of neck ultrasound. The most commonly used neck ultrasound examinations include salivary glands, mass lesions, lymph nodes, infection/trauma and the endocrine exam [2].

11.1 Assessment of the Neck Using Handheld Ultrasound (Fig. 11.1)

11.1.1 Evaluation of Vascular Anatomy and Carotid Triangle

Inferior to the posterior belly of the digastric muscle is the carotid triangle. It is bounded anteriorly by the superior belly of the omohyoid muscle and posteriorly by the sternocleidomastoid muscle. Within the carotid triangle, immediately under the skin are the vascular structures of the carotid sheath: the carotid artery and the internal jugular vein (Video 11.1). In this region, color flow doppler may be used to help distinguish blood vessels from other structures. During the POCUS examination, it is important to scan these vascular structures in both the transverse (Fig. 11.2) and longitudinal planes (Video 11.2). The vessels are round, mostly hypoechoic when the transducer is in the transverse plane of the neck. When the transducer is in the longitudinal plane of the neck, the vessels appear as anechoic linear structures [1, 3].

Lateral and slightly more superficial to the carotid artery (Fig. 11.3) is the internal jugular vein (IJV). The IJV is usu-

Electronic Supplementary Material The online version of this chapter (https://doi.org/10.1007/978-3-319-73855-0_11) contains supplementary material, which is available to authorized users.

B. K. Mathews, M.D. (✉) · O. Dickinson, M.D.
Department of Medicine, University of Minnesota Medical School, Minneapolis, MN, USA

Department of Hospital Medicine, HealthPartners, St. Paul, MN, USA
e-mail: Benji.K.Mathews@HealthPartners.com

B. P. Nelson et al. (eds.), *Atlas of Handheld Ultrasound*, https://doi.org/10.1007/978-3-319-73855-0_11

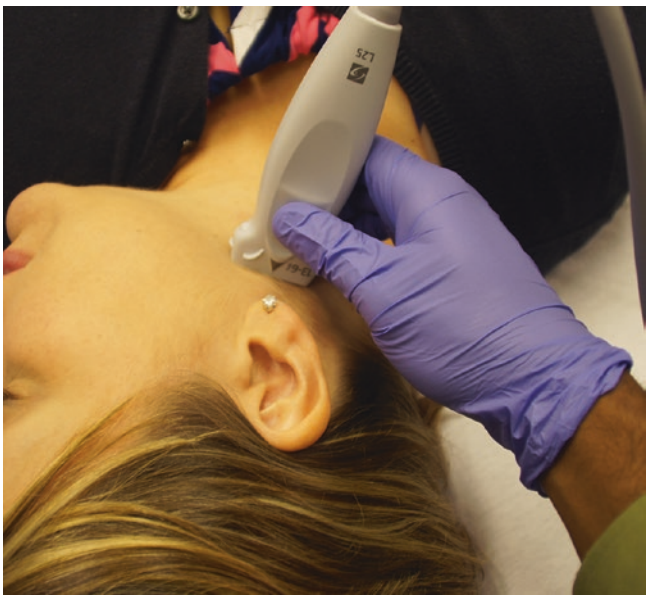

Fig. 11.1 POCUS of the neck should be performed with the patient in the supine position with neck in extension. The transducer is positioned in the transverse plane with the head rotated to the side opposite the area of evaluation. High-frequency linear array transducer with mean frequencies between 8 and 12 MHz is used. The probe marker will point to operator's left side. If standing at the head of the bed, the probe marker is pointing to the left shoulder of the patient and corresponds to the marker on the left side of the ultrasound screen. A systematic examination should be completed. The recommendation is to proceed in a general sequence starting with the upper neck, proceeding to the mid-neck (area near the thyroid gland), then the area of the posterior triangle along the supraclavicular region. Image courtesy of Benji Mathews, MD

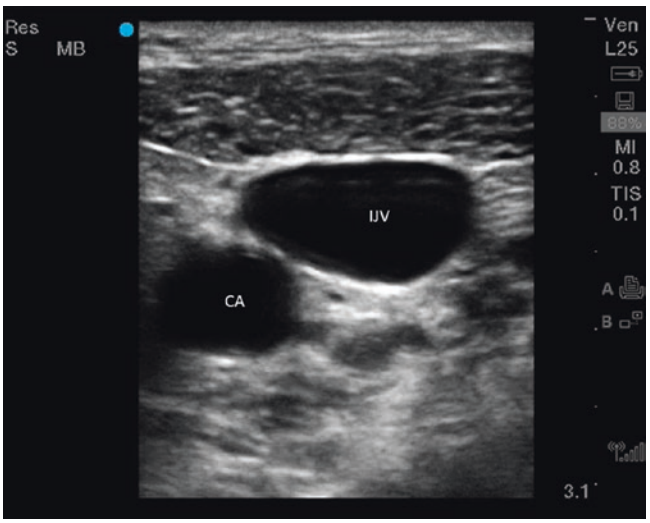

Fig. 11.2 Transverse (short axis) view along the right internal jugular vein (IJV) and carotid artery (CA). Internal jugular vein has notable respirophasic variation and is easily compressible. The internal jugular vein lies lateral to the carotid artery, below the sternocleidomastoid muscle, and is generally more ovoid than the carotid artery. Image courtesy of Benji Mathews, MD

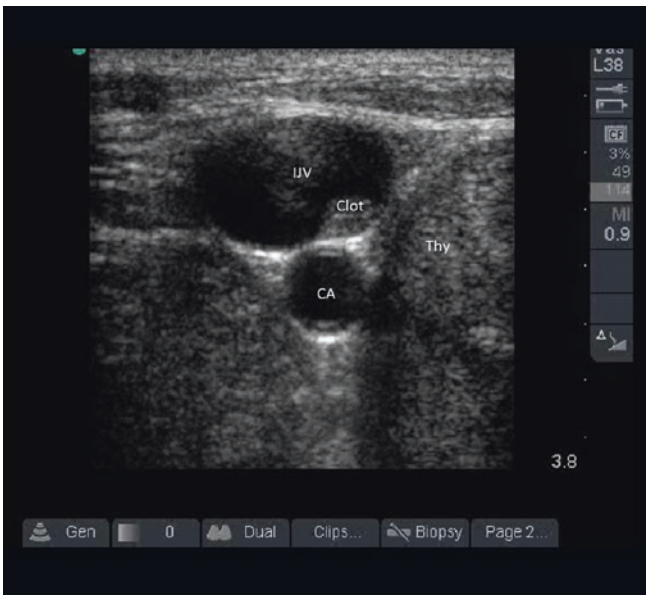

Fig. 11.3 Transverse view of the internal jugular vein (IJV), thrombus (clot), carotid artery (CA). The thyroid gland (thy) is also seen in this view. Image courtesy of Mangala Narasingham, DO

ally larger in size on the right side of the neck than on the left. The IJV is easily compressible with gentle pressure from the transducer when compared with the carotid artery, which is not easily compressible and pulsates with cardiac cycles. Moreover, during a Valsalva maneuver a moderate distension of the IJV can be noticed [1].

If the transducer is gradually advanced superior on the neck in the carotid triangle, anterior to the hypoechoic sternocleidomastoid muscle, the internal and external carotid arteries and their bifurcation can be seen. If the transducer is moved more caudally in the carotid triangle, the common carotid artery and its junction with the subclavian artery can be seen [1, 3].

Many studies have used the ultrasound to evaluate the anatomic variations between the IJV and common carotid artery (CCA) [3–6]. Troianos et al. found >75% overlap of the IJV and CCA among 54% of all patients whose heads were rotated to the contralateral side. Additionally, two thirds of older patients (age > 60 years) had >75% overlap of the IJV and CCA [3].

In the past, continuous wave doppler ultrasound was used extensively for guidance for IJV cannulation. This technique is now discouraged because it was not shown to benefit over the 2-dimensional (B-mode) ultrasound imaging [7]. Adjunctive use of color doppler may help distinguish venous from arterial anatomy, as well as vessel patency.

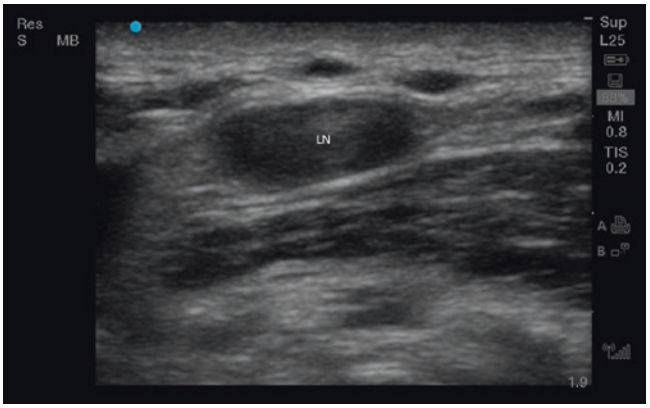

Fig. 11.4 Transverse view of a lymph node. Pathologic lymph nodes are often asymmetric, heterogeneous in echotexture and markedly hypoechoic. In the presence of know malignancy, a lymph node without a normal sonographic appearance should be considered suspicious for metastatic spread. Cystic degeneration of all or part of the node, large dimensions, a rounded appearance with nearly equal transverse, anteroposterior, and longitudinal measurements, micro calcifications, irregular margins, cortical thickening, peripheral and/or transnodal vascularity on power Doppler imaging can be features concerning for malignancy [8]. Image courtesy of Benji Mathews, MD

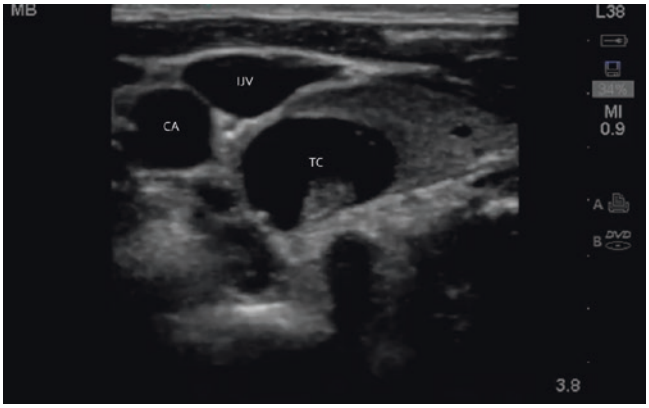

Fig. 11.5 Common mimic of vasculature in the neck. Thyroid cyst is seen in this image. Image courtesy of Mangala Narasingham, DO

11.1.2 Evaluation of Lymph Nodes

The cervical lymph nodes can be easily evaluated by POCUS. Each node has a fibrous capsule and is divided into a medulla and a cortex. Each node has a hilum with both the artery and the vein. If a lymph node is palpable on neck exam, the clinician can follow this up with a POCUS examination (Video 11.3). General POCUS evaluation for lymph nodes in the neck includes assessment of size, shape, boundaries, vascularity, echogenicity and cortical thickness (Fig. 11.4) [2, 9, 10].

Usually, a minimum of six lymph nodes are identified in the cervical chain. Most lymph nodes are between 0.3 and 0.8 cm with the submandibular lymph node often being larger [10]. Normal lymph nodes are generally oval or kidney bean-shaped, hypoechoic, with an echogenic hilum. In the hilum are afferent and efferent lymphatics as well as arterial and venous vessels that can often be seen on color flow Doppler (Video 11.4). The size criteria for consideration as a pathologic lymph node is controversial. 1.0 cm is often used as the upper limit of normal for an ordinary-appearing lymph node (exception being the jugulodigastric node, which may have a normal upper limit of 1.5 cm) [1].

If on physical exam a neck mass is identified, a subsequent POCUS evaluation is recommended. This thorough evaluation will allow the clinician to identify other nodes that may not be palpable and to access cytology with ultrasound-guided fine-needle aspiration (FNA).

AIUM describes the following indications for POCUS examination of enlarged cervical lymph nodes:

- Determination of inflammation from metastatic malignant lymph nodes.
- Determination of a lymph node from another mass lesion such as a cyst (Fig. 11.5), schwannoma, paraganglioma, lipoma, or parathyroid adenoma.
- Determination of possible lymphomatous nodes.
- Determination of the presence of metastatic lymphadenopathy at specific levels to determine the required type of neck dissection.
- Determination of the specific level of metastatic squamous cell carcinoma within lymph nodes to assist in defining the primary source.
- FNA for cytology.
- Core sampling for lymphoma [2].

11.1.3 Evaluation of Neck Infections

POCUS can be an important tool for the initial identification and sequential treatment determination of various infectious. POCUS is relevant in locating abscess formation and identifying the confluent adenopathy.

In patients with infections in the maxillofacial region, a comparative analysis of both clinical and ultrasonographic findings has showed that ultrasonography has 65% sensitivity and 80% specificity in identifying an infection when compared with the clinical exam alone [11].

Indications for POCUS assessment of inflammatory conditions of the neck can include:

- Identification of multiple enlarged lymph nodes with benign structure.
- Differentiating cellulitis from abscess formation.
- Differentiating an abscess from confluent lymphadenopathy.
- Detection of subcutaneous emphysema or hematoma [2].

11.1.4 Evaluation for Vascular Access and Procedural Guidance

Based on evidence and the consensus opinion of the collaborating organizations, ultrasound should be used whenever feasible in higher-risk procedures such as internal jugular central venous access and for all elective jugular vein dialysis catheter placement [12]. According to AIUM, there are no absolute contraindications to using ultrasound as a procedural adjunct for vascular guidance when it is administered appropriately by qualified personnel [2]. POCUS can offer a substantial benefit in terms of procedural safety and success improving venipuncture accuracy and procedural success [13].

To maximize the IJV size and minimize the possibility of air embolism during IJV access, the patient should be placed in the Trendelenburg position prior to procedure. A slight head rotation may be required to maneuver the probe and cannulation equipment but the amount of rotation could increase the overlap of the IJV and carotid artery, so this should be minimized (Fig. 11.1). The vascular access site should be chosen where the IJV is lateral to the carotid artery, as close as possible to the surface of the skin. Whether using either in-plane or out-of-plane needle visualization with ultrasound, it is important that the tip of the needle to be identified throughout the procedure. If the needle tip is not clearly seen, very slight movement of the needle may help visualize the tip by showing adjacent tissue movement. A "target sign" is seen in the short axis when a catheter enters the vessel. When the needle has entered the vessel, ultrasound should be used to confirm that the needle and/or guide wire is in the target vessel and is not visible in adjacent vessels not intended for cannulation [14].

It is recommended that the tip of the catheter be in the distal third of the superior vena cava (SVC) or close to the junction of the SVC with right atrium. This location allows the catheter to flow freely within the vein lumen and lie parallel with the vessel wall, resulting in considerable reduction of complications such as venous thrombosis, venous perforation, and catheter-related blood stream infections [15]. Also, POCUS may permit a more rapid identification of catheter malposition and allow for readjustment of the catheter before completion of the initial procedure. It also helps avoid other vascular structures and decreases the incidence of pneumothorax. The impact of ultrasound guidance in improving success and reducing complications is greatest in difficult patients, particularly in patients who are obese, have short necks, or are uncooperative [16, 17].

References

1. Klem C. Head and neck anatomy and ultrasound correlation. Otolaryngol Clin N Am. 2010;43(6):1161–8.
2. AIUM practice guideline for the performance of ultrasound examinations of the head and neck. J Ultrasound Med. 2014;33(2):366–82.
3. Troianos CA, Kuwik RJ, Pasqual JR, Lim AJ, Odasso DP. Internal jugular vein and carotid artery anatomic relation as determined by ultrasonography. Anesthesiology. 1996;85(1):43–8.
4. Gordon AC, Wright I, Pugh ND. Duplication of the superficial femoral vein: recognition with duplex ultrasonography. Clin Radiol. 1996;51(9):622–4.
5. Sulek CA, Gravenstein N, Blackshear RH, Weiss L. Head rotation during internal jugular vein cannulation and the risk of carotid artery puncture. Anesth Analg. 1996;82(1):125–8.
6. Lin BS, Kong CW, Tarng DC, Huang TP, Tang GJ. Anatomical variation of the internal jugular vein and its impact on temporary haemodialysis vascular access: an ultrasonographic survey in uremic patients. Nephrol Dial Transplant. 1998;13:134–8.
7. Gilbert TB, Seneff MG, Becker RB. Facilitation of internal jugular venous cannulation using an audio-guided Doppler ultrasound vascular access device: results from a prospective, dual-center, randomized, crossover clinical study. Crit Care Med. 1995;23(1):60–5.
8. Ying M, Ahuja A, Brook F, Metreweli C. Power Doppler sonography of normal cervical lymph nodes. J Ultrasound Med. 2000;19:511–7.
9. Rubaltelli L, Khadivi Y, Tregnaghi A, Stramare R, Ferro F, Borsato S, et al. Evaluation of lymph node perfusion using continuous mode harmonic ultrasonography with a second-generation contrast agent. J Ultrasound Med. 2004;23:829–36.
10. Soni NJ, Arntfield R, Kory PD. Point of care ultrasound. Philadelphia: Elsevier/Saunders; 2015.
11. Pandey PK, Umarani M, Kotrashetti S, Baliga S. Evaluation of ultrasonography as a diagnostic tool in maxillofacial space infections. J Oral Maxillofac Res. 2011;2(4):e4.
12. KDOQI clinical practice guidelines and clinical practice recommendations for 2006 updates: hemodialysis adequacy, peritoneal dialysis adequacy and vascular access. Am J Kidney Dis. 2006;48(suppl 1):S1–S322.
13. Randolph AG, Cook DJ, Gonzales CA, Pribble CG. Ultrasound guidance for placement of central venous catheters: a meta-analysis of the literature. Crit Care Med. 1996;24:2053–8.
14. AIUM practice guideline for the use of ultrasound to guide vascular access procedures. J Ultrasound Med. 2013;32(1):191–215.
15. Vesely TM. Central venous catheter tip position: a continuing controversy. J Vasc Interv Radiol. 2003;14:527–34.
16. Hosokawa K, Shime N, Kato Y, Hashimoto S. A randomized trial of ultrasound image-based skin surface marking versus real-time ultrasound-guided internal jugular vein catheterization in infants. Anesthesiology. 2007;107:720–4.
17. Karakitsos D, Labropoulos N, De Groot E, Patrianakos AP, Kouraklis G, Poularas J, et al. Real-time ultrasound-guided catheterisation of the internal jugular vein: a prospective comparison with the landmark technique in critical care patients. Crit Care. 2006;10:R162.

Tonsils

12

Jennifer V. Huang and Kevin Hu

Peritonsillar abscess (PTA) is a complication of tonsillitis and other upper respiratory infections; it is the most common deep space infection that presents to the emergency department. Diagnosis is often challenging, and even among experienced otolaryngologists, clinical exam has been shown to be only 78% sensitive and 50% specific in diagnosis of this pathology. Sonography is used both diagnostically and to provide procedural guidance in real time.

Several studies have shown that intraoral ultrasound (IOU) is an effective method of identifying and assisting with drainage of these abscesses. An endocavitary or "hockey-stick" probe is placed on the respective tonsil. PTAs are described as having an isoechoic rim with a hypoechoic center. Alternatively, a telescopic submandibular approach has also been described as an alternative method if the patient does not tolerate the IOC due to trismus. Another benefit of the telescopic submandibular approach is that it is easier to track the needle during drainage using ultrasound guidance.

See Figs. 12.1, 12.2, 12.3, 12.4, 12.5, and 12.6 and Videos 12.1, 12.2, 12.3, 12.4, 12.5 and 12.6 for details.

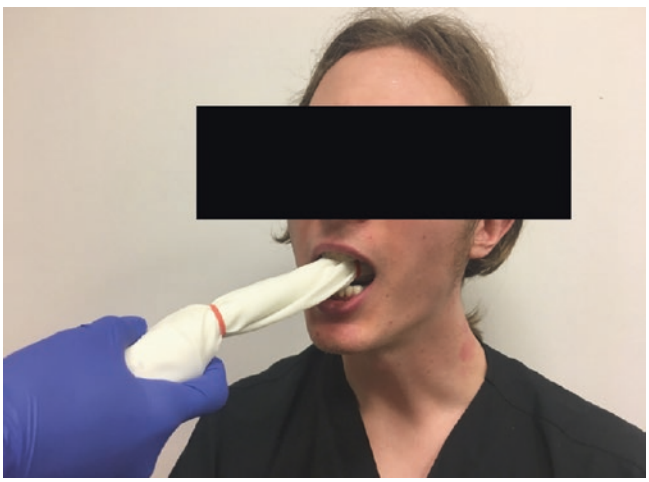

Fig. 12.1 Intraoral ultrasound (IOU) method: Gently place an endocavitary probe covered with a probe cover on the suspected tonsillar abscess. The probe marker should be pointed cephalad

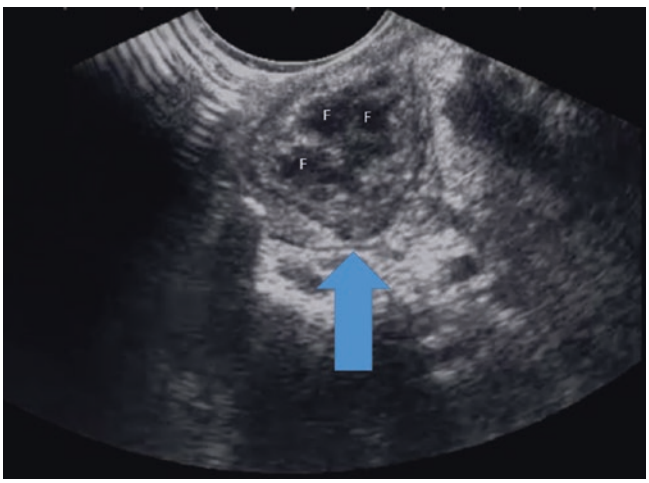

Fig. 12.2 IOU ultrasound: The blue arrow marks the abscess filled with fluid (F). Image courtesy of Phillip Andrus

Electronic Supplementary Material The online version of this chapter (https://doi.org/10.1007/978-3-319-73855-0_12) contains supplementary material, which is available to authorized users.

J. V. Huang, D.O. (✉) · K. Hu, M.D.
Department of Emergency Medicine, Icahn School of Medicine at Mount Sinai, New York, NY, USA

B. P. Nelson et al. (eds.), *Atlas of Handheld Ultrasound*, https://doi.org/10.1007/978-3-319-73855-0_12

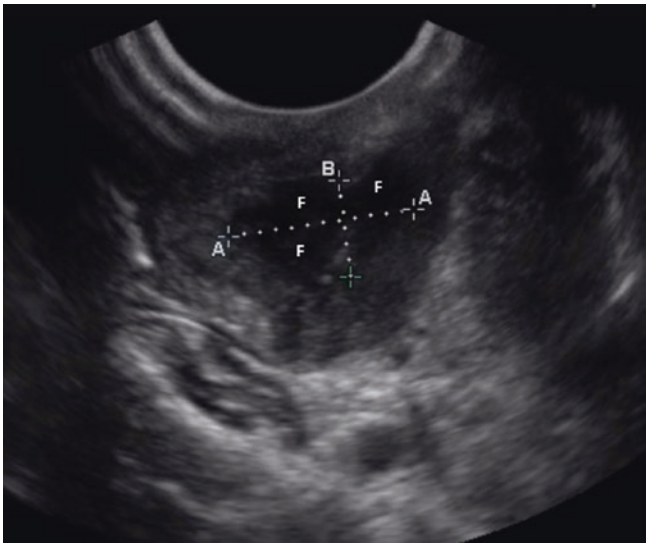

Fig. 12.3 IOU ultrasound: Abscess filled with fluid (F). Measurements of the size of the abscess are represented by A and B. Image courtesy of Ee Tay

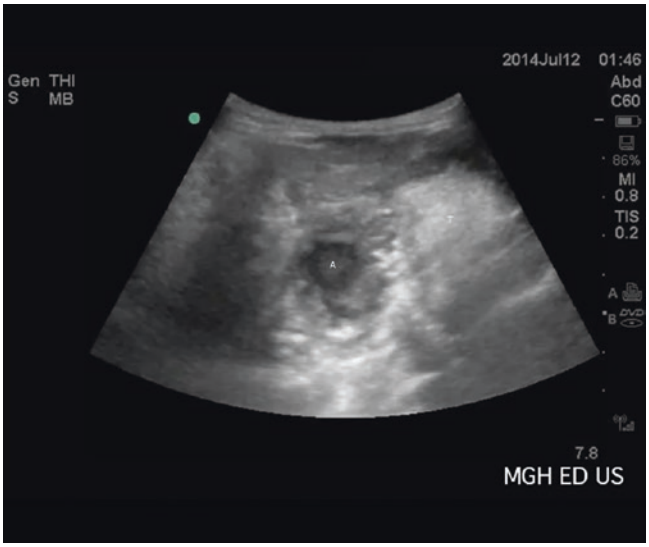

Fig. 12.5 This view demonstrates a peritonsillar abscess using the telescopic submandibular approach. Note the hypoechoic abscess (A) and the tongue (T). Image courtesy of Andrew Liteplo

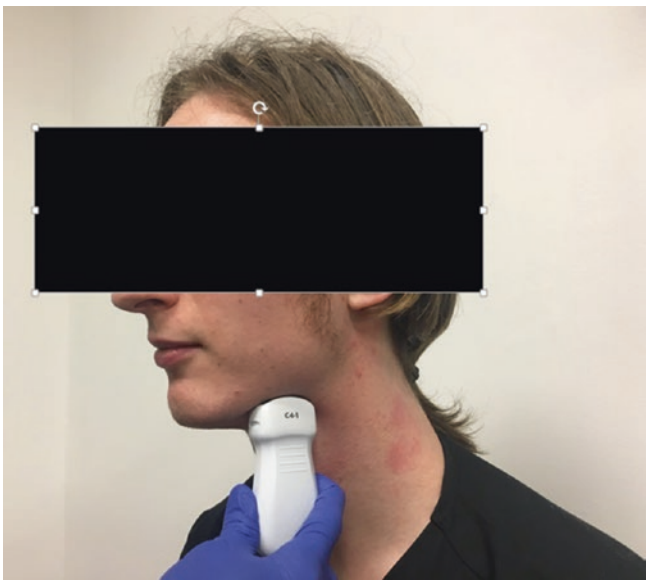

Fig. 12.4 Telescopic submandibular approach: Place a high-frequency linear probe or low-frequency curvilinear probe on the anterior cervical side of the neck ipsilateral to the suspected tonsillar abscess in a sagittal plane with the probe marker pointed posteriorly

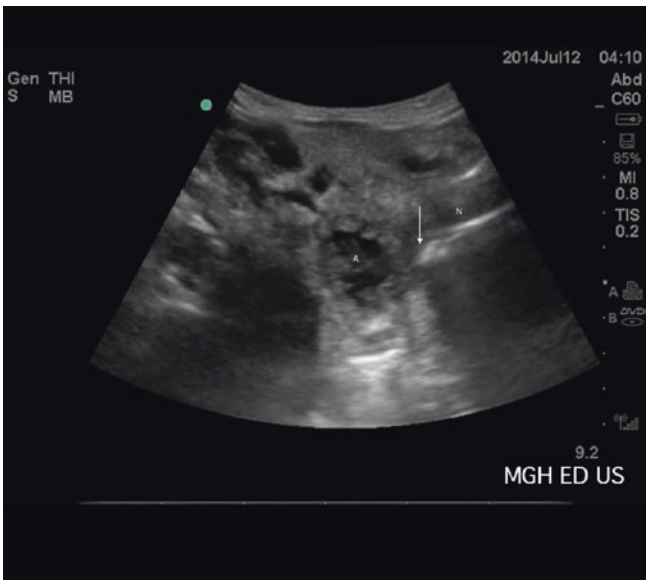

Fig. 12.6 This telescopic submandibular image demonstrates ultrasound guided needle aspiration of a peritonsillar abscess (A). A longitudinal view of the entire needle (N) can be seen using this method. The arrow points to the needle tip. Image courtesy of Andrew Liteplo

Suggested Reading

1. Blaivas M, Theodoro D, Duggal S. Ultrasound-guided drainage of peritonsillar abscess by the emergency physician. Am J Emerg Med. 2003;21(2):155–8.
2. Costantino TG, Satz WA, Dehnkamp W, Goett H. Randomized trial comparing intraoral ultrasound to landmark-based needle aspiration in patients with suspected peritonsillar abscess. Acad Emerg Med. 2012;19(6):626–31.
3. Kew J, Ahuja A, Loftus WK, Scott PM, Metreweli C. Peritonsillar abscess appearance on intra-oral ultrasonography. Clin Radiol. 1998;53(2):143–6.
4. Lyon M, Blaivas M. Intraoral ultrasound in the diagnosis and treatment of suspected peritonsillar abscess in the emergency department. Acad Emerg Med. 2005;12(1):85–8.
5. Prokofieva A, Modayil V, Chiricolo G, Ash A, Raio C. Ultrasound-guided drainage of peritonsillar abscess: shoot with your hockey-stick. Intern Emerg Med. 2016;11(6):883–4.
6. Rehrer M, Mantuani D, Nagdev A. Identification of peritonsillar abscess by transcutaneous cervical ultrasound. Am J Emerg Med. 2013;31(1):267.e1–3.
7. Scott PM, Loftus WK, Kew J, Ahuja A, Yue V, van Hasselt CA. Diagnosis of peritonsillar infections: a prospective study of ultrasound, computerized tomography and clinical diagnosis. J Laryngol Otol. 1999;113(3):229–32.
8. Ungkanont K, Yellon RF, Weissman JL, Casselbrant ML, González-Valdepeña H, Bluestone CD. Head and neck space infections in infants and children. Otolaryngol Head Neck Surg. 1995;112(3):375–82.

Thyroid

13

Stella S. Hahn and Mangala Narasimhan

The thyroid gland is easily to visualize due to its superficial location, size, and echogenicity. Many of the abnormalities of the thyroid need evaluation and close monitoring, making point-of-care ultrasound a useful bedside tool. Thyroid ultrasound can easily identify nodules, cysts, masses and also help in visualization during a diagnostic procedure [1].

See Figs. 13.1, 13.2, 13.3, 13.4, 13.5, and 13.6; Videos 13.1, 13.2 and 13.3 for details.

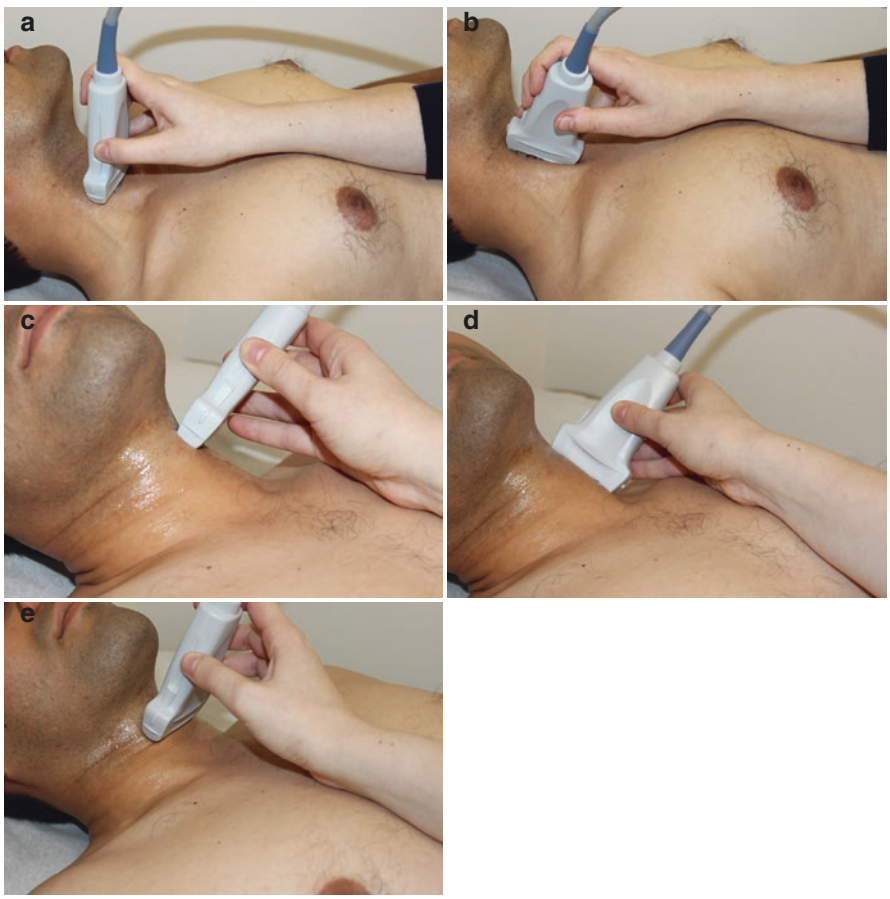

Fig. 13.1 A high-frequency linear array transducer should be used. The patient should be in the supine position with a pillow under their shoulders with their neck extended. The anterior neck is scanned both in the transverse (**a**) and longitudinal planes (**b**) to visualize the entire thyroid. In the transverse plane, the right thyroid lobe should be scanned from superior to inferior poles. The transducer should be then rotated 90° to the longitudinal plane and the thyroid should be inspected medial to laterally. The same should be repeated for the left thyroid lobe (**c**, **d**) [2]. (**e**) Imaging the isthmus. Image courtesy of Stella Hahn, Margarita Oks, and Atul Palkar

Electronic Supplementary Material The online version of this chapter (https://doi.org/10.1007/978-3-319-73855-0_13) contains supplementary material, which is available to authorized users.

S. S. Hahn, M.D. (✉) · M. Narasimhan, D.O.
Donald and Barbara Zucker School of Medicine at Hofstra/Northwell, New Hyde Park, NY, USA
e-mail: sthahn@northwell.edu

B. P. Nelson et al. (eds.), *Atlas of Handheld Ultrasound*, https://doi.org/10.1007/978-3-319-73855-0_13

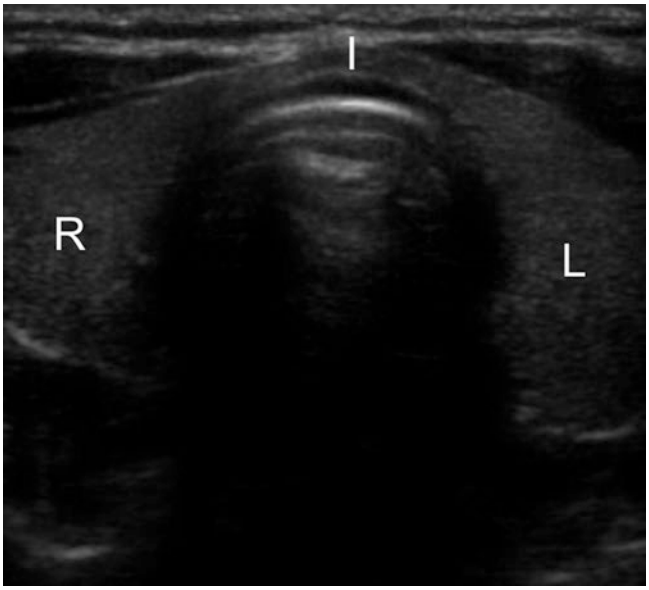

Fig. 13.2 The normal thyroid gland has two lobes right (R) and left (L) and an isthmus (I) that bridges them [3]. Normal thyroid tissue is brighter (hyperechoic) than muscle tissue but darker (hypoechoic) compared to connective tissue. It has a relatively homogenous echogenicity. Image courtesy of Stella Hahn

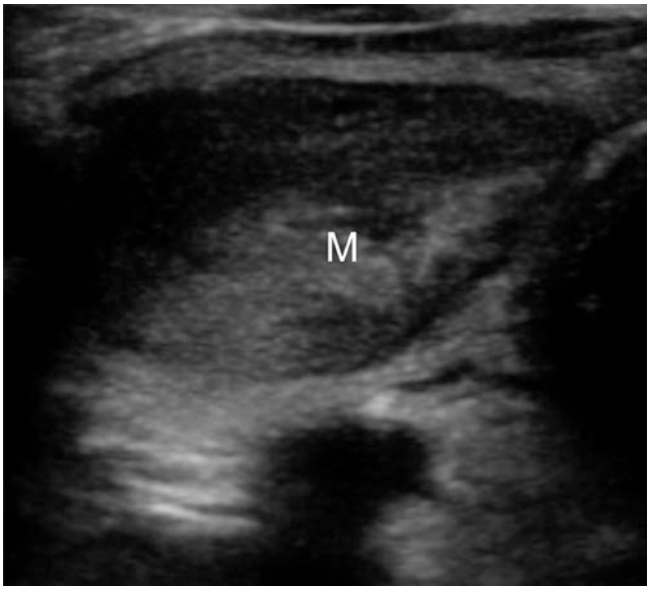

Fig. 13.4 An enlarged right lobe of the thyroid (M) is seen on this image. It is hyperechoic compared to a normal thyroid. Diffuse enlargement of the thyroid can be seen in Grave's disease or thyroiditis. Image courtesy of Mangala Narasimhan

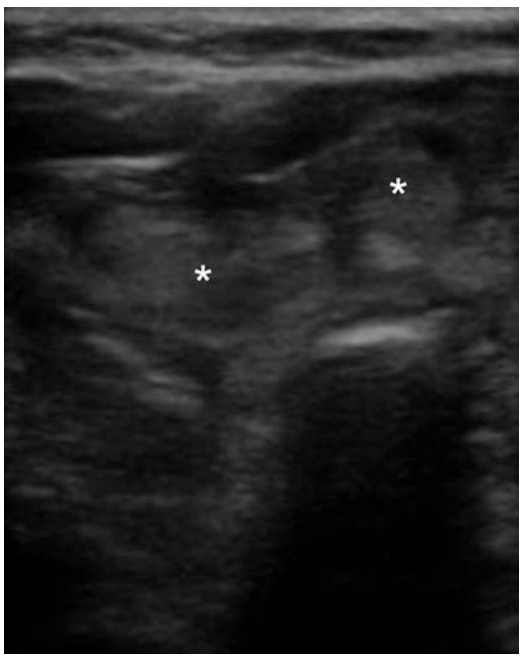

Fig. 13.3 Nodular disease of the thyroid is very common, with the majority being benign. Nodules (*) are the most common cause of thyroid enlargement. Image courtesy of Mangala Narasimhan

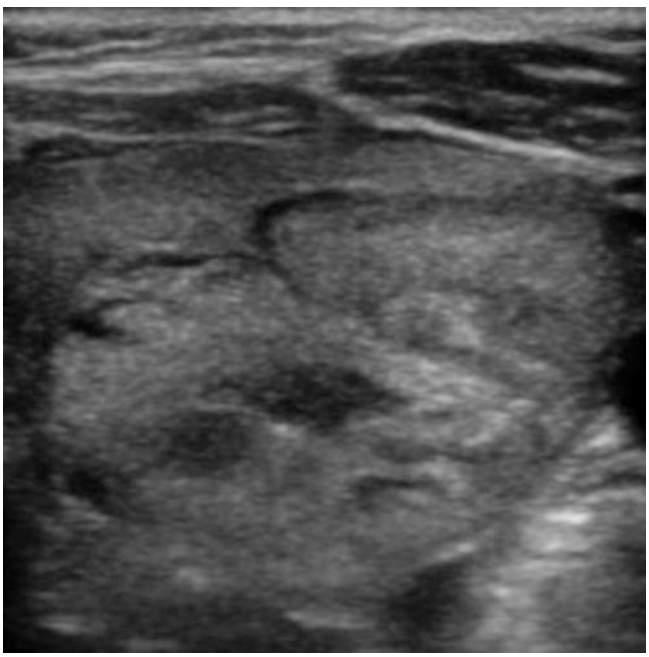

Fig. 13.5 A thyroid mass (M) is seen on the image. Note the heterogeneous echogenicity and the abnormal contour of the thyroid. Ultrasound is sensitive in diagnosing malignant lesions of the thyroid. Image courtesy of Mangala Narasimhan

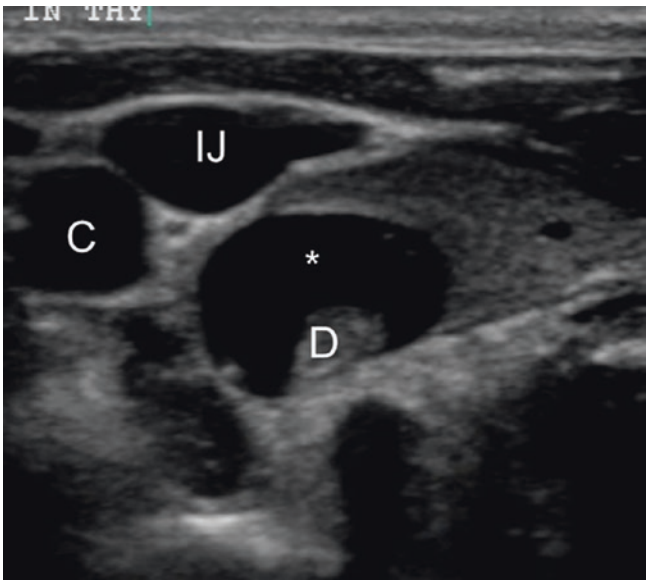

Fig. 13.6 A cyst (*) is seen within the right lobe of the thyroid. Debris (D) is seen within the cyst which can be indicative of infection. The right internal jugular vein (IJ) and the carotid artery (C) is also seen in this image. Image courtesy of Mangala Narasimhan

References

1. Levine RA. History of thyroid ultrasound. In: Baskin Sr HJ, Duick DS, Levine RA, editors. Thyroid ultrasound and ultrasound-guided FNA. 3rd ed. New York: Springer; 2013.
2. Treadwell DR. Normal neck anatomy and method of performing ultrasound examination. In: Baskin Sr HJ, Duick DS, Levine RA, editors. Thyroid ultrasound and ultrasound-guided FNA. 3rd ed. New York: Springer; 2013.
3. Chaudhary V, Bano S. Thyroid ultrasound. Indian J Endocrinol Metab. 2013;17(2):219–27.

Pleura

14

Brendan H. A. Milliner and James W. Tsung

Lung ultrasound is increasingly recognized as a critical element of bedside sonography [1]. The pleura is generally very well-visualized as a bright white (hyperechoic) horizontal line just deep to the ribs. Pleural ultrasound is used widely for the diagnosis of pneumothorax and pleural effusion, and new studies demonstrate its utility for the evaluation of suspected pneumonia [2–5]. The images in Figs. 14.1, 14.2, 14.3, 14.4, 14.5, 14.6, 14.7, 14.8, 14.9, and 14.10 demonstrate these diagnoses, as well as depictions of basic scanning technique and normal ultrasonographic lung anatomy.

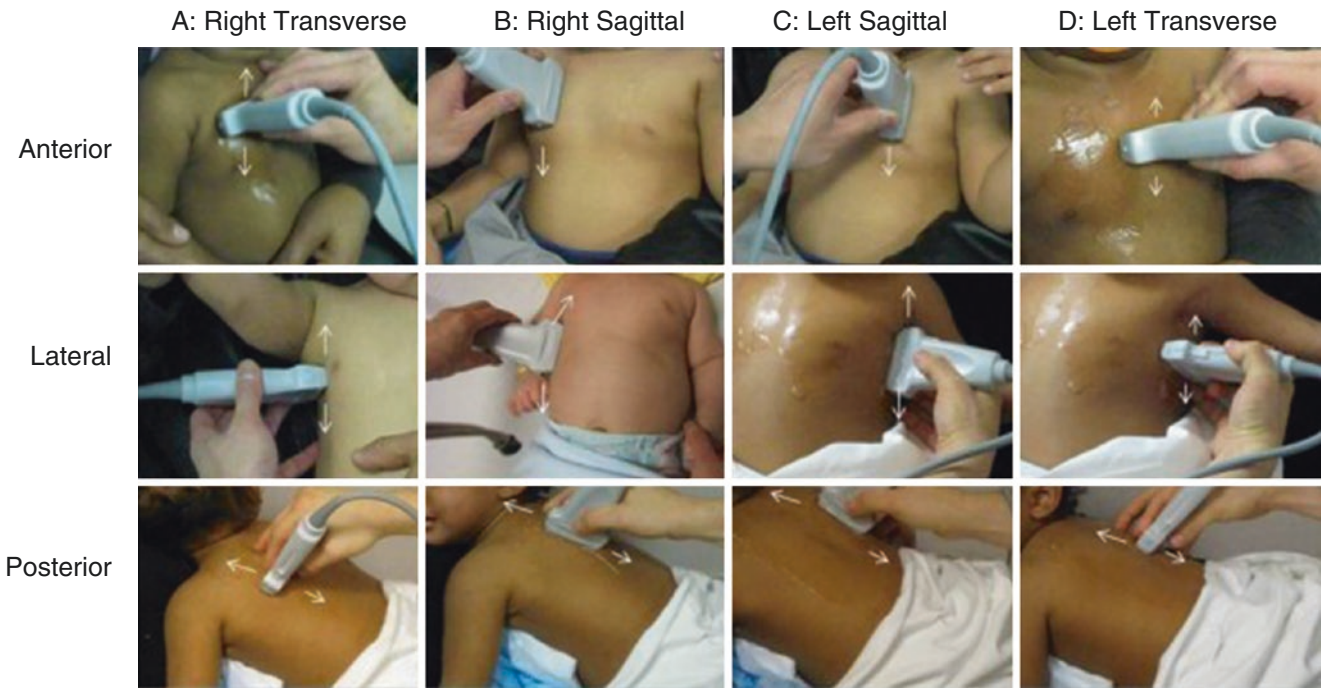

Fig. 14.1 Six-zone lung scanning protocol. *Top row*: anterior midclavicular line; *Middle row*: lateral midaxillary line; *Bottom row*: posterior paraspinal line. Probes in transverse (columns A and D) and parasagittal planes (columns B and C) in anterior and posterior lung fields, and in transverse and coronal planes (middle row) in lateral lung fields

B. H. A. Milliner, M.D. (✉)
Division of Emergency Medicine, University of Utah Hospital, Salt Lake City, UT, USA

J. W. Tsung, M.D., M.P.H.
Department of Emergency Medicine, Mount Sinai Health System, Icahn School of Medicine at Mount Sinai, New York, NY, USA

B. P. Nelson et al. (eds.), *Atlas of Handheld Ultrasound*, https://doi.org/10.1007/978-3-319-73855-0_14

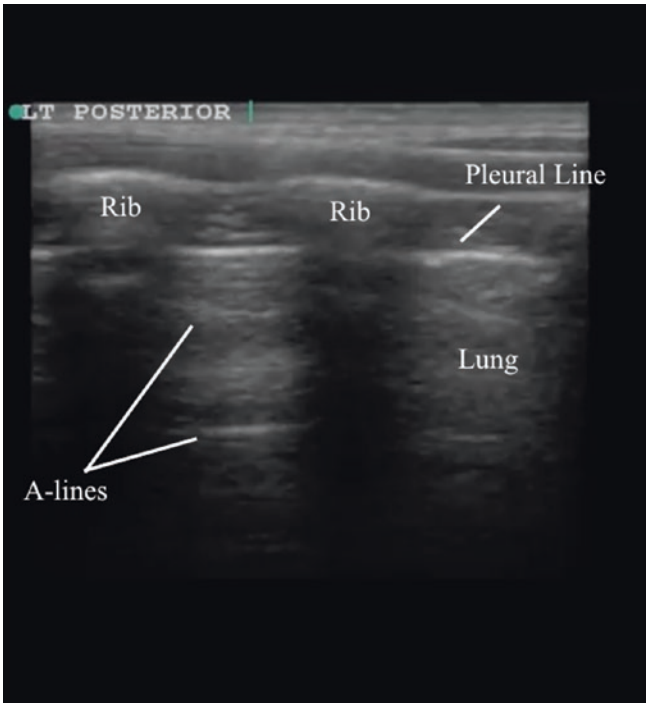

Fig. 14.2 Normal lung anatomy and A-lines: sagittal view

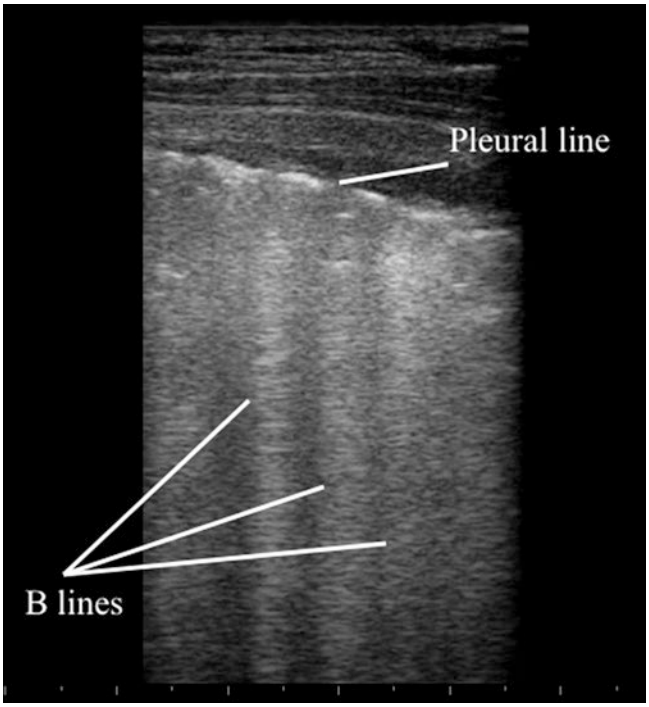

Fig. 14.4 B-lines: sagittal view. The presence of B-lines indicates extravascular lung water. These lines can be seen in pulmonary edema, interstitial fibrosis, or viral lower respiratory tract infection (e.g., viral pneumonia or bronchiolitis)

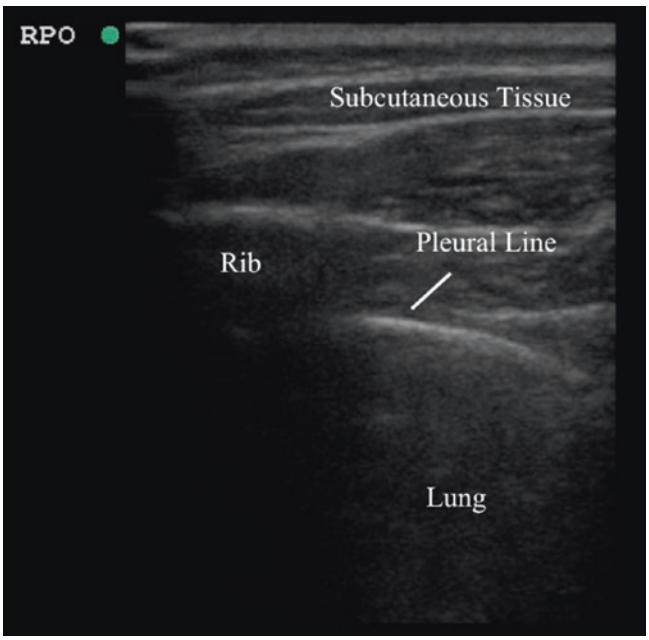

Fig. 14.3 Normal lung anatomy: transverse view

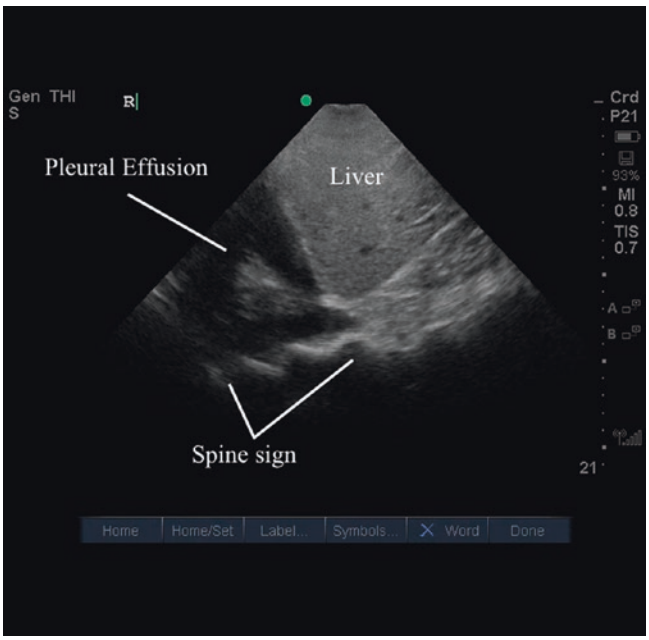

Fig. 14.5 Pleural effusion and spine sign. This image demonstrates the presence of fluid layering above the diaphragm. "Spine sign" refers to the vertebral bodies visible in the lower half of the image and is diagnostic of pleural effusion. In patients without effusion, the aerated lung parenchyma obscures these vertebrae

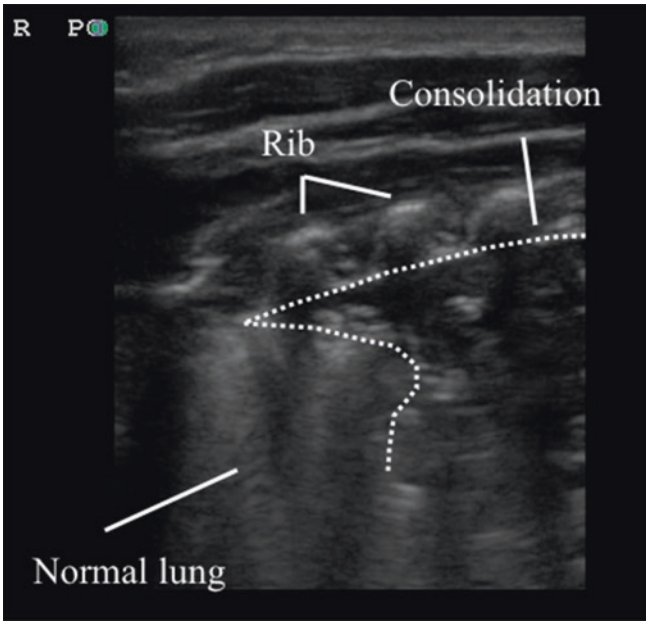

Fig. 14.6 Lung consolidation with sonographic air bronchograms: sagittal view

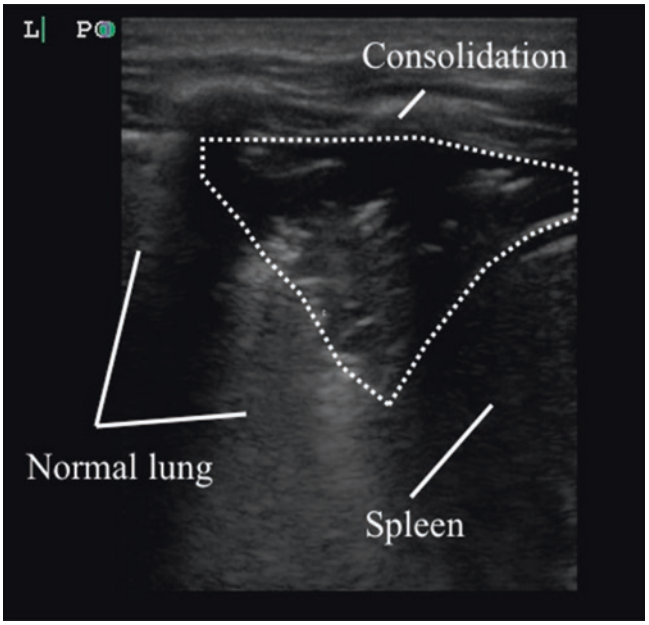

Fig. 14.8 Inferior lung consolidation: sagittal view. Consolidations are often found in the inferior lung abutting the liver or spleen. This picture demonstrates the sonographic differences between lung consolidation and splenic parenchyma

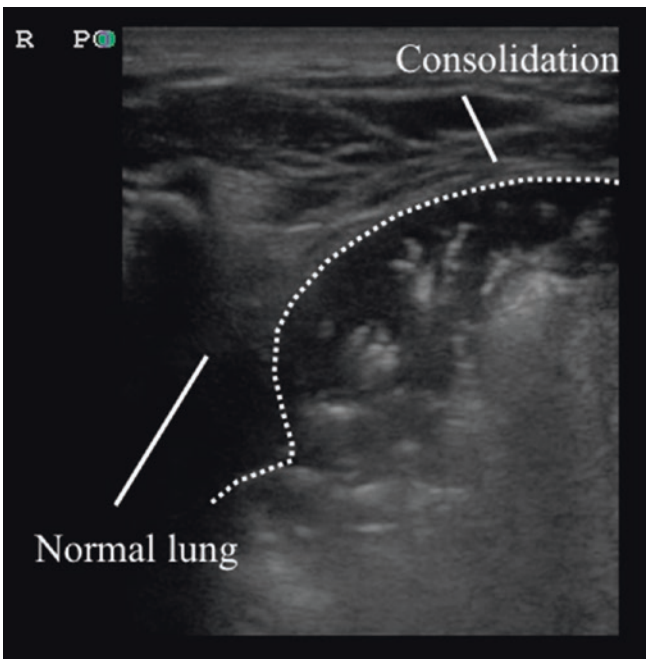

Fig. 14.7 Lung consolidation with sonographic air bronchograms: transverse view

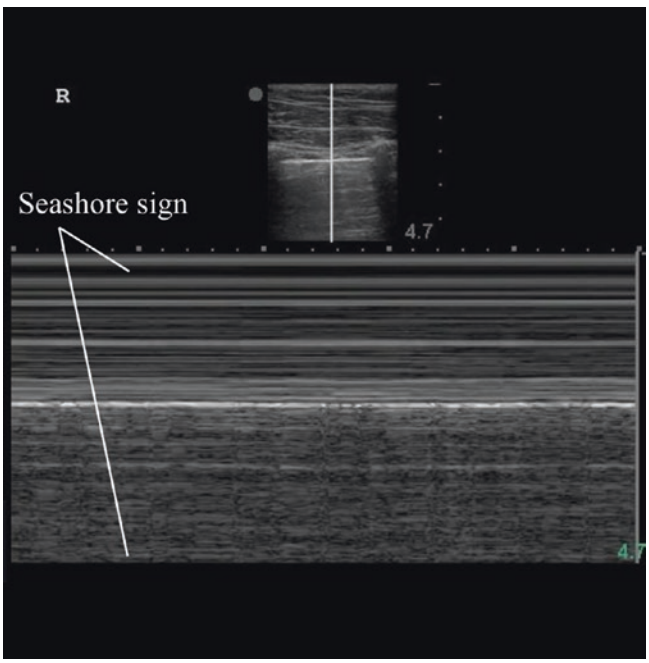

Fig. 14.9 M-mode for the diagnosis of pneumothorax: normal lung. Using M-mode gives a snapshot of a focused lung area over time. This image demonstrates "seashore" sign, a visual representation of normal lung sliding. The demarcation between the mobile lung parenchyma and the static subcutaneous tissue is clearly seen

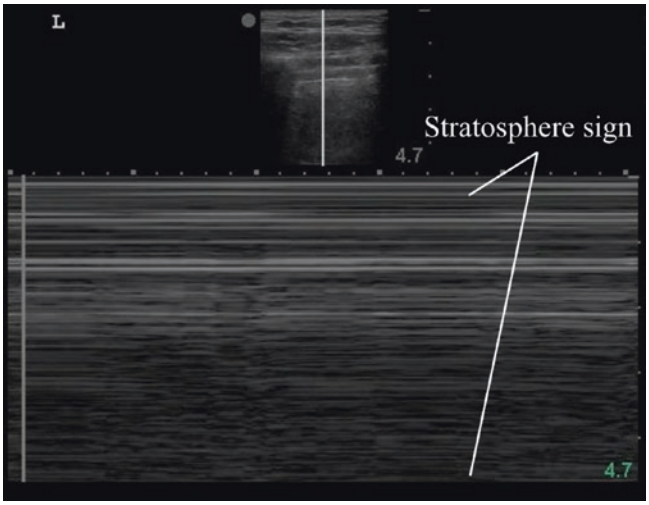

Fig. 14.10 M-mode for the diagnosis of pneumothorax: presence of pneumothorax. This image demonstrates "stratosphere sign," the absence of normal lung sliding. Note the lack of demarcation between lung and subcutaneous tissue

References

1. Lichtenstein DA. Ultrasound in the management of thoracic disease. Crit Care Med. 2007;35(5 Suppl):S250–61.
2. Lichtenstein DA, Lascols N, Mezière G, Gepner A. Ultrasound diagnosis of alveolar consolidation in the critically ill. Intensive Care Med. 2004;30(2):276–81.
3. Tsung JW, Kessler DO, Shah VP. Prospective application of clinician-performed lung ultrasonography during the 2009 H1N1 influenza A pandemic: distinguishing viral from bacterial pneumonia. Crit Ultrasound J. 2012;4(1):16.
4. Shah VP, Tunik MG, Tsung JW. Prospective evaluation of point-of-care ultrasonography for the diagnosis of pneumonia in children and young adults. JAMA Pediatr. 2013;167(2):119–25.
5. Jones BP, Tay ET, Elikashvili I, Sanders JE, Paul AZ, Nelson BP, et al. Feasibility and safety of substituting lung ultrasonography for chest radiography when diagnosing pneumonia in children: a randomized controlled trial. Chest. 2016;150(1):131–8.

Breast Ultrasound

15

Sharon L. Mulvagh and Tara L. Anderson

15.1 Introduction

Breast ultrasound is primarily utilized in conjunction with diagnostic mammography to evaluate breast concerns identified by the patient or during clinical breast exam, and to further characterize findings identified on mammogram, breast MRI, and molecular breast imaging. Breast symptoms evaluated by ultrasound include breast pain, nipple discharge, and palpable masses. Ultrasound is also used to guide breast biopsies when the targeted lesion is well seen by ultrasound and occasionally to evaluate breast implants [1]. At some institutions, whole breast ultrasound is being utilized for cancer screening in select groups of patients, including those at high risk for breast cancer who are unable to undergo MRI, pregnant women, and women with increased breast density [2]. Breast ultrasound is rarely performed in isolation without concurrent mammography. Primary exceptions are for patients under 30 years old with a focal area of concern, clinical signs of mastitis with concern for breast abscess, and for targeted follow-up. Point-of-care breast ultrasound should be followed by formal breast diagnostic evaluation performed by an experienced breast imager.

15.2 Technique

Ultrasound is operator-dependent and knowledge of scanning technique and image optimization is important for accurate characterization of breast lesions. Firm pressure should be applied while scanning the breast. The patient is typically positioned supine with the ipsilateral arm flexed above the head. Flat supine positioning is usually ideal for evaluation of medial lesions. Lesions in the lateral breast are often better evaluated with the patient in the contralateral oblique position [1].

Linear 12–5-MHz transducer is most commonly used in breast ultrasound. When evaluating superficial lesions, a linear 17–5-MHz transducer may be used [1]. This high-frequency transducer results in improved spatial resolution, which increases lesion conspicuity against the background of normal breast tissue. However, higher resolution results in loss of acoustic penetration and deeper tissues are suboptimally evaluated. If scanning a palpable lesion, the operator should first palpate the area and then the ultrasound probe should be placed directly on the same area.

The breast can be scanned in the transverse and longitudinal planes or radial and anti-radial planes. Images of any abnormalities should always be obtained in two planes. Breast lesion location is typically described by right or left, clock face position, and centimeters from the nipple, which should be annotated on the images. Evaluation of lesion vascularity with Doppler imaging is recommended.

S. L. Mulvagh, M.D., F.R.C.P.C. (✉)
Department of Medicine, Division of Cardiology,
Dalhousie University, Halifax, NS, Canada
e-mail: Sharon.Mulvagh@nshealth.ca

T. L. Anderson, M.D.
Department of Radiology, Mayo Clinic Health System,
Austin, MN, USA

B. P. Nelson et al. (eds.), *Atlas of Handheld Ultrasound*, https://doi.org/10.1007/978-3-319-73855-0_15

15.3 Anatomy

The breast is composed of 15–20 lobes containing lobules and ducts that converge at the nipple areolar complex [3]. Each lobe is covered by fascia with the most anterior fascia separating the lobes from the subcutaneous fat and the most posterior fascia separating the lobes from the retro-mammary fat and pectoralis musculature. This fascial division creates three anatomic zones within the breast (Fig. 15.1). The pre-mammary (subcutaneous) zone contains Cooper's suspensory ligaments and sometimes a small number of peripheral ducts and lobules. The central mammary zone contains all the central ducts and most of the peripheral ducts and lobules, as well as fat and fibrous tissue. The deep retro-mammary zone contains only fat and ligaments [3].

The breast contains tissues of differing composition, including fat tissue, glandular tissue, and fibrous connective tissue. Fat is typically hypoechoic on ultrasound, while glandular tissue is typically hyperechoic. The fibrous connective tissue or Cooper's ligaments provide support to the breast from the chest wall. Cooper's ligaments are identifiable on ultrasound as thin, echogenic bands, which may demonstrate posterior acoustic shadowing. Ducts can be seen as thin hypoechoic tubular structures that converge at the nipple. The nipple areolar complex can also cause posterior acoustic shadowing and should be evaluated carefully with rocking of the ultrasound probe if needed. An offset pad of thick gel may be helpful when evaluating the nipple [4].

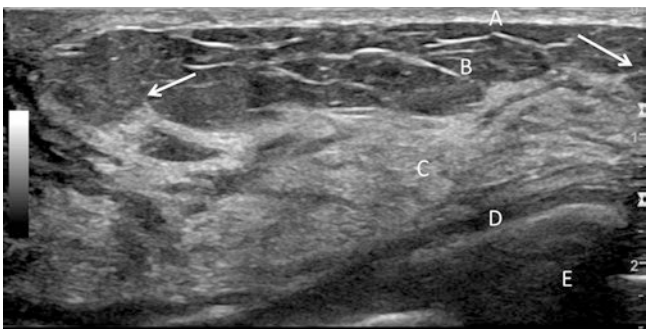

Fig. 15.1 Normal ultrasound breast anatomy. From superficial to deep: A, skin; B, pre-mammary subcutaneous fat; C, mammary zone containing fibroglandular tissue; D, retro-mammary fat; and E, chest wall. Arrows show Cooper's ligaments anteriorly at the junction of the pre-mammary and mammary zones

15.4 Pathology

Ultrasound is helpful in distinguishing solid from cystic breast masses. Lesions in the breast should be characterized by shape, orientation, margin, echo pattern, and posterior features. Associated features should also be noted, including architectural distortion, duct or skin changes, edema, and Doppler vascularity. Specific imaging criteria must be met to diagnose a simple breast cyst. Those criteria include: anechoic mass with circumscribed margins, a thin imperceptible wall, and increased through transmission (Fig. 15.2) [4]. Increased through transmission is seen as a brighter area behind a low-echogenicity or anechoic structure because fewer of the sound waves are attenuated or reflected by that tissue. Simple cysts may contain a single thin septation. These classic findings can be masked in lesions that are deep in the breast or in very small cysts. Simple cysts should not contain any solid component or thick septation, nor should they demonstrate wall thickening or internal vascularity.

Solid masses may be benign or malignant. Characteristics of benign masses include orientation parallel to the chest (wider than tall), circumscribed margins, and oval or round shape (Fig. 15.3). Suspicious features of solid masses include irregular shape, spiculated, micro-lobulated or angular margins, marked hypoechogenicity, posterior acoustic shadowing, and associated micro-calcifications (Fig. 15.4a) [4]. Posterior acoustic shadowing is seen as a darker area deep to a mass caused by attenuation or reflection of the sound waves by the mass. Micro-calcifications can be identified on ultrasound as tiny echogenic foci, which may have posterior shadowing. Malignant masses are more likely to be oriented antiparallel to the chest (taller than wide). Doppler evaluation of solid masses may demonstrate internal blood flow (Fig. 15.4b). Benign and malignant masses cannot always be reliably delineated by imaging, and biopsy may be indicated for tissue diagnosis.

Breast abscesses occur as a complication of mastitis and generally occur in young women. Abscess in a breast-feeding woman is called a puerperal or lactational abscess. Abscess in a non-lactating woman is classified by either central or peripheral location, with central abscess being more common [5]. Risk factors for non-puerperal abscesses include black race, obesity, diabetes, and smoking [5]. Imaging evaluation is often indicated when there is concern for abscess in the setting of clinically apparent breast infection, including symptoms of breast pain, redness, and heat. An abscess is seen by ultrasound as a hypoechoic or mixed echogenicity collection of inconstant shape and size with a thick, echogenic peripheral rim and increased peripheral blood flow (Fig. 15.5a, b). Posterior increased through transmission is often present due to internal fluid. Ultrasound can also be used to guide percutaneous drainage and for follow-up after treatment. Inflammatory breast carcinoma can mimic breast infection, presenting with skin erythema and breast swelling with or without an associated mass. This underscores the importance of follow-up with comprehensive clinical and breast imaging evaluation.

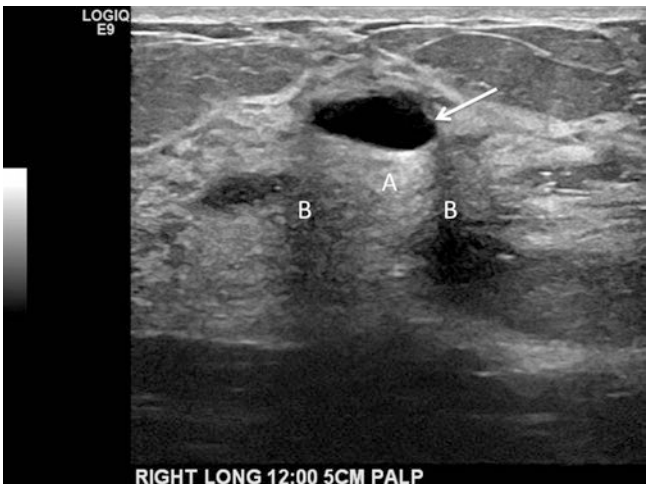

Fig. 15.2 Benign breast cyst. A cyst (arrow) is anechoic, oval-shaped with circumscribed margins, an imperceptible wall, and increased through-transmission (A). This image also shows edge shadowing artifact (B), created by refraction of the sound waves as they encounter the edge of a cyst wall or curved surface

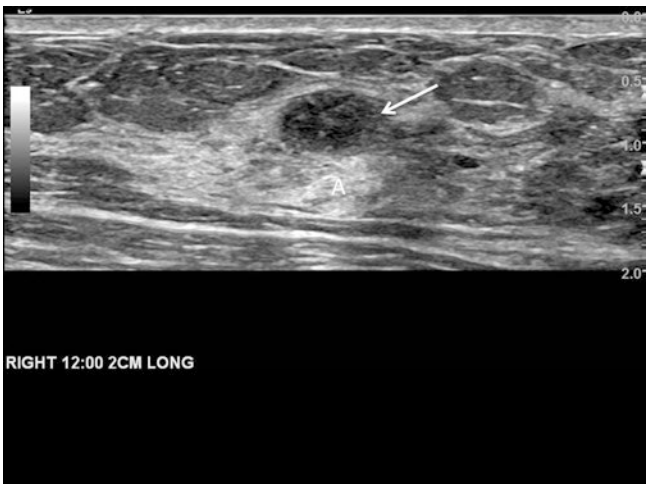

Fig. 15.3 Benign breast mass, biopsy proven fibroadenoma (arrow). This mass demonstrates benign features, including oval shape with parallel orientation, and circumscribed margins. This mass also demonstrates some increased through transmission (A)

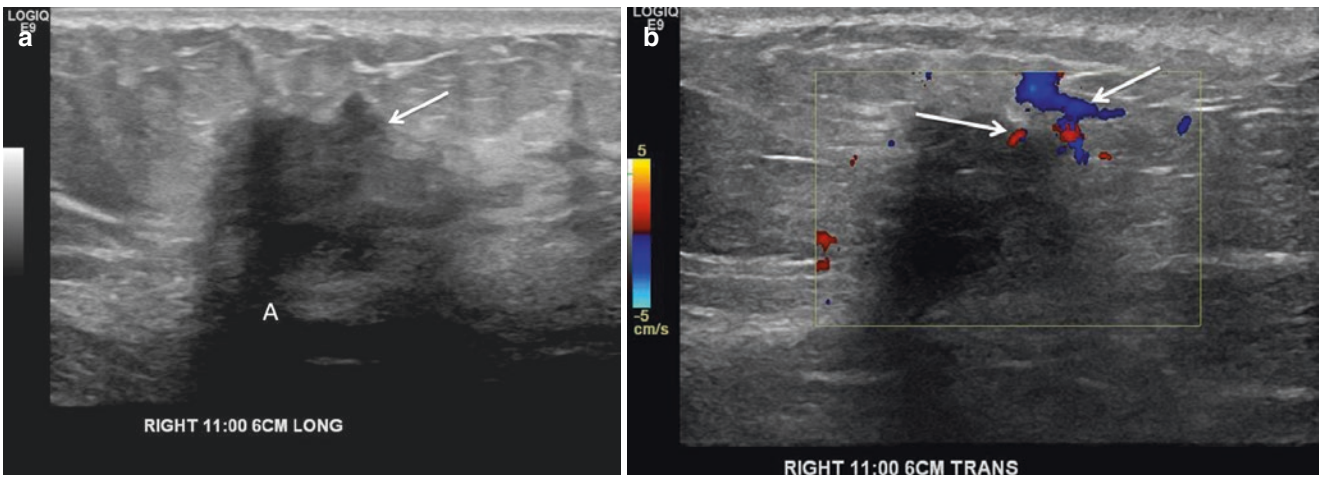

Fig. 15.4 (**a**) Malignant breast mass, biopsy proven invasive ductal carcinoma (arrow). This mass demonstrates malignant features including irregular shape, spiculated margins, antiparallel orientation, and posterior acoustic shadowing (A). (**b**) The same malignant breast mass evaluated with color Doppler demonstrates areas of internal and peripheral vascularity (arrows)

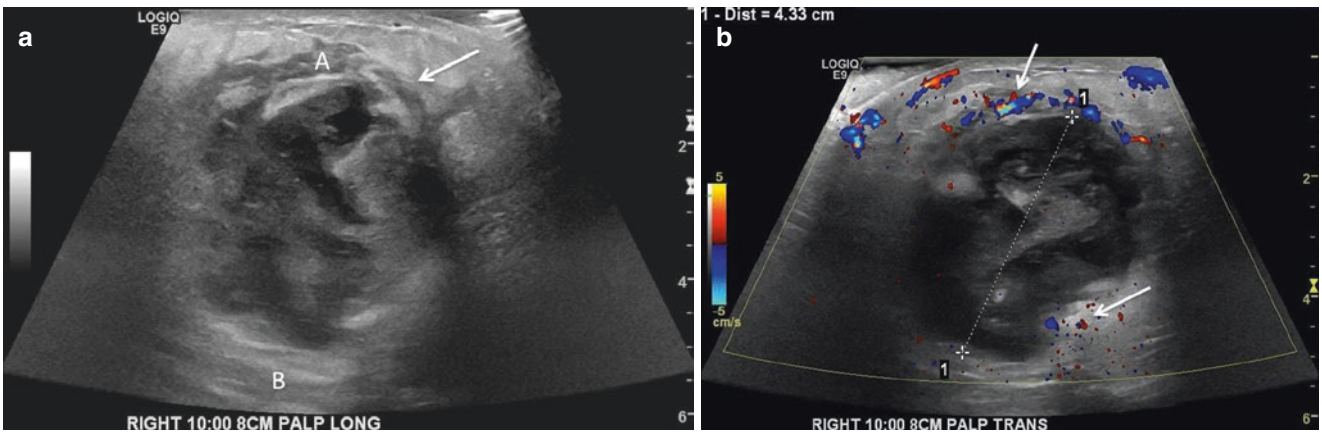

Fig. 15.5 (**a**) Breast abscess, cultures demonstrated staphylococcus aureus (arrow). This mass is a mixed echogenicity collection with a thick peripheral rim (A), compatible with an abscess in a patient with clinically apparent infection. Increased through transmission is seen due to the fluid component (B). (**b**) The same breast abscess evaluated with color Doppler demonstrates increased peripheral blood flow (arrows)

References

1. Hooley RJ, Scoutt LM, Philpotts LE. Breast ultrasonography: state of the art. Radiology. 2013;268:642–59.
2. Ultrasound—breast. In: RadiologyInfo.org. http://www.radiology-info.org/en/info.cfm?pg=breastus. Accessed 30 Aug 2016.
3. Stavros AT. Breast ultrasound. Philadelphia: Lippincott Williams & Wilkins; 2004.
4. Mendelson EB, Böhm-Vélez M, Berg WA, et al. ACR BI-RADS® ultrasound. In: D'Orsi CJ, editor. ACR BI-RADS® atlas: breast imaging reporting and data system. 5th ed. Reston, VA: American College of Radiology; 2013.
5. Trop I, Dugas A, David J, El Khoury M, Boileau JF, Larouche N, et al. Breast abscesses: evidence-based algorithms for diagnosis, management, and follow-up. Radiographics. 2011;31:1683–99.

Normal Cardiac Anatomy and Common Views

16

Edgar Argulian and Jagat Narula

16.1 Introduction

There is no universally accepted imaging protocol for point-of-care cardiac ultrasound. Image acquisition and interpretation skills of the examiner are crucial in order to diagnose common conditions and comprehend the limitations of the approach [1]. Certain imaging views are easier to obtain (such as parasternal and subcostal views), others need more expertise (such as apical views), and certain techniques require comprehensive training (such as color and spectral Doppler) [2]. The following abnormalities can be accurately detected using point of care cardiac ultrasound: left ventricular enlargement, hypertrophy, and systolic dysfunction; right ventricular enlargement and dysfunction; pericardial effusion; and elevated central venous pressure [3]. Correct quantification of the detected abnormalities requires comprehensive echocardiography. The current chapter (Figs. 16.1, 16.2, 16.3, 16.4, 16.5, 16.6, 16.7, 16.8, 16.9, 16.10, 16.11, 16.12, 16.13, and 16.14; Videos 16.1, 16.2, 16.3, 16.4, 16.5, 16.6, 16.7, and 16.8; and Table 16.1) reviews some common views that can be obtained and interpreted during point of care ultrasound examination.

Electronic Supplementary Material The online version of this chapter (https://doi.org/10.1007/978-3-319-73855-0_16) contains supplementary material, which is available to authorized users.

E. Argulian, M.D., M.P.H. (✉)
Mount Sinai St. Luke's Hospital, Icahn School of Medicine at Mount Sinai, New York, NY, USA
e-mail: Edgar.Argulian@mountsinai.org

J. Narula, M.D., Ph.D.
Mount Sinai Hospital, Icahn School of Medicine at Mount Sinai, New York, NY, USA

B. P. Nelson et al. (eds.), *Atlas of Handheld Ultrasound*, https://doi.org/10.1007/978-3-319-73855-0_16

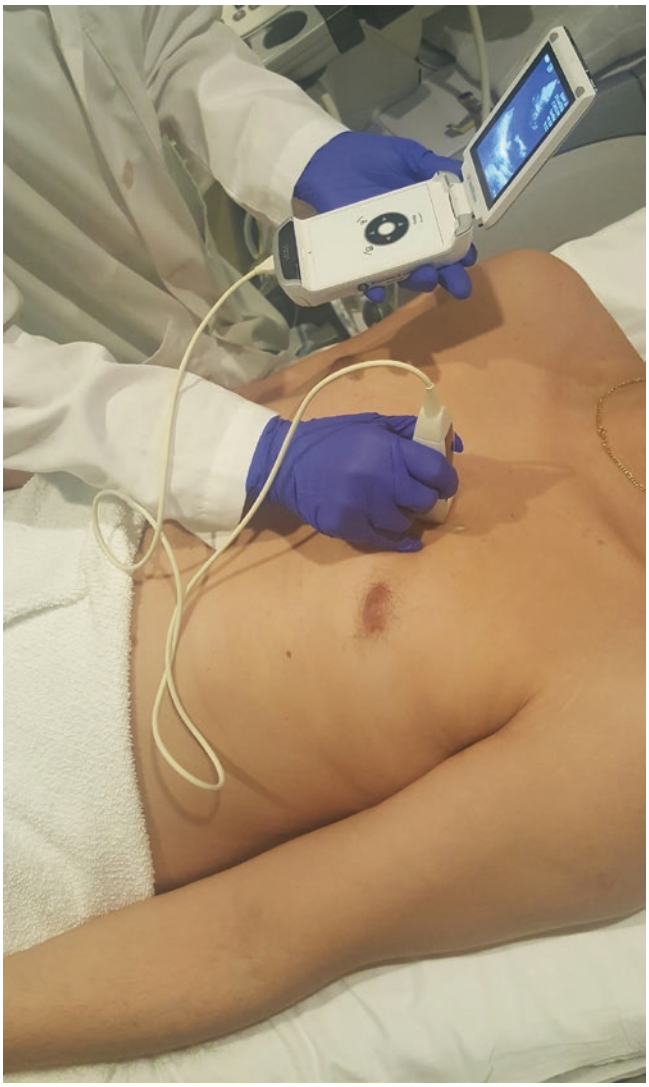

Fig. 16.1 Obtaining the parasternal long axis view using a handheld ultrasound device. Unlike apical views, the parasternal views are less dependent on patient positioning and are easier to obtain. The patient is in supine position; if necessary and feasible the patient can be turned to the left lateral decubitus position to optimize imaging. The examiner should begin scanning in the third left intercostal space with the probe marker pointing toward the patient's right shoulder. The examiner should adjust the transducer to align the scanning plane along the major axis of the left ventricle. To optimize the image, it may be necessary to move up or down one or two intercostal spaces

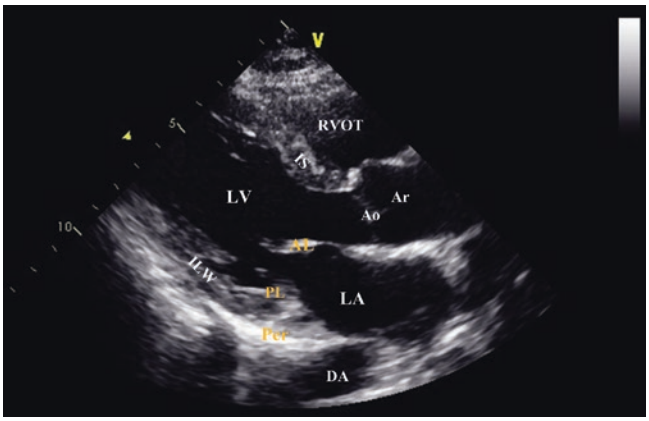

Fig. 16.2 Parasternal long axis view. This view allows visualization of the right ventricular outflow tract (RVOT), left atrium (LA) and left ventricle (LV). The interventricular septum (IS) and the inferolateral wall (ILW) of the left ventricle are also seen. Bright pericardium (Per) is seen behind the left ventricle. This view also allows identification of the aortic valve (Ao) and aortic root (Ar), anterior (AL) and posterior (PL) leaflets of the mitral valve, and descending aorta (DA). Color Doppler examination in this view allows visualization of mitral regurgitation and aortic regurgitation. See also Video 16.1

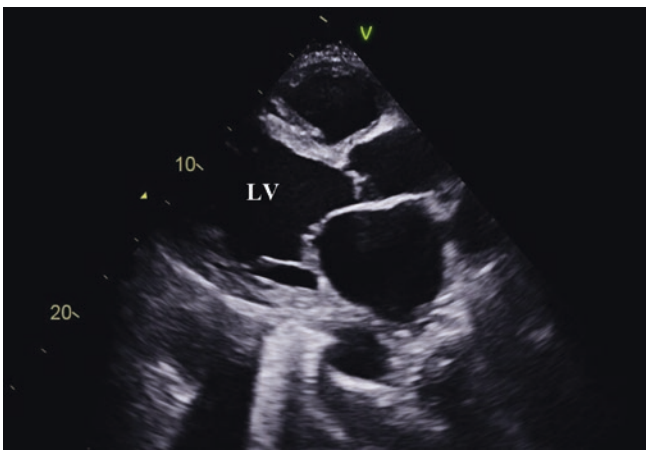

Fig. 16.3 Parasternal long axis view in a patient with shortness of breath. The left ventricle (LV) is dilated and left ventricular ejection fraction is reduced. Parasternal views allow approximate assessment of the left ventricular size and identification of significant left ventricular systolic dysfunction. See also Video 16.2

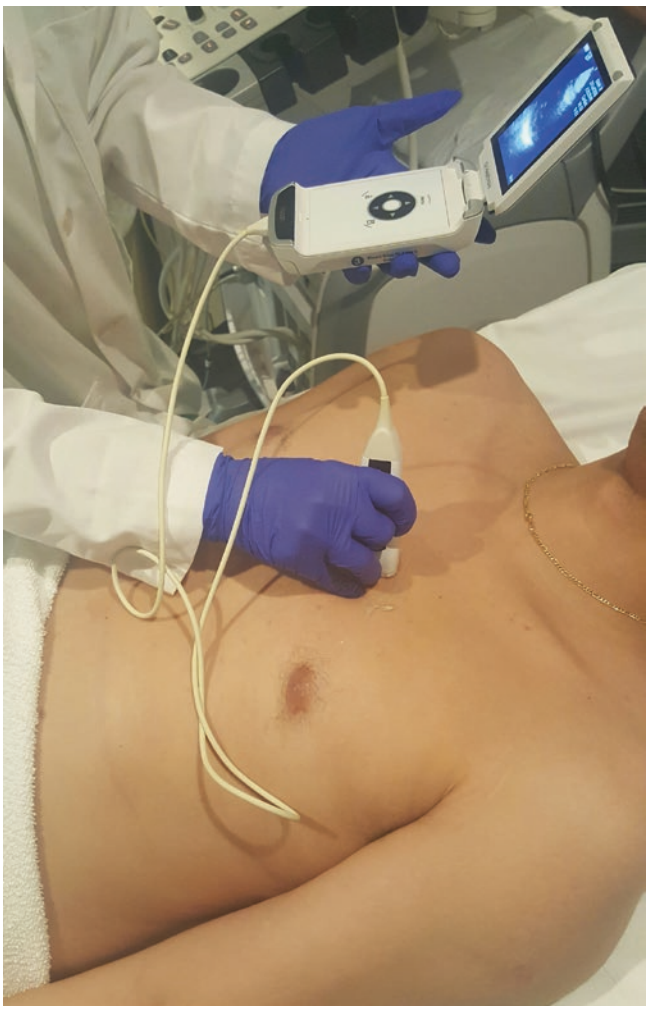

Fig. 16.4 Obtaining parasternal short axis views using handheld ultrasound device. From the parasternal long axis view the transducer is rotated clockwise approximately 90°. The probe marker is now pointing toward the patient's left shoulder. Different short axis planes can be obtained by tilting the transducer up and down in this position. These include the basal level (level of the aortic valve), mitral valve level, papillary muscle level, and apical level. These planes are not exactly parallel and require good examination skills to acquire

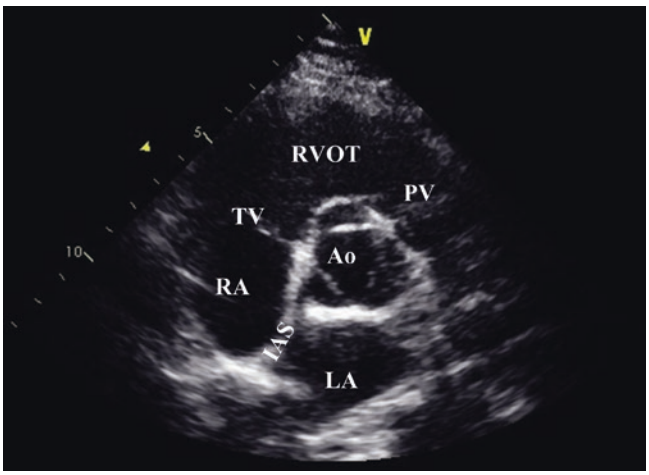

Fig. 16.5 Parasternal short axis view at the level of the aortic valve. The short axis view of the aortic valve is obtained and all three leaflets of the aortic valve (Ao) are seen in the middle. This view also allows identification of right ventricular outflow tract (RVOT), right atrium (RA), left atrium (LA) and interatrial septum (IAS), tricuspid valve (TV) and pulmonary valve (PV)

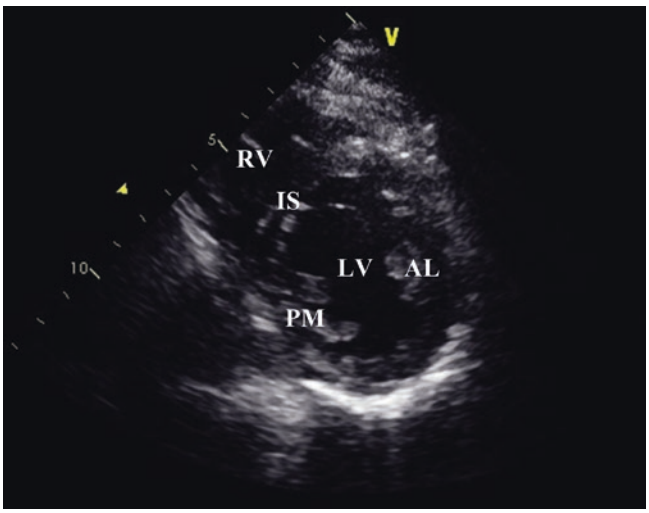

Fig. 16.6 Parasternal short axis view at the level of the papillary muscles. Left ventricle (LV), interventricular septum (IS) and right ventricle (RV) are seen. The left ventricle appears round and symmetric. Anterolateral (AL) and posteromedial (PM) papillary muscles are the landmarks at this level. This view is useful for rough assessment of the left ventricular systolic function. See also Video 16.3

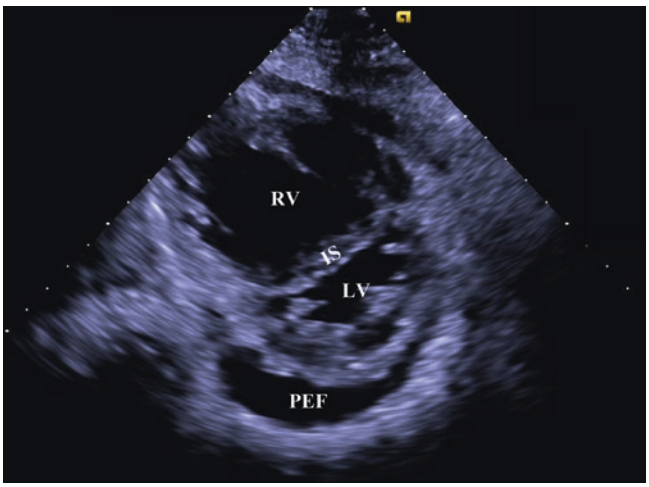

Fig. 16.7 The parasternal short axis view in a patient with shortness of breath. The right ventricle (RV) is dilated while the left ventricle (LV) appears smalls and hyperdynamic. The interventricular septum (IS) is flattened making the left ventricle D-shaped instead of the normal round shape. Pericardial effusion (PEF) is also seen. This patient has pulmonary hypertension with right ventricular failure. See also Video 16.4

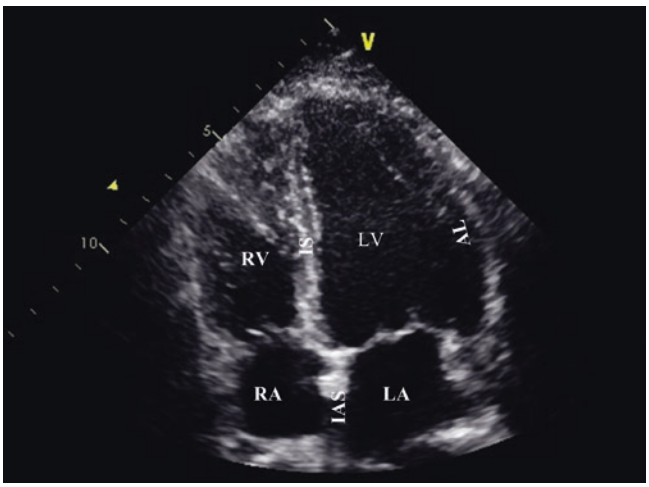

Fig. 16.9 Apical four-chamber view. The left ventricle (LV), right ventricle (RV), interventricular septum (IS) and the anterolateral wall (AL) of the left ventricle, left atrium (LA), right atrium (RA) and interatrial septum (IAS) are seen. Adequate visualization of the apex is essential for correct estimation of the left ventricular ejection fraction. Apical foreshortening may result in overestimation of the ejection fraction. See also Video 16.5

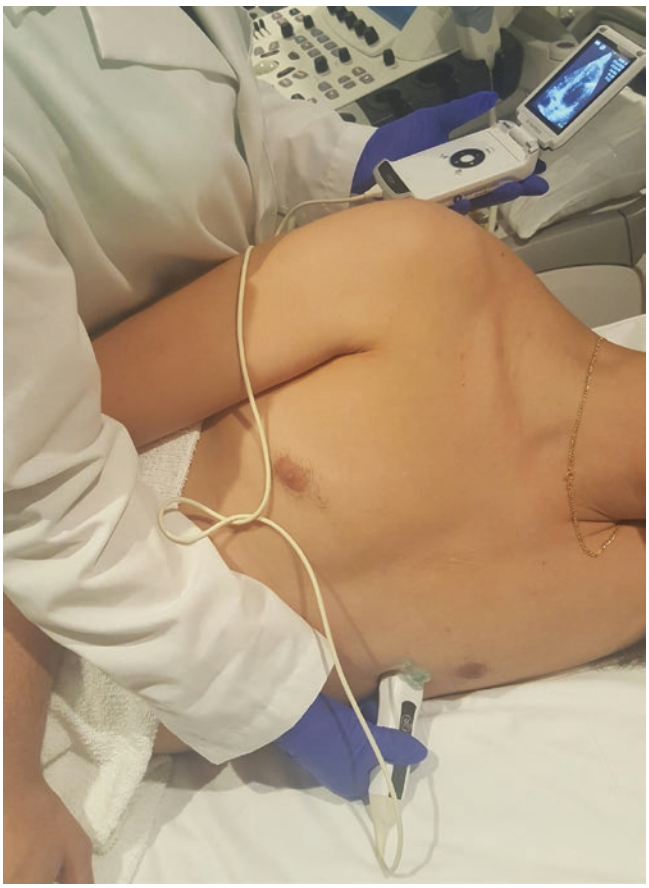

Fig. 16.8 Obtaining apical four-chamber view using handheld ultrasound device. The patient is positioned on the left side to optimize the imaging. The transducer is placed in the apical position with the probe marker turned toward the patient's left. Rotation of the transducer from this position allows the examiner to obtain the two-chamber and apical long axis views but these require more advanced examination skills and may not be practical for routine point-of-care cardiac ultrasound

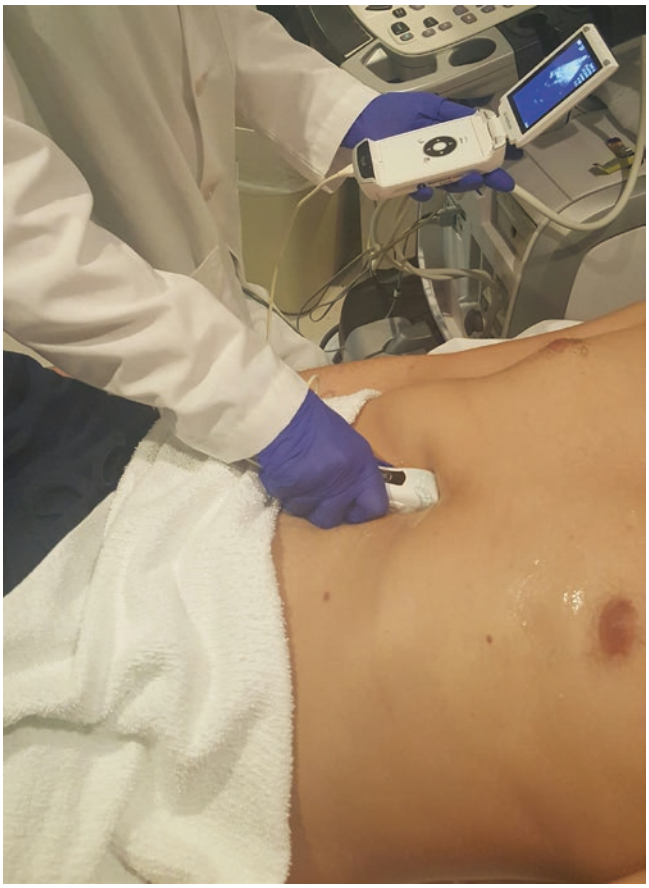

Fig. 16.10 Obtaining subcostal views using handheld ultrasound device. The patient is positioned supine and the transducer is placed under the xiphoid process. Bending patient's knees may help with imaging. From subcostal position, the four-chamber view can be obtained. Short axis planes can also be obtained by rotating the transducer and the inferior vena cava can be interrogated. These views can be especially helpful in settings when the standard parasternal and apical views are technically difficult, such as in patients with advanced obstructive lung disease or intubated patients on mechanical ventilation

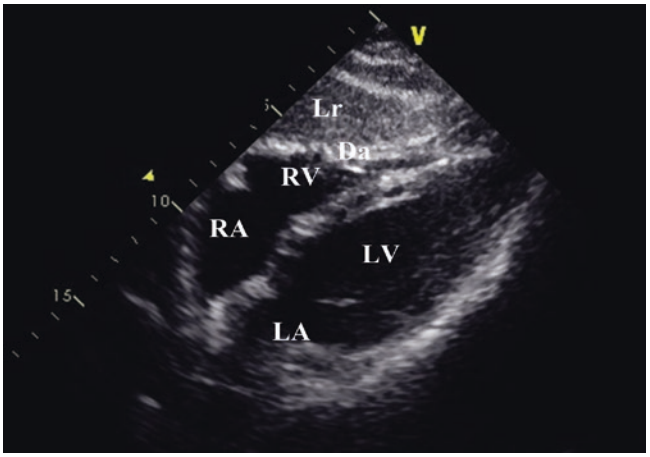

Fig. 16.11 Subcostal four-chamber view. The liver (Lr) and the bright line of diaphragm (Da) are seen. The right heart, including right ventricle (RV) and right atrium (RA) are closer to the transducer in this view, while the left ventricle (LV) and left atrium (LA) are in the far field. See also Video 16.6

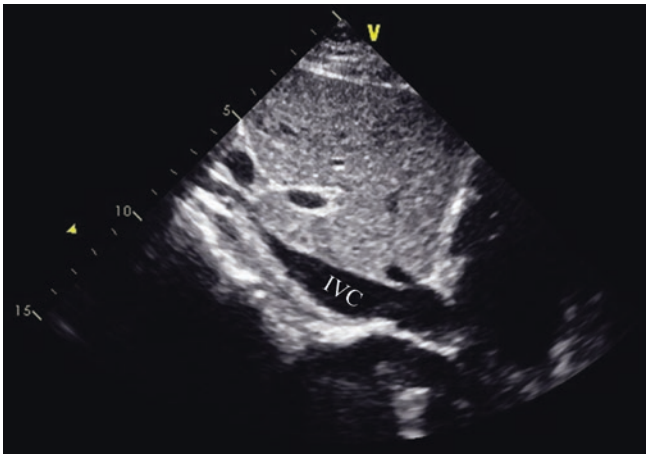

Fig. 16.13 Inferior vena cava assessment. The inferior vena cava (IVC) is seen in the subcostal view. The diameter of the inferior vena cava and collapsibility with respiration (or a brief sniff) should be noted. See also Video 16.8

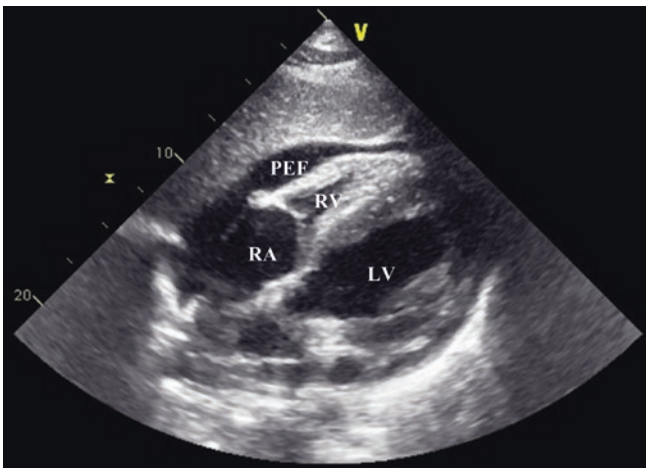

Fig. 16.12 Subcostal view in a patient with shortness of breath. The pericardial effusion (PEF) is seen as an echo-free space around the heart, most prominent over the diaphragm underlying the right ventricle (RV) and right atrium (RA). Also, systolic function of the left ventricle (LV) is reduced. This patient has systolic heart failure and pericardial effusion. See also Video 16.7

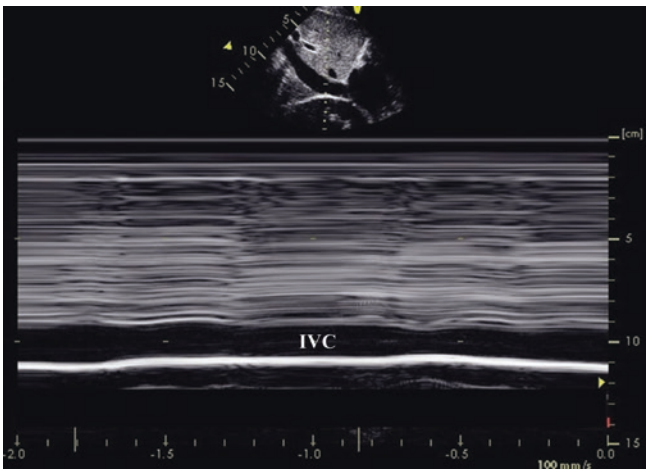

Fig. 16.14 Inferior vena cava assessment using M-mode echocardiography. M mode echocardiogram provides a single-slice view of the structures along the time axis. Due to very high temporal resolution, M mode is helpful in recording and measuring motion over time. It can supplement 2D echocardiogram if it is available on the ultrasound platform. The inferior vena cava (IVC) is seen on the M mode display; it demonstrates little variability in size/collapsibility during the recording

Table 16.1 Estimating right atrial pressure based on the inferior vena cava size (1–2 cm from right atrial junction) and collapsibility [4]

Inferior vena cava (IVC) size and collapsibility	Estimate of right atrial pressure
Dilated (>2.1 cm) and little collapsibility (<50%)	Elevated (10–20 mmHg)
Normal (<2.1 cm) but little collapsibility (<50%) Dilated (>2.1 cm) but collapsible (>50%)	Intermediate (5–10 mmHg)
Normal (<2.1 cm) and collapsible (>50%)	Normal/low (0–5 mmHg)

References

1. Arntfield RT, Millington SJ. Point of care cardiac ultrasound applications in the emergency department and intensive care unit--a review. Curr Cardiol Rev. 2012;8(2):98–108.
2. Martin LD, Howell EE, Ziegelstein RC, Martire C, Shapiro EP, Hellmann DB. Hospitalist performance of cardiac hand-carried ultrasound after focused training. Am J Med. 2007;120(11):1000–4.
3. Spencer KT, Kimura BJ, Korcarz CE, Pellikka PA, Rahko PS, Siegel RJ. Focused cardiac ultrasound: recommendations from the American Society of Echocardiography. J Am Soc Echocardiogr. 2013;26(6):567–81.
4. Lang RM, Badano LP, Mor-Avi V, Afilalo J, Armstrong A, Ernande L, et al. Recommendations for cardiac chamber quantification by echocardiography in adults: an update from the American Society of Echocardiography and the European Association of Cardiovascular Imaging. J Am Soc Echocardiogr. 2015;28(1):1–39.e14.

Assessment of Cardiac Function

17

Amer M. Johri

17.1 Introduction

Cardiac point-of-care ultrasound (POCUS) can be used to enhance the cardiac physical examination. POCUS of the heart may be useful in the assessment of ventricular systolic function, wall motion assessment, and disease states such as cardiomyopathy and pulmonary embolism [1]. In general, views obtained by POCUS are not meant to provide precise and accurate quantitative information such as a quantified ejection fraction, pulmonary artery systolic pressure, and diastolic parameters; they can, however, provide an overall visual estimation of the severity of systolic dysfunction as well as be the initial screen for wall motion abnormality or cardiomyopathy. In this chapter, the initial views to obtain an assessment of ventricular function are introduced. It is critical for the operator to understand the need for adequate scanning training (hands-on image acquisition) and ongoing quality control to avoid false positive diagnosis [2]. As wall motion assessment is the most difficult skill in echocardiography, a skilled POCUS operator understands the limitations of her cardiac scan, and possesses the experience to know when formal echocardiography is indicated.

17.2 Scanning Technique

The parasternal long axis (PLAX) view is the initial view recommended to assess ventricular function (Video 17.1a). In the PLAX, the functioning of the basal and mid left ventricle is visualized. This view is optimal when the apex is not seen; however, both the mitral and aortic valves are visualized (Fig. 17.1a). The longest axis of the left ventricle is visualized to avoid foreshortening. In this view, myocardial contraction of the anteroseptal region of the left ventricle and the basal posterior wall can be visually assessed (Video 17.1a). The change in size of the cavity from systole and diastole can be appreciated. Following training, severe impairment can be discerned from a normal functioning or a hyperdynamic ventricle. With further training and experience, mild or moderate impairment of systolic function may be determined. A quantitative ejection fraction (using Simpson's method of discs, for example) is not recommended unless performed by a trained sonographer or operator [3].

The parasternal long axis view additionally allows for determination of the right ventricular size, again by visual

Electronic Supplementary Material The online version of this chapter (https://doi.org/10.1007/978-3-319-73855-0_17) contains supplementary material, which is available to authorized users.

A. M. Johri, M.D., M.Sc., F.R.C.P.C.
Department of Medicine, Division of Cardiology,
Kingston General Hospital, Kingston, ON, Canada

B. P. Nelson et al. (eds.), *Atlas of Handheld Ultrasound*, https://doi.org/10.1007/978-3-319-73855-0_17

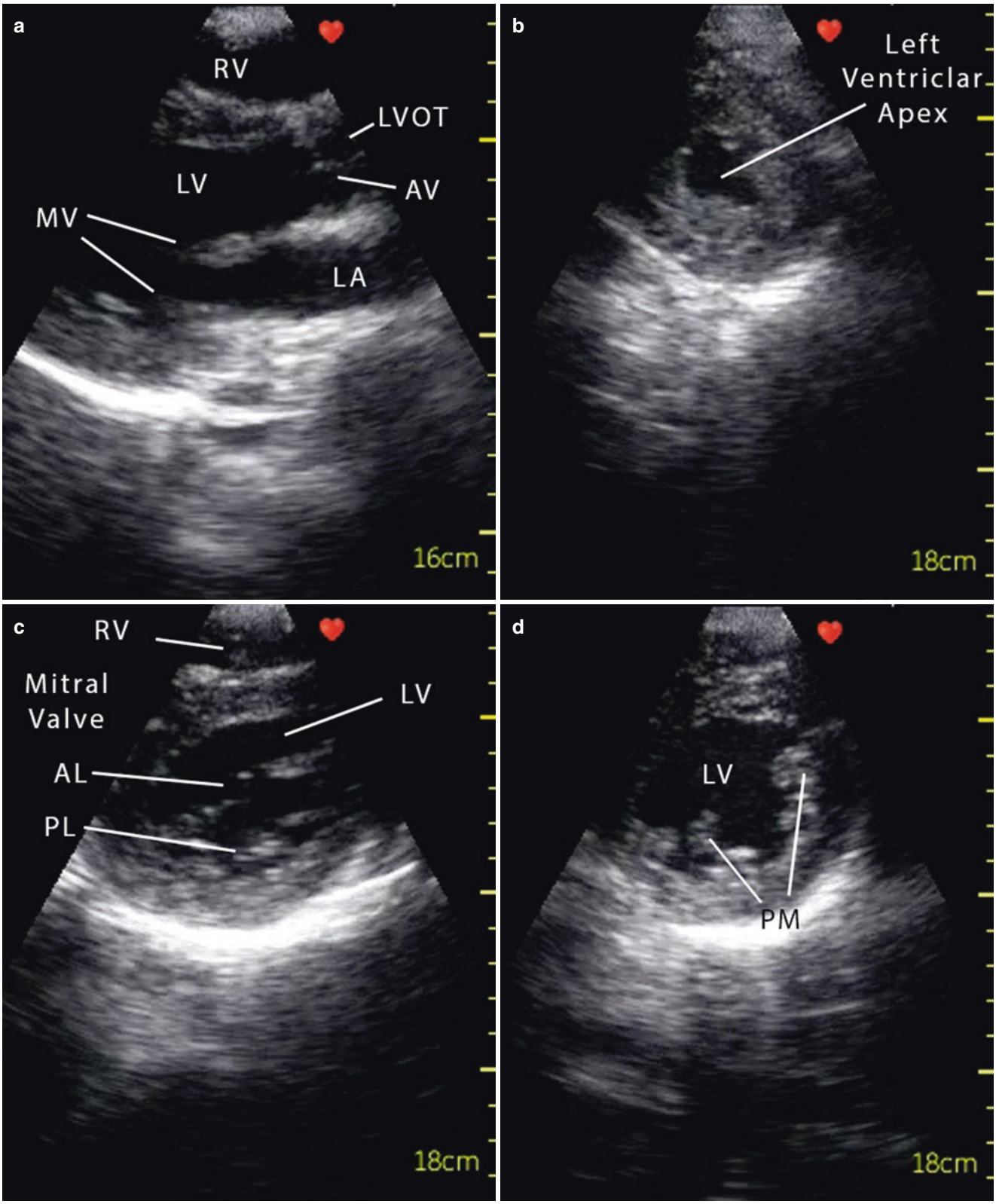

Fig. 17.1 (**a**) Parasternal long axis (PLAX) view of the left ventricle (LV). *RV* right ventricle, *LVOT* left ventricular outflow tract, *LA* left atrium, *MV* mitral valve. (**b**) Parasternal short axis view of the left ventricle, apical region. (**c**) Parasternal short axis view of the left ventricle, mitral leaflet level (base of the heart). *LV* left ventricle, *RV* right ventricle, *AL* anterior leaflet, *PL* posterior leaflet. (**d**) Parasternal short axis view of the left ventricle, papillary level (mid region of the left ventricle). *LV* left ventricle, *PM* papillary muscles. (**e**) Four chamber view of the heart. *LV* left ventricle, *LA* left atrium, *RV* right ventricle, *RA* right atrium, *MV* mitral valve, *TV* tricuspid valve. (**f**) Two chamber view of the heart. *LV* left ventricle, *LA* left atrium, *MV* mitral valve

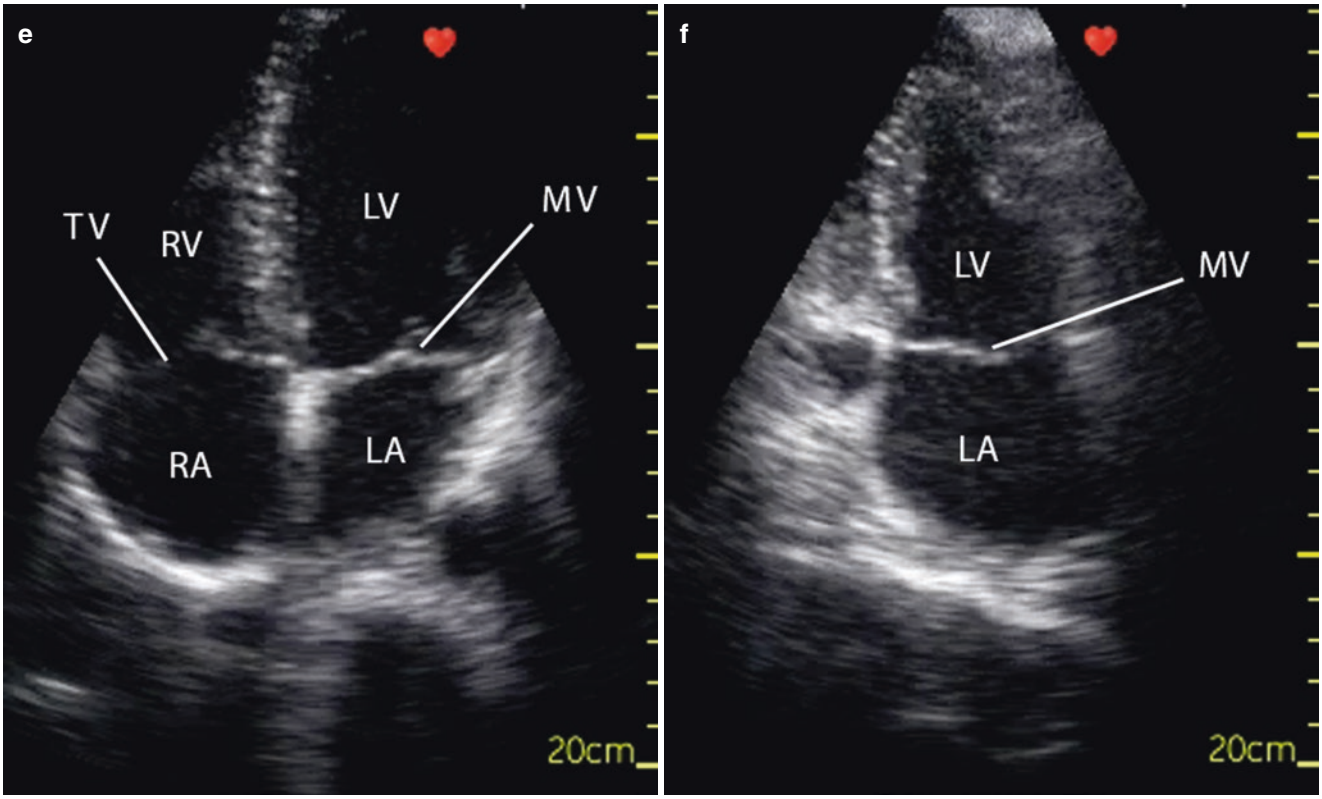

Fig. 17.1 (continued)

estimation. Caution should be used to comment on right ventricular size and functioning from only this view, and it should be interpreted in context of the clinical situation and multiple other views of the right ventricle.

The parasternal short axis (PSAX) view is the next view recommended to assess ventricular function, and follows immediately from the PLAX, often from the same rib space, but with clockwise probe rotation (Video 17.1b). Following this initial rotation, the base of the left ventricle and the mitral valve enface are seen. Angulation of the tail of the probe toward the patient's right shoulder allows scanning from the base to the mid and apical portion of the left ventricular cavity in short axis (Fig. 17.1b). This view allows visual assessment of ventricular wall thickness and contraction, and can also help determine the presence of a wall motion abnormality at the apex (Fig. 17.1b), base of the heart (Fig. 17.1c), or mid portion of the ventricle (Fig. 17.1d).

The next views for assessment of ventricular chambers occur from the apical window (Video 17.1c). In this view, the four-chamber is produced demonstrating the septal, apical, and lateral walls of the left ventricle, as well as the septal and lateral walls of the right ventricle (Fig. 17.1e). Foreshortening needs to be avoided so that the longest axis into the apical tip of the left ventricle is produced, rather than a "rounded" left ventricular apex. This view again is helpful for the assessment of myocardial contraction, thickness, and wall motion, as well as cavity size. The right ventricular lateral wall is often difficult to visualize due to lung artefact and body habitus, but can be sought following off-axis imaging (Video 17.1c).

Rotation of the probe in a counter-clockwise motion produces the two-chamber view of the left ventricle, demonstrating the inferior and anterior walls of this chamber (Fig. 17.1f).

17.3 Common Pathology

17.3.1 The Left Ventricle

17.3.1.1 Ischemic Heart Disease

The mismatch between myocardial demand and coronary artery supply may manifest as a wall motion abnormality (hypokinesis or akinesis) detected by cardiac ultrasound. However, the assessment of wall motion abnormality is one of the most difficult skills in echocardiography and is associated with important inter-observer variability [4]. POCUS of the heart may allow detection of global or regional impairment of systolic function, but it is limited to providing a visual estimate of the range of impairment rather than providing a quantified ejection fraction. Generally, the degree of impaired systolic function could be categorized as mild, moderate, or severe, after the operator gains sufficient experience. Regionality of wall motion abnormality may also be detected. The operator must recognize that systolic dysfunction can easily be missed; if it is not detected, this could be a reflection of the operator's experience or skill rather than the absence of a finding. Videos 17.2a and 17.2b demonstrate a large, easily seen anteroseptal wall motion abnormality in a patient presenting with chest pain (Fig. 17.2). The remaining segments of the left ventricle are relatively hyperdynamic. In this case, the patient presented with chest pain, was diagnosed to have a myocardial infarction, and upon angiography had a flow-limiting lesion in the left anterior descending coronary artery.

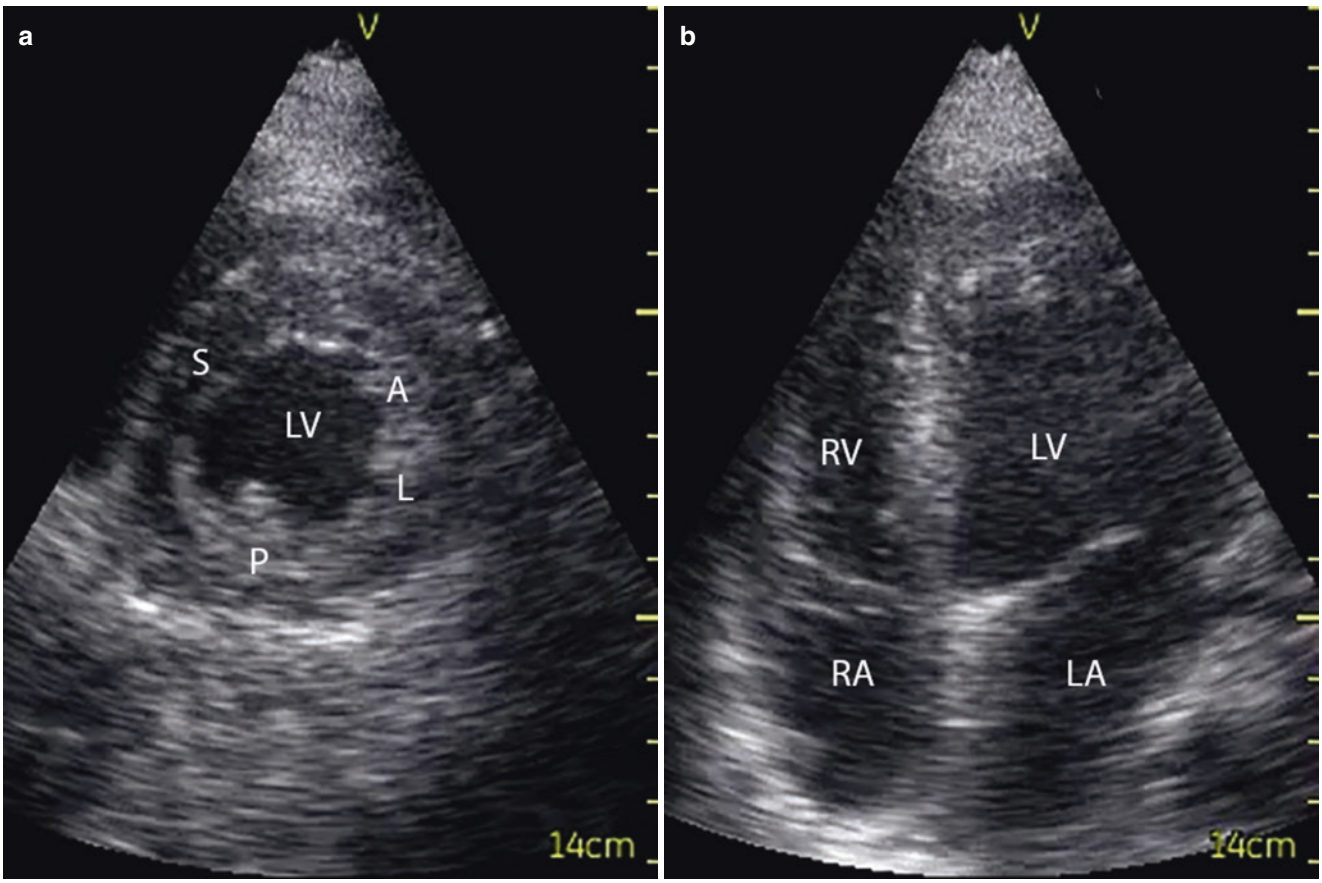

Fig. 17.2 (**a**) Still image of the parasternal short axis to demonstrate anatomic landmarks in Video 17.2a (*LV* left ventricle, *A* anterior, *L* lateral, *P* posterior, *S* septal). (**b**) Still image of the four-chamber view of the heart in Video 17.2b. *LV* left ventricle, *RV* right ventricle, *LA* left atrium, *RA* right atrium

17.3.1.2 Dilated Cardiomyopathy

Dilated cardiomyopathy may also be caused by ischemic heart disease, among other etiologies (including tachycardia, arrhythmia, drugs/toxins, and immune and inflammatory diseases). Although left ventricular dimensions may not be possible to ascertain with some ultrasound devices applied at the bedside, an obviously dilated left ventricle, as seen in Videos 17.3a and 17.3b (see also Fig. 17.3a, b) could be detected. This young woman presented with dyspnea to the emergency department one week post-partum. Although measurements were not made, the systolic function was visually estimated as severely impaired, and a severely enlarged ventricular cavity was noted precipitating rapid admission and urgent formal transthoracic echocardiography. In this case, application of POCUS assisted in the triage of the patient and helped recognize the acuity of her condition early.

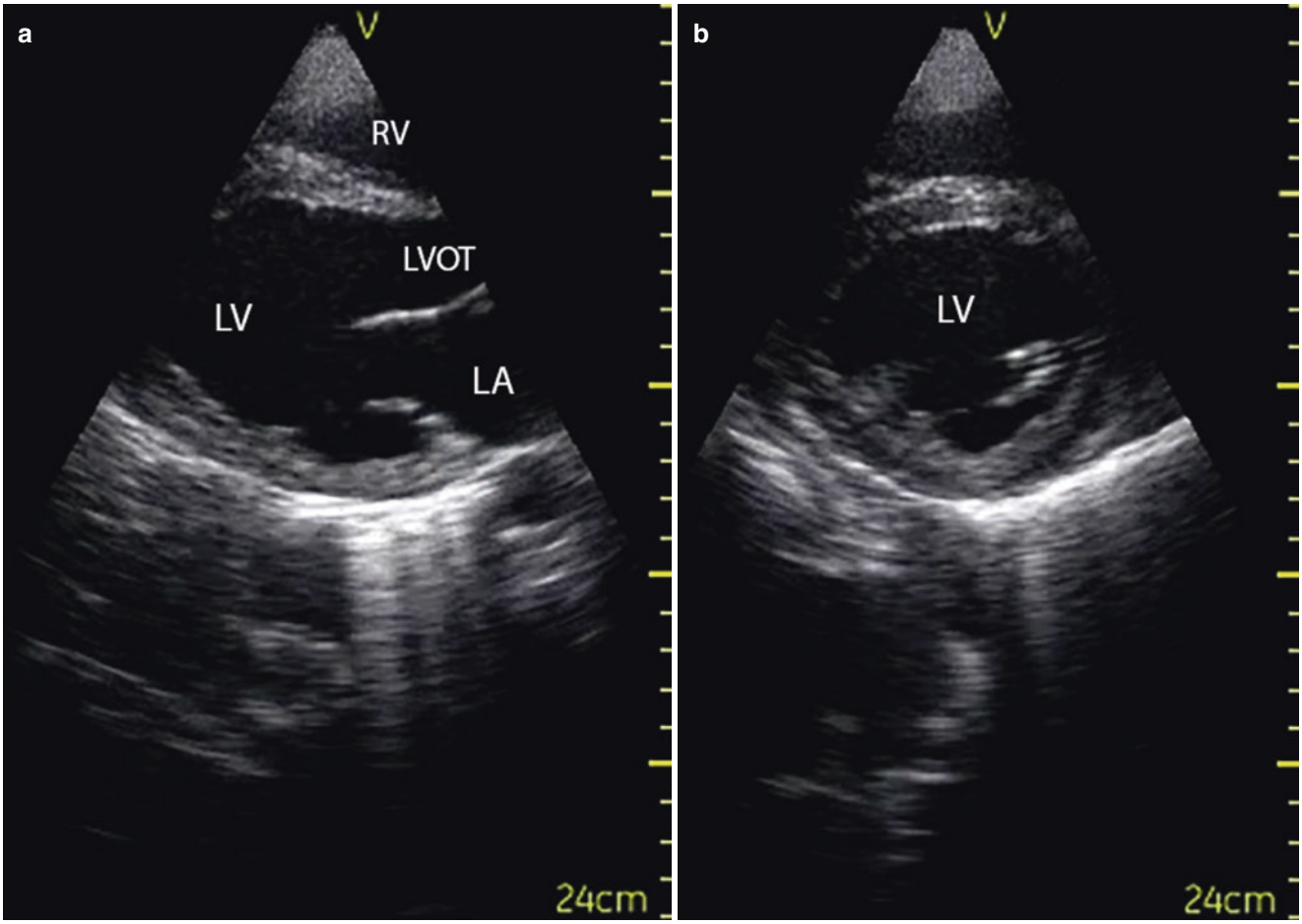

Fig. 17.3 (**a**) Still image of the parasternal long axis to demonstrate anatomic landmarks in Video 17.3a (*LV* left ventricle, *RV* right ventricle, *LVOT* left ventricular outflow tract, *LA* left atrium). (**b**) Still image of the parasternal short axis to demonstrate anatomic landmarks in Video 17.3b (*LV* left ventricle)

17.3.1.3 Hypertrophic Cardiomyopathy

Hypertrophic cardiomyopathy (HCM) is challenging to diagnose because the finding of left ventricular hypertrophy (LVH) is non-specific. Other causes of LVH include aortic stenosis, hypertension, and athlete's heart. Generally LVH, due to causes other than HCM, may appear as global hypertrophy of the ventricle. Thickening of only a discrete segment of the left ventricle may represent a variant of HCM such as apical HCM or asymmetric septal hypertrophy. However, even this finding is non-specific. For example, Videos 17.4a and 17.4b (see also Fig. 17.4a, b) are images of septal hypertrophy of the left ventricle initially thought to be hypertrophic cardiomyopathy. Such a finding in a young athlete can have a profound impact on an athlete's career if further participation in competitive sports had been prohibited. This patient was further investigated by transthoracic echocardiography, and following cardiology consultation, was fortunately diagnosed with athlete's heart instead of HCM.

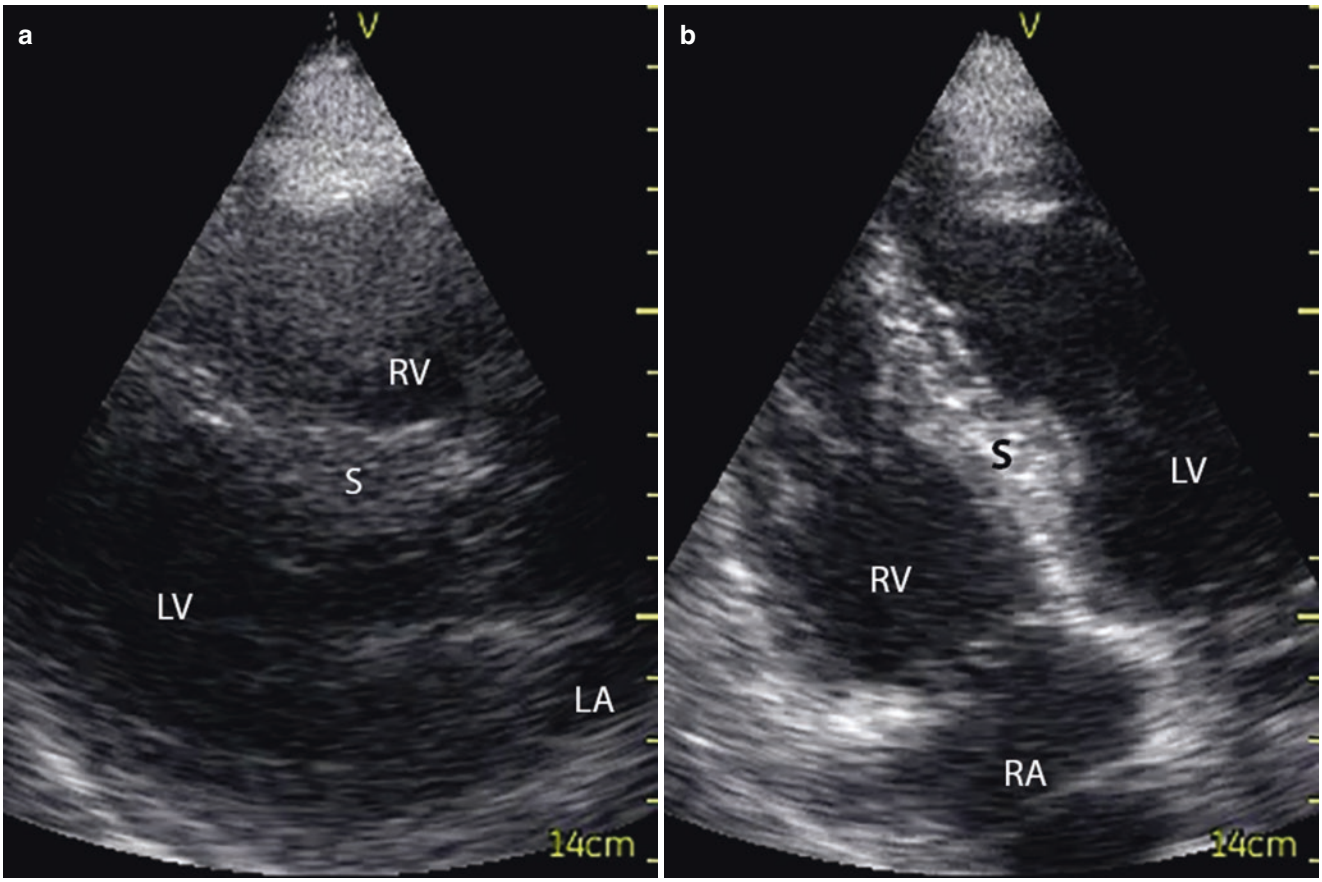

Fig. 17.4 (**a**) Still image of the parasternal long axis to demonstrate anatomic landmarks in Video 17.4a (*LV* left ventricle, *RV* right ventricle, *S* septum LVOT, *LA* left atrium). (**b**) Still image of the four-chamber view of the heart in Video 17.4b. *S* septum, *LV* left ventricle, *RV* right ventricle, *RA* right atrium

17.3.1.4 Restrictive Cardiomyopathy

Restrictive cardiomyopathy is commonly caused by infiltrative disease and can be a challenge to diagnose in the early stages. An important cause of restrictive cardiomyopathy is cardiac amyloid, which can be characterized by severe diastolic dysfunction, relatively normal systolic function depending on the stage of disease, valvular and ventricular thickening, and atrial enlargement. These findings are nonspecific but when present together may point to this diagnosis. Videos 17.5a, 17.5b, 17.5c, and 17.5d; and Fig. 17.5a–e demonstrate POCUS of a patient with cardiac amyloid past the early stages of disease. The ventricle is severely thickened and systolic function is noted to appear normal. Diastolic parameters are generally not conducted on a bedside scan by POCUS operators, but would be consistent with severe filling impairment by formal TTE. The right ventricle is severely thickened in this example as well. Also noted in this video are inferior vena cava plethora, valvular thickening, and atrial enlargement, assessment of which is described elsewhere in this book.

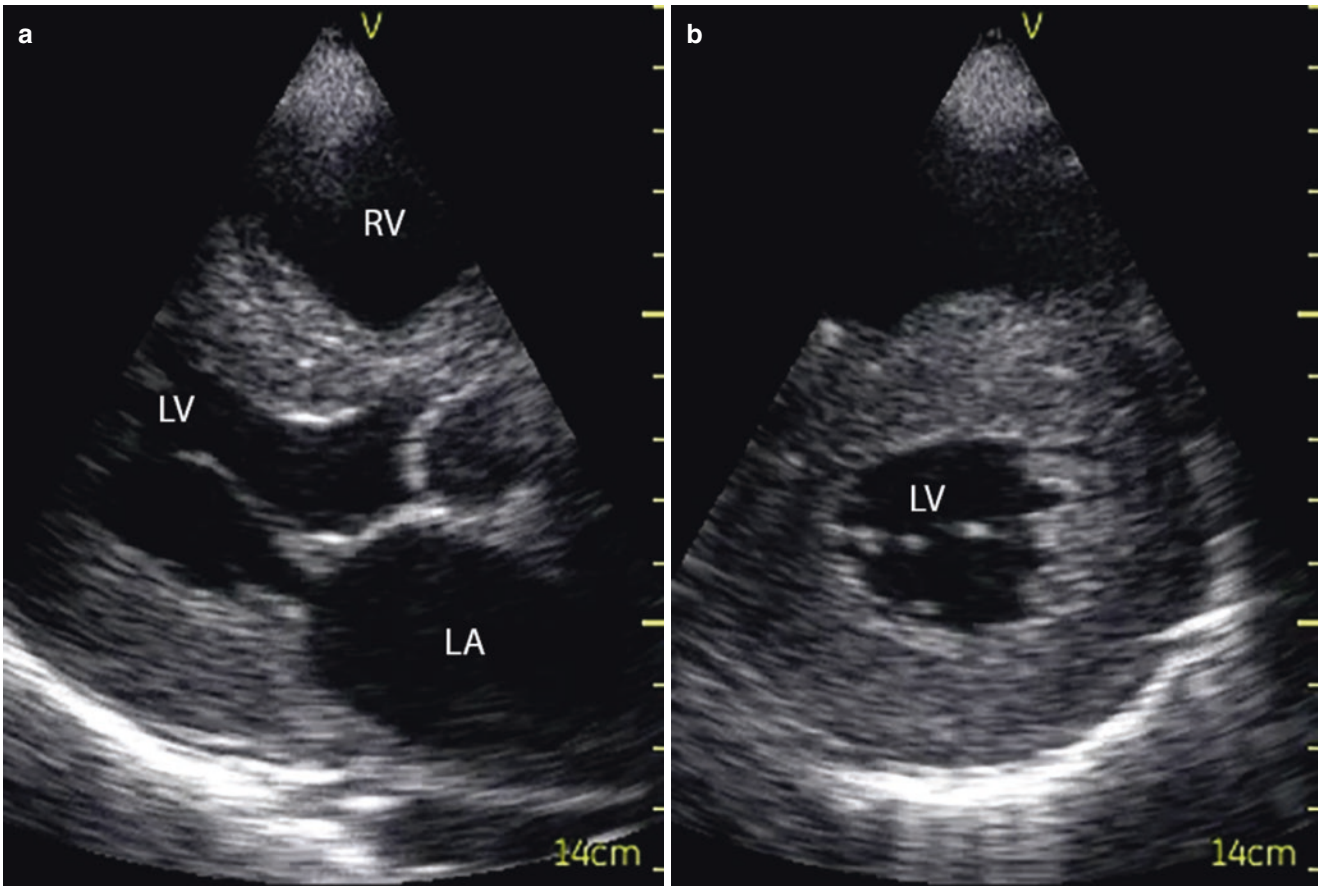

Fig. 17.5 (**a**) Parasternal long axis demonstrating a restrictive cardiomyopathy due to amyloid *LV* left ventricle, *RV* right ventricle, *LA* left atrium. (**b**) Parasternal short axis view of the left ventricle demonstrating ventricular wall thickening due to amyloid (*LV* left ventricle). (**c**) Subcostal view of the heart demonstrating restrictive cardiomyopathy, thickening of chamber walls. *LV* left ventricle, *RV* right ventricle, *LA* left atrium, *RA* right atrium. (**d**) Subcostal view demonstrating inferior vena cava (IVC) plethora. (**e**) Four-chamber view with focus on left ventricle demonstrating wall thickening due to amyloid. *LV* left ventricle, *LA* left atrium

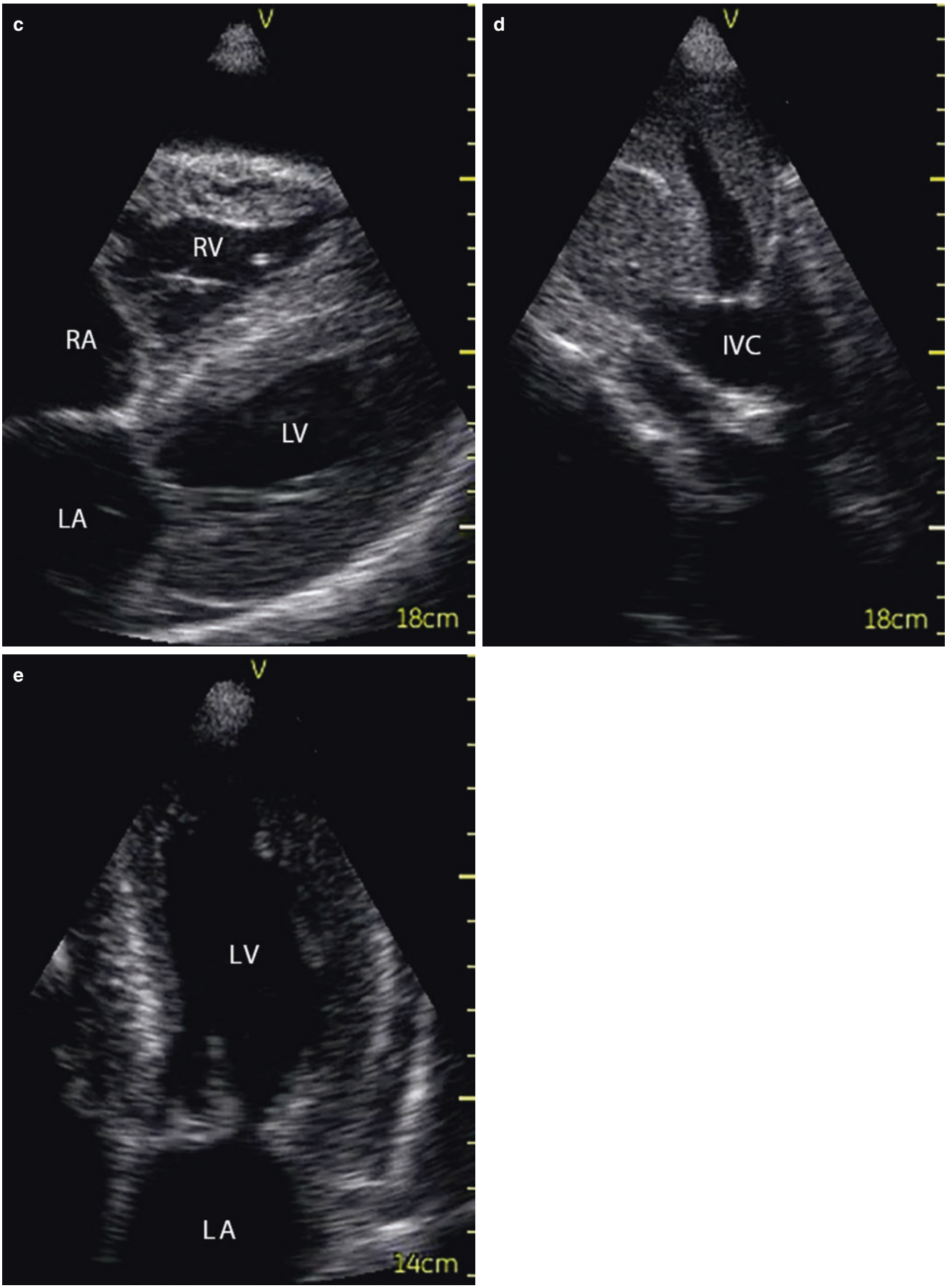

Fig. 17.5 (continued)

17.4 The Right Ventricle

17.4.1 Pulmonary Hypertension: Pulmonary Embolism/Right ventricular Dysfunction

POCUS is helpful in the diagnosis of right ventricular dysfunction, especially when a patient may be presenting with acute symptoms of pulmonary embolism. The presenting complaint of dyspnea may be further differentiated by POCUS if right ventricular dysfunction is noted. For example, a patient presented to the clinic with sudden onset of dyspnea, and was found to have a severely enlarged, hypokinetic right ventricle (Videos 17.6a and 17.6b). This finding precipitated an urgent echocardiogram followed by a CTPA confirming a pulmonary embolism. The main finding in the POCUS is the right ventricular size and function; the right ventricle is a highly challenging to scan even by skilled sonographers. Using formal echocardiography, pulmonary artery systolic pressure (PASP) can be calculated from the velocity of the tricuspid regurgitant jet. PASP calculation is not estimated by the POCUS operator because of known variability in the input of the various parameters required to calculate the estimate, nor is POCUS used for serial monitoring of pulmonary hypertension patients (Fig. 17.6).

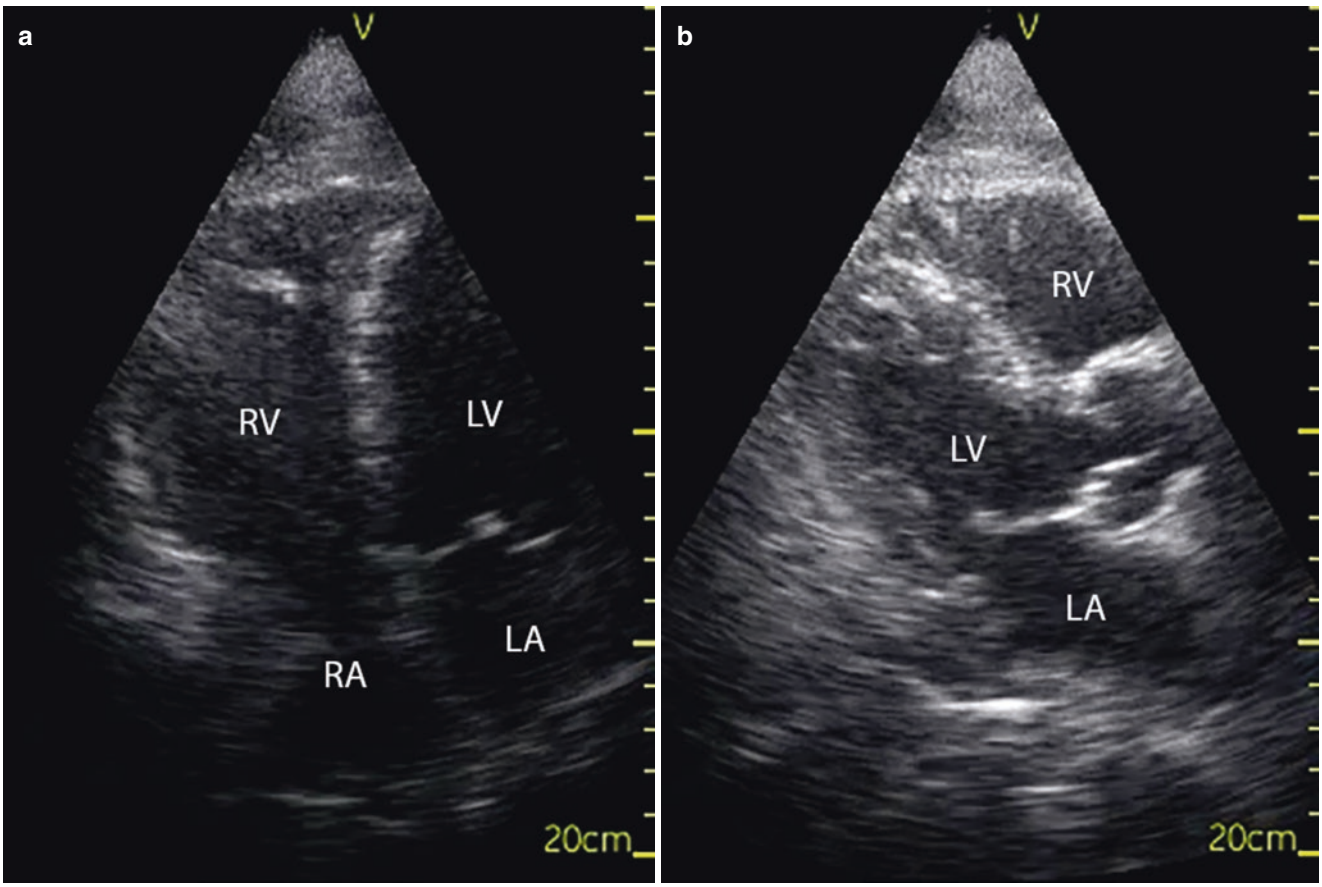

Fig. 17.6 (**a**) Four chamber view demonstrating right ventricular enlargement and impaired systolic function. (**b**) Parasternal long axis view demonstrating enlarged, hypokinetic right ventricle

Acknowledgments All videos courtesy of Atul Jaidka, MD.

Appendix

Patient positioning (Video 17.1d).

References

1. Meloche J. Use of POCUS for assessment of dyspnea in the Emergency Department. POCUS J. 2016;1:2.
2. Wilkinson JS, Barake W, Smith C, Thakrar A, Johri AM. Limitations of condensed teaching strategies to develop hand-held cardiac ultrasonography skills in internal medicine residents. Can J Cardiol. 2016;32(8):1034–7.
3. Spencer KT, Kimura BJ, Korcarz CE, Pellikka PA, Rahko PS, Siegel RJ. Focused cardiac ultrasound: recommendations from the American Society of Echocardiography. J Am Soc Echocardiogr. 2013;26(6):567–81.
4. Johri AM, Picard MH, Newell J, Marshall JE, King ME, Hung J. Can a teaching intervention reduce interobserver variability in LVEF assessment: a quality control exercise in the echocardiography lab. JACC Cardiovasc Imaging. 2011;4(8):821–9.

Pericardial Effusion and Tamponade

18

Edgar Argulian and Jagat Narula

18.1 Introduction

Pericardial effusion is a relatively common finding in high-risk patients evaluated in the emergency department [1]. It should be considered in differential diagnosis for patients with different clinical presentations such as shortness of breath, chest pain, and hypotension [2]. Physical examination alone may not be very accurate in identifying patients with cardiac tamponade and point-of-care ultrasound has been shown to be a very useful clinical tool [3]. Pericardial effusion is easily identified by ultrasound examination. Hemodynamic significance of the effusion can be assessed by a set of additional findings such as chamber collapse, flow variation across the atrioventricular valves, and inferior vena cava engorgement. These require good understanding of tamponade physiology, training in spectral Doppler and M-mode echocardiography, and advanced examination skills.

Assessment for pericardial effusion and tamponade is best done utilizing multiple cardiac views. Thus, hypotheses about potential pathology can be confirmed or refuted from different angles (Figs. 18.1, 18.2, 18.3, 18.4, 18.5, 18.6, 18.7, 18.9, and 18.10; Videos 18.1, 18.2, 18.3, 18.4, 18.5, and 18.6). Common pitfalls and caveats in evaluating pericardial effusion and tamponade ae summarized in Table 18.1.

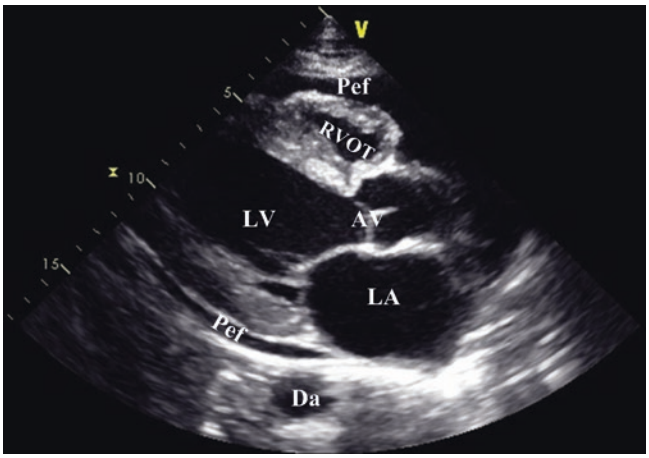

Fig. 18.1 Pericardial effusion in the parasternal long axis view. In this view, the left atrium (LA), left ventricle (LV), right ventricular outflow tract (RVOT) and aortic valve (AV) are seen. Left ventricular ejection fraction is reduced. Pericardial effusion (Pef) appears as an echo free space around the heart, both anteriorly and posteriorly. Descending aorta (DA) allows differentiation of pericardial effusion from left pleural effusion: it is seen behind the echo bright pericardium. See also Video 18.1

Electronic Supplementary Material The online version of this chapter (https://doi.org/10.1007/978-3-319-73855-0_18) contains supplementary material, which is available to authorized users.

E. Argulian, M.D., M.P.H. (✉)
Mount Sinai St. Luke's Hospital,
Icahn School of Medicine at Mount Sinai, New York, NY, USA
e-mail: Edgar.Argulian@mountsinai.org

J. Narula, M.D., Ph.D.
Mount Sinai Hospital, Icahn School of Medicine at Mount Sinai,
New York, NY, USA

B. P. Nelson et al. (eds.), *Atlas of Handheld Ultrasound*, https://doi.org/10.1007/978-3-319-73855-0_18

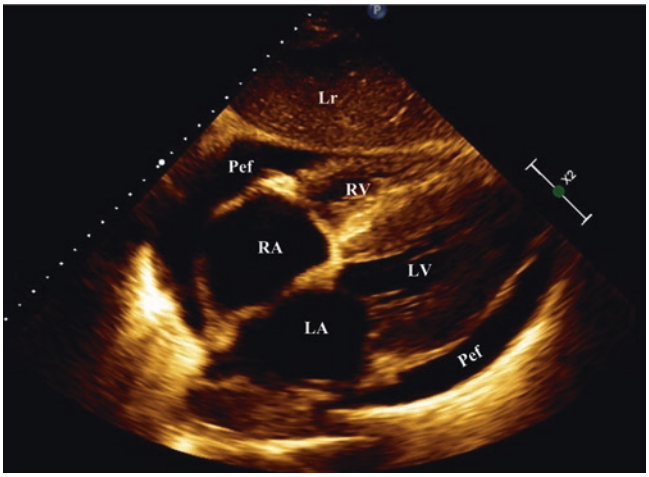

Fig. 18.2 Pericardial effusion in the subcostal view. In this view, the right ventricle (RV) and right atrium (RA) are closer to the transducer, while the left ventricle (LV) and left atrium (LA) are in the far field. Pericardial effusion (Pef) appears as an echo free space around the heart, both along the diaphragm above the liver (Lr) and along the lateral wall of the left ventricle. See also Video 18.2

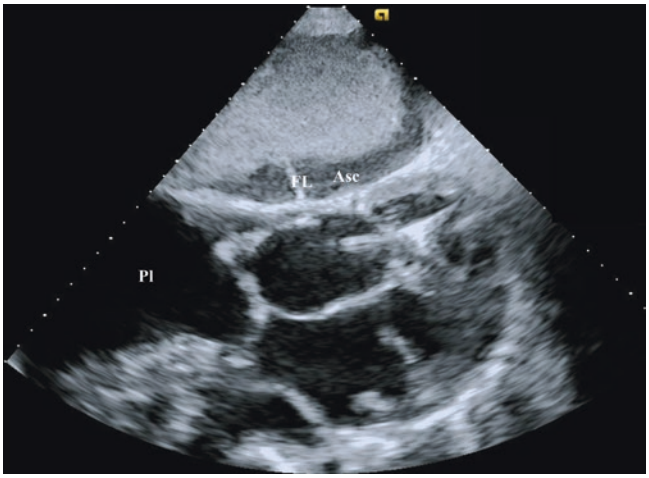

Fig. 18.4 Ascites and right pleural effusion in the subcostal view. This patient with biventricular dysfunction has anasarca. Ascites (Asc) is seen as an echo free space below the diaphragm; one can also identify the falciform ligament (FL). Right pleural effusion (Pl) is seen as an echo free space above the diaphragm. The highly echogenic implantable defibrillator lead is seen in the right ventricle. See also Video 18.4

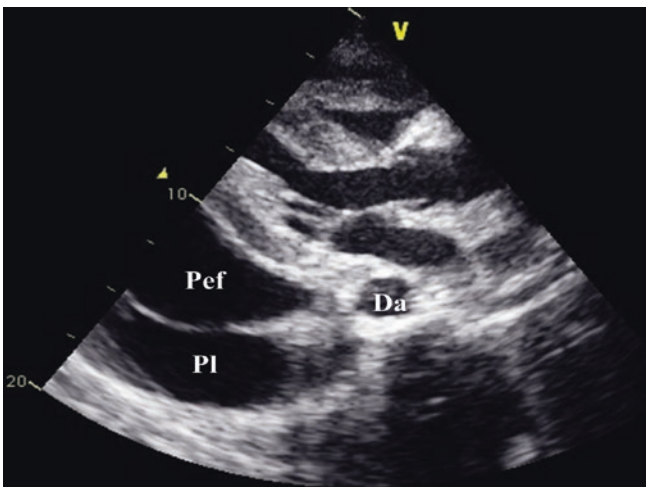

Fig. 18.3 Pericardial effusion and pleural effusion in the parasternal long axis view. Pericardial effusion can occasionally be confused with left pleural effusion, right pleural effusion, ascites, and pericardial fat. In this patient, a large pericardial effusion (Pef) is seen as an echo free space behind the inferolateral wall of the left ventricle. Left pleural effusion (Pl) is also seen. Note the position of the descending aorta (Da) behind the bright line of the pericardium. See also Video 18.3

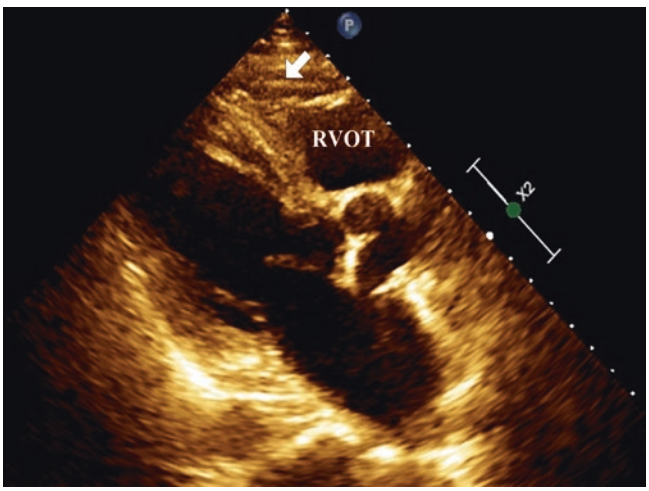

Fig. 18.5 Pericardial fat in the parasternal long axis view. Pericardial fat commonly appears as hypoechoic area overlying the right ventricular outflow tract (RVOT) in the parasternal long axis view. It should not be confused with pericardial effusion. The thin and bright line of the parietal pericardium is seen (*arrow*) separating the anterior pericardial fat from posterior epicardial fat. See also Video 18.5

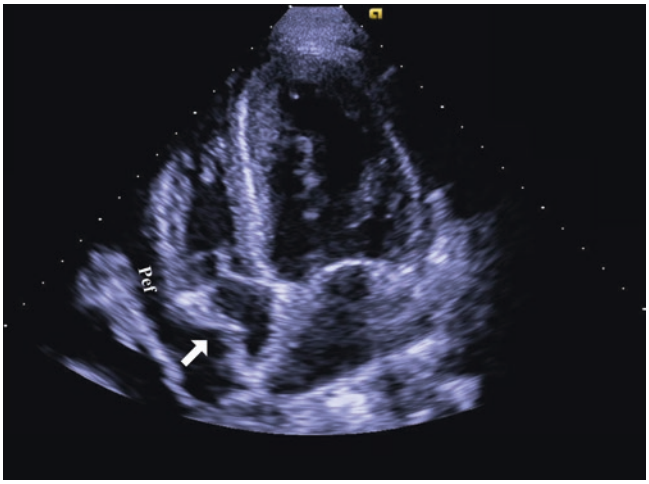

Fig. 18.6 Pericardial effusion with right atrial collapse. Pericardial effusion (Pef) is seen as echo free space around the right atrium and right ventricle. Right atrial collapse (*arrow*) is seen as the intrapericardial pressure transiently exceeds the right atrial pressure. Short-lived right atrial collapse is a non-specific finding. Sustained right atrial collapse lasting more than one-third of the cardiac cycle is more specific for cardiac tamponade. See also Video 18.6

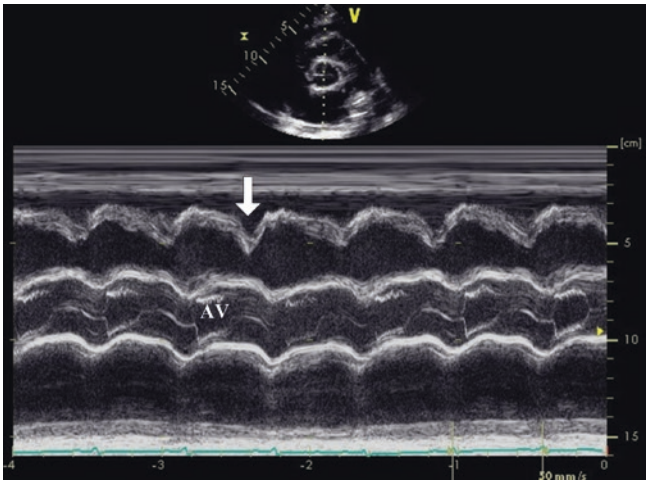

Fig. 18.7 Pericardial effusion with right ventricular collapse. Early diastolic right ventricular collapse has a high specificity for cardiac tamponade. M-mode is recorded in the short axis view through the right ventricular outflow tract and the aortic valve. Please note box-like opening of the aortic valve (AV) that helps to time the systole. Early diastolic collapse of the right ventricular outflow tract is marked by the *arrow*

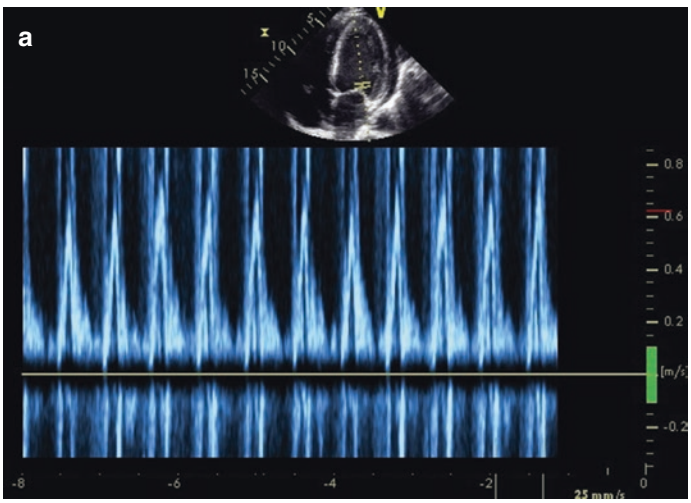

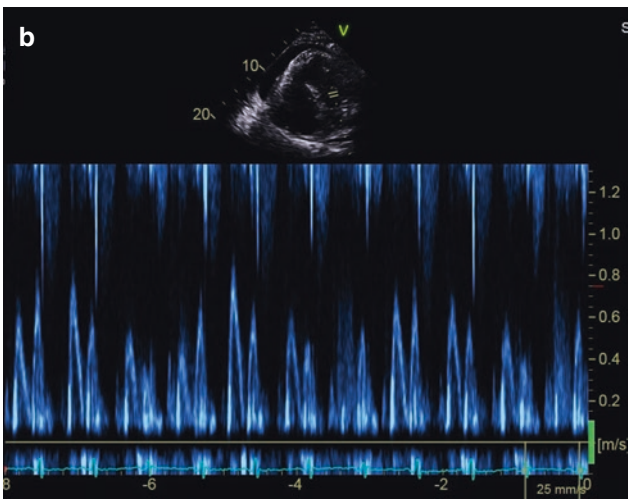

Fig. 18.8 Flow velocity variation across the mitral valve. Mitral inflow velocities can be recorded by pulse wave or continuous wave spectral Doppler. Doppler recording requires a proper cursor positioning, adequate scale and appropriate sweep speed. Normally and in patients with asymptomatic effusions, there is insignificant variation in flow velocities across the mitral valve (around 5%) related to inspiration: flow velocities increase with expiration and decrease with inspiration. Figure 18.8a demonstrates little variation of the mitral inflow velocities. In patients with tamponade, this variation is greatly exaggerated and typically exceeds 30% as seen in Fig. 18.8b. Due to ventricular interdependence similar changes can be recorded for tricuspid, aortic and pulmonary valve velocities in patients with cardiac tamponade

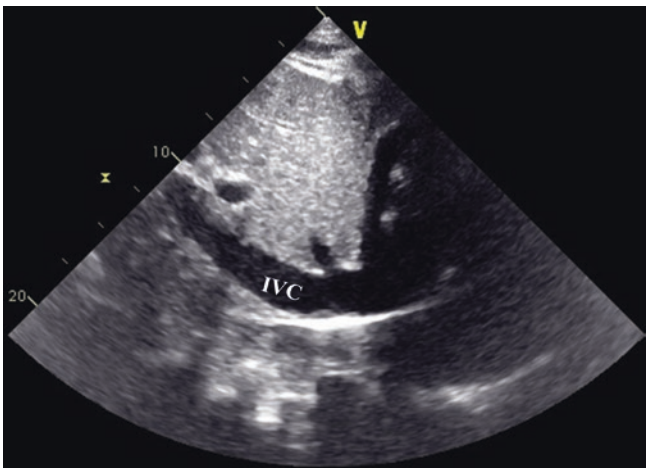

Fig. 18.9 Inferior vena cava and estimation of the right atrial pressure. Inferior vena cava (IVC) assessment is essential when evaluating a patient for cardiac tamponade. Dilated (>2.1 cm) inferior vena cava with little collapsibility (<50%) suggests elevated systemic venous pressures and it is a sensitive (but not specific) sign for pericardial tamponade. M-mode echocardiography can also be used to assist in documenting inferior vena cava size and collapsibility

Table 18.1 Selected caveats in evaluating pericardial effusion and tamponade [3, 4]

Caveats	Description
Correct identification of pericardial effusion	Pericardial effusion can be confused with pericardial fat and pleural effusion
Localized pericardial effusion	Pericardial effusion and/or clot after open heart surgery can be localized and cause specific heart chamber compression (regional tamponade)
Pulmonary hypertension	Significant pulmonary hypertension can mask right-sided chamber collapse
Hypertensive cardiac tamponade	27–43% of patients with tamponade are hypertensive upon presentation; hypertension does not rule out tamponade
Low-pressure cardiac tamponade	Inferior vena cava engorgement may not be present

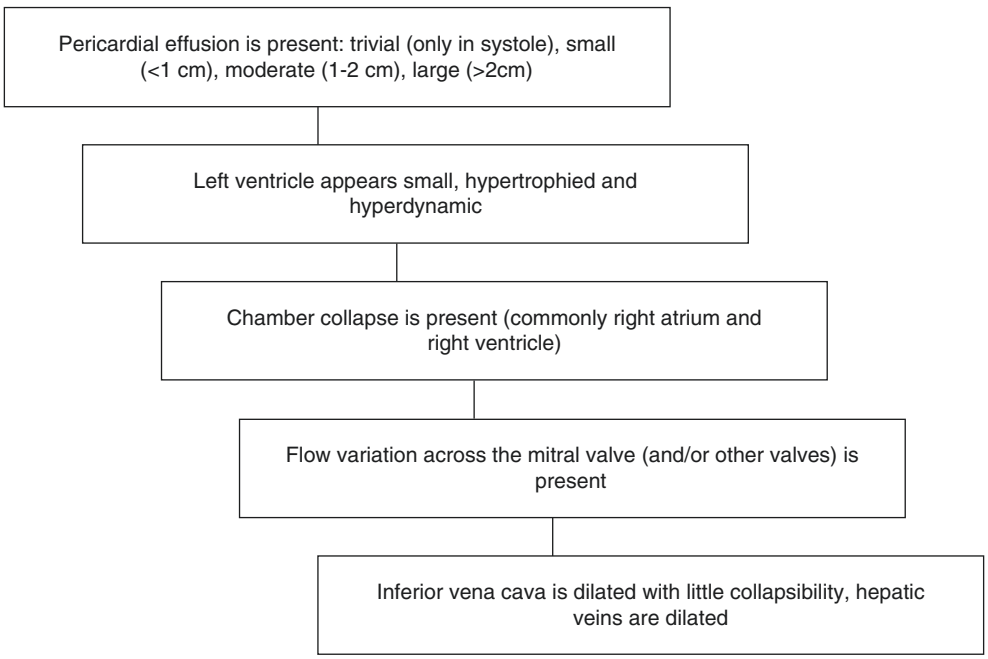

Fig. 18.10 Stepwise simplified approach to recognizing cardiac tamponade. Identification of all components requires proper understanding of pathophysiology as well as excellent ultrasound examination and interpretation skills. Diagnosing and sizing pericardial effusion is the essential initial step. The left ventricle commonly appears small and hyperdynamic. Chamber collapse indicates that the pericardial pressure transiently exceeding the intracardiac pressure; exact timing and duration of the collapse commonly requires M-mode echocardiography. Finally, elevated systemic venous pressures are indentified by engorged hepatic veins and inferior vena cava

Acknowledgments All images courtesy of Dr. Edgar Argulian.

References

1. Mandavia DP, Hoffner RJ, Mahaney K, Henderson SO. Bedside echocardiography by emergency physicians. Ann Emerg Med. 2001;38(4):377–82.
2. Arntfield RT, Millington SJ. Point of care cardiac ultrasound applications in the emergency department and intensive care unit--a review. Curr Cardiol Rev. 2012;8(2):98–108.
3. Argulian E, Messerli F. Misconceptions and facts about pericardial effusion and tamponade. Am J Med. 2013;126(10):858–61.
4. Argulian E, Herzog E, Halpern DG, Messerli FH. Paradoxical hypertension with cardiac tamponade. Am J Cardiol. 2012;110(7):1066–9.

Cardiac Masses

19

Kyle W. Klarich and Kevin Ka-Ho Kam

Echocardiography is an invaluable tool for cardiac structure evaluation. It is often the first imaging modality for assessing space-occupying masses in the heart. Point-of-care cardiovascular ultrasound has been increasingly used as an extension of the physical examination [1]. It allows non-invasive, real-time assessment of the heart at the bedside without the need for radiation [1]. Cardiac masses are considered to be benign in most circumstances. In fact, the majority of cardiac masses are discovered incidentally. However, some cardiac masses (such as left atrial myxoma) may lead to significant clinical consequences if left untreated. As a result, it is important to make a timely diagnosis, especially for those who are symptomatic (presenting with chest pain, syncope, or previous embolic events). Ultrasound allows for a detailed assessment of cardiac masses, including location (intracardiac vs. extracardiac), size, mobility, embolic potential, hemodynamic impact to surrounding structures, etc. Having gathered all this information, the physician may suggest further confirmatory testing such as transesophageal echocardiography, cardiac computer tomography or cardiac magnetic resonance imaging. However, if the cardiac mass appears to be complex and is difficult to assess by point-of-care ultrasound, a standard formal echocardiography with hemodynamic assessment should be pursued [2].

There are a wide variety of masses associated with each cardiac chamber; these can be differentiated by their location, sonographic appearance, and clinical history (Tables 19.1, 19.2, 19.3, and 19.4). Figures 19.1, 19.2, 19.3, 19.4, 19.5, 19.6, 19.7, 19.8, and 19.9 detail the typical appearance of some common cardiac masses.

K. W. Klarich, M.D. (✉)
Department of Cardiovascular Medicine, Mayo Clinic,
Rochester, MN, USA
e-mail: klarich.kyle@mayo.edu

K. Ka-Ho Kam, M.B., Ch.B.
Department of Medicine and Therapeutics,
Prince of Wales Hospital, The Chinese University of Hong Kong,
Hong Kong, China

B. P. Nelson et al. (eds.), *Atlas of Handheld Ultrasound*, https://doi.org/10.1007/978-3-319-73855-0_19

Table 19.1 Approach to RA mass by point-of-care ultrasound of heart

	Location	Size	Echocardiographic features	Additional Ix	Manifestation	DDx
Crista Terminalis	Posterior wall of RA	Variable	Muscular ridge connecting from IVC to SVC	3D Echo, TEE	Incidental finding, normal cardiac structure	Atrial tumor, atrial thrombus cor triatriatum dexter
Eustachian valve	Junction of posterior margin of IVC and RA	>2 cm	Free floating horizontal linear structure	TEE	Incidental finding, normal variant	Tricuspid valve endocarditis, flail tricuspid leaflets, DVT in-transit, tumor thrombus
Chiari network	Near the orifice of IVC	>5 cm	Free floating thin network-like structure	TEE	Incidental finding, normal variant	Tricuspid endocarditis, flail tricuspid leaflets, DVT in-transit, tumor thrombus
Atrial septal aneurysm	Bulging of interatrial septum towards RA	>1.5 cm beyond the plane of interatrial septum	Phasic excursion with respiration	TEE	Incidental finding, normal cardiac structure, may represent elevated RA pressure	Atrial tumor
Lipomatous hypertrophy	Within interatrial septum	1–2 cm	Dumbbell-shaped interatrial septum sparing fossa ovalis	TEE, MRI	Incidental finding, benign structure	Atrial tumor, atrial thrombus
Atrial thrombus	Arise from right atrial appendage	Variable	Mobile, irregular mass floating at RA	TEE	Present with cardioembolic events such as stroke, history of atrial fibrillation	Atrial tumor
Cor triatriatum dexter	Mid RA	Variable	Incomplete membrane dividing RA into upper and lower chambers	CT, TEE	May cause RV inflow obstruction	Crista Terminalis, atrial tumor, atrial thrombus
Atrial myxoma	Attach to interatrial septum	5–6 cm	Large globular intracavitary mass with a stalk attaching to interatrial septum, heterogeneous echogenicity	MRI, CT, TEE	Benign tumor, obstructive, embolic or systemic symptoms	Atrial tumor, atrial thrombus
Angiosarcoma	RA free wall	Variable	RA mural mass associates with haemopericardium	MRI, CT	Malignant tumor, right heart failure, cardiac tamponade	Atrial tumor, atrial thrombus
Lymphoma	RA free wall	Variable	RA mural mass with adjacent pericardial effusion	MRI, CT	Malignant tumor, B symptoms, lymphadenopathy on physical exam	Atrial tumor, atrial thrombus
Renal cell carcinoma	RA cavity with IVC involvement	Variable	Long slender structure floating at RA chamber	MRI, CT	Malignant tumor, may present with haematuria	Eustachian valve, Chiari's network, DVT in-transit
DVT in-transit	RA cavity +/– IVC involvement	Variable	Long slender structure floating at RA chamber	USG Doppler of lower limbs	Acute pulmonary embolism, may have dyspnea, chest pain, lower limb sweating, recent immobilization history	Eustachian valve, Chiari's network, renal cell carcinoma

Table 19.2 Approach to RV mass by Point-of-care ultrasound of heart

	Location	Size	Echocardiographic features	Additional Ix	Manifestation	DDx
Moderator band	Lower third of RV	Variable	Prominent muscular ridge extending from interventricular septum to right ventricular lateral wall, best seen in apical 4-chamber view	Nil	Incidental finding, normal cardiac structure	Right ventricular thrombus
Annular calcification	Tricuspid annulus	Variable	Circumscribed, echo-dense structure at the base of tricuspid valve leaflet	CT	Degenerative change, common in elderly and patients with chronic renal failure	Right atrial/ventricular thrombus, tricuspid endocarditis
Loeffler endomyocarditis	Right ventricular apex	2–3 cm	Right apical obliteration with thrombus, increase in myocardial thickness	Contrast echo, MRI	Present with heart failure symptoms, blood profile shows high eosinophil count	Right ventricular thrombus
Right ventricular thrombus	Anywhere in RV	Variable	Mobile echogenic mass floating at RV	Contrast echo, CT	Found in low output state such as right ventricular infarction or in acute pulmonary embolism	Loeffler's endomyocarditis
Papillary fibroelastoma	Attach to RV wall with a stalk	Variable	Highly mobile, homogeneous, relatively circular intracavitary mass	TEE	Incidental finding, may present with cardioembolic stroke	Atrial myxoma
Fibroma	Interventricular septum, RV free wall	3–10 cm	Usually solitary, associate with central calcification	MRI, CT	Benign tumor, rare among adult population, may cause RV outflow tract obstruction and arrhythmia	Rhabdomyoma
Rhabdomyoma	Anywhere in RV	Variable	Multiple nodular masses in several chambers of heart	MRI, CT	Benign tumor, very rare among adult population, may cause RV outflow tract obstruction, associate with tuberous sclerosis	Fibroma
Atrial myxoma	Attach to Interatrial septum	5–6 cm	Large globular mass with a stalk attaching to myocardium, heterogeneous echogenicity	MRI, CT, TEE	Benign tumor, obstructive, embolic or systemic symptoms	Papillary fibroelastoma

Table 19.3 Approach to LA mass by Point-of-care ultrasound of heart

	Location	Size	Echocardiographic features	Additional Ix	Manifestation	DDx
Atrial septal aneurysm	Bulging of interatrial septum towards LA	>1.5 cm beyond the plane of interatrial septum	Phasic excursion with respiration	TEE	Incidental finding, normal cardiac structure, may represent elevated LA pressure	Atrial tumor
Lipomatous hypertrophy	Within interatrial septum	1–2 cm	Dumbbell-shaped interatrial septum sparing fossa ovalis	TEE, MRI	Incidental finding, benign structure	Atrial tumor, atrial thrombus
Atrial thrombus	Arise from left atrial appendage	Variable	Mobile, irregular mass floating at RA	TEE	Present with cardioembolic events such as stroke, history of atrial fibrillation	Atrial tumor
Cor triatriatum sinister	Mid LA	Variable	Incomplete fibrous membrane dividing LA into upper and lower chambers	CT, TEE	May cause LV inflow obstruction, associate with partial anomalous pulmonary venous drainage	Supravalvular mitral ring, atrial tumor, atrial thrombus
Supravalvular mitral ring	Arise from the base of atrial aspect of mitral leaflets	Variable	Fibrous membrane encroaches on the mitral inlet	TEE, CT	May cause LV inflow obstruction, may associate with coarctation of aorta (Shone's complex)	Cor triatriatum sinister
Atrial myxoma	Attach to Interatrial septum	5–6 cm	Large globular intracavitary mass with a stalk attaching to interatrial septum, heterogeneous echogenicity	MRI, CT, TEE	Benign tumor, obstructive, embolic or systemic symptoms	Atrial tumor, atrial thrombus
Osteosarcoma	Posterior wall of LA near pulmonary vein	Variable	Large mobile mass with calcification, may prolapse through mitral valve orifice	MRI, CT	Malignant tumor, usually represent metastatic disease	Atrial tumor, atrial thrombus
Leiomyosarcoma	Attach to interatrial septum	Variable	May involve both mitral valve and pulmonary veins	MRI, CT	Malignant tumor	Atrial tumor, atrial thrombus

Table 19.4 Approach to LV mass by Point-of-care ultrasound of heart

	Location	Size	Echocardiographic features	Additional Ix	Manifestation	DDx
False tendon	Within LV cavity	Variable	Linear fibrous structure that traverse LV cavity, may be single or multiple	Nil	Incidental finding, normal cardiac structure, may associate with arrhythmia	Left ventricular thrombus or tumor
Annular calcification	Mitral annulus	Variable	Circumscribed, echo-dense structure at the base of mitral valve leaflet	CT	Degenerative change, common in elderly and patients with chronic renal failure	Left atrial/ventricular thrombus, mitral valve endocarditis
Loeffler endomyocarditis	Left ventricular apex	2–3 cm	Left apical obliteration with thrombus, increase in myocardial thickness	Contrast echo, MRI	Present with heart failure symptoms, blood profile shows high eosinophil count	Left ventricular thrombus
Left ventricular thrombus	Usually at left ventricular apex	Variable	Mobile echogenic mass	Contrast echo, CT	Associate with myocardial infarct especially apical infarct	Loeffler's endomyocarditis
Papillary fibroelastoma	Attach to LV wall with a stalk	Variable	Highly mobile, homogeneous, relatively circular intracavitary mass	TEE	Incidental finding, may present with cardioembolic stroke	Atrial myxoma
Fibroma	Interventricular septum, LV free wall	3–10 cm	Usually solitary, associate with central calcification	MRI, CT	Benign tumor, rare among adult population, may cause LV outflow tract obstruction and arrhythmia	Rhabdomyoma
Rhabdomyoma	Anywhere in LV	Variable	Multiple nodular masses in several chambers of heart	MRI, CT	Benign tumor, very rare among adult population, may cause LV outflow tract obstruction, associate with tuberous sclerosis	Fibroma
Atrial myxoma	Attach to Interatrial septum	5–6 cm	Large globular mass with a stalk attaching to myocardium, heterogeneous echogenicity	MRI, CT, TEE	Benign tumor, obstructive, embolic or systemic symptoms	Papillary fibroelastoma

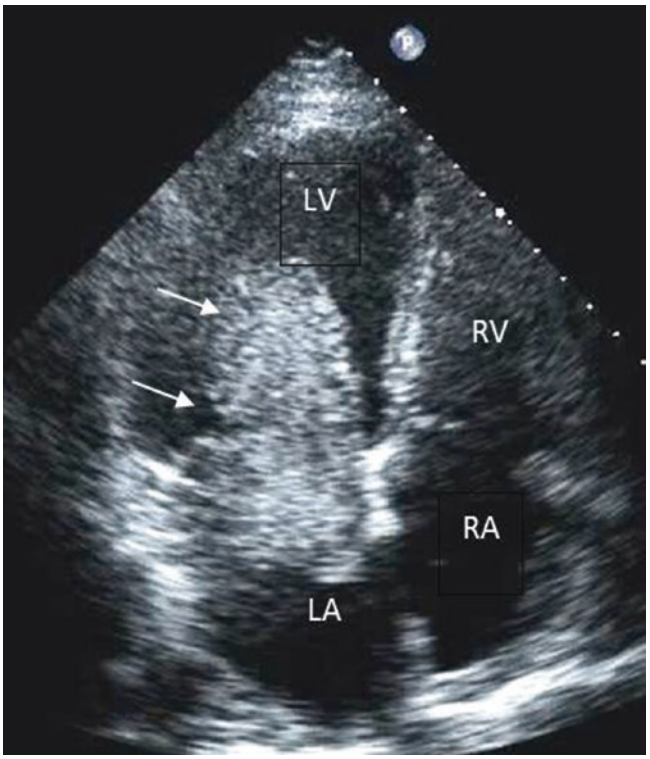

Fig. 19.1 Apical 4-chamber view POCUS in patient whose chest X-ray demonstrated cardiomegaly. A large mobile globular mass (arrows) was found attached to the interatrial septum; it was noted to move to and fro between the left atrium and left ventricle. Overall features favored left atrial myxoma given its attachment and classical 2D features. *LA* left atrium, *LV* left ventricle, *RA* right atrium, *RV* right ventricle

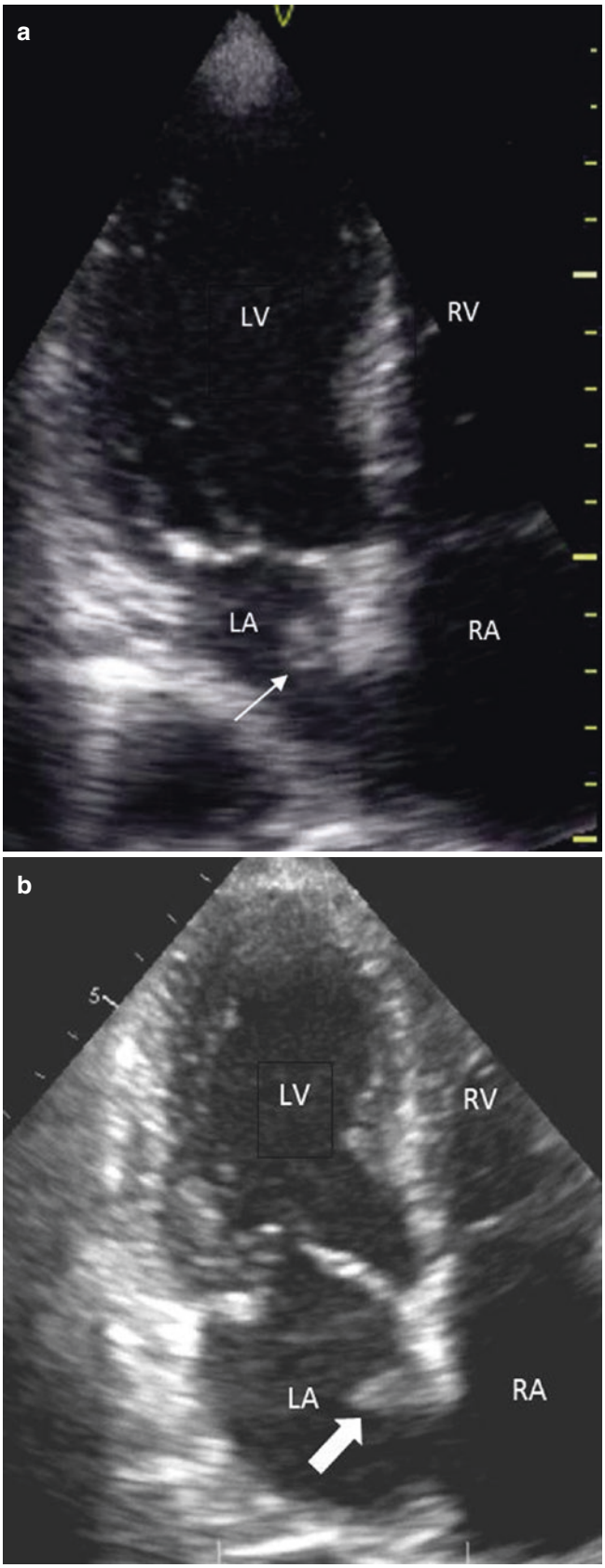

Fig. 19.2 (**a**) POCUS Apical 4-chamber view in patient with persistent fever. A small echogenic circular mass (small arrow) measuring 2 cm is attached to interatrial septum. (**b**) Apical 4-chamber view echo lab TTE imaging confirms the diagnosis of cardiac myoxma; note the echocardiographic features are similar to the POC image. *LA* left atrium, *LV* left ventricle, *RA* right atrium, *RV* right ventricle

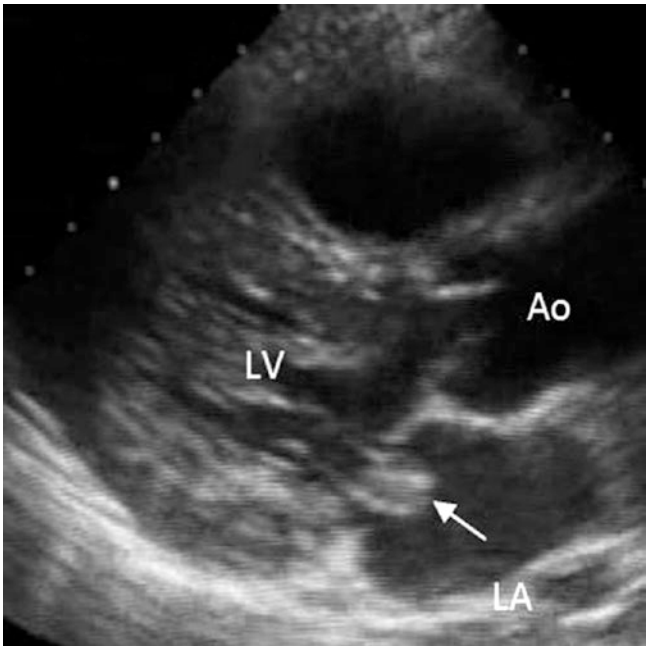

Fig. 19.3 Parasternal long axis view POC imaging of a 60-year-old patient who presented with acute embolic stroke. A highly mobile roundish mass (*arrow*) with moderate size attaches to the atrial aspect of the mitral valve, consistent with a diagnosis of papillary fibroelastoma. It is prudent to exclude infective endocarditis in these cases. *LA* left atrium, *LV* left ventricle, *Ao* aorta

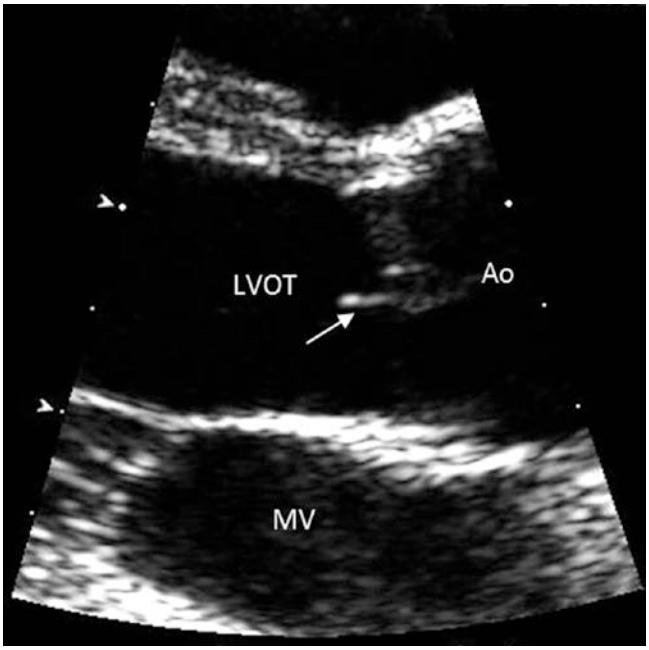

Fig. 19.5 Parasternal long axis POC imaging of a 70-year-old man with recent history of palpitations. The mass (arrow) measured 3.5 mm in diameter, was highly mobile and attached to the interventricular septum with a stalk. It is located at the closure margin of aortic valve without any regurgitation. This is an example of Lambl's excrescence, which are thin, mobile filiform structures located at valve closures. They are thought to be degenerative processes with low risk of embolization. *Ao* aorta, *LVOT* left ventricular outflow tract, *MV* mitral valve

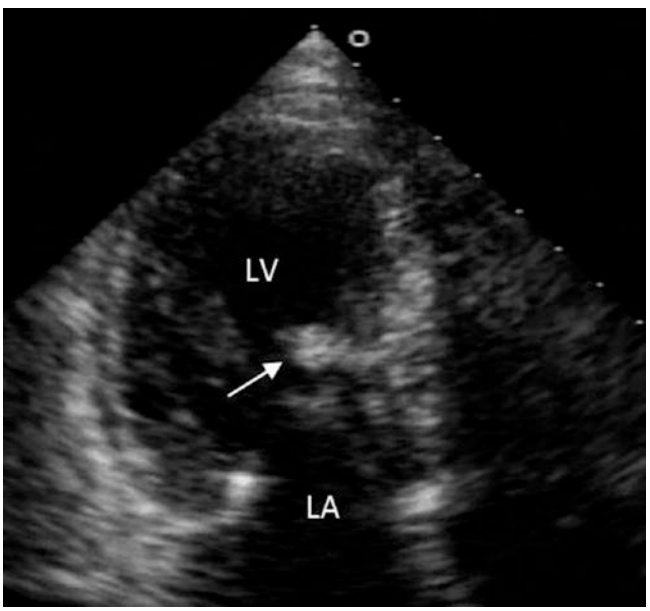

Fig. 19.4 Apical 4-chamber view POC imaging of a hypertrophic cardiomyopathy with incidental finding of papillary fibroelastoma. It measures 3.5 cm in diameter; it is highly mobile and attaches to interventricular septum with a stalk. *LA* left atrium, *LV* left ventricle

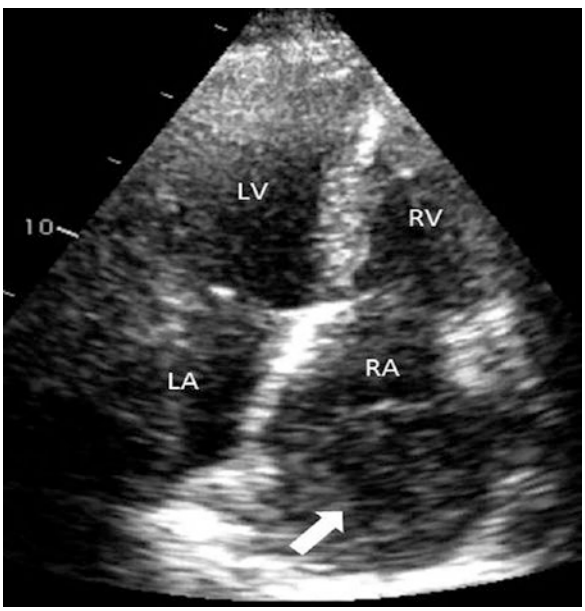

Fig. 19.6 Apical 4-chamber view POC imaging in newly diagnosed angiosarcoma. The tumor is large, multilobulated, and adheres to right atrial free wall (*arrow*). It is usually associated with hemopericardium, but there is no significant pericardial involvement in this case. *LA* left atrium, *LV* left ventricle, *RA* right atrium, *RV* right ventricle

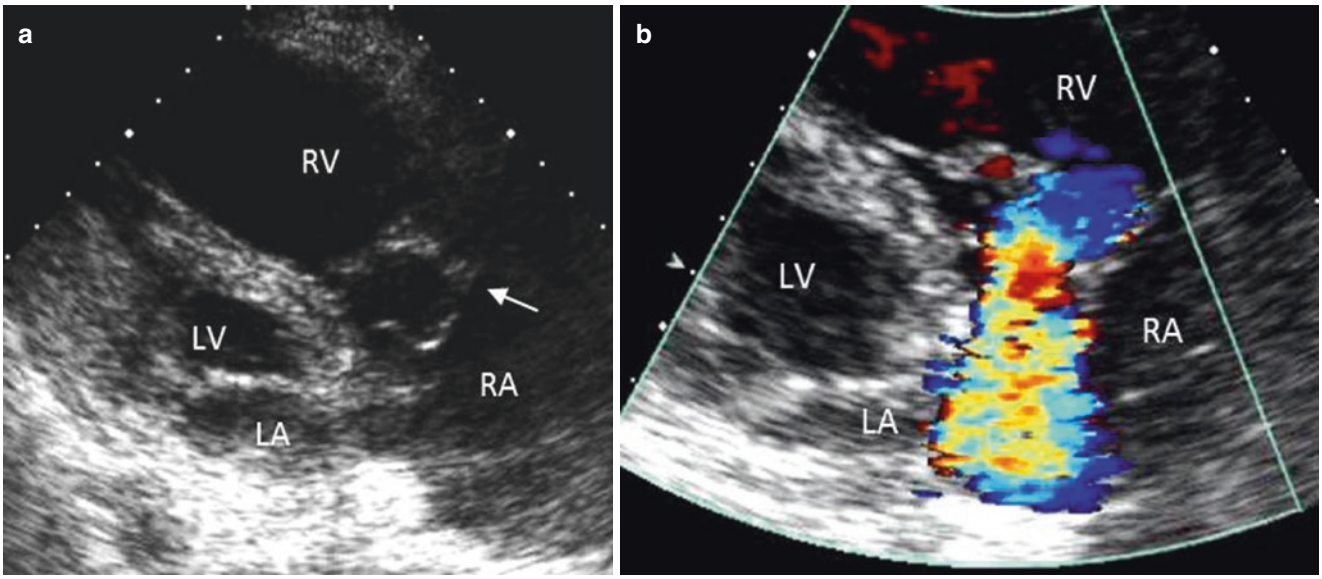

Fig. 19.7 (**a**) Non-standard apical 4-chamber view POC imaging in a patient presenting with right heart failure. There is a mobile, thin-walled cystic-like lesion attached to the tricuspid valve. (**b**) It is associated with severe tricuspid regurgitation. The diagnosis of blood cyst is established by agitated saline test in transthoracic echocardiography. *LA* left atrium, *LV* left ventricle, *RA* right atrium, *RV* right ventricle

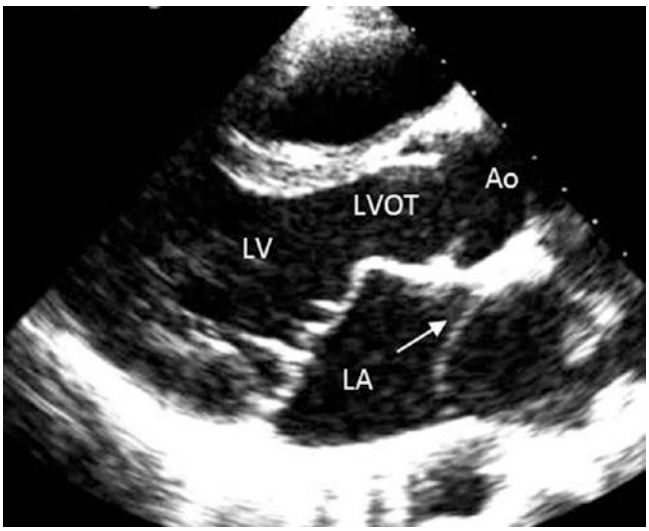

Fig. 19.8 Parasternal long axis POC imaging of a 32-year-old man with new onset of atrial fibrillation. A flap-like structure (arrow) is found at the left atrium (LA), which separates the LA into two distinct chambers. This is highly suspicious for cor triatriatum, which was confirmed on subsequent transesophageal echocardiography. *LV* left ventricle, *LA* left atrium, *Ao* aorta

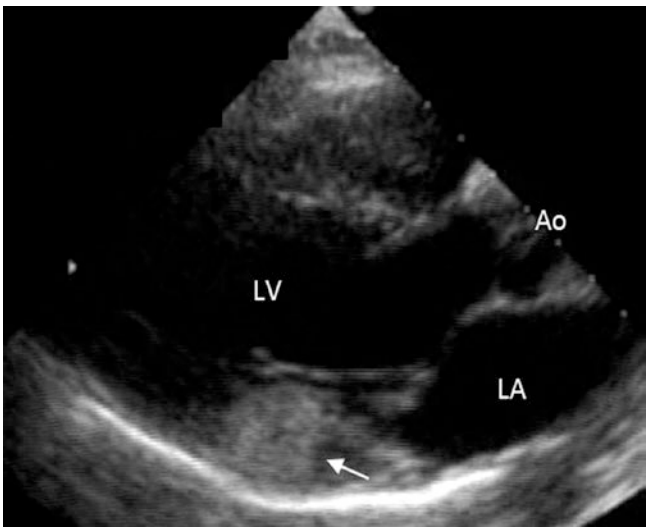

Fig. 19.9 Parasternal long axis POC imaging. There is a solitary, well circumscribed, relatively immobile mass (arrow) situated at the basal posterior wall of the heart which is incidentally discovered by echocardiography. The echocardiographic feature is suggestive of ventricular fibroma. The *LV* left ventricle, *LA* left atrium, *Ao* aorta

References

1. Spencer KT, Kimura BJ, Korcarz CE, Pellikka PA, Rahko PS, Siegel RJ. Focused cardiac ultrasound: recommendations from the American Society of Echocardiography. J Am Soc Echocardiogr. 2013;26(6):567–81.
2. Neskovic AN, Edvardsen T, Galderisi M, Garbi M, Gullace G, Jurcut R, et al. Focus cardiac ultrasound: the European Association of Cardiovascular Imaging viewpoint. Eur Heart J Cardiovasc Imaging. 2014;15(9):956–60.

Valvular Heart Disease

20

Edgar Argulian and Jagat Narula

20.1 Introduction

Valvular heart disease is an important consideration in patients with different clinical presentations such as shortness of breath, chest pain, syncope, and hypotension [1]. Correct identification of valvular heart disease requires good knowledge of anatomy, pathophysiology and advanced ultrasound applications (such as color and spectral Doppler), as well as excellent ultrasound examination skills. In most cases, precise quantification of the valvular pathology requires comprehensive echocardiography using a high-end ultrasound platform [2]. Point-of-care ultrasound may assist in identification of common valvular diseases, but caution should be exercised in interpreting the abnormalities by less experienced examiners, especially ruling out significant valvular heart disease based on limited ultrasound examination (Figs. 20.1, 20.2, 20.3, 20.4, 20.5, 20.6, 20.7, 20.8, 20.9, 20.10, and 20.11; Videos 20.1, 20.2, 20.3, 20.4, 20.5, 20.6, 20.7, 20.8 and 20.9) [3].

Electronic Supplementary Material The online version of this chapter (https://doi.org/10.1007/978-3-319-73855-0_20) contains supplementary material, which is available to authorized users.

E. Argulian, M.D., M.P.H. (✉)
Mount Sinai St. Luke's Hospital, Icahn School of Medicine at Mount Sinai, New York, NY, USA
e-mail: Edgar.Argulian@mountsinai.org

J. Narula, M.D., Ph.D.
Mount Sinai Hospital, Icahn School of Medicine at Mount Sinai, New York, NY, USA

B. P. Nelson et al. (eds.), *Atlas of Handheld Ultrasound*, https://doi.org/10.1007/978-3-319-73855-0_20

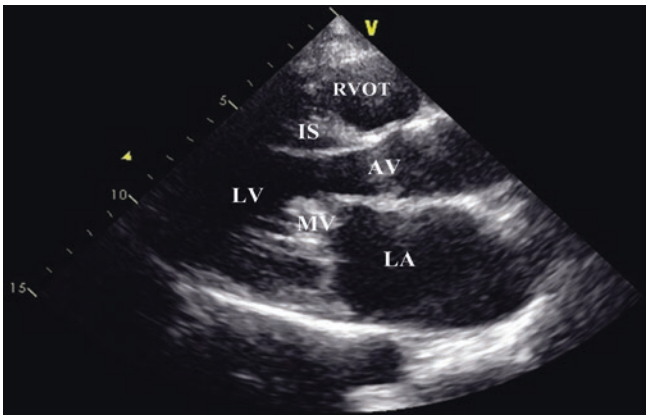

Fig. 20.1 Mitral stenosis, parasternal long axis view. Mitral valve can be visualized from multiple views. In parasternal long axis view, the left atrium (LA), left ventricle (LV), right ventricular outflow tract (RVOT) and interventricular septum (IS) are seen. Aortic valve (AV) appears echo dense but it is opening normally. Mitral valve (MV) appears echo dense and thickened with highly restricted leaflet opening. This is consistent with rheumatic mitral valve stenosis. See also Video 20.1

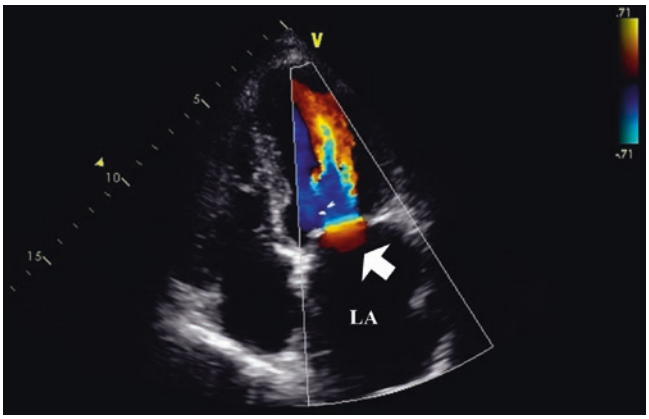

Fig. 20.3 Mitral stenosis, color Doppler examination in the apical four-chamber view. Color Doppler examination in this view shows color flow convergence (*arrow*) in the left atrium (LA) which indicates blood flow acceleration toward the narrowed orifice of the mitral valve in diastole. See also Video 20.3

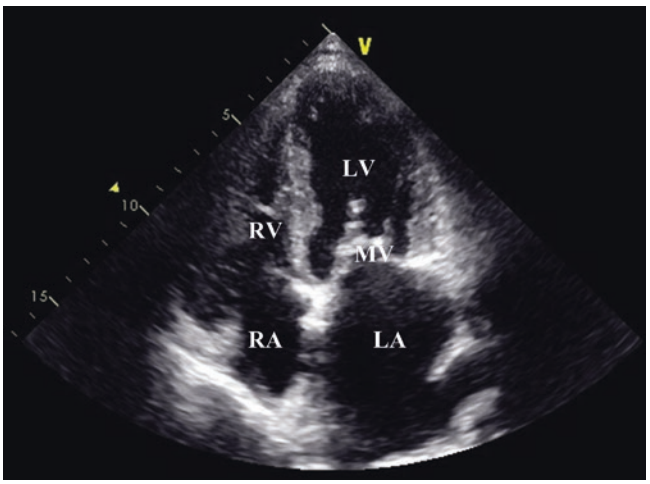

Fig. 20.2 Mitral stenosis, apical four-chamber view. In this view, the left atrium (LA), right atrium (RA), left ventricle (LV), and right ventricle (RV) are seen. The left atrium is markedly enlarged. The mitral valve (MV) appears echo dense and thickened, the posterior leaflet is immobile and anterior leaflet has restricted mobility. This is consistent with rheumatic mitral valve stenosis. See also Video 20.2

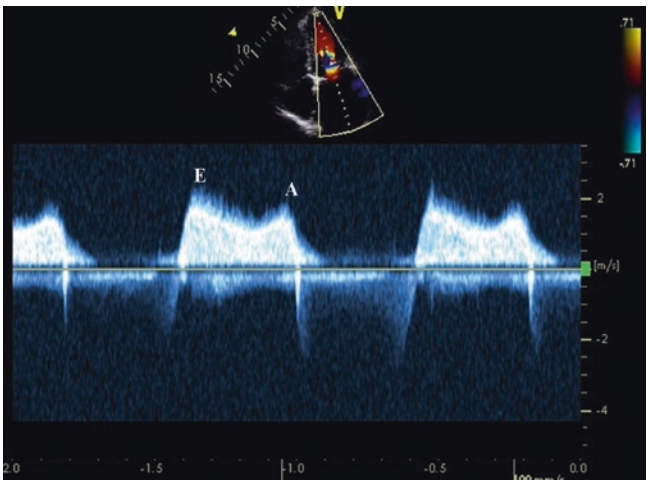

Fig. 20.4 Mitral inflow interrogation using continuous wave Doppler. In ultrasound systems equipped with spectral Doppler continuous wave interrogation through the mitral valve can be obtained. Early diastolic velocity (E) is high exceeding 2 m/sec and the deceleration slope of E wave appears flat. This is consistent with significant mitral stenosis. Atrial contraction wave (A) is not seen in patients with atrial fibrillation. Tracing the contour of the spectral Doppler signal can be used to calculate mean transmitral gradient

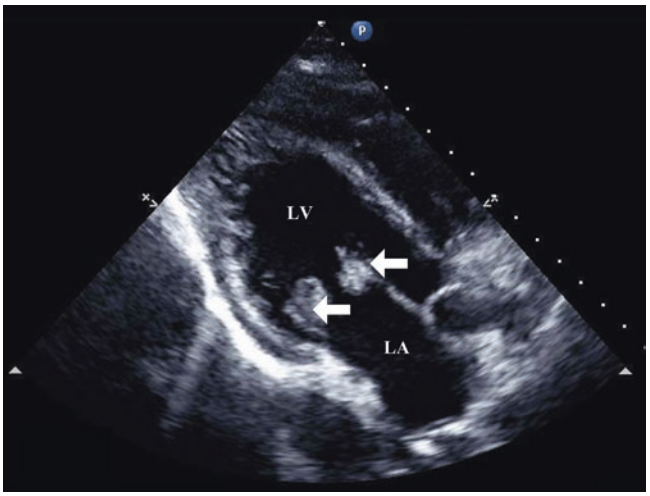

Fig. 20.5 Infective endocarditis involving the mitral valve in a patient with shortness of breath and fever. Point-of-care ultrasound can identify gross structural abnormalities involving the mitral valve. In this patient, a modified parasternal long-axis view is obtained with the left ventricle (LV) and the left atrium (LA) in focus. Large mobile echo densities with soft consistency (*arrows*) are seen attached to both mitral valve leaflets; there are consistent with vegetations. See also Video 20.4

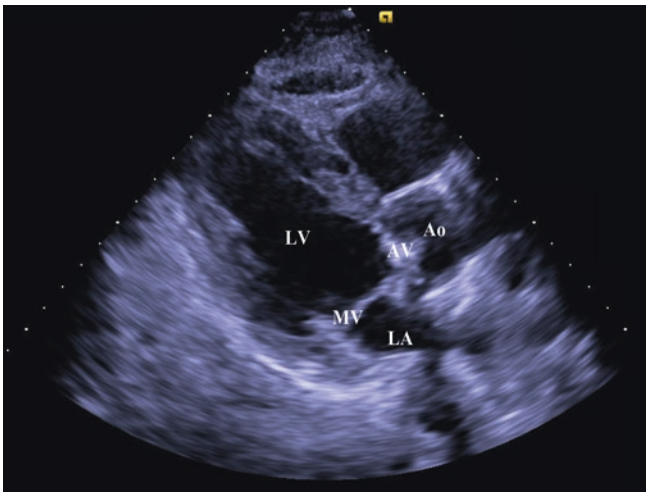

Fig. 20.7 Aortic stenosis in the parasternal long-axis view. An attempt to visualize the aortic valve opening should be made in the parasternal views. In this parasternal long axis view the left ventricle (LV), left atrium (LA), mitral and aortic valves, and the aortic root (Ao) are seen. The mitral valve (MV) appears echo bright but opens normally. The aortic valve (AV) appears echo bright with very restricted leaflet opening suggestive of aortic stenosis. See also Video 20.6

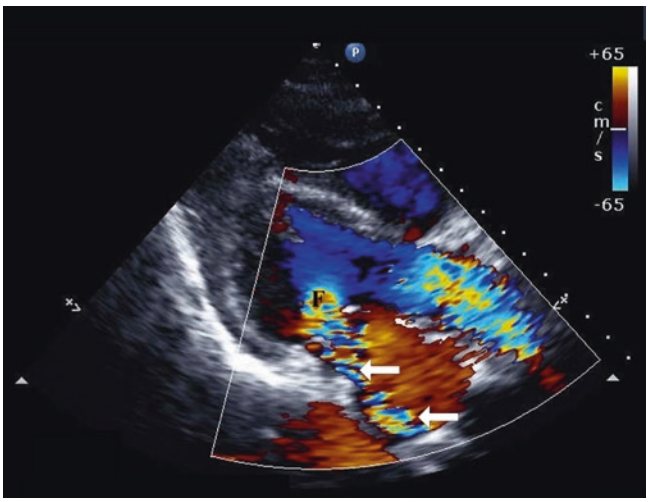

Fig. 20.6 Infective endocarditis involving the mitral valve in a patient with shortness of breath and fever. Color Doppler echocardiography can identify mitral regurgitation and can help in gross estimation of the lesion severity. Careful attention must be paid to color Doppler settings such as Nyquist limit and color Doppler gain. In this patient, color Doppler demonstrates a jet of severe mitral regurgitation (*arrows*) with a large area of flow convergence (F). Quantitative assessment of the mitral regurgitation severity by the size of the regurgitant jet can be misleading and can result in both under- and overestimating lesion severity. Eccentric mitral regurgitation jets can have small jet areas and can be missed by the limited assessment using point of care ultrasound. Therefore, comprehensive echocardiography is required for accurate mitral regurgitation assessment and quantification. See also Video 20.5

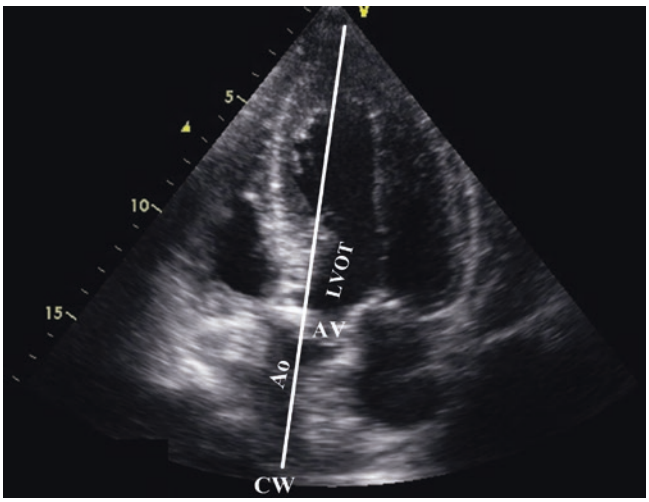

Fig. 20.8 Five-chamber view for evaluation of aortic stenosis. Doppler interrogation of the transaortic velocities is essential in diagnosing aortic stenosis and other causes of left ventricular outflow obstruction. This can be achieved by obtaining a five-chamber view: from the usual four-chamber view the transducer is tilted anteriorly (shallower relative to the chest) to visualize the left ventricular outflow tract (LVOT), aortic valve (AV) and the ascending aorta (Ao). Continuous wave (CW) spectral Doppler can be aligned parallel to the left ventricular outflow using this view to capture the transaortic velocity. While this interrogation can assist in diagnosing aortic stenosis, proper aortic stenosis grading requires multiple interrogations from different insonation angles and should be performed during comprehensive echocardiography. See also Video 20.7

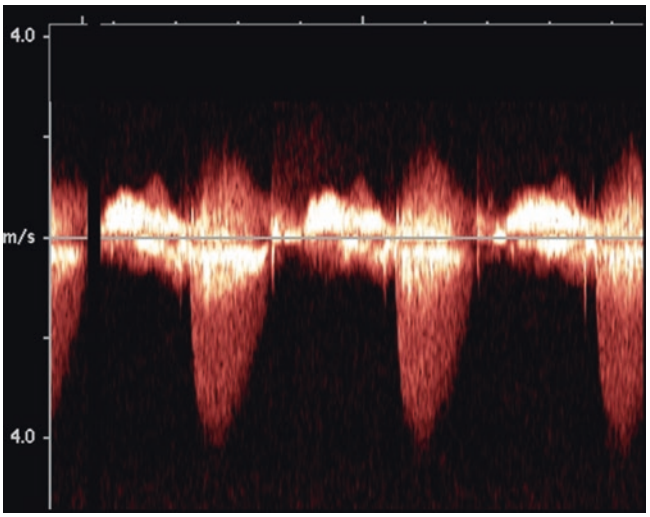

Fig. 20.9 Interrogation of the aortic valve using continuous wave spectral Doppler. The examination shows a high transaortic flow velocity (approximately 4 m/sec) consistent with severe aortic stenosis. Interpretation of the Doppler findings requires excellent ultrasound examination and interpretation skills. The velocity can be underestimated if a single acoustic window is used. The flow signal should not be confused with other flows (like mitral regurgitation). Also, other causes of left ventricular outflow obstruction can cause elevated transaortic velocities; these include hypertrophic obstructive cardiomyopathy, subaortic membrane, and supravalvular obstruction

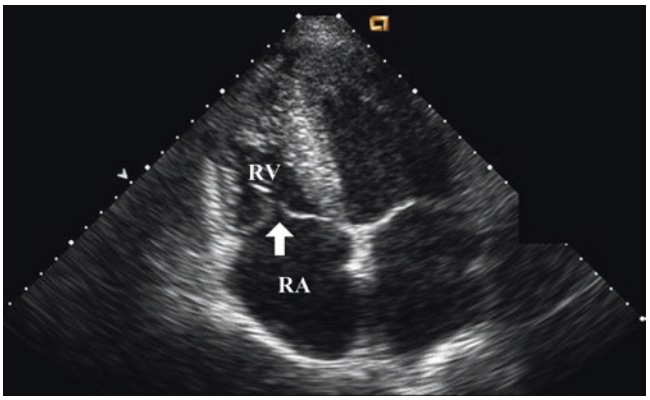

Fig. 20.10 Structural assessment of the tricuspid valve using point-of-care ultrasound. Tricuspid valve assessment can be accomplished in different views including parasternal, apical and subcostal views. The apical four-chamber view is commonly used for point-of-care ultrasound. Tricuspid regurgitation is a relatively common finding. Most commonly, moderate-to-severe tricuspid regurgitation is secondary to right ventricular dilation. In this example, the right ventricle (RV) and right atrium (RA) are enlarged. A coaptation gap can be seen between the tricuspid valve leaflets in systole due to tricuspid annular dilation. See also Video 20.8

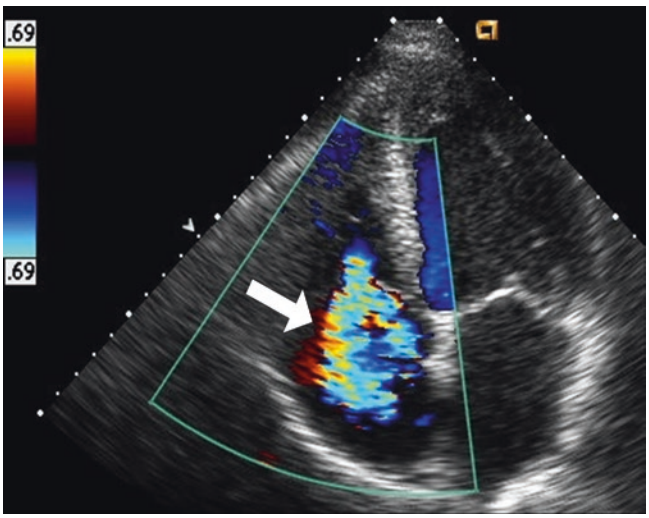

Fig. 20.11 Tricuspid valve assessment using color Doppler. Color Doppler allows gross assessment of the tricuspid regurgitation severity but examination limited to a single view can be misleading. Careful attention must be paid to color Doppler settings such as Nyquist limit and color Doppler gain. In this example, color Doppler examination demonstrates a large jet of tricuspid regurgitation (*arrow*) consistent with significant tricuspid regurgitation. Spectral Doppler assessment of the tricuspid regurgitant jet can also be performed in this view. Although it can be used to estimate pulmonary artery systolic pressure, interrogation from multiple angles is required for complete assessment which is typically accomplished by comprehensive echocardiography. See also Video 20.9

Acknowledgments All videos courtesy of Dr. Edgar Argulian.

References

1. Millington SJ, Arntfield RT. Advanced point-of-care cardiac ultrasound examination: doppler applications, valvular assessment, and advanced right heart examination. Glob Heart. 2013;8(4):305–12.
2. Spencer KT, Kimura BJ, Korcarz CE, Pellikka PA, Rahko PS, Siegel RJ. Focused cardiac ultrasound: recommendations from the American Society of Echocardiography. J Am Soc Echocardiogr. 2013;26(6):567–81.
3. Via G, Hussain A, Wells M, Reardon R, ElBarbary M, Noble VE, et al. International evidence-based recommendations for focused cardiac ultrasound. J Am Soc Echocardiogr. 2014;27(7):683.e1–e33.

Congenital Heart Disease

21

William R. Miranda and Crystal R. Bonnichsen

Owing to the advances in diagnosis and management, more than one million adults in the United States are known to have congenital heart disease (CHD). Some forms of CHD, including atrial septal defect (ASD) and bicuspid aortic valve (BAV), often present for the first time in the adult patient. Complex forms of CHD, such as cyanotic CHD, require thorough echocardiographic evaluation for accurate diagnoses; however, simpler lesions could be easily diagnosed with point-of-care ultrasound, distinguishing them from other causes of cardiac murmurs or heart disease. If CHD is identified or suspected with point-of-care ultrasound, formal echocardiographic evaluation and consultation with an expert in CHD is recommended.

Atrial septal defect (ASD) consists of a communication between the atria and accounts for one-tenth of congenital heart abnormalities (Figs. 21.1, 21.2, 21.3, and 21.4). Ostium secundum ASD corresponds to a defect within the oval fossa and is the most common form of ASD. In ostium primum ASD, the communication lies in the most apical portion of the atrial septum, near the atrioventricular valves (no ventricular septal defect is present). Two other rare types of interatrial communication exist: sinus venous ASD (the defect is typically superior to the oval fossa) and coronary sinus ASD (a communication between the coronary sinus—the largest cardiac vein—and the left atrium). Atrial septal defects can lead to right atrial and ventricular enlargement secondary to volume overload and, therefore, should be suspected in patients with otherwise unexplained right heart enlargement.

Ventricular septal defect (VSD) is the second most common form of CHD, but most defects close spontaneously in childhood. VSDs can be classified into four major types: (1) membranous VSD (most common in the United States), a defect in the thin, non-muscular portion of the ventricular septum (the membranous septum); (2) muscular VSD, an interventricular communication surrounded by muscle in the trabecular portion of the septum; (3) infundibular VSD (also described as supracristal, subarterial or doubly committed), where the communication lies below the aortic and pulmonary valves; and (4) inlet VSD, in which the defect lies below the mitral and tricuspid valves and is classically associated with Down syndrome (Figs. 21.5, 21.6, 21.7, and 21.8) [1]. Ventricular septal defects are typically suspected when a loud holosystolic murmur, often associated with a thrill, is heard at the bedside. In contrast to ASDs, VSDs lead to left heart enlargement and should be suspected in a patient with a loud murmur and a dilated left heart.

Bicuspid aortic valve (BAV) affects 1–2% of the population and is the most common congenital heart lesion (Fig. 21.9). It results from fusion (partial or complete) of two of the three aortic valve cusps, most frequently the right and left cusps. BAV can cause aortic valve stenosis or regurgitation and the presence of a murmur associated with a systolic click is a clue to the diagnosis. Dilatation of the ascending aorta—*aortopathy*—occurs in at least 20% of patients with BAV; aortic dissection is a rare complication in those patients. The aortic root and ascending aorta can usually be well visualized by transthoracic echocardiography and should always be assessed in patients with BAV. Lastly, 5% of patients with BAV have coarctation of the aorta so an evaluation of the descending thoracic aorta by two-dimensional and echo-Doppler should also be routinely performed (Fig. 21.10). Coarctation of the aorta should always be considered in a young patient presenting with hypertension.

W. R. Miranda, M.D. · C. R. Bonnichsen, M.D. (✉)
Department of Cardiovascular Diseases,
Mayo Clinic, Rochester, MN, USA
e-mail: miranda.william@mayo.edu; Bonnichsen.Crystal@mayo.edu

B. P. Nelson et al. (eds.), *Atlas of Handheld Ultrasound*, https://doi.org/10.1007/978-3-319-73855-0_21

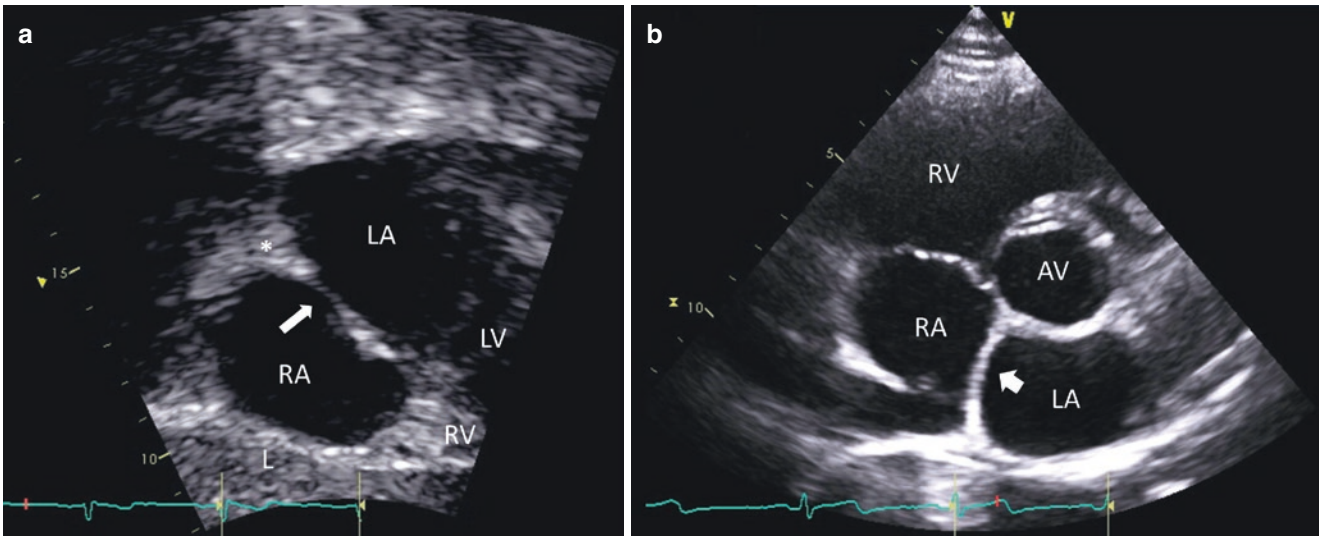

Fig. 21.1 Normal atrial septum. (**a**) Subcostal four-chamber (congenital format) view showing the normal atrial septal anatomy. The transducer is placed in the subxiphoid region, lying almost horizontal with the probe marker in the 3-o'clock position. Alternatively, if the "adult format" is chosen (liver on the top of the screen), the probe marker should be held at the 9-o'clock position. The thin arrow points to the oval fossa, located between the superior (asterisk) and inferior limbi. This is the most commonly used view for the evaluation of the atrial septum. (**b**) The parasternal short-axis view also provides excellent visualization of the atrial septum (thick arrow). The transducer is placed vertically (probe marker around 12-o'clock) and angled slightly toward the left shoulder at the third or fourth left intercostal spaces. Assessment of atrial septum using the apical four-chamber view can be misleading due to "dropout" giving the false impression that an interatrial communication is present. Thus, this imaging format should be avoided when looking for an ASD (*AV* aortic valve, *LA* left atrium, *LV* left ventricle, *L* liver, *RA* right atrium, *RV* right ventricle)

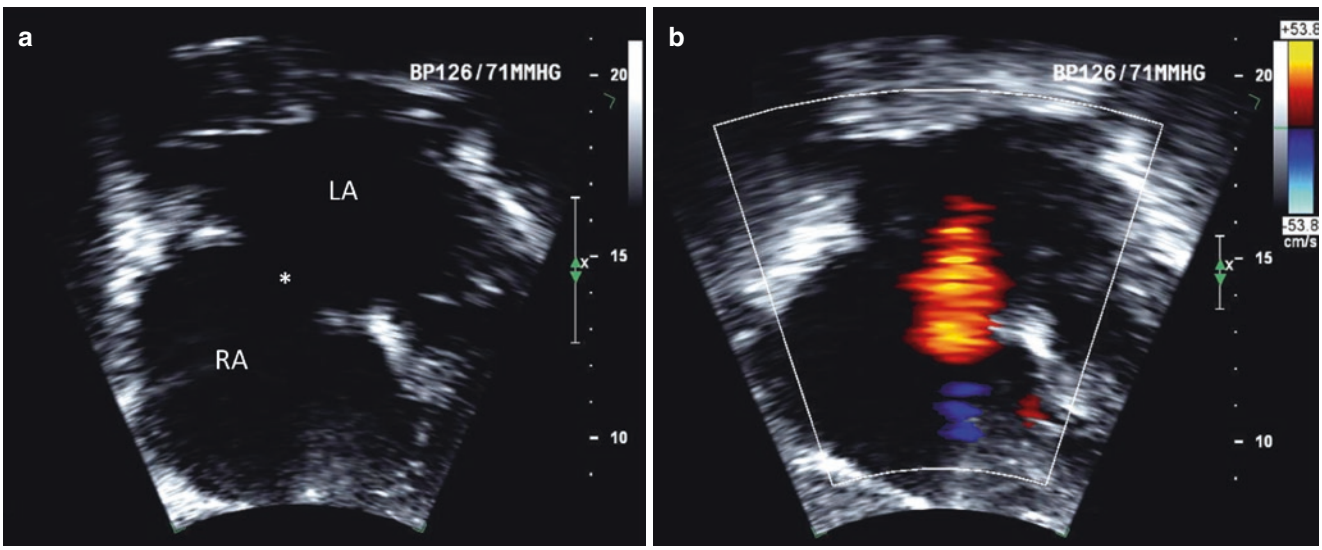

Fig. 21.2 Secundum atrial septal defect. (**a**) Subcostal four-chamber view (panel A; congenital format) showing a large secundum atrial septal defect (asterisk). Bi-atrial enlargement is also present. (**b**) Color-flow Doppler illustrates the presence of left-to-right shunting (red jet) associated the secundum atrial septal defect demonstrated in panel A (*LA* left atrium, *RA* right atrium)

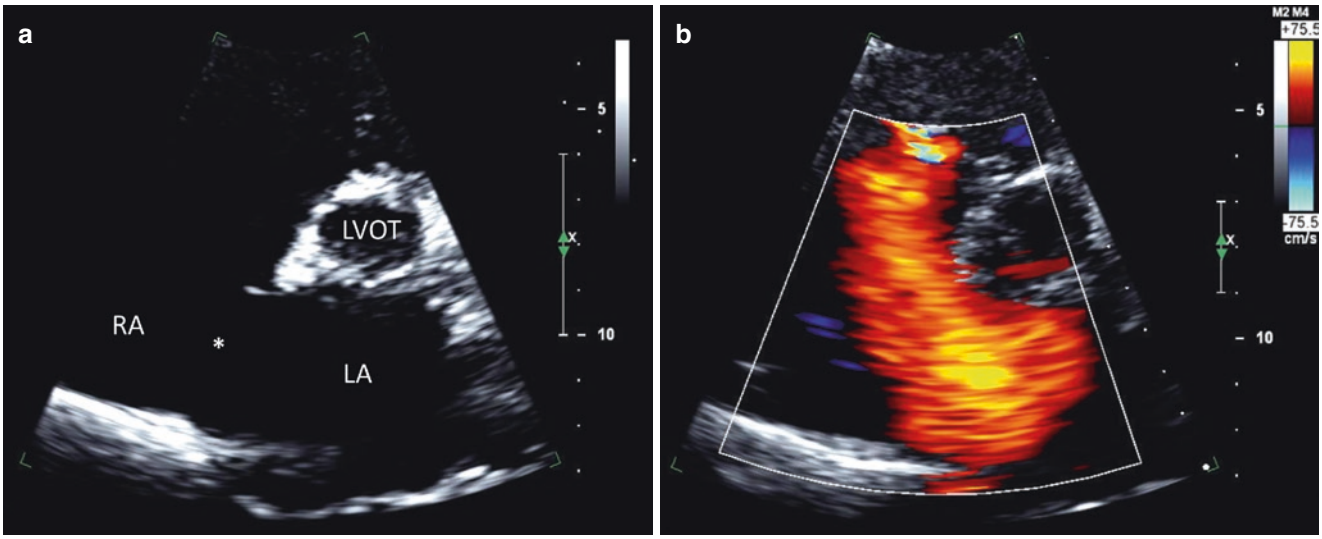

Fig. 21.3 Secundum atrial septum defect. (**a**) Parasternal short-axis view showing a large secundum atrial septal defect (asterisk). (**b**) Color-flow Doppler shows a large left-to-right shunt across the atrial septal defect shown in panel A. These images are from the same patient depicted in Fig. 21.2 (*LA* left atrium, *LVOT* left ventricular outflow tract, *RA* right atrium)

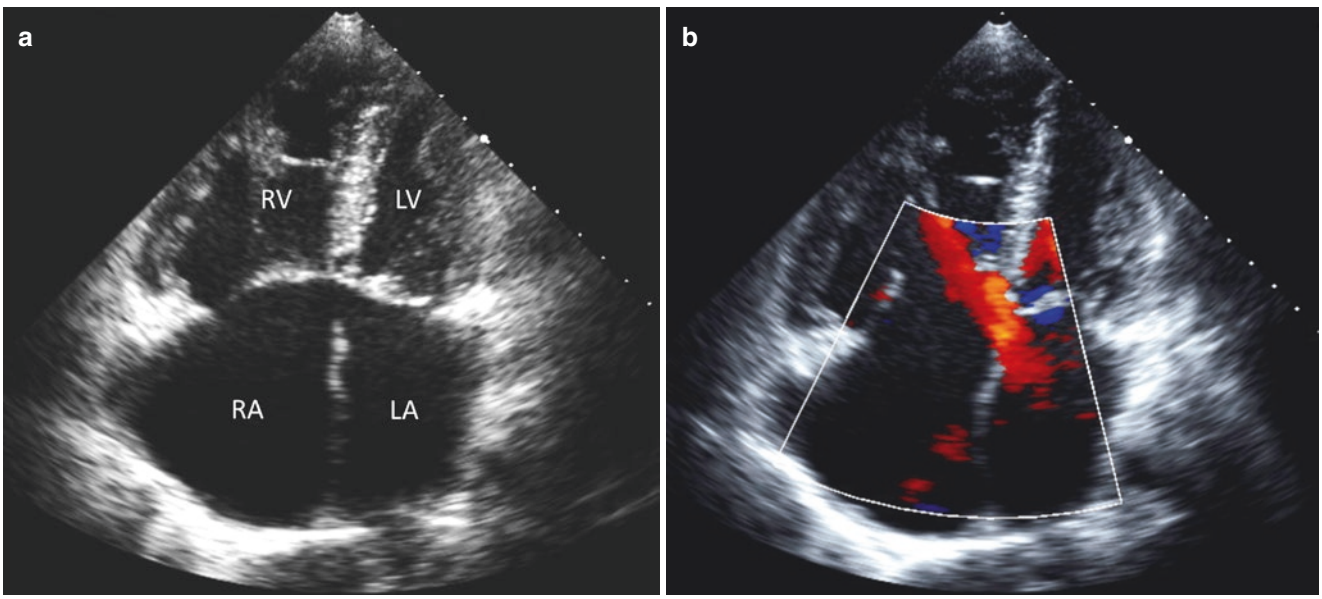

Fig. 21.4 Ostium primum atrial septal defect. (**a**) Apical four-chamber view showing an ostium primum atrial septum defect. The probe is placed fifth left intercostal space, mid-clavicular line, angled toward the right shoulder; probe marker is at the 2–3-o'clock position. The atrial septal defect is located at the apical portion of the atrial septum (inferior limbus). Note that the right and left atrioventricular valves are on the same level, the anatomic hallmark of partial (ostium primum) and complete atrioventricular canal defects. In normal heart, the tricuspid valve is more apically positioned than the mitral valve. Bi-atrial and right ventricular enlargement is also present. (**b**) Color-flow Doppler shows left-to-right shunting across the interatrial communication demonstrated in panel A (*LA* left atrium, *LV* left ventricle, *RA* right atrium, *RV* right ventricle)

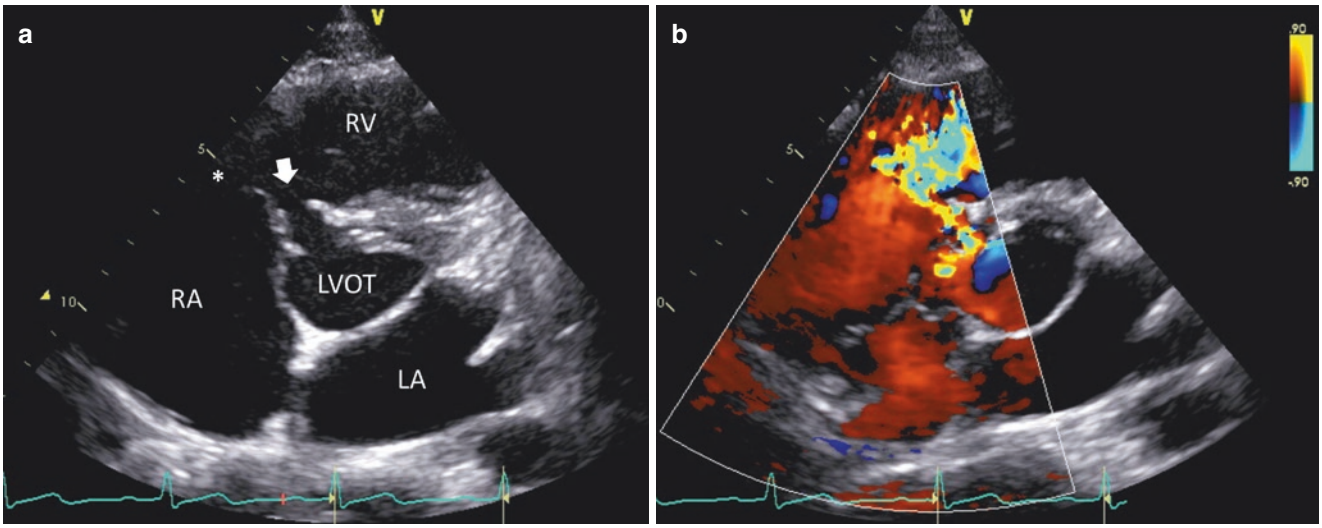

Fig. 21.5 Membranous ventricular septal defect. (**a**) Parasternal short-axis view demonstrating a membranous ventricular septal defect (arrow). Due to the proximity of the tricuspid valve (asterisk), this type of defect is also described as sub-tricuspid. (**b**) Color-flow Doppler shows left-to-right shunt across the ventricular septal defect demonstrated in panel A (*LA* left atrium, *LVOT* left ventricular outflow tract, *RA* right atrium, *RV* right ventricle)

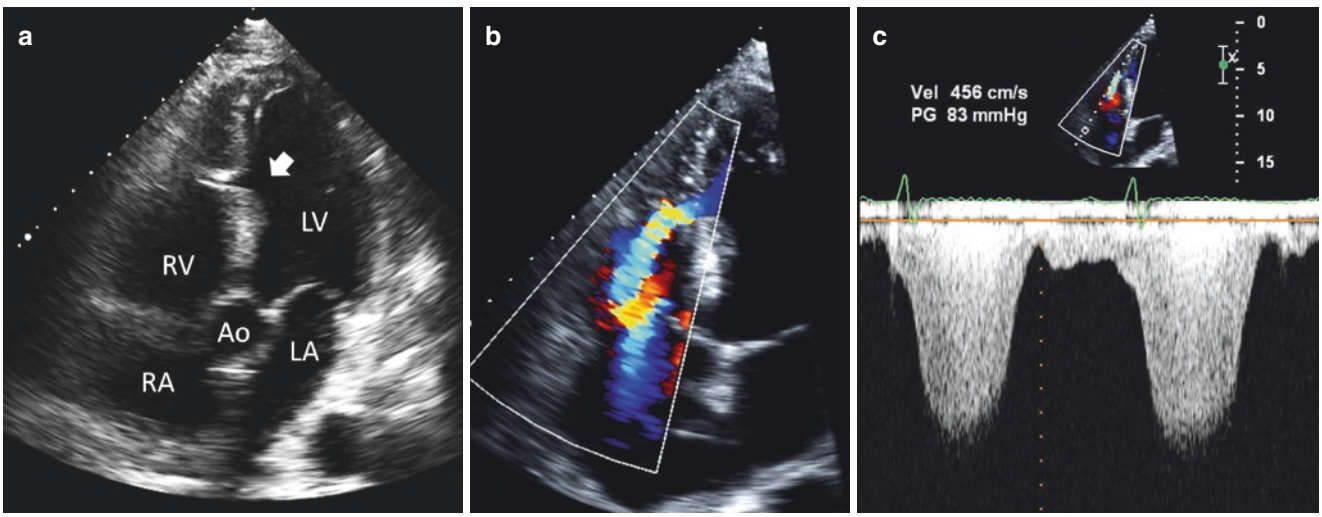

Fig. 21.6 Muscular ventricular septal defect. (**a**) Apical five-chamber view showing a small muscular ventricular septal defect (arrow), located at the mid portion of the ventricular septum. Muscular ventricular septal defects are typically well seen in parasternal short-axis or apical views (except for the two-chamber view). In this picture, the transducer was slightly rotated clockwise and angled anteriorly from a four-chamber view, hence the visualization of the aorta. (**b**) Color-flow Doppler shows left-to-right shunting through the muscular ventricular septal defect. Note the left ventricular size is normal, which is in keeping with a small ventricular septal defect. (**c**) Continuous-wave Doppler interrogation of the ventricular septal defect illustrates the typical Doppler profile with left-to-right shunt during systole and ventricular diastole (*LA* left atrium, *LV* left ventricle, *RA* right atrium, *RV* right ventricle, *Ao* aorta)

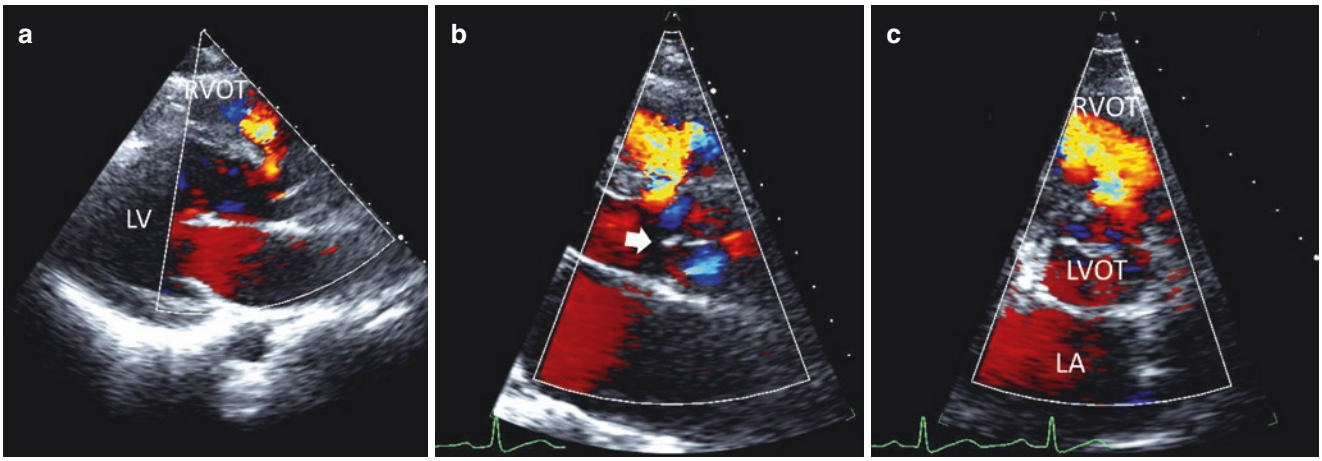

Fig. 21.7 Subarterial ventricular septal defect. (**a**) Parasternal long-axis view showing left-to-right shunt (red jet) arising immediately below (apical to) the aortic valve. Note left ventricular enlargement, suggesting a significant left-to-shunt shunt. (**b**) Parasternal long-axis, zoomed-in view, demonstrating the proximity of the ventricular septal defect to the aortic valve (arrow) and right sinus of Valsalva. (**c**) Parasternal short-axis view demonstrating the subarterial ventricular septal defects demonstrated in Panel A and B. Note the location, in proximity to the pulmonary valve (between the 12- and 3-o'clock position). In contrast, a membranous ventricular septal defect is in close proximity to the tricuspid valve (around the 9-o'clock position; see Fig. 21.5) (*LA* left atrium, *LV* left ventricle, *RA* right atrium, *RV* right ventricle, *RVOT* right ventricular outflow tract)

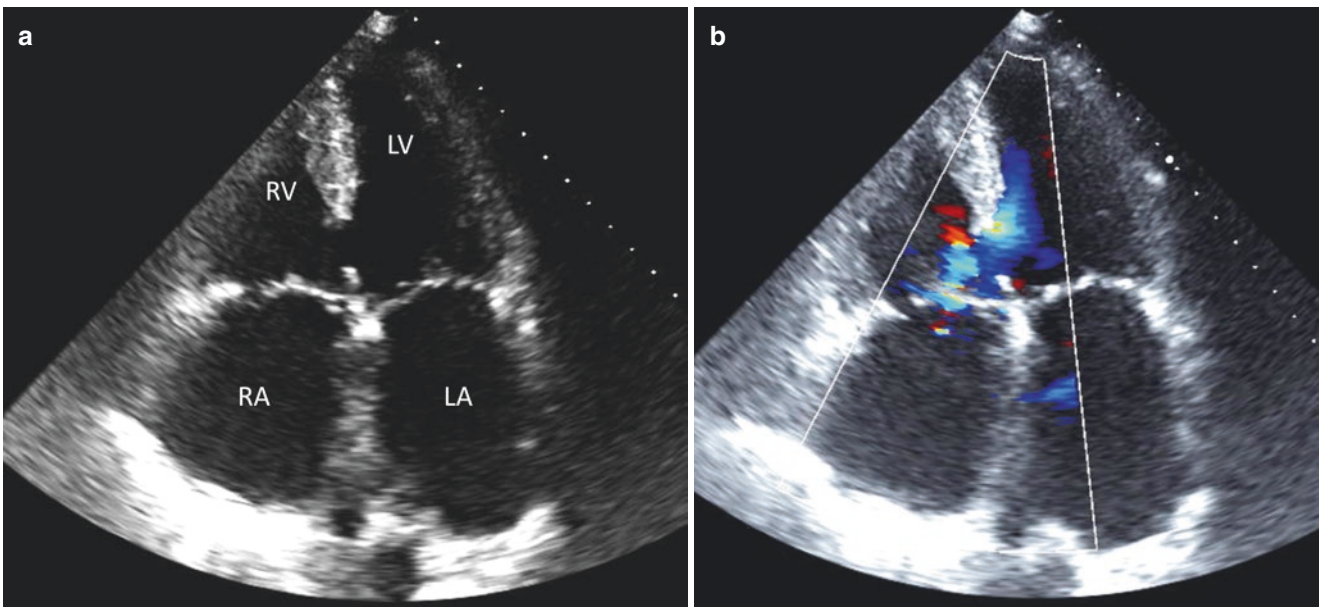

Fig. 21.8 Inlet ventricular septal defect. (**a**) Apical four-chamber view showing a small ventricular septal defect in the superior portion of the ventricular septum, close to the atrioventricular valves. (**b**) Color-flow Doppler illustrates left-to-right shunt associated with the defect demonstrated in Panel A. Also note that the atrioventricular valves are at the same level. This finding in combination with location of the interventricular communication is consistent with an inlet ventricular septal defect (*LA* left atrium, *LV* left ventricle, *RA* right atrium, *RV* right ventricle)

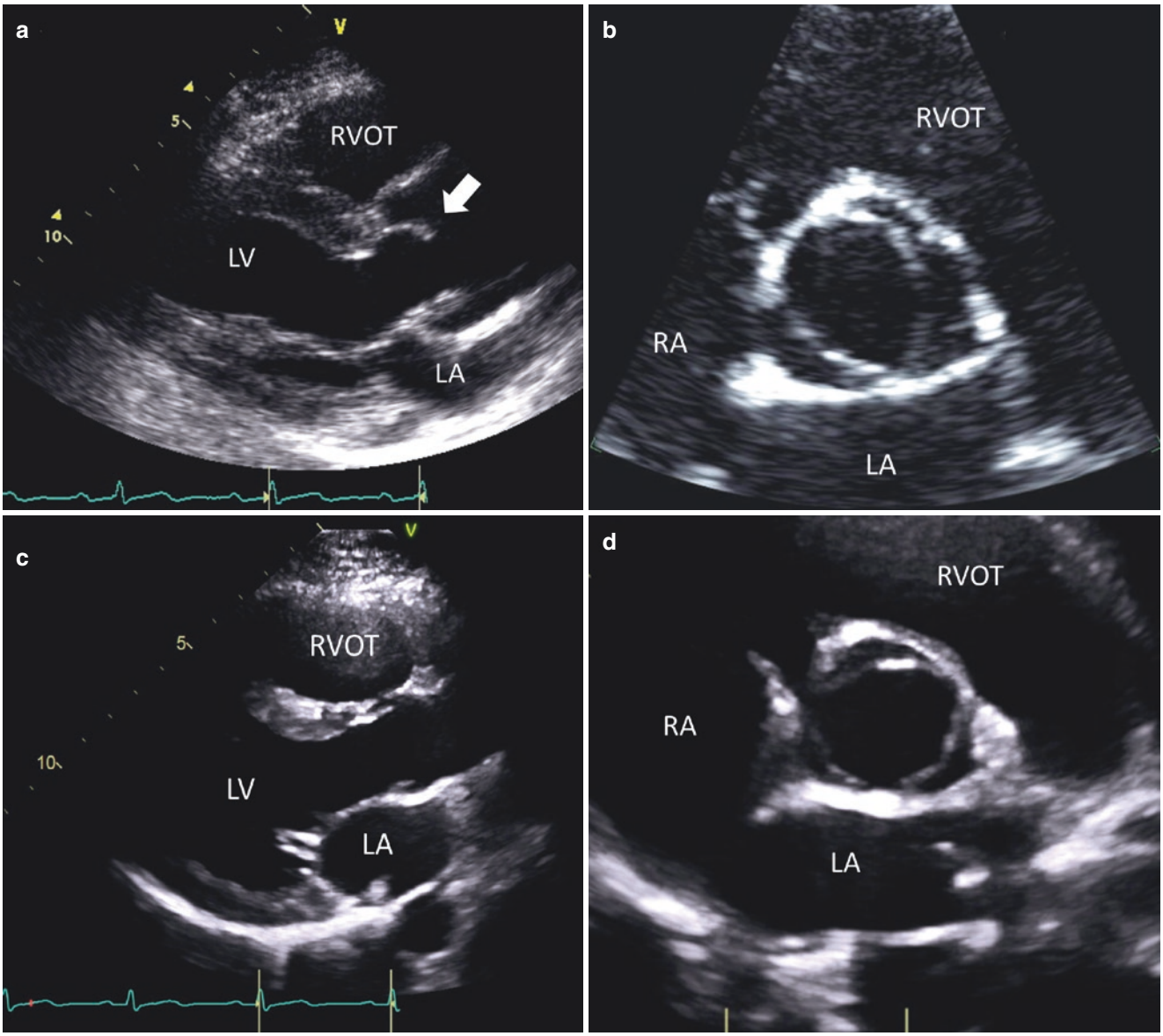

Fig. 21.9 Bicuspid aortic valve. (**a**) Parasternal long-axis view in a patient with a bicuspid aortic valve. Note the systolic doming of the thickened bicuspid aortic valve (arrow), in contrast to the normal systolic excursion seen in a patient with tricuspid aortic valve (panel C). (**b**) Parasternal short-axis view demonstrates an oval-shaped aortic valve orifice in a different patient with bicuspid aortic valve (fusion of right and left cusps). In contrast, note the triangular-shaped opening of a normal aortic valve (panel D). Assessment of aortic valve anatomy is performed during ventricular systole, when the aortic valve is fully opened. (**c**) Normal systolic excursion in a patient with tricuspid aortic valve. (**d**) Normal aortic valve (*LA* left atrium, *LV* left ventricle, *RA* right atrium, *RV* right ventricle, *RVOT* right ventricular outflow tract)

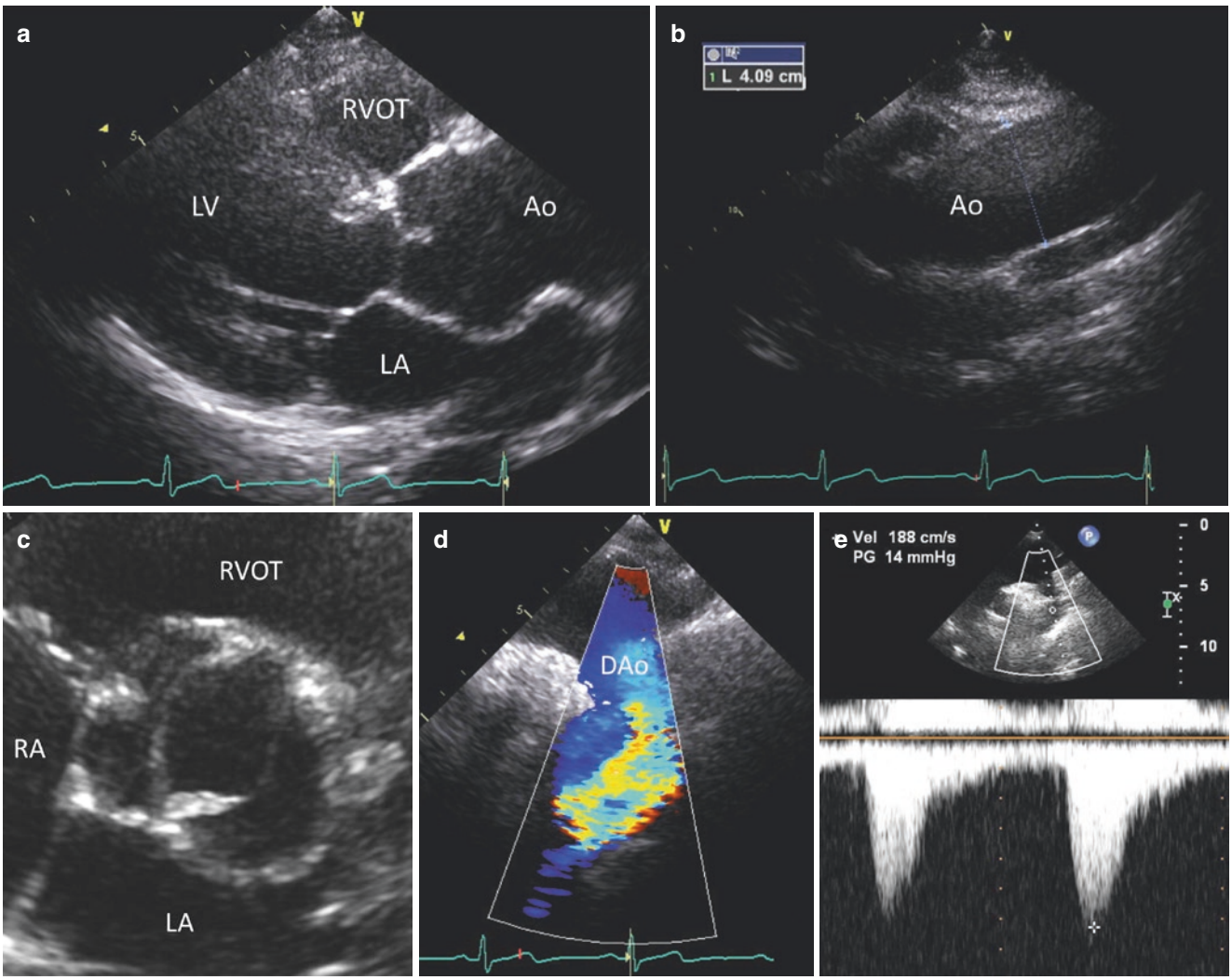

Fig. 21.10 Coarctation of the aorta. (**a**) and (**b**) Parasternal long-axis views demonstrate dilatation of the sinuses of Valsalva (panel A) and mid ascending aorta (panel B). For better visualization of the mid ascending aorta, the transducer is moved superiorly and toward the right axilla in panel B. (**c**) Parasternal short-axis view showing a bicuspid aortic valve, with fusion of the right and noncoronary cusps. (**d**) Color-flow Doppler assessment of the descending aorta from the suprasternal notch shows color flow aliasing, suggesting obstruction to flow. In this view, the transducer is located at the suprasternal notch with the probe marked at 12 o'clock and slightly angled toward the left hip. (**e**) The presence of mild coarctation of the aorta was confirmed by continuous wave Doppler (peak-to-peak gradient 14 mmHg) (*LA* left atrium, *LV* left ventricle, *RA* right atrium, *RV* right ventricle, *RVOT* right ventricular outflow tract, *Ao* aorta, *Dao* descending aorta)

Reference

1. Jacobs JP, Burke RP, Quintessenza JA, Mavroudis C. Congenital heart surgery nomenclature and database project: ventricular septal defect. Ann Thorac Surg. 2000;69(4 Suppl):S25–35.

Inferior Vena Cava

22

Alaa M. Omar, Edgar Argulian, and Jagat Narula

22.1 Introduction

Venous blood is derived back to the right side of the heart from the lower part of the body through the inferior vena cava (IVC). The IVC opens into the lowest part of the right atrium (RA) directed upward and backward by a rudimentary valve (Eustachian valve) at the level of the lower third of the ninth thoracic vertebra. The IVC is usually visualized and assessed by echocardiography using the subcostal approach. Respiratory changes and collapsibility of the IVC can be effectively used for the assessment of the right sided pressures and intravascular volume status [1–3]. IVC measurements can be done on the 2D- or M-mode recording of the IVC during at least one whole respiratory cycle. The recording should start from end expiration and involves inspiratory effort "sniff" followed by return to expiration again [1, 3]. IVC measurements should be done 2 cm away from the RA inlet [4]. IVC visualization can also help in assessment of several anatomical obstruction conditions such as IVC stenosis, thrombosis, and masses, in addition to several congenital abnormalities.

Figures 22.1, 22.2, 22.3, 22.4, 22.5, 22.6, 22.7, 22.8, 22.9, 22.10, 22.11, 22.12, and 22.13; Videos 22.1, 22.2a, 22.2b, 22.2c, 22.3, 22.4, 22.5, 22.6a, 22.6b, 22.7a, 22.7b, and 22.8; and Tables 22.1, 22.2, 22.3, and 22.4 provide details about visualization of the inferior vena cava.

Electronic Supplementary Material The online version of this chapter (https://doi.org/10.1007/978-3-319-73855-0_22) contains supplementary material, which is available to authorized users.

A. M. Omar, M.D., M.Sc., Ph.D. (✉)
Department of Cardiology, Icahn School of Medicine at Mount Sinai, New York, NY, USA

Department of Internal Medicine, Bronx Lebanon Hospital Center, Bronx, NY, USA

Department of Internal Medicine, National Research Center, Cairo, Egypt

E. Argulian, M.D., M.P.H.
Mount Sinai St. Luke's Hospital, Icahn School of Medicine at Mount Sinai, New York, NY, USA

J. Narula, M.D., Ph.D.
Mount Sinai Hospital, Icahn School of Medicine at Mount Sinai, New York, NY, USA

B. P. Nelson et al. (eds.), *Atlas of Handheld Ultrasound*, https://doi.org/10.1007/978-3-319-73855-0_22

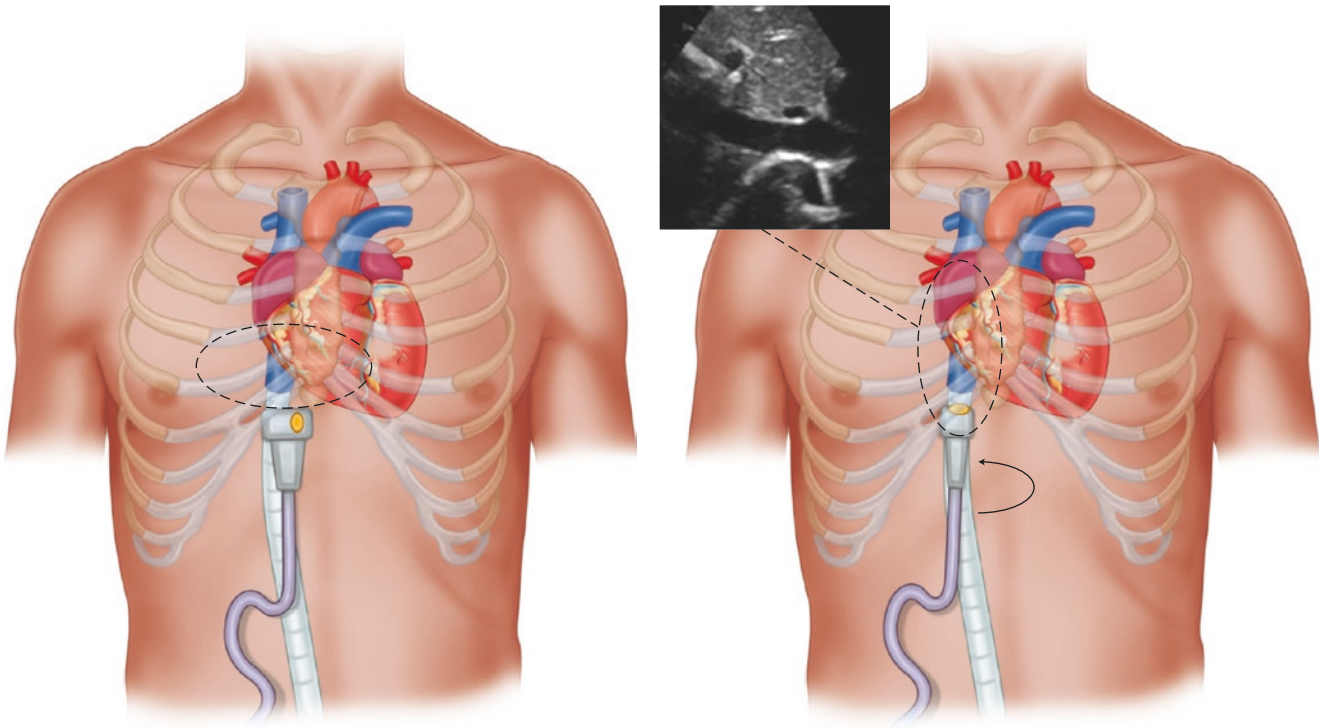

Fig. 22.1 Subcostal approach for assessment of the inferior vena cava (IVC). Left panel: With the patient in supine position, the subcostal view is obtained by placing the probe below the xiphoid process with the acoustic marker facing to the right (*yellow dot*). Right panel: Once the subcostal view of the heart is obtained, the probe is rotated to the right with the marker pointing upward (*arrow*). As such, the IVC should be visualized entering the right atrium (RA) in its longitudinal axis. Image courtesy of Alaa M. Omar, MD, PhD

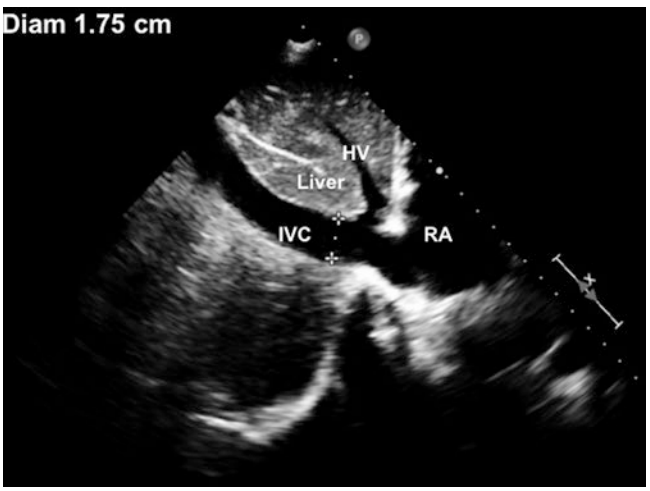

Fig. 22.2 Normal IVC Diameter measured from 2D image in the subcostal approach. The normal diameter of the IVC is ≤20 mm measured 2 cm from the inlet of the IVC into the right atrium. *HV* hepatic vein, *IVC* inferior vena cava, *RA* right atrium. Image courtesy of Alaa M. Omar, MD, PhD

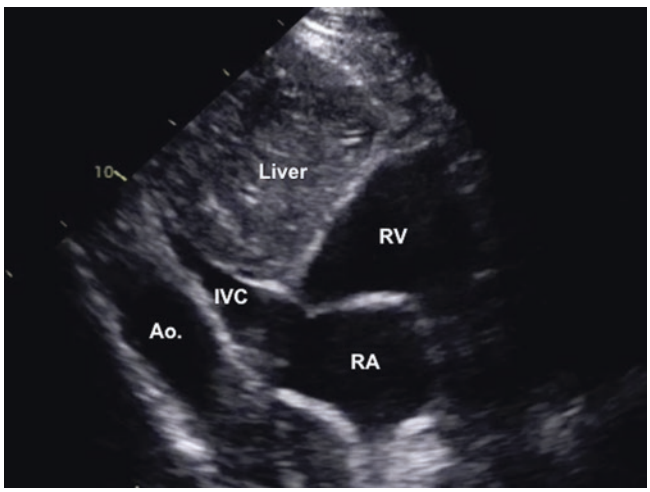

Fig. 22.3 IVC visualization using anterior axillary approach. This view uses the liver as an acoustic window. With the patient in supine position, the probe is placed in the right anterior axillary line with acoustic marker pointing toward the patient's head. From this approach, the IVC can be seen crossing the diaphragmatic opening longitudinally adjacent to the liver and parallel to the aorta. Visualizing the IVC entering the RA confirms its identity and differentiates it from the aorta. See Video 22.1. Image courtesy of Piedad Lerena Saenz, MD

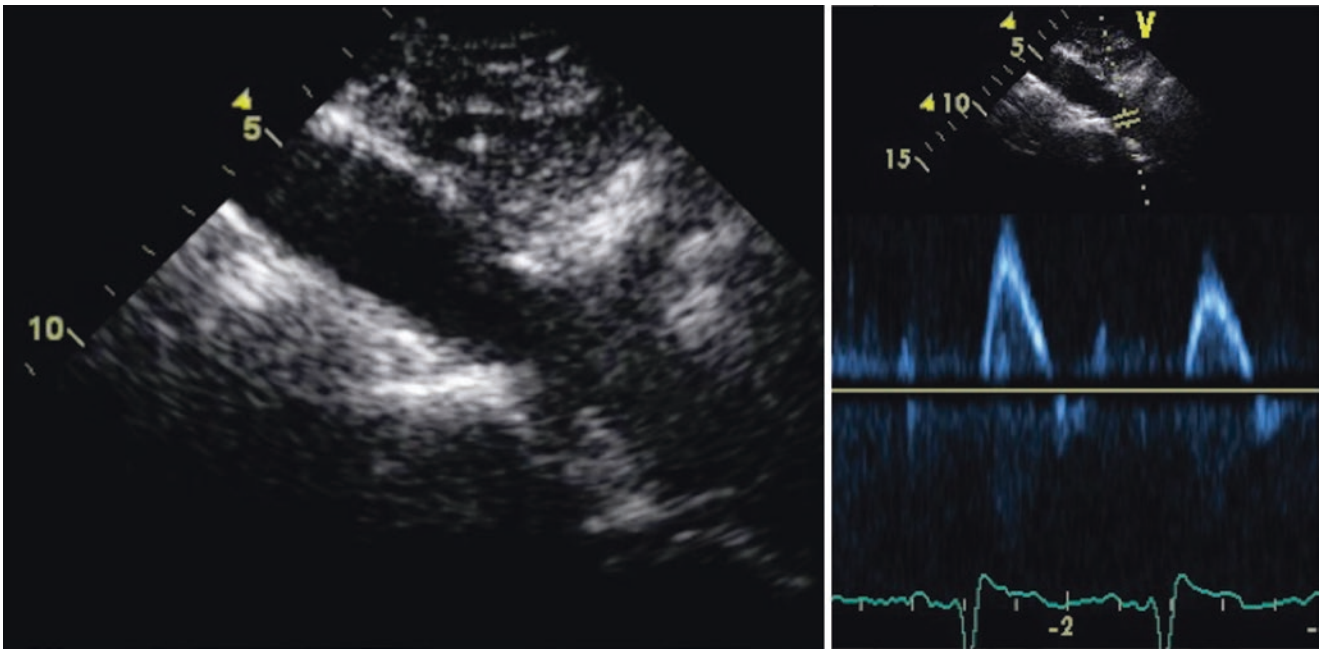

Fig. 22.4 Echocardiographic assessment of the aorta for differentiation from IVC. In comparison to the IVC, the aorta is an incompressible thick-wall vessel that does not change its diameter with respiration (left panel), and Doppler velocity signals are of high velocities (right panel). See Videos 22.2a–22.2c. Image courtesy of Alaa M. Omar, MD, PhD

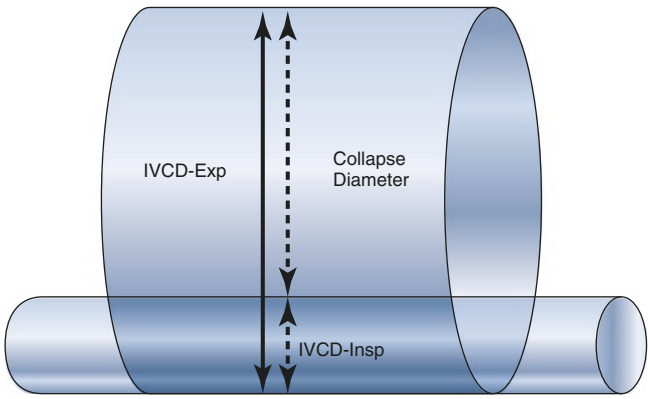

Fig. 22.5 Respiratory changes in IVC diameter. During inspiration: The drop in intra-thoracic pressure increases venous return to the right side of the heart. The drop of pressures in all thoracic structures increase the gradient between the right side of the heart and the thoracic part of the IVC on one side and the extra-thoracic IVC and venous circulation resulting in an increase in the velocity of venous return. The outcome of these changes is significant collapse of the IVC. During expiration: Intra-thoracic pressure returns to resting values leading to reversal of the aforementioned changes causing the return of IVC size. This can be used for the calculation of IVC collapsibility index (IVCCI), which is defined as the percentage of inspiratory collapse in relation to end expiratory IVCD (normally >50%). Image courtesy of Alaa M. Omar, MD, PhD

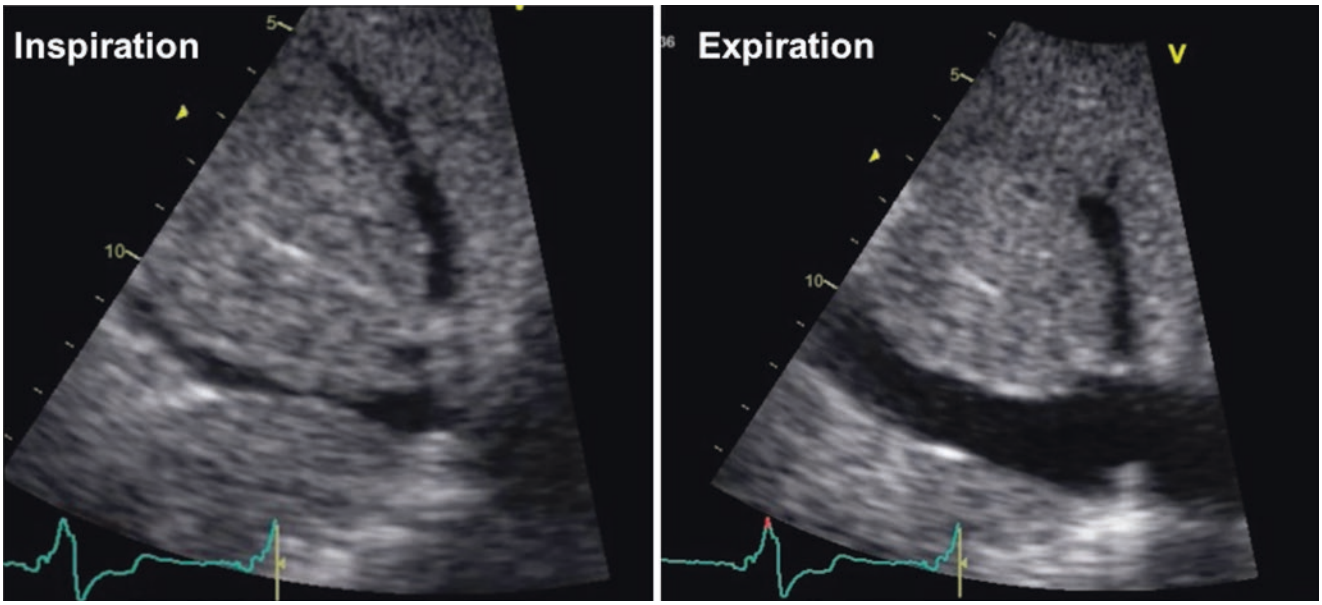

Fig. 22.6 2D echocardiographic assessment of IVC showing normal inspiratory collapse. See Video 22.3. Image courtesy of Alaa M. Omar, MD, PhD

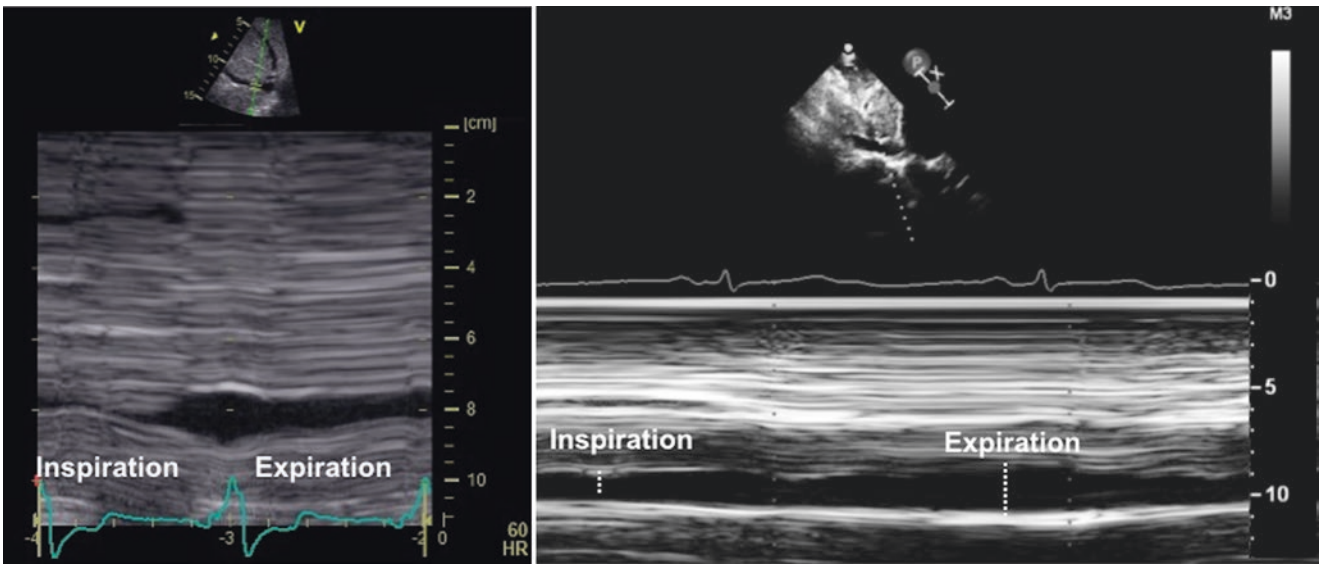

Fig. 22.7 M-Mode echocardiographic assessment of the IVC. The interrogation line is positioned across the IVC such that the inspiratory collapse of the IVC can be appreciated with return to its normal values with expiration. Be mindful of IVC movement cranial and caudal during respirations—if there is significant longitudinal displacement of the IVC the M-mode tracing will not demonstrate the same area of the IVC throughout the respiratory cycle. In this case, measurements of the IVC should be taken using B-mode in inspiration and expiration rather than measuring different areas of the same M-mode tracing. Image courtesy of Alaa M. Omar, MD, PhD

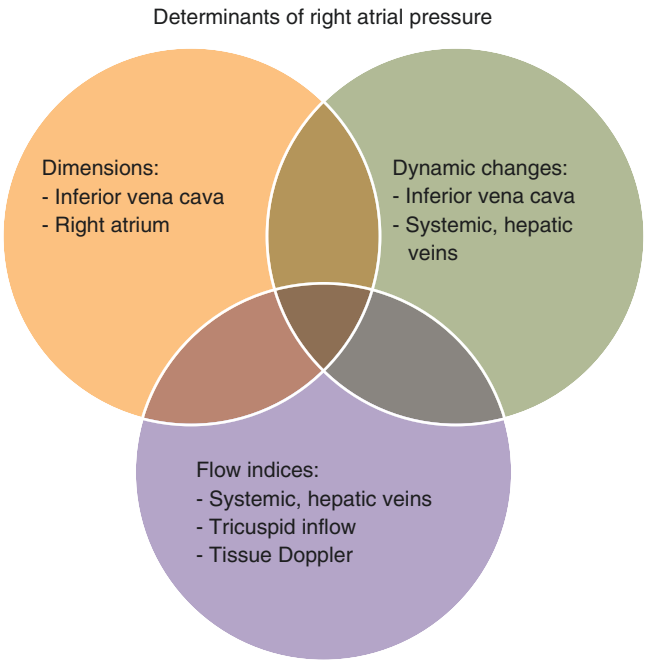

Fig. 22.8 Echocardiographic determinants of right atrial pressure (RAP). The IVC diameter and collapsibility play a major role in the assessment of RAP; however, multiple factors must be taken into account to provide an accurate estimate of RAP including right atrial dimensions, Doppler and tissue Doppler assessments of the tricuspid flow, hepatic veins and tricuspid annulus. (*Reproduced from* Beigel et al. [1]; *with permission*.)

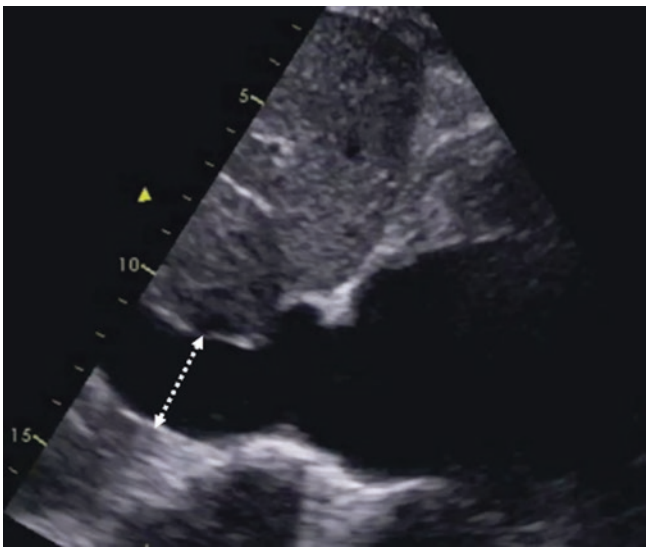

Fig. 22.9 IVC plethora in a patient with pulmonary hypertension. The IVC is engorged and does not demonstrate normal inspiratory collapse. These findings suggest elevated right atrial pressures. See Video 22.4. Image courtesy of Alaa M. Omar, MD, PhD

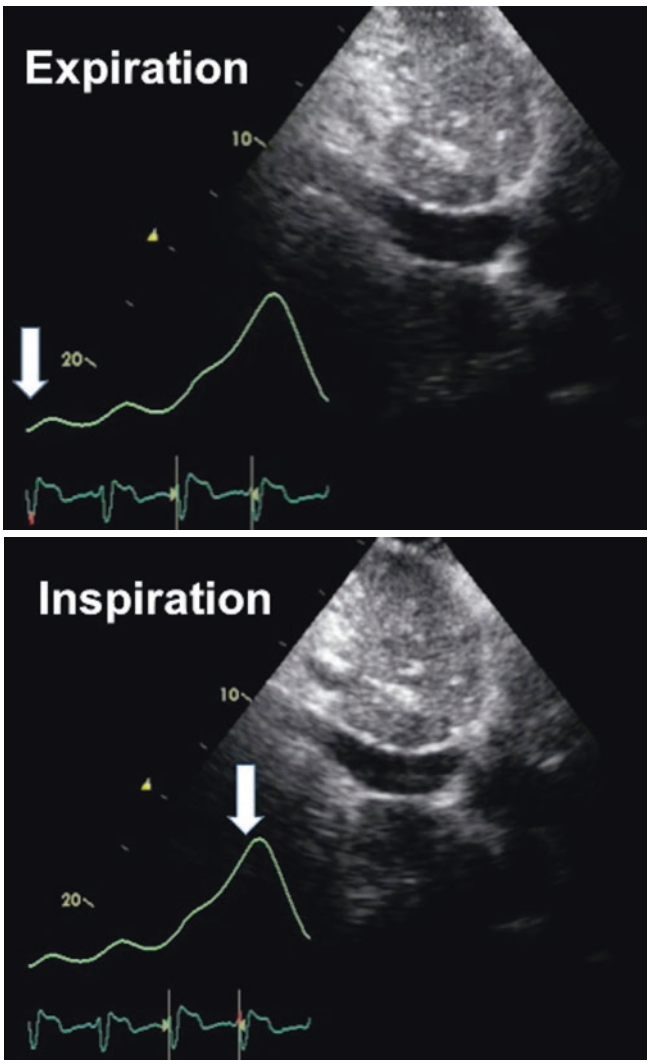

Fig. 22.10 Loss of IVC collapse in a patient with constrictive pericarditis. The IVC is assessed at end-expiration and with inspiration (sniff). These phases can be confirmed in the image using a respirometer for recording of the respiratory movements (arrows). See Video 22.5. Image courtesy of Alaa M. Omar, MD, PhD

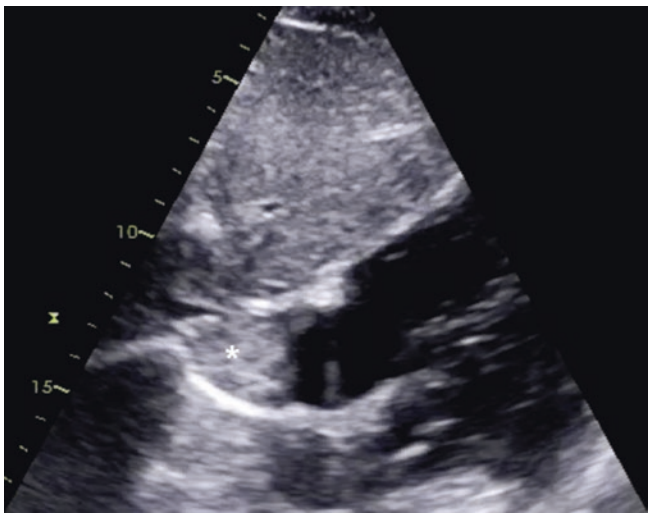

Fig. 22.11 Renal cell carcinoma extending to the IVC and the RA. See Videos 22.6a, 22.6b. Image courtesy of Piedad Lerena Saenz, MD

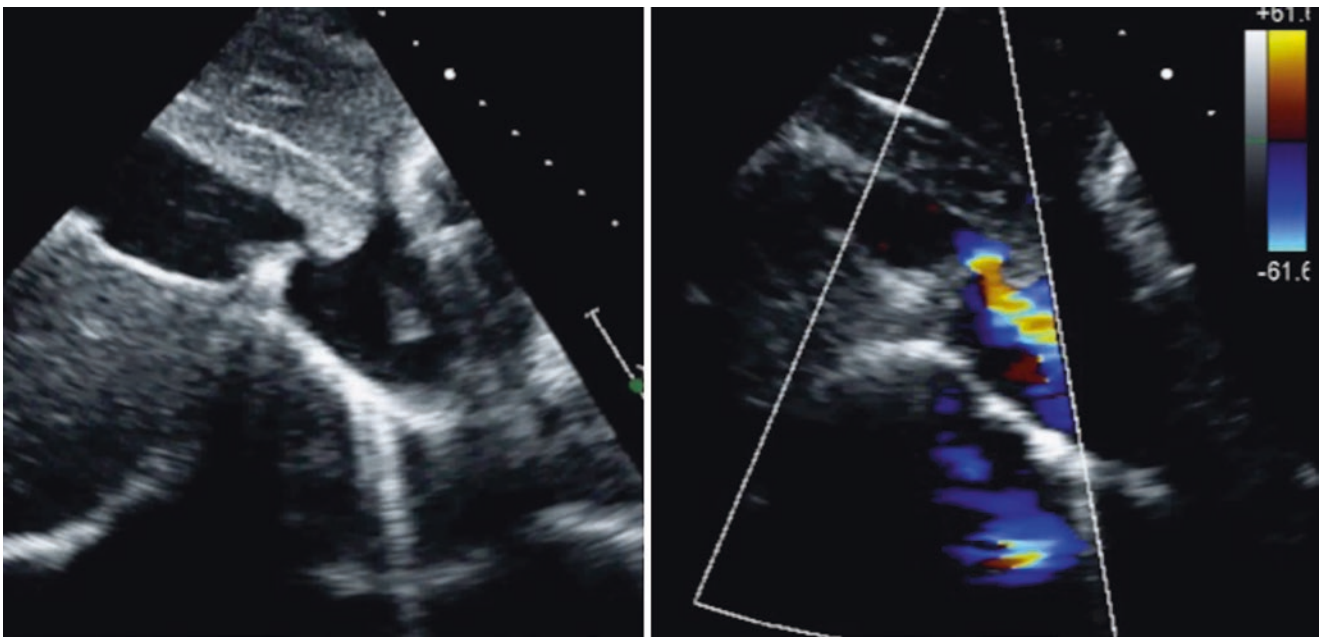

Fig. 22.12 IVC stenosis. Left panel showing focal narrowing of the IVC just before its opening into the RA, right panel with color flow Doppler showing turbulence and acceleration of the blood flow with a convergence zone developing at the stenotic end. See Video 22.7a, 22.7b. Image courtesy of Piedad Lerena Saenz, MD

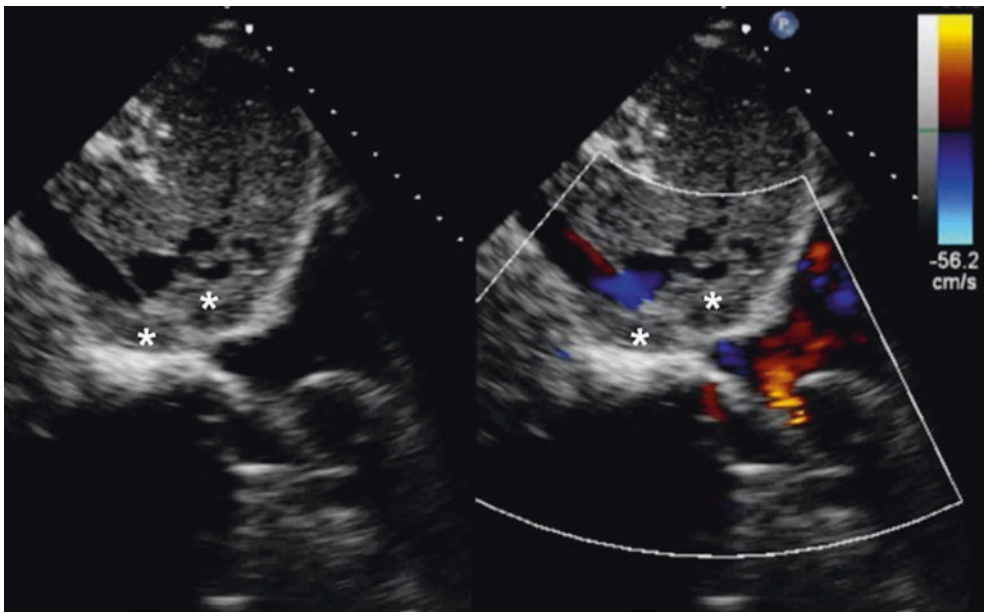

Fig. 22.13 Budd Chiari syndrome. Thrombosis developed at the middle hepatic vein as it joins the IVC. The thrombosis extends to the IVC (star, left panel), with color flow Doppler showing significant flow impingement (right panel). See Video 22.8. Image courtesy of Piedad Lerena Saenz, MD

Table 22.1 Echocardiographic measures of IVC assessment

Measurement	Definition	Normal range	Significance
IVCD	The anteroposterior diameter of inferior vena cava measured using frozen 2D images or M-mode echocardiography at end expiration	<20 mm	An increase in the IVCD usually reflects an increase in the RAP. E.g., pulmonary hypertension, significant tricuspid regurgitation, right ventricular failure, pericardial constriction and tamponade
IVCCI	Percentage of inspiratory collapse in relation to end expiratory IVCD	>50%	Attenuates or becomes lost with increased right atrial pressures

CVP central venous pressure, *IVCCI* inferior vena cava collapsibility index, *IVCD* inferior vena cava diameter, *RAP* right atrial pressure

Table 22.2 Interpretation of different IVC measures

	IVCD	IVCCI	Others
RAP value			
<5 mmHg (mean 3)	≤20 mm	>50%	
5–10 mmHg (mean 8)	≤20 mm	<50%	
5–10 mmHg (mean 8)	>20 mm	>50%	
>10 mmHg (mean 15)	>20 mm	>50%	Restrictive tricuspid flow pattern, tricuspid E/e' > 6 and hepatic vein diastolic flow reversal
Volume status			
Depleted	Decreased	>50%	
Overload	Increased	Minimal	

E/e' ratio between tricuspid early diastolic Doppler derived velocity and tricuspid annular early diastolic tissue Doppler derived velocity, *IVCCI* inferior vena cava collapsibility index, *IVCD* inferior vena cava diameter, *RAP* right atrial pressure

Table 22.3 Accuracy, sensitivity, and specificity of echocardiographic measurements for identification of RAP >10 mmHg according to Patel et al. [2]

	IVCD > 20 mm	IVCD > 20 IVCCI < 40%	IVCD > 20 IVCCI < 40% + 3D–RA volume index ≥35 ml/m^2
Accuracy	83	68	88
Sensitivity	89	60	92
Specificity	67	83	86

IVCCI inferior vena cava collapsibility index, *IVCD* inferior vena cava diameter

Table 22.4 Challenges and pitfalls in IVC assessment

	Challenges	
Bowel gas	Bowel gas masking IVC	Applying single-graded pressure to uncover the IVC; excessive pressure might compress the IVC giving the false impression of collapse Or Consider the anterior mid-axillary approach.
Mechanical ventilation	In patients receiving positive pressure ventilation, respiratory changes in IVCD become reversed. Thus, IVCD does not correlate with CVP and RAP	Can only be used in these patients to assess the response to volume loading.
Differentiating IVC from aorta	Both lie parallel, in close proximity, in the subcostal area. Especially challenging when using the anterior mid-axillary approach and in pediatric patients.	2D: IVC is a compressible thin walled vessel that changes diameter with respiration and the aorta is an incompressible thick wall vessel that does not change its diameter with respiration. IVC drains into RA; aorta does not. Hepatic veins drain from liver into IVC. Doppler velocities: aortic signal is of high velocity compared to the low velocity signals of the IVC. Color Doppler: will also show pulsatility of the aortic flow.
Clinical situations	Constriction in a dehydrated patients, volume depletion might mask IVC changes	Fluid challenge should be given to assess the IVC size while other echocardiographic assessments of CP should be also considered before excluding the diagnosis.

CP constrictive pericarditis, *CVP* central venous pressure, *IVC* inferior vena cava, *IVCD* inferior vena cava diameter, *RAP* right atrial pressure

References

1. Beigel R, Cercek B, Luo H, Siegel RJ. Noninvasive evaluation of right atrial pressure. J Am Soc Echocardiogr. 2013;26(9):1033–42.
2. Patel AR, Alsheikh-Ali AA, Mukherjee J, Evangelista A, Quraini D, Ordway LJ, et al. 3D echocardiography to evaluate right atrial pressure in acutely decompensated heart failure correlation with invasive hemodynamics. JACC Cardiovasc Imaging. 2011;4(9):938–45.
3. Nagdev AD, Merchant RC, Tirado-Gonzalez A, Sisson CA, Murphy MC. Emergency department bedside ultrasonographic measurement of the caval index for noninvasive determination of low central venous pressure. Ann Emerg Med. 2010;55:290–5.
4. Fields JM, Lee PA, Jenq KY, Mark DG, Panebianco NL, Dean AJ. The interrater reliability of inferior vena cava ultrasound by bedside clinician sonographers in emergency department patients. Acad Emerg Med. 2011;18:98–101.

Aorta

23

Peter C. Spittell, Anjali Bhagra, and Sharon L. Mulvagh

23.1 Introduction

Nontraumatic disorders of the aorta may be acute or chronic. Chronic disorders include aortic aneurysm, atherosclerosis, and aortitis, while acute aortic syndromes include acute aortic dissection, penetrating aortic ulcer, and aortic intramural hematoma. The aorta may be transected acutely, due to trauma, often seen after a motor vehicle accident. Congenital anomalies of the aorta most commonly include coarctation. The aorta can also become afflicted with a tumor. Transthoracic echocardiography can be utilized to evaluate the proximal to mid portion of the ascending aorta and abdominal aorta; evaluation of the aortic arch and descending thoracic aorta require more invasive (transesophageal echocardiography) or advanced imaging (CT/MRI/aortography) techniques. POCUS assessment of the aorta is thus limited to the proximal to mid ascending portion of the thoracic aorta, and the abdominal aorta. In the context of the history, physical examination, and clinical assessment, POCUS may be useful in identifying aortic abnormalities limited to these areas, particularly aneurysms and dissections, initiating additional confirmatory imaging, but cannot be considered definitive for exclusion of aortic pathologies.

23.2 Technique/Views

The aorta may be visualized from numerous acoustic windows, providing multiple views (Fig. 23.1). The aortic root and proximal ascending thoracic aorta are most readily visualized from the parasternal long-axis (PLAX) view where they are seen in the longitudinal plane; a portion of the descending thoracic aorta can also be seen posterior to the left atrium in cross-section (Fig. 23.2, Video 23.1). Moving the transducer slightly cephalad often enables further visualization of the ascending aorta beyond the proximal to the mid-level. Adjustment of the acoustic window to a high right parasternal view is sometimes necessary to maximize visualization of the mid-to-distal ascending thoracic aorta (Fig. 23.3, Video 23.2). Descending thoracic aneurysms can also be seen from the PLAX view (Videos 23.3a and 23.3b). The suprasternal acoustic window can also be used to view portions of the aortic arch, but this is a challenging view in most patients and is not considered to provide definitive structural information. The abdominal aorta is visualized with the transducer held at the midline of the abdomen starting from the subcostal region, and extending caudally to the bifurcation, in longitudinal and transverse (short axis) views (Fig. 23.4, Videos 23.4a, 23.4b, 23.4c, 23.4d, 23.4e, and 23.4f). Measurements of the ascending aorta are done using the "leading edge to leading edge technique" at end-diastole (Fig. 23.3, Video 23.2), and the upper threshold of normal is 3.5–4.0 cm [1]. Measurements of the abdominal aorta are done using the "outer edge to outer edge technique" (Fig. 23.4d), and the upper threshold of normal is 2.5–3.0 cm [2].

Electronic Supplementary Material The online version of this chapter (https://doi.org/10.1007/978-3-319-73855-0_23) contains supplementary material, which is available to authorized users.

P. C. Spittell, M.D. (✉)
Department of Cardiovascular Medicine, Mayo Clinic, Rochester, MN, USA
e-mail: Spittell.peter@mayo.edu

A. Bhagra, M.D.
Department of General Internal Medicine, Mayo Clinic, Rochester, MN, USA

S. L. Mulvagh, M.D., F.R.C.P.C.
Department of Medicine, Division of Cardiology, Dalhousie University, Halifax, NS, Canada

B. P. Nelson et al. (eds.), *Atlas of Handheld Ultrasound*, https://doi.org/10.1007/978-3-319-73855-0_23

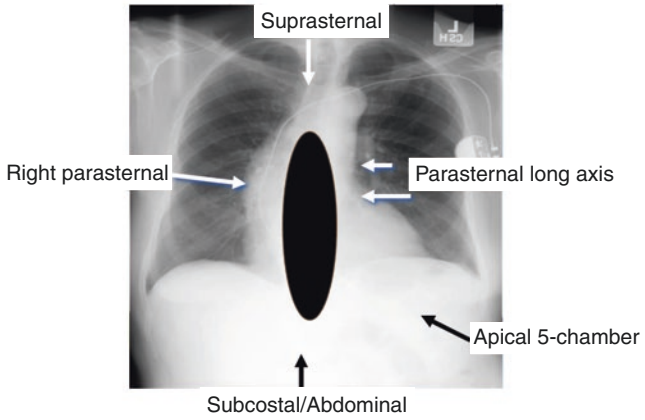

Fig. 23.1 Available acoustic windows to view the aorta, superimposed upon a chest X-ray, for anatomic reference. Images courtesy of Drs. Peter Spittell, Anjali Bhagra, and Sharon Mulvagh

23.2.1 Aortic Aneurysms

Aortic aneurysms are classified according to their anatomic location: thoracic or abdominal. Diagnostic evaluation techniques include: Chest x-ray, TEE, CT/CTA, MRI/MRA, and aortography. POCUS can be utilized as a screening tool for the presence of aneurysms in the proximal-to-mid ascending thoracic, arch, and abdominal aorta. The natural history of thoracoabdominal aneurysms is progressive enlargement, on average 2.5 mm/year. The rate of enlargement can be influenced by clinical (hypertension, associated atherosclerotic disease) and morphologic factors [3, 4].

23.2.1.1 Thoracic Aortic Aneurysms

Thoracic aortic aneurysms (Fig. 23.3, Videos 23.2, 23.3a, and 23.3b) are not usually diagnosed early, and, because most are asymptomatic, are often discovered incidentally. As they progress, however, chest and/or back pain may occur, and compression of adjacent structures may result in hoarseness, cough, dyspnea, stridor, plethora, edema, and dysphagia. Physical examination may demonstrate hypertension, fixed distension of one or more neck veins, aortic regurgitation, a fixed vocal cord, and systemic and/or cerebral embolism. Once diagnosed, serial follow-up surveillance assessment intervals are size-adjusted: 3.5–4.5 cm annually; 4.5–5.4 cm semi-annually. The yearly risk of rupture in ascending aortic aneurysms greater than 6.0 cm is approximately 30% [5]. Indications for surgical intervention include: Ascending aortic diameter ≥ 5.5 cm (*but threshold is lower [4.0–5.0 cm] in genetically mediated disorders*); descending aortic diameter ≥ 6.0 cm; symptomatic, rapid enlargement; traumatic origin; infectious etiology; and patients undergoing AVR with ascending aorta >4.5 cm [6].

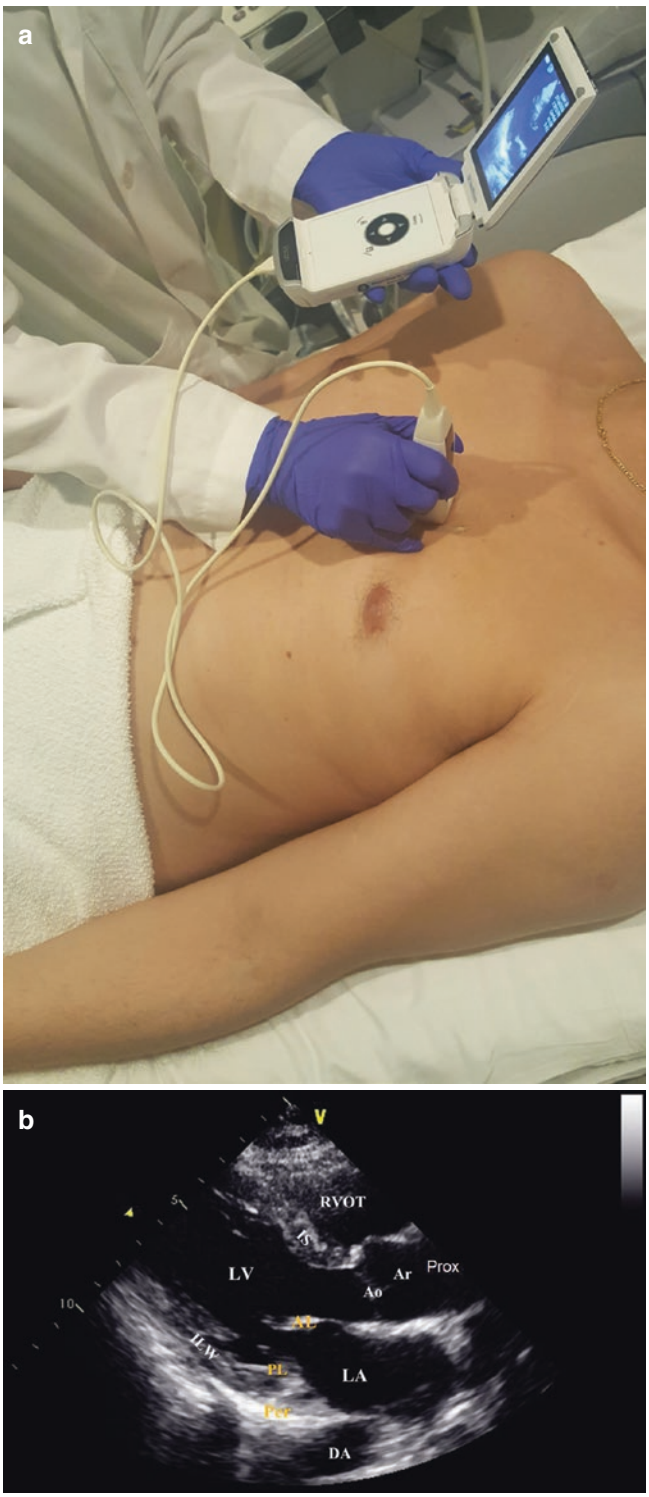

Fig. 23.2 (**a**) The transducer is positioned just to the left of the sternal border at about the second to third intercostal space, in the usual manner for achievement of the standard parasternal long axis view (PLAX). (**b**) In the PLAX view, the aortic valve (Ao), aortic root (Ar), and proximal (Prox) ascending thoracic aorta are seen. The left atrium (LA), left ventricle (LV), right ventricular outflow tract (RVOT) and aortic valve (AV) are also seen. Descending thoracic aorta (DA) is seen posterior to the left atrium. See also Video 23.1. Images courtesy of Drs. Peter Spittell, Anjali Bhagra, and Sharon Mulvagh

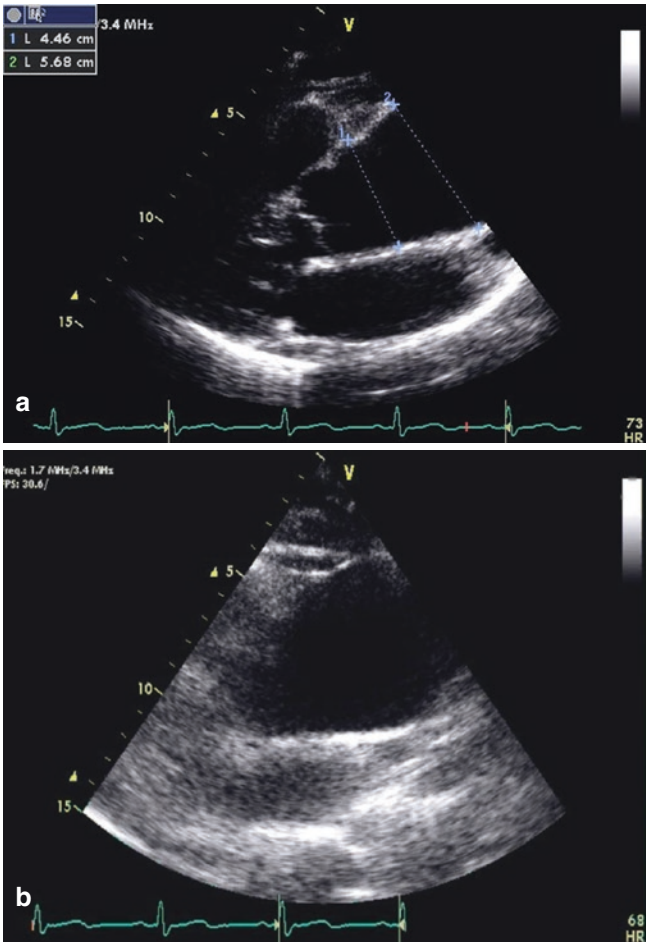

Fig. 23.3 From the PLAX position, the transducer can be slid slightly cephalad along the left sternal border edge to see more of the ascending aorta, including the mid ascending aorta, and revealing an ascending thoracic aortic aneurysm (see Video 23.2a). Additionally, the transducer can be moved to the right of the sternal border, at about the first to second intercostal space, to achieve the high right parasternal view (see Video 23.2b) and obtain an image of the mid-to distal ascending aorta. Measurements of the ascending aorta using the "leading edge to leading edge" method are demonstrated (**a** proximal and mid; **b** distal). See also Video 23.2. Images courtesy of Drs. Peter Spittell, Anjali Bhagra, and Sharon Mulvagh

23.2.1.2 Abdominal Aortic Aneurysms

Abdominal aortic aneurysms (AAA) (Fig. 23.4, Videos 23.4a, 23.4b, 23.4c, 23.4d, 23.4e, and 23.4f) are usually occult, and asymptomatic until they enlarge. Symptoms may include: pulsation in abdomen, abdominal pain, back pain, flank pain, groin pain, and those symptoms associated with atheroembolic phenomenon. Physical exam may include: pulsatile abdominal mass, hypertension, evidence of atheroembolism, peripheral arterial disease. Abdominal aortic aneurysm screening is done using ultrasound because the physical examination lacks sensitivity, early detection reduces mortality, and single screening ultrasound identifies most AAA. The U.S. Preventive Services Task Force (USPTF) provides a Grade B recommendation that men aged 65–75 years who have ever smoked should undergo ultrasound screening for AAA [7]. Serial follow-up surveillance assessment intervals are the same as for thoracic aneurysms. The one-year risk for AAA rupture is about 10% if less than 7.0 cm and increases dramatically with increasing size, to almost 40% when greater than 7.0 cm [8]. Indications for AAA surgery include: symptomatic; rupture/contained rupture; diameter > 5.5 cm; rapid expansion (>0.5 cm in 12 mo.); inflammatory or infectious etiology [9].

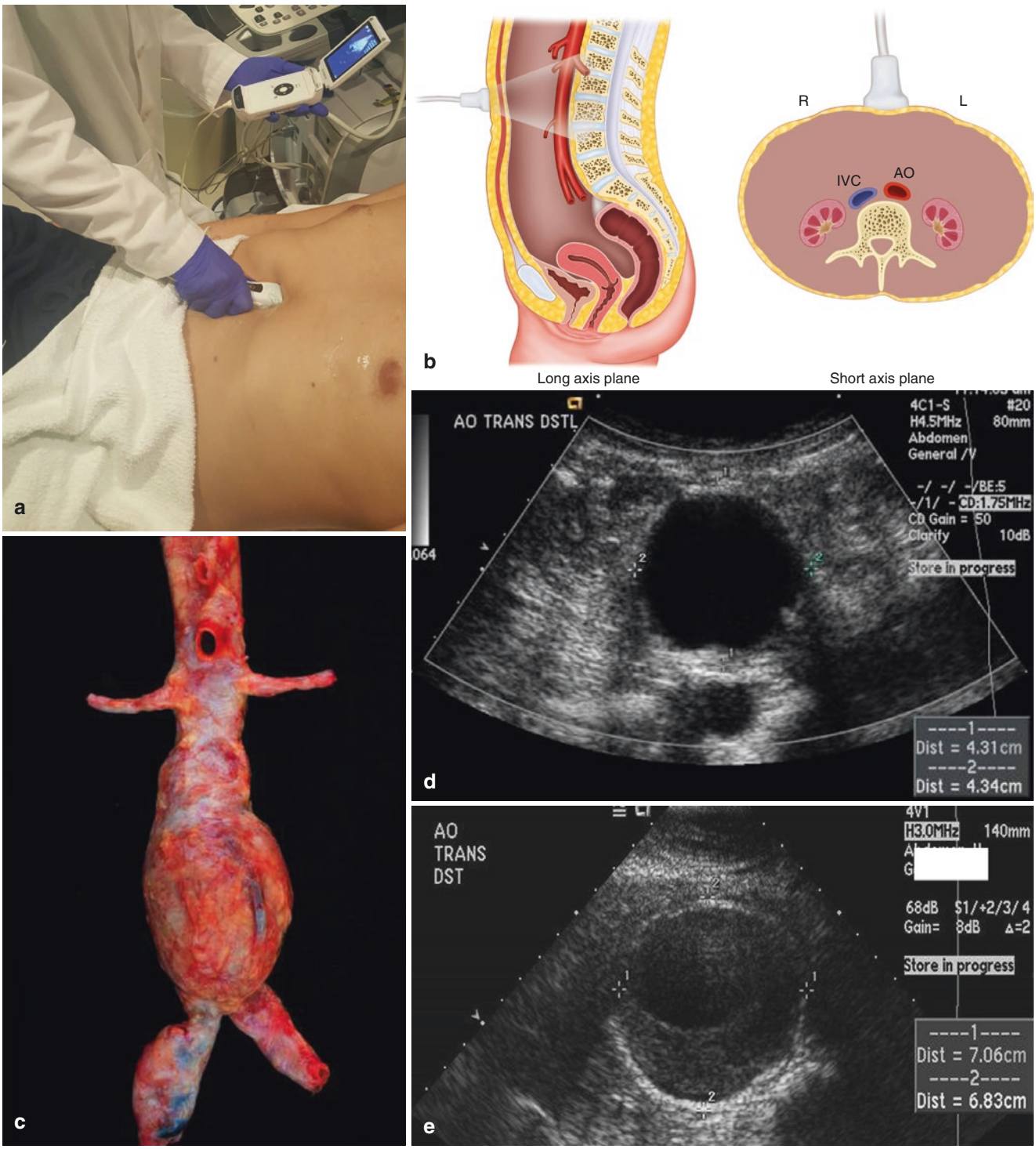

Fig. 23.4 The abdominal aorta is visualized and screening for aneurysmal disease is done with the transducer held in the midline of the abdomen starting at the subcostal region and then slowly swept caudally towards the umbilicus, until the aortic bifurcation is seen (Images **a** and **b**). This is done for both longitudinal and transverse views; normal findings are presented for each of these respective views in Videos 23.4a and 23.4b. See Videos 23.4c, 23.4d, 23.4e, and 23.4f for examples of patient screenings which revealed abdominal aortic aneurysms of varying complexities (true and false lumina, thrombus, debris). Measurements of the abdominal aorta in the transverse view using the "outer edge to outer edge" method is demonstrated (images **d** and **e**) in two different patients with different sizes of abdominal aortic aneurysms; note the true and false lumina in image **e**, with layered thrombus within the false lumen. Image **c** is an autopsy specimen from a patient who expired from rupture of a large abdominal aortic aneurysm. See also Videos 23.4a, 23.4b, 23.4c, 23.4d, 23.4e, and 23.4f. Images courtesy of Drs. Peter Spittell, Anjali Bhagra, and Sharon Mulvagh

23.3 Aortic Dissection

Aortic dissection (Fig. 23.5, Videos 23.4a, 23.4b, 23.4c, 23.4d, 23.4e, 23.4f; 23.5a, 23.5b, 23.5c, and 23.5d) is a potentially fatal aortic condition with a high mortality (1% per hour in the first 48 h; 70% die within the first two weeks), which is notoriously difficult to diagnose clinically, requiring a high index of suspicion and rapid performance of definitive noninvasive testing (TTE/TEE, MRI/MRA, CT/CTA) to achieve accurate diagnosis (pooled sensitivity and specificity of TEE, CT, MRI is 95–98% [10]. The choice of test depends upon the patient's stability and test availability. POCUS can be a valuable tool in the emergency setting, also for identifying associated high-risk features including pericardial effusion and/or cardiac tamponade (a surgical emergency); negative findings on transthoracic echo, however, *do not* exclude dissection [11]. Aortic dissections are classified as Type A or B, depending on extent: Type A (proximal) includes the ascending thoracic aorta, and Type B is limited to the distal thoracic aorta. Symptoms and signs can include sudden onset, of severe chest, back or abdominal pain (sensitivity: 90%, specificity: 84%), congestive heart failure, shock, cerebrovascular accident, syncope, paraplegia, or acute arterial occlusion [12, 13]. Physical examination may reveal elevated blood pressure (36% [type A], 70% [type B]), pulse deficit or asymmetric blood pressure differential (19–30% [type A], 9–21% [type B]), new diastolic murmur (of aortic regurgitation −28%); focal neurologic deficits: 17% [12]. Management depends on the classification of the aortic dissection; Type A requires immediate surgical repair, while Type B is initially managed medically, with delayed surgical approach [6, 13, 14].

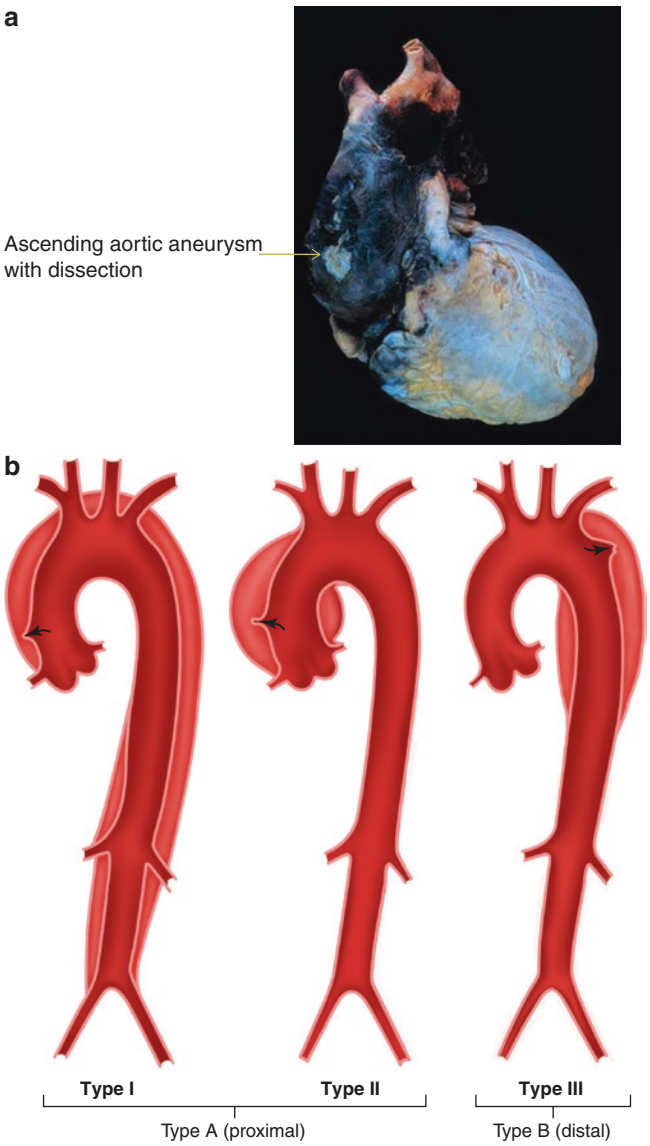

Fig. 23.5 57-year-old female presented with acute low back pain and paraplegia, and suffered hemodynamic collapse. Image (**a**) is a pathology specimen of patient who succumbed to sudden death due to aortic dissection. Image (**b**) displays the classification of aortic dissection. See also Videos 23.5a, 23.5b, 23.5c, and 23.5d. Images courtesy of Drs. Peter Spittell, Anjali Bhagra, and Sharon Mulvagh

References

1. Lang RM, Badano LP, Mor-Avi V, Afilalo J, Armstrong A, Ernande L, et al. Recommendations for cardiac chamber quantification by echocardiography in adults: an update from the American Society of Echocardiography and the European Association of Cardiovascular Imaging. J Am Soc Echocardiogr. 2015;28(1):1–39.e14.
2. Campens L, Demulier L, De Groote K, Vandekerckhove K, De Wolf D, Roman MJ, et al. Reference values for echocardiographic assessment of the diameter of the aortic root and ascending aorta spanning all age categories. Am J Cardiol. 2014;114(6):914–20.
3. Kuzmik GA, Sang AX, Elefteriades JA. Natural history of thoracic aortic aneurysms. J Vasc Surg. 2012;56(2):565–71.
4. Yiu RS, Cheng SW. Natural history and risk factors for rupture of thoracic aortic arch aneurysms. J Vasc Surg. 2016;63(5):1189–94.
5. Elefteriades JA. Natural history of thoracic aortic aneurysms: indications for surgery, and surgical versus nonsurgical risks. Ann Thorac Surg. 2002;74(5):S1877–80; discussion S1892–8.
6. Tsai TT, Fattori R, Trimarchi S, Isselbacher E, Myrmel T, Evangelista A, et al. Long-term survival in patients presenting with type B acute aortic dissection: insights from the International Registry of Acute Aortic Dissection. Circulation. 2006;114(21):2226–31.
7. Bird AN, Davis AM. Screening for abdominal aortic aneurysm. JAMA. 2015;313(11):1156–7.
8. Lederle FA, Johnson GR, Wilson SE, Ballard DJ, Jordan WD Jr, Blebea J, et al. Rupture rate of large abdominal aortic aneurysms in patients refusing or unfit for elective repair. JAMA. 2002;287(22):2968–72.
9. Brewster DC, Cronenwett JL, Hallett JW Jr, Johnston KW, Krupski WC, Matsumura JS, et al. Guidelines for the treatment of abdominal aortic aneurysms. Report of a subcommittee of the Joint Council of the American Association for Vascular Surgery and Society for Vascular Surgery. J Vasc Surg. 2003;37(5):1106–17.
10. Shiga T, Wajima Z, Apfel CC, Inoue T, Ohe Y. Diagnostic accuracy of transesophageal echocardiography, helical computed tomography, and magnetic resonance imaging for suspected thoracic aortic dissection: systematic review and meta-analysis. Arch Intern Med. 2006;166(13):1350–6.
11. Evangelista A, Avegliano G, Aguilar R, Cuellar H, Igual A, González-Alujas T, et al. Impact of contrast-enhanced echocardiography on the diagnostic algorithm of acute aortic dissection. Eur Heart J. 2010;31(4):472–9.
12. Park SW, Hutchison S, Mehta RH, Isselbacher EM, Cooper JV, Fang J, et al. Association of painless acute aortic dissection with increased mortality. Mayo Clin Proc. 2004;79:1252–7.
13. ACCF/AHA/AATS/ACR/ASA/SCA/SCAI/SIR/STS/SVM Guidelines for the diagnosis and management of patients with thoracic aortic disease representative members*, Hiratzka LF, Creager MA, Isselbacher EM, Svensson LG, 2014 AHA/ACC Guideline for the Management of Patients With Valvular Heart Disease Representative Members*, Nishimura RA, Bonow RO, et al. Surgery for aortic dilatation in patients with bicuspid aortic valves: a statement of clarification from the American College of Cardiology/American Heart Association Task Force on Clinical Practice Guidelines. Circulation. 2016;133(7):680–6.
14. Rogers AM, Hermann LK, Booher AM, Nienaber CA, Williams DM, Kazerooni EA, et al. Sensitivity of the aortic dissection detection risk score, a novel guideline-based tool for identification of acute aortic dissection at initial presentation: results from the international registry of acute aortic dissection. Circulation. 2011;123(20):2213–8.

Peripheral Veins

24

Stephen Alerhand

Bedside ultrasound (US) is an extremely valuable tool to increase success rates for acquiring difficult intravenous (IV) access [1–3]. Patients for whom the landmark method is technically difficult include: obese or edematous patients, those undergoing dialysis, chemotherapy treatments, frequent IV placement for any other chronic illness, or a history of IV drug use. Safe and effective US-guided IV access has also been shown to decrease the utilization of central venous catheters in non-critical patients [4, 5], while also increasing patient satisfaction in those who are discharged from the emergency department [6]. In pediatric patients as well, use of US may decrease the number of attempts made to attain IV access [7, 8]. This skill can be learned by physicians, nurses [9–11], and technicians [12] alike.

For procedural guidance, recognizing the appearance of a vein can be helpful to avoid vessel puncture during incision and drainage of abscesses. Moreover, in the correct clinical picture, thrombophlebitis of peripheral veins can be diagnosed by visualizing echogenic material within a non-compressible lumen.

The figures that follow demonstrate proper probe position in assessing the anatomy and collapsibility of the peripheral veins (Figs. 24.1, 24.2, 24.3, 24.4, 24.5, and 24.6) (Videos 24.1 and 24.2).

Electronic Supplementary Material The online version of this chapter (https://doi.org/10.1007/978-3-319-73855-0_24) contains supplementary material, which is available to authorized users.

S. Alerhand, M.D.
Department of Emergency Medicine, Icahn School of Medicine at Mount Sinai, New York, NY, USA

B. P. Nelson et al. (eds.), *Atlas of Handheld Ultrasound*, https://doi.org/10.1007/978-3-319-73855-0_24

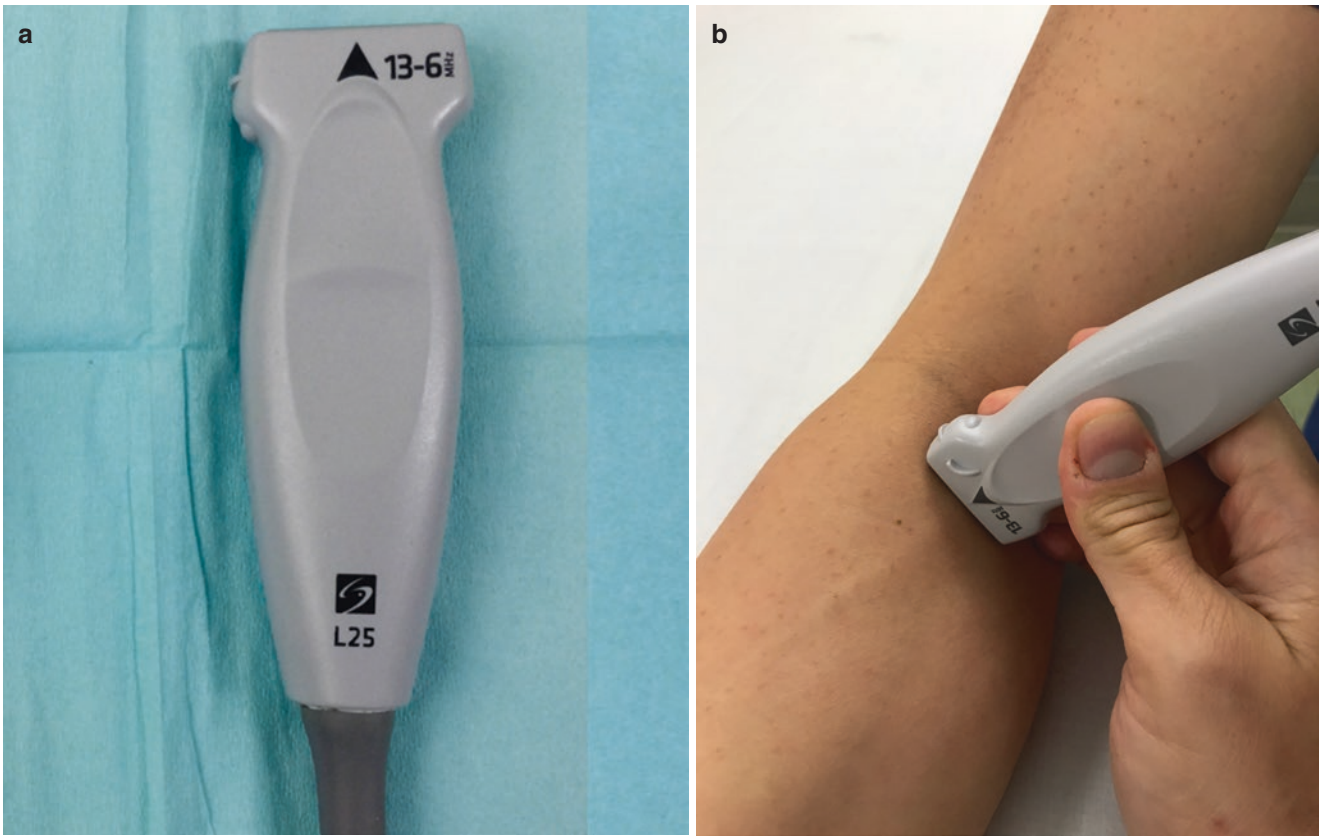

Fig. 24.1 Ultrasound probe position in the right antecubital fossa. (**a**) The linear (high-frequency) probe should be placed transversely in the antecubital fossa. (**b**) The probe marker should be placed toward the patient's right, so that from the physician's perspective, the left side of the probe corresponds to the left side of the ultrasound screen. Image courtesy of Bret Nelson

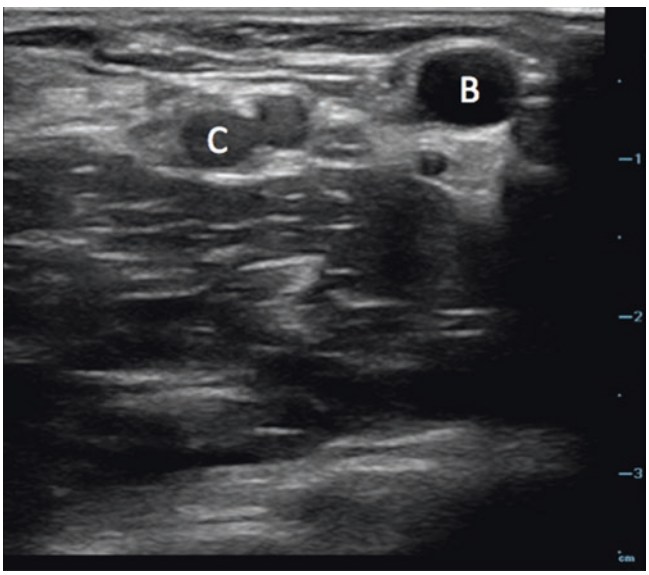

Fig. 24.2 Ultrasound image of the right antecubital fossa. Circular blood vessel walls appear hyperechoic, while blood within the lumen appears anechoic. The basilic vein (B) can be visualized medially and the cephalic vein (C) laterally. Image courtesy of Stephen Alerhand

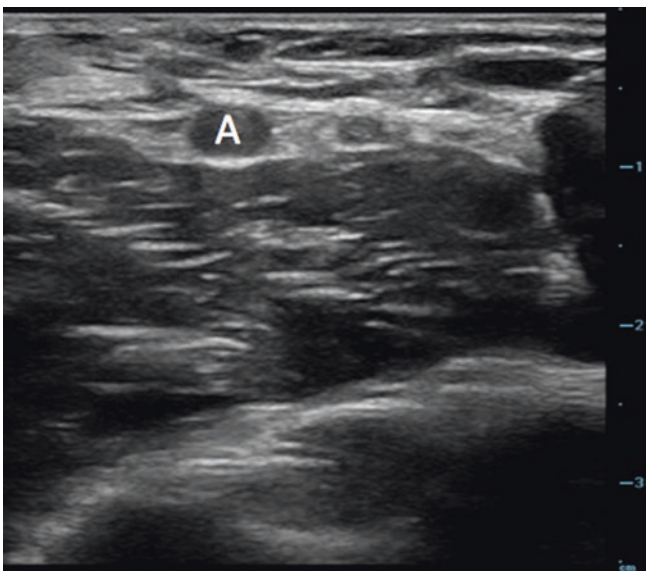

Fig. 24.3 Ultrasound image of the right antecubital fossa under compression. Veins have thin compressible walls, whereas arteries (A) have thicker walls that do not fully compress upon application of pressure. Image courtesy of Stephen Alerhand

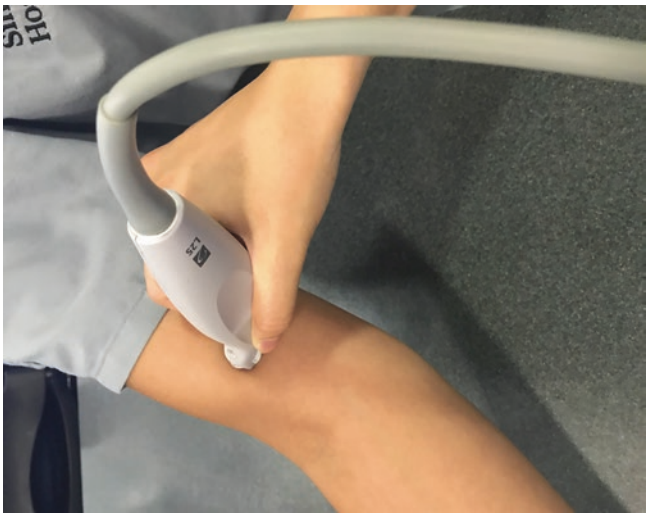

Fig. 24.4 Ultrasound probe position in the right medial upper arm. The linear (high-frequency) probe should be placed transversely in the median upper arm. The probe marker should be placed toward the patient's right, so that from the physician's perspective, the left side of the probe corresponds to the left side of the ultrasound screen. Image courtesy of Stephen Alerhand

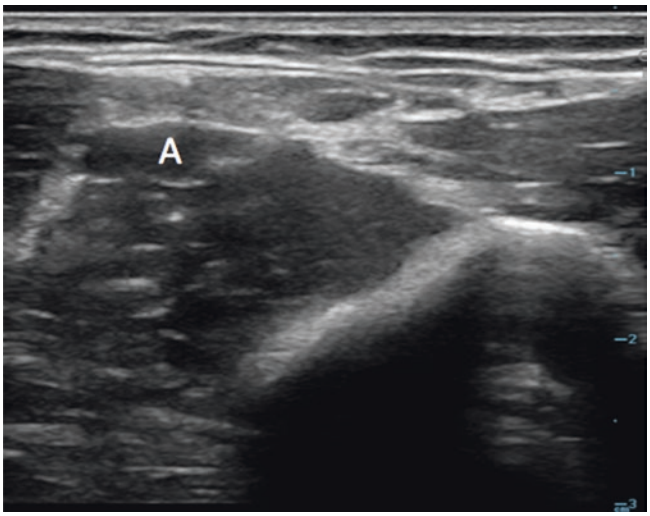

Fig. 24.6 Ultrasound image of the medial upper arm veins under compression. The thin-walled veins fully compress with application of pressure, whereas the thicker-walled brachial artery (A) remains patent. Image courtesy of Stephen Alerhand

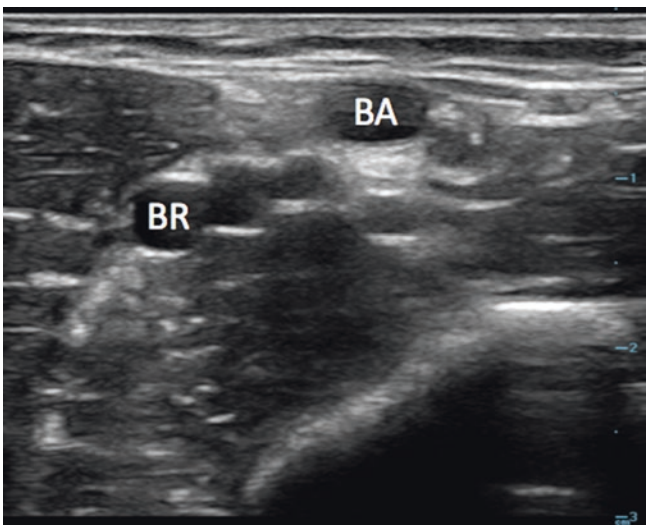

Fig. 24.5 Ultrasound image of the right medial upper arm. The basilic (BA) and deep brachial veins (BR) can be visualized in this region. Image courtesy of Stephen Alerhand

References

1. Egan G, Healy D, O'Neill H, Clarke-Moloney M, Grace PA, Walsh SR. Ultrasound guidance for difficult peripheral venous access: systematic review and meta-analysis. Emerg Med J. 2013;30(7):521–6.
2. Stolz LA, Stolz U, Howe C, Farrell IJ, Adhikari S. Ultrasound-guided peripheral venous access: a meta-analysis and systematic review. J Vasc Access. 2015;16(4):321–6.
3. Costantino TG, Parikh AK, Satz WA, Fojtik JP. Ultrasonography-guided peripheral intravenous access versus traditional approaches in patients with difficult intravenous access. Ann Emerg Med. 2005;46(5):456–61.
4. Au AK, Rotte MJ, Grzybowski RJ, Ku BS, Fields JM. Decrease in central venous catheter placement due to use of ultrasound guidance for peripheral intravenous catheters. Am J Emerg Med. 2012;30(9):1950–4.
5. Shokoohi H, Boniface K, McCarthy M, Khedir Al-tiae T, Sattarian M, Ding R, et al. Ultrasound-guided peripheral intravenous access program is associated with a marked reduction in central venous catheter use in noncritically ill emergency department patients. Ann Emerg Med. 2013;61(2):198–203.
6. Schoenfeld E, Shokoohi H, Boniface K. Ultrasound-guided peripheral intravenous access in the emergency department: patient-centered survey. West J Emerg Med. 2011;12(4):475–7.

7. Doniger SJ, Ishimine P, Fox JC, Kanegaye JT. Randomized controlled trial of ultrasound-guided peripheral intravenous catheter placement versus traditional techniques in difficult-access pediatric patients. Pediatr Emerg Care. 2009;25(3):154–9.
8. Heinrichs J, Fritze Z, Vandermeer B, Klassen T, Curtis S. Ultrasonographically guided peripheral intravenous cannulation of children and adults: a systematic review and meta-analysis. Ann Emerg Med. 2013;61(4):444–54.e1.
9. Carter T, Conrad C, Wilson JL, Dogbey G. Ultrasound guided intravenous access by nursing versus resident staff in a community based teaching hospital: a "Noninferiority" trial. Emerg Med Int. 2015;2015:563139.
10. Bahl A, Pandurangadu AV, Tucker J, Bagan M. A randomized controlled trial assessing the use of ultrasound for nurse-performed IV placement in difficult access ED patients. Am J Emerg Med. 2016;34(10):1950–4.
11. Stolz LA, Cappa AR, Minckler MR, Stolz U, Wyatt RG, Binger CW, et al. Prospective evaluation of the learning curve for ultrasound-guided peripheral intravenous catheter placement. J Vasc Access. 2016;17(4):366–70.
12. Duran-Gehring P, Bryant L, Reynolds JA, Aldridge P, Kalynych CJ, Guirgis FW. Ultrasound-guided peripheral intravenous catheter training results in physician-level success for emergency department technicians. J Ultrasound Med. 2016;35(11):2343–52.

Peritoneum

25

Pimpa Limphan-udom

Bedside ultrasound is an optimal first-line imaging modality for the evaluation of peritoneal free fluid. The focused assessment with sonography in trauma (FAST) examination is one of the first point-of-care, multi-organ system assessments described in literature. Although computed tomography (CT) is generally more sensitive and specific for diagnosing solid organ injury, pneumothorax, hemoperitoneum and other acute injuries, ultrasound involves no ionizing radiation, intravenous contrast, and can generally be performed and interpreted much more rapidly [1, 2]. This is especially helpful in patients too unstable for transport to Radiology. The benefits of bedside ultrasound are now commonly extended beyond trauma evaluations to search for free fluid in the non-traumatic patient and in other disease processes. It can be used to evaluate for free peritoneal fluid in patients with end-stage liver disease, renal disease, congestive heart failure, or ruptured ectopic pregnancy and guide the optimal site for paracentesis. Bedside ultrasound for free fluid can expedite patient care and definitive treatment [3].

Although not the primary imaging modality, bedside ultrasound can be used to diagnose perforations [4]. Previous prospective studies of patients with abdominal trauma or abdominal pain have confirmed that ultrasound is as accurate as plain radiography, although CT remains the imaging gold standard for perforations (Figs. 25.1, 25.2, 25.3, 25.4, 25.5, 25.6, 25.7, 25.8, 25.9, and 25.10; Videos 25.1, 25.2, 25.3, 25.4, and 25.5) [5–11].

Electronic Supplementary Material The online version of this chapter (https://doi.org/10.1007/978-3-319-73855-0_25) contains supplementary material, which is available to authorized users.

P. Limphan-udom, M.D.
Emergency Medicine Department, Icahn School of Medicine at Mount Sinai, New York, NY, USA

B. P. Nelson et al. (eds.), *Atlas of Handheld Ultrasound*, https://doi.org/10.1007/978-3-319-73855-0_25

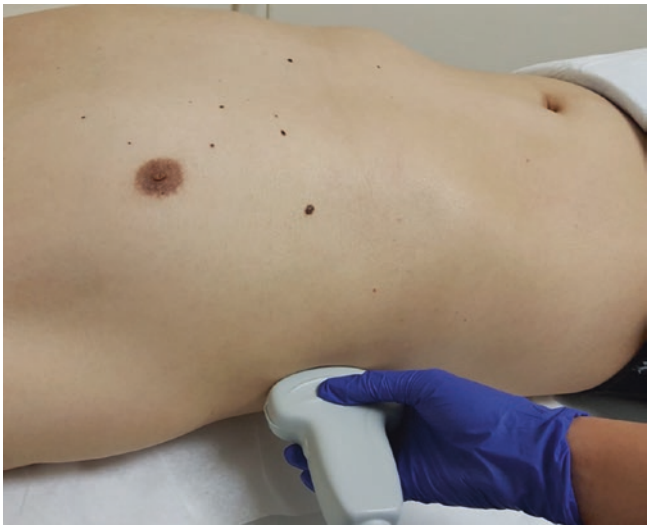

Fig. 25.1 Ultrasound probe position on the right upper quadrant. The transducer should be placed in a coronal plane in the midaxillary line between the 9th and 11th intercostal spaces with the transducer marker pointing cephalad. Image courtesy of Pimpa Limphan-udom

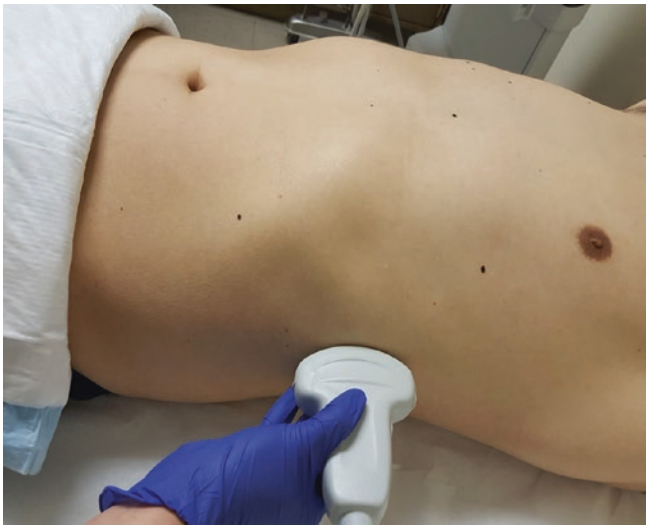

Fig. 25.3 Ultrasound probe position on the left upper quadrant. The transducer should be placed in a coronal plane in the posterior axillary line between the sixth and nineth intercostal spaces with the transducer marker pointing cephalad. The image may be improved by rotating the transducer 10–20° clockwise with the transducer marker pointing slightly posteriorly. Angle the transducer superiorly to image below the diaphragm in the perisplenic space. Again, the area immediately above (cephalad to) the diaphragm can be visualized to exclude fluid in the thorax. Image courtesy of Pimpa Limphan-udom

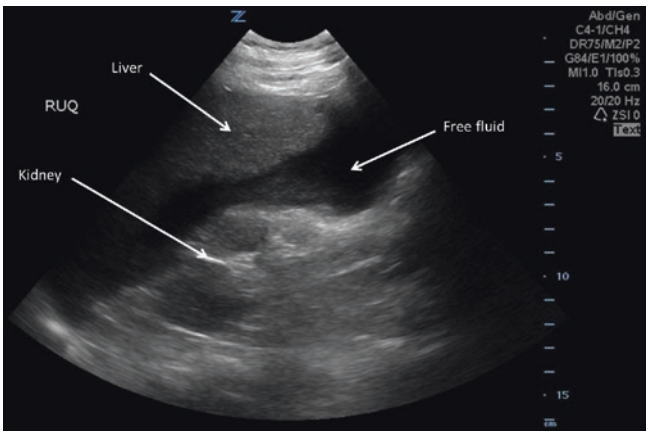

Fig. 25.2 Ultrasound image of free fluid in the right upper quadrant. Peritoneal free fluid (anechoic) in the hepatorenal recess. Image courtesy of Pimpa Limphan-udom

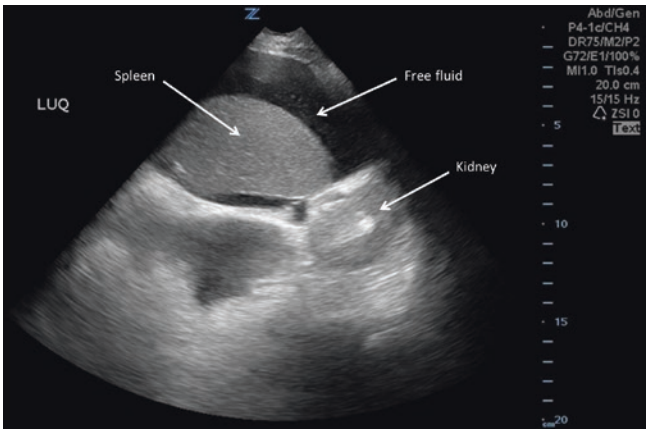

Fig. 25.4 Ultrasound image of free fluid in the left upper quadrant. Peritoneal free fluid in the subdiaphragmatic space in the left upper quadrant. Image courtesy of Pimpa Limphan-udom

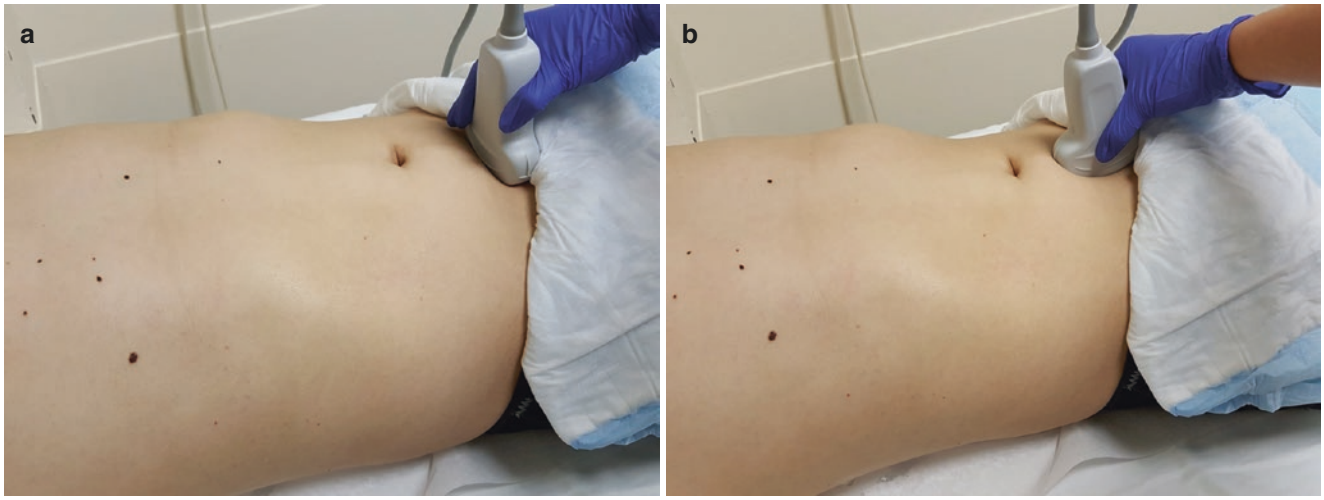

Fig. 25.5 Ultrasound probe position for visualizing the pelvis. For a transverse view, the transducer should be placed in a transverse plane just superior to the pubic symphysis with the transducer marker pointed toward the patient's right. For a sagittal view, rotate the transducer 90° clockwise to obtain sagittal views of the bladder with the transducer marker pointing cephalad. Image courtesy of Pimpa Limphan-udom

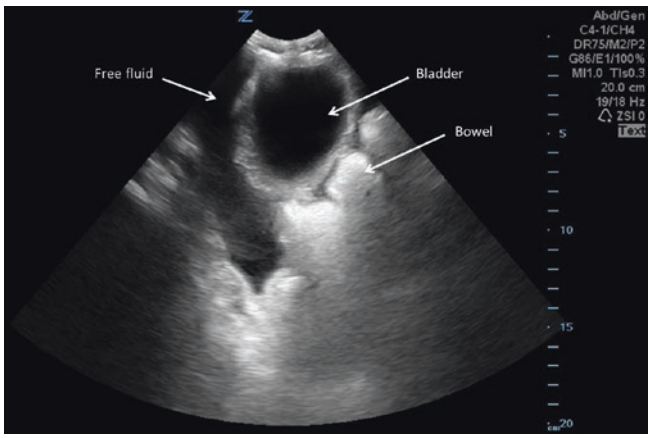

Fig. 25.6 Ultrasound image of free fluid in the transverse plane of the pelvis. Pelvis with free fluid collecting in the rectovesical space. Image courtesy of Pimpa Limphan-udom

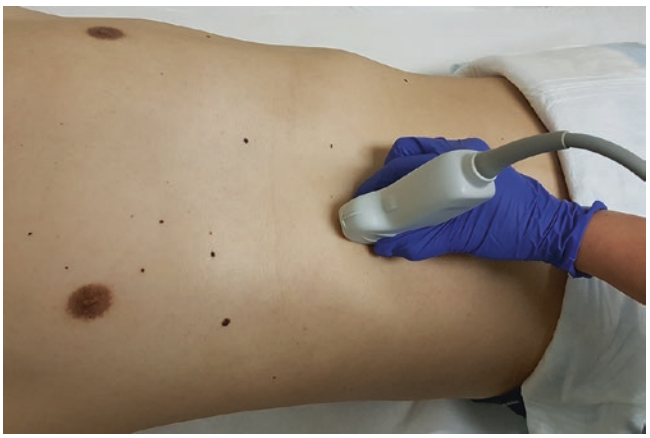

Fig. 25.8 Ultrasound probe position on the right hypochondrium. Patients should be scanned in the supine position concentrating on the midline and right hypochondrium. Image courtesy of Pimpa Limphan-udom

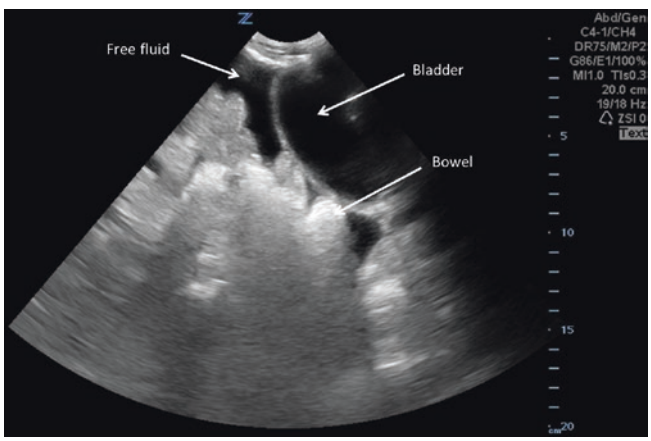

Fig. 25.7 Ultrasound image of free fluid in the longitudinal plane of the pelvis. Pelvis with free fluid collecting in the rectovesical space. Image courtesy of Pimpa Limphan-udom

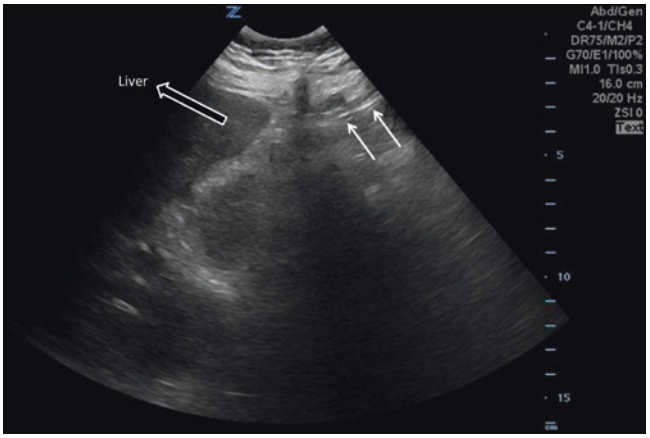

Fig. 25.9 Ultrasound image of the normal peritoneum. The normal peritoneal stripe (*white arrow*) is identified by US as a single or double echogenic line posterior to the anterior abdominal wall. Normal air within the lumen of the gastrointestinal tract is recognizable by its association with bowel and moves with peristalsis in this scan of the right hypochondrium, performed with a convex probe. Image courtesy of Pimpa Limphan-udom

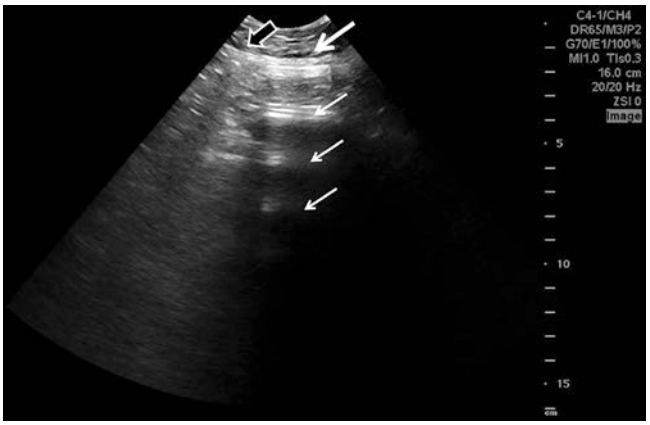

Fig. 25.10 Ultrasound image of the pneumoperitoneum. Enhancement of peritoneal stripe (*large* arrow) and reverberation artifacts (*small* arrow) detected in the right hypochondrium scan with convex probe in a patient with pneumoperitoneum with adjacent area of normal air within the lumen of the gastrointestinal tract (*empty arrow*). Image courtesy of Bret Nelson

References

1. Rozycki GS, Ochsner MG, Jaffin JH, Champion HR. Prospective evaluation of surgeons' use of ultrasound in the evaluation of trauma patients. J Trauma. 1993;34:516–26.
2. Boulanger BR, Kearney PA, Brenneman FD, Tsuei B, Ochoa J. Utilization of FAST (focused assessment with sonography for trauma) in 1999: results of a survey of North American trauma centers. Am Surg. 2000;66:1049–55.
3. Thierman JS. Ultrasound evaluation of peritoneal fluid. In: Carmody KA, Moore CL, Feller-Kopman D, eds. Handbook of critical care and emergency ultrasound. New York: McGraw-Hill; 2011. http://accessanesthesiology.mhmedical.com/content.aspx?bookid=517&sectionid=41066795. Accessed 27 June 2017.
4. Goudie A. Detection of intraperitoneal free gas by ultrasound. Australas J Ultrasound Med. 2013;16(2):56–61.
5. Hoffmann B, Nürnberg D, Westergaard MC. Focus on abnormal air: diagnostic ultrasonography for the acute abdomen. Eur J Emerg Med. 2012;19(5):284–91.
6. Braccini G, Lamacchia M, Boraschi P, Bertellotti L, Marrucci A, Goletti O, et al. Ultrasound versus plain film in the detection of pneumoperitoneum. Abdom Imaging. 1996;21(5):404–12.
7. Karahan OI, Kurt A, Yikilmaz A, Kahriman G. New method for the detection of intraperitoneal free air by sonography: scissors maneuver. J Clin Ultrasound. 2004;32(8):381–5.
8. Chen SC, Yen ZS, Wang HP, Lin FY, Hsu CY, Chen WJ. Ultrasonography is superior to plain radiography in the diagnosis of pneumoperitoneum. Br J Surg. 2002;89(3):351–4.
9. Moriwaki Y, Sugiyama M, Toyoda H, Kosuge T, Arata S, Iwashita M, et al. Ultrasonography for the diagnosis of intraperitoneal free air in chest-abdominal-pelvic blunt trauma and critical acute abdominal pain. Arch Surg. 2009;144(2):137–41.
10. Asrani A. Sonographic diagnosis of pneumoperitoneum using the 'enhancement of the peritoneal stripe sign.' A prospective study. Emerg Radiol. 2007;14(1):29–39.
11. Noble VE, Nelson BP. Manual of emergency and critical care ultrasound. New York: Cambridge University Press; 2011.

Gallbladder

26

Huidong Kang

It is not possible to diagnose gallbladder pathology with a reasonable degree of certainty using history and physical examination alone [1]. Bedside ultrasound (US) is currently considered the preferred initial imaging technique for patients who are clinically suspected of having acute calculous cholecystitis [2]. Bedside US of the biliary system has been shown to decrease the costs [3] as well as emergency department length of stay [4] in patients with cholelithiasis. Bedside US can detect gallstones, a thickened gallbladder wall, pericholecystic fluid, and a sonographic Murphy sign to assist in diagnosis of acute cholecystitis. More than 90% of cases of acute cholecystitis are associated with cholelithiasis (acute calculous cholecystitis) [5] and absence of gallstone alone more reliably excludes acute calculous cholecystitis [6]. Point-of-care ultrasound has been shown to be accurate in diagnosing cholelithiasis [7]. Also, point-of-care US for gallbladder disease is a skill that can be learned by physicians at all levels of training [8]. However, ultrasound findings must be carefully interpreted in the context of the clinical presentation (Figs. 26.1, 26.2, 26.3, 26.4, 26.5, 26.6, 26.7, 26.8, 26.9, 26.10, 26.11, 26.12, 26.13, and 26.14; Videos 26.1, 26.2, 26.3, 26.4, 26.5, and 26.6).

Electronic Supplementary Material The online version of this chapter (https://doi.org/10.1007/978-3-319-73855-0_26) contains supplementary material, which is available to authorized users.

H. Kang, M.D., Ph.D.
Department of Emergency Medicine, University of Ulsan,
College of Medicine, Gangneung Asan Hospital,
Gangneung, Gangwon, South Korea

B. P. Nelson et al. (eds.), *Atlas of Handheld Ultrasound*, https://doi.org/10.1007/978-3-319-73855-0_26

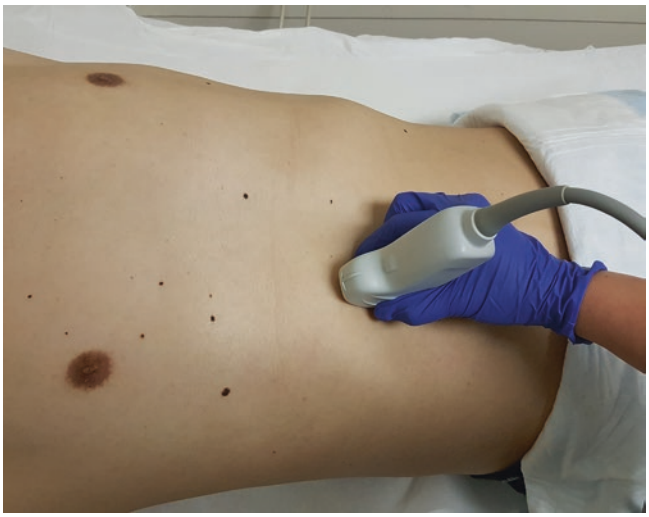

Fig. 26.1 Ultrasound probe position for visualizing the gallbladder. A curvilinear (low frequency) probe is typically used to scan the gallbladder. To obtain longitudinal views, place the probe under the right costal margin with the prove marker toward the patient's head, and start the scan at the costal margin in the right mid-clavicular line. Slide the probe along the costal margin to visualize the gallbladder. Once the gallbladder is visualized, slightly rotate and tilt the probe until the longest axis is seen. And then, fan through the entire gallbladder to identify any pathology. Note that "longitudinal" view of the gallbladder refers to the long axis of the gallbladder, not to the probe orientation with relation to the patient's body planes. Another approach toward visualization of the gallbladder is to place the probe in a transverse orientation (probe marker to patient right) in the midclavicular line at the costal margin. Angle the ultrasound beam cephalad and caudal to find the gallbladder. Image courtesy of Huidong Kang

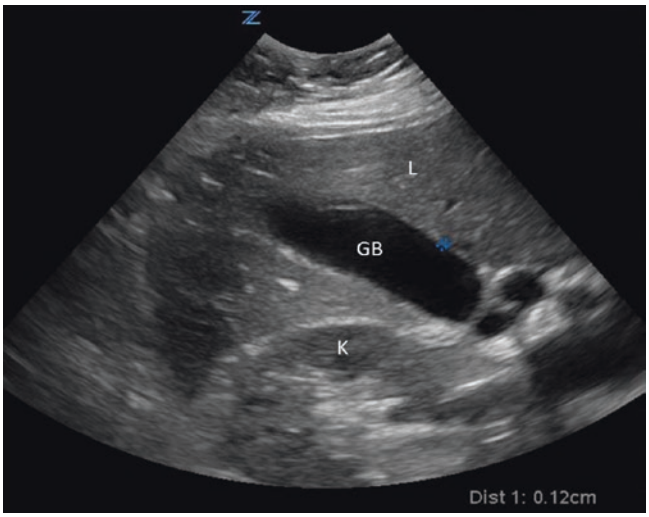

Fig. 26.3 Ultrasound image of the gallbladder in the longitudinal plane. A normal gallbladder should be thin-walled (<3 mm) and anechoic. *GB* Gallbladder, *L* liver, *K* kidney. Image courtesy of Huidong Kang

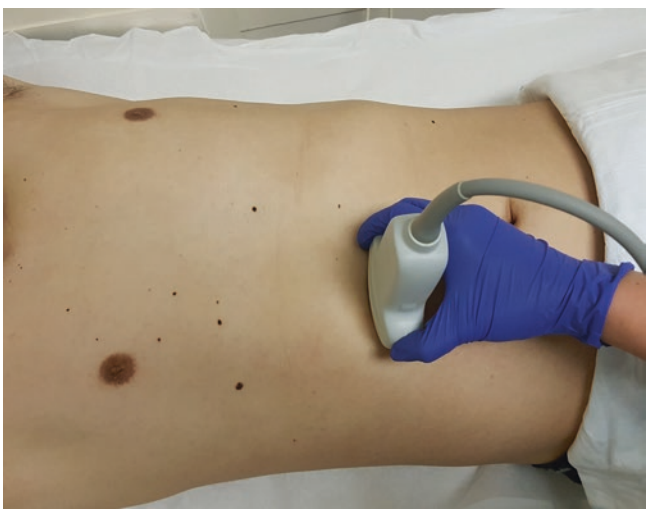

Fig. 26.2 Ultrasound probe position for visualizing the gallbladder. After the long axis is thoroughly examined, rotate the probe 90 degrees counterclockwise to obtain transverse views. Fan through the entire gallbladder in a short axis plane. Again, the short axis or transverse plane of the gallbladder may or may not correspond to the transverse plane of the patient's body. Image courtesy of Huidong Kang

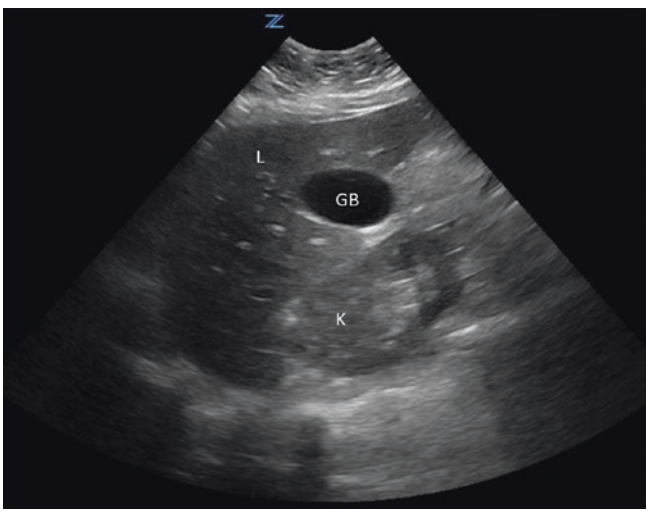

Fig. 26.4 Ultrasound image of the gallbladder in the transverse plane. *GB* Gallbladder, *L* Liver, *K* kidney. Image courtesy of Huidong Kang

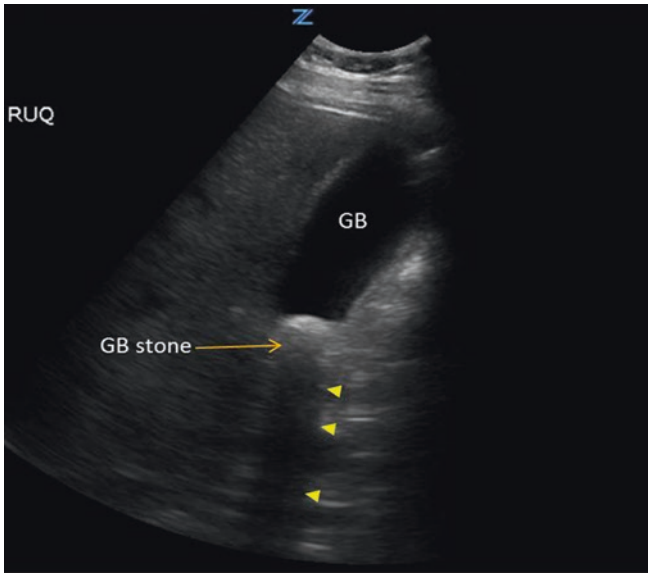

Fig. 26.5 Ultrasound image of gallstone in the longitudinal plane. Impacted gallstone with posterior shadowing (*arrowhead*). Image courtesy of Pimpa Limphan-udom

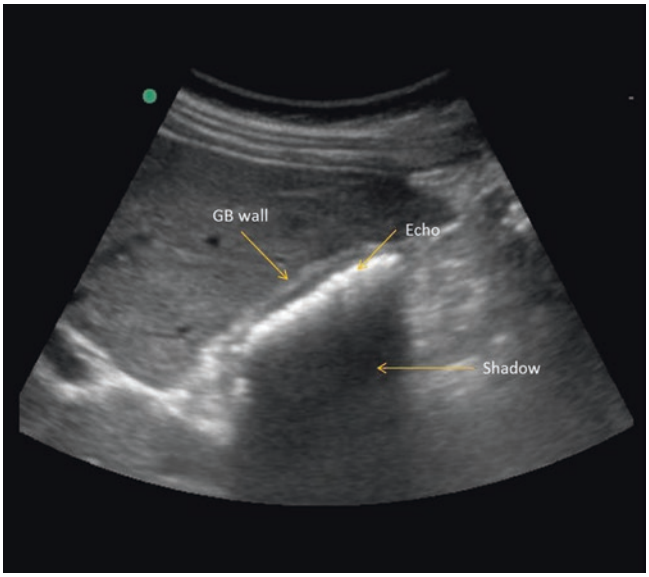

Fig. 26.7 Wall-echo-shadow (WES) sign. When the gallbladder is entirely filled with stones, the wall-echo-shadow sign can be seen. In this case the gallbladder may be difficult to appreciate, since the characteristic fluid-filled, anechoic appearance is replaced by shadow deep to the stones. Image courtesy of Bret Nelson

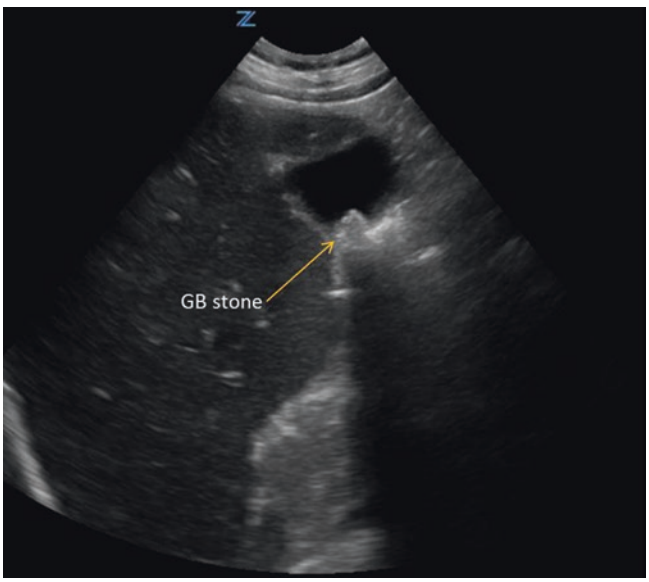

Fig. 26.6 Impacted gallstone with posterior shadowing in the transverse plane. Image courtesy of Pimpa Limphan-udom

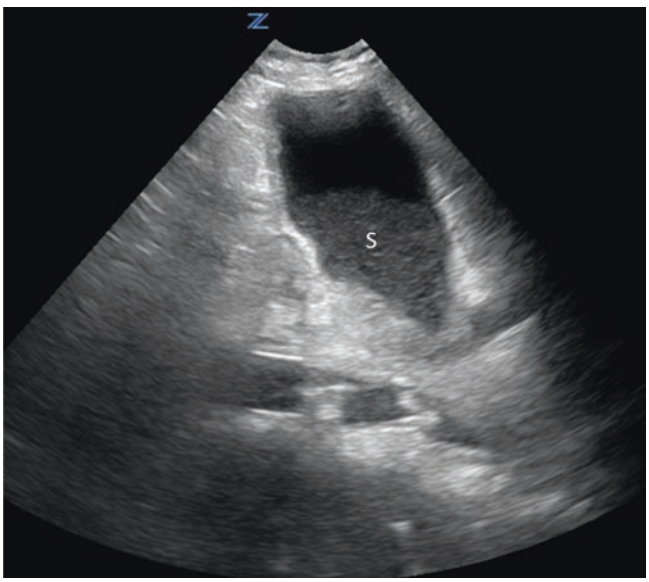

Fig. 26.8 Ultrasound image of the gallbladder sludge. Sludge (S) appears as a low amplitude homogenous echoes, layering on the posterior wall. Sludge does not typically cause shadowing. Image courtesy of Pimpa Limphan-udom

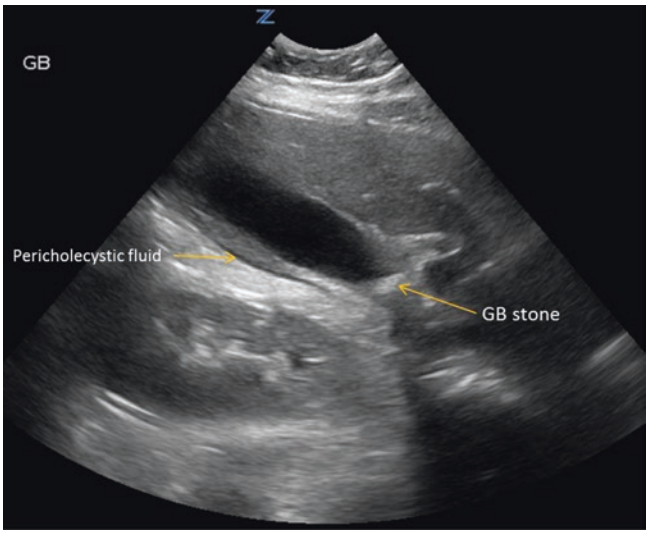

Fig. 26.9 Acute cholecystitis with associated gallstone and pericholecystic fluid. *Arrow* indicates stone with associated posterior acoustic shadowing. Image courtesy of Huidong Kang

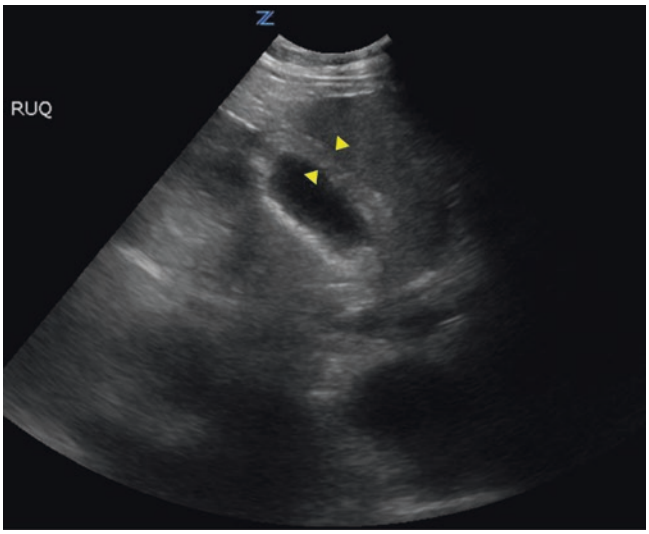

Fig. 26.11 Nonspecific gallbladder wall thickening. GB wall thickening (*arrowhead*) due to ascites in a patient with liver cirrhosis. This appearance may also be seen with diabetes, interstitial edema, congestive heart failure, and other chronic disease processes. Image courtesy of Bret Nelson

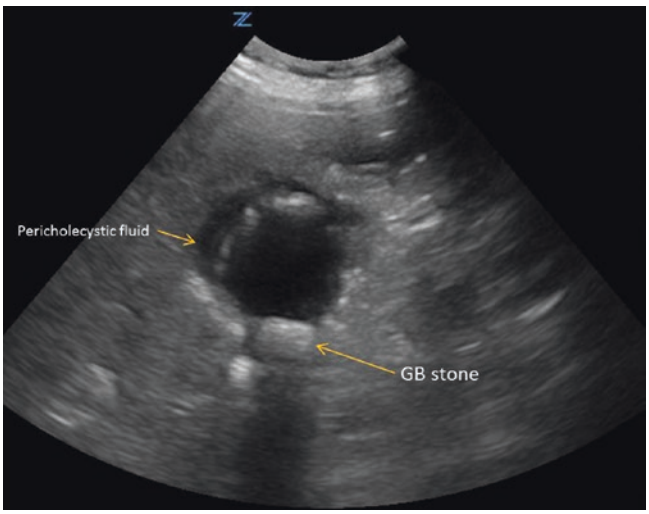

Fig. 26.10 Acute cholecystitis with associated gallstone, irregular wall and pericholecystic fluid. Image courtesy of Huidong Kang

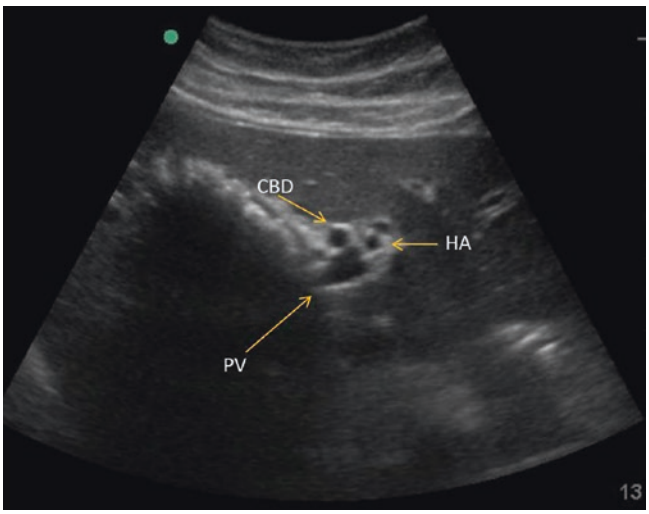

Fig. 26.12 Portal triad in a transverse view. The CBD is most easily identified through its association with portal vein. The portal vein will appear as a large anechoic circle with echogenic border (vein wall). The CBD and hepatic artery will appear as two small circles anterior to portal vein. Often, these three circles are called a 'Mickey Mouse' sign. *CBD* common bile duct, *PV* portal vein, HA hepatic artery. Image courtesy of Bret Nelson

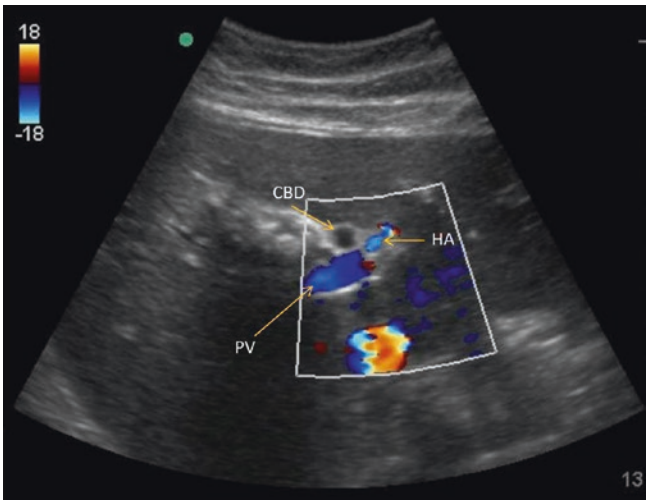

Fig. 26.13 Color flow Doppler of the portal triad in a transverse view. Color flow doppler can be used to differentiate common bile duct from hepatic artery and portal vein. The hepatic artery and portal vein will demonstrate flow and the common bile duct will not. *CBD* common bile duct, *PV* portal vein, *HA* hepatic artery. Image courtesy of Bret Nelson

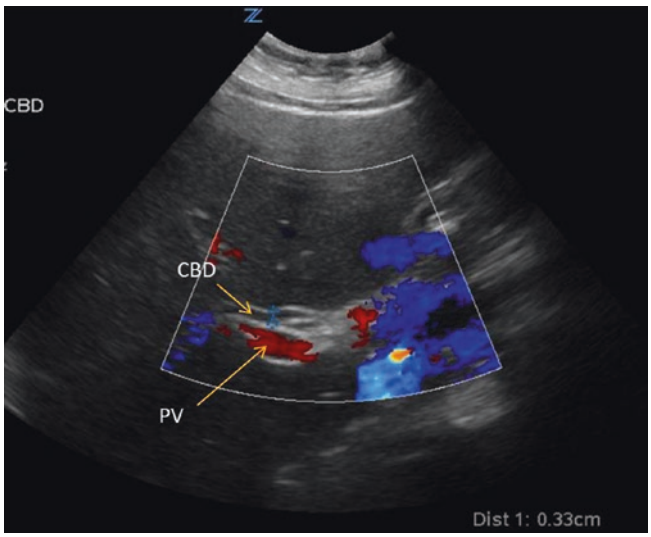

Fig. 26.14 Color flow Doppler of the portal triad in a longitudinal view. *CBD* common bile duct, *PV* portal vein. Image courtesy of Pimpa Limphan-udom

References

1. Trowbridge RL, Rutkowski NK, Shojania KG. Does this patient have acute cholecystitis? JAMA. 2003;289(1):80–6.
2. Pinto A, Reginelli A, Cagini L, Coppolino F, Stabile Ianora AA, Bracale R, et al. Accuracy of ultrasonography in the diagnosis of acute calculous cholecystitis: review of the literature. Crit Ultrasound J. 2013;5(Suppl 1):S11.
3. Durston W, Carl ML, Guerra W, Eaton A, Ackerson L, Rieland T, et al. Comparison of quality and cost-effectiveness in the evaluation of symptomatic cholelithiasis with different approaches to ultrasound availability in the ED. Am J Emerg Med. 2001;19(4):260–9.
4. Blaivas M, Harwood RA, Lambert MJ. Decreasing length of stay with emergency ultrasound examination of the gallbladder. Acad Emerg Med. 1999;6(10):1020–3.
5. Strasberg SM. Clinical practice. Acute calculous cholecystitis. N Engl J Med. 2008;358(26):2804–11.
6. Villar J, Summers SM, Menchine MD, Fox JC, Wang R. The absence of gallstones on point-of-care ultrasound rules out acute cholecystitis. J Emer Med. 2015;49(4):475–80.
7. Scruggs W, Fox JC, Potts B, Zlidenny A, McDonough J, Anderson CL, et al. Accuracy of ED bedside ultrasound for identification of gallstones: retrospective analysis of 575 studies. West J Emerg Med. 2008;9(1):1–5.
8. Gaspari RJ, Dickman E, Blehar D. Learning curve of bedside ultrasound of the gallbladder. J Emerg Med. 2009;37(1):51–6.

Bowel

27

Errel Khordipour and Ee Tay

Bowel sonography has been recognized as a powerful diagnostic tool. While ultrasound retains an important role for abdominal evaluation, the use of CT scans is preferred as CT scans are less operator-dependent and allow rapid evaluation of vessels, mesentery, and major organs. Ultrasound is limited by large patient body habitus and availability of qualified sonographers. Recently there has been a focus on resource utilization reduction, providing cost-effective care, and limiting radiation and contrast exposure for abdominal diagnostic tests [1–3]. When compared to CT, the use of ultrasound as a diagnostic tool reduces time to diagnosis and treatment, as well as overall length of stay [4–7].

The reduction in radiation exposure is especially imperative in the management of pediatric patients [8]. Ultrasound can be used as the initial imaging modality and be rapidly detected at bedside in disease states such as appendicitis, intussusception, and pyloric stenosis in children [9–11].

The images that follow illustrate normal bowel anatomy as well as a variety of different bowel and peritoneal pathologies (Figs. 27.1, 27.2, 27.3, 27.4, 27.5, 27.6, 27.7, 27.8, 27.9, 27.10, 27.11, 27.12, 27.13, 27.14, 27.15, 27.16, 27.17, 27.18, 27.19, 27.20, and 27.21; Videos 27.1, 27.2, 27.3, 27.4, 27.5, 27.6, 27.7, 27.8, and 27.9).

Electronic Supplementary Material The online version of this chapter (https://doi.org/10.1007/978-3-319-73855-0_27) contains supplementary material, which is available to authorized users.

E. Khordipour, D.O. (✉)
Emergency Department, Maimonides Medical Center, Brooklyn, NY, USA

E. Tay, M.D.
Department of Emergency Medicine, Icahn School of Medicine at Mount Sinai, New York, NY, USA

B. P. Nelson et al. (eds.), *Atlas of Handheld Ultrasound*, https://doi.org/10.1007/978-3-319-73855-0_27

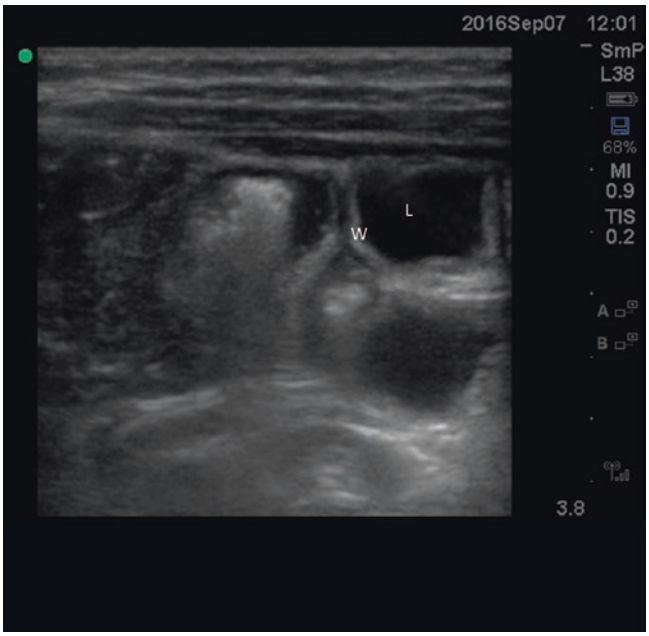

Fig. 27.1 Normal bowel will appear as a single circular hyperechoic layer which represents the wall of the muscular layer (W) surrounding a mixture of hyperechoic and hypoechoic bowel contents with the intestinal lumen (L). The normal thickness of this layer during the contraction stage is 2–3 mm. the hyperechoic normal bowel walls become thinner during relaxation of bowel

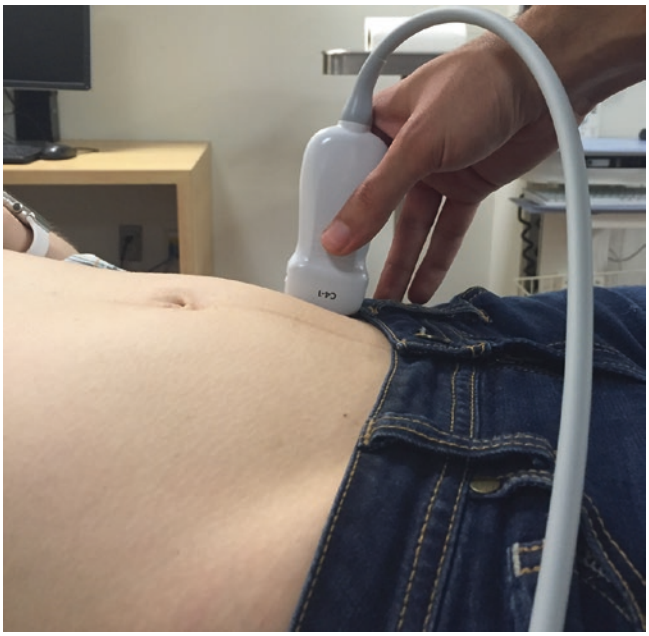

Fig. 27.3 With the probe marker toward the patient's head, start in the LLQ, moving up to LUQ, then across to RUQ, then down to RLQ. Evaluate through all four quadrants in the longitudinal plane. Use sequential graded compression

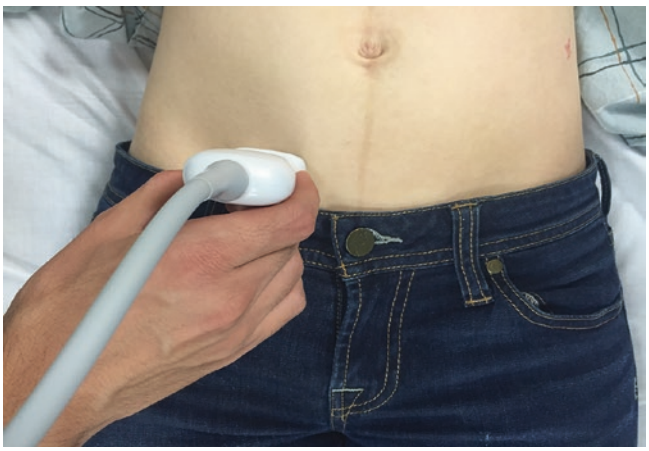

Fig. 27.2 With a low frequency curvilinear probe, evaluate the abdomen in different quadrants. Start with the probe marker toward the patient's right. Using sequential graded compression in the transverse plane, move from the RLQ, to RUQ, then across to LUQ, and down to LLQ. Sequential graded compression is a technique used to decompress bowel in order to decrease air artifact. Apply gentle downward pressure every few centimeters

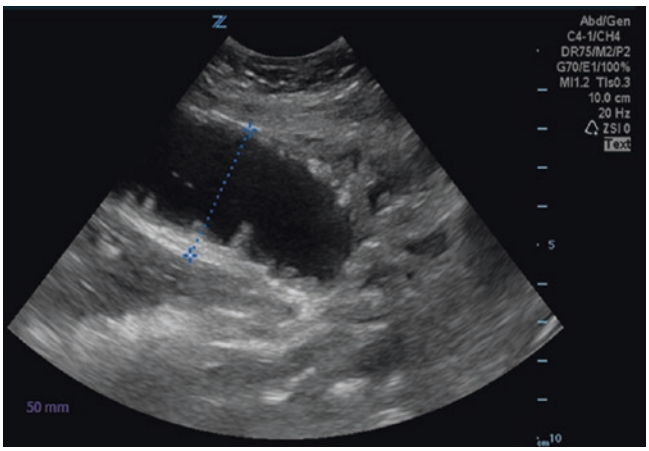

Fig. 27.4 Look for dilated loops of bowel with hyperechoic bright spots representing food particles or gas. Bowel diameter should not be >25 mm for jejunum or >15 mm for ileum when measured from outer wall to outer wall. Once a dilated loop of bowel is found, attempt to compress it. Non-compressible small bowel is highly suspicious of small bowel obstruction

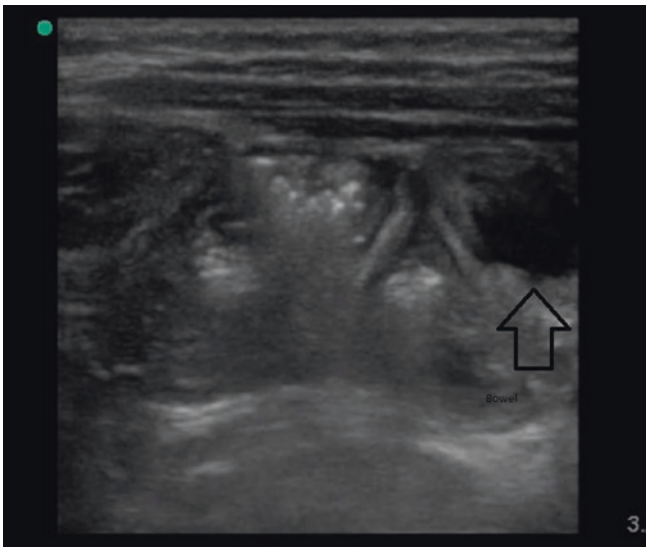

Fig. 27.5 Bowel movement represents peristalsis, as demonstrated by bowel contents moving back and forth. In normal bowel, peristalsis should push contents forward, and not the opposite direction

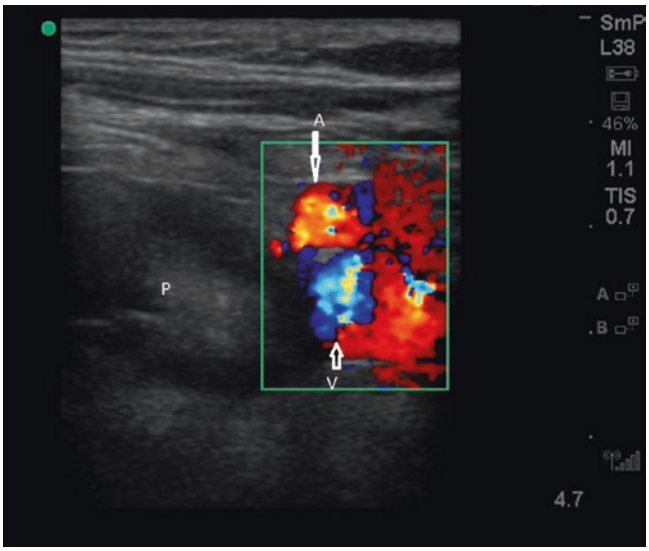

Fig. 27.7 With graded compression, normal bowel loops are displaced allowing for better visualization of the iliac artery (A) and iliac vein (V) in the right iliac fossa as well as the psoas muscle (P). The appendix often overlays or is next to the iliac artery or medial to the psoas muscle

Fig. 27.6 A high-frequency linear probe or a curvilinear probe may be used. Curvilinear probes are preferred in patients with larger body habitus when anatomy cannot be detected by a linear probe. Place the probe over the point of maximum tenderness as indicated by the patient. Start with the probe either in the longitudinal (probe marker to patient's head) or transverse plane by (probe marker to the patient's right)

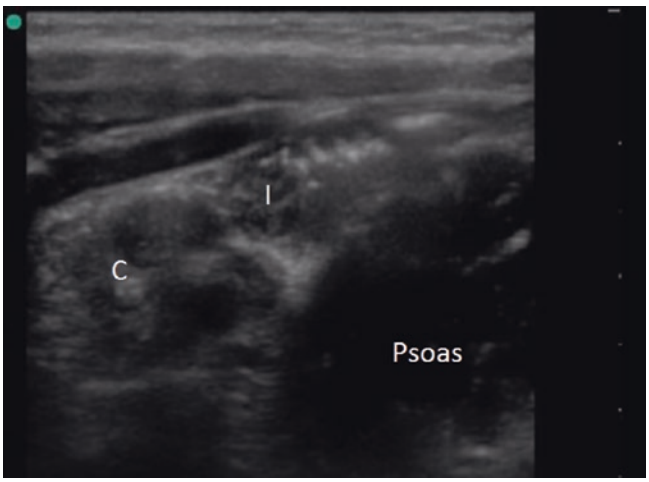

Fig. 27.8 Ascending colon is visualized as non-peristalsing structures containing gas and fluid. Move the probe inferiorly towards the cecum (C). Using compression to release the gas and fluid from the bowel, the right psoas muscle can be identified. The adjacent terminal ileum (I) can be visualized and distinguished from appendix as it is compressible and undergoes peristalsis

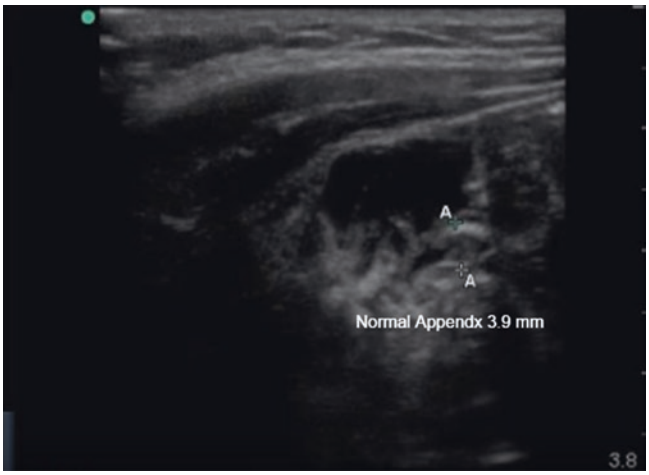

Fig. 27.9 Once the cecum has been located, the appendix should be visualized coming off it. Follow this smaller tubular structure down its entire length as the appendix should end as a blind-ending pouch while the terminal ileum will not. The measurement of a normal appendix should be <6 mm when measured from outer wall to outer wall. The appendix lumen should be empty of gas or fecal matter, and should be compressible

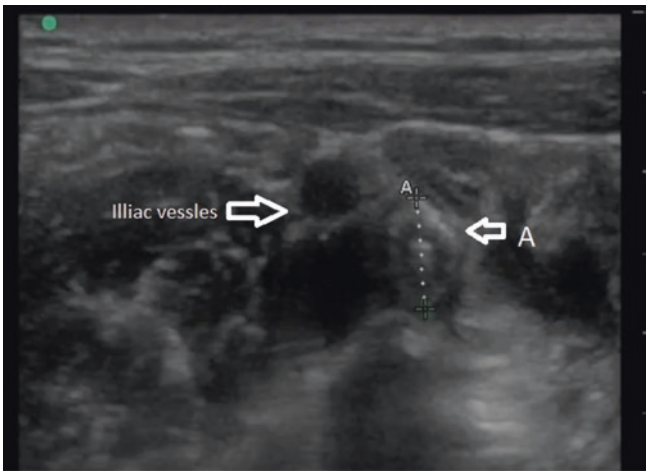

Fig. 27.11 The appendix (A) may have a target sign appearance. This is caused by a fluid-filled center surrounded by a hyperechoic ring which represents the mucosa. This layer is surrounded by a hypoechoic muscularis layer causing a target appearance on axial imaging

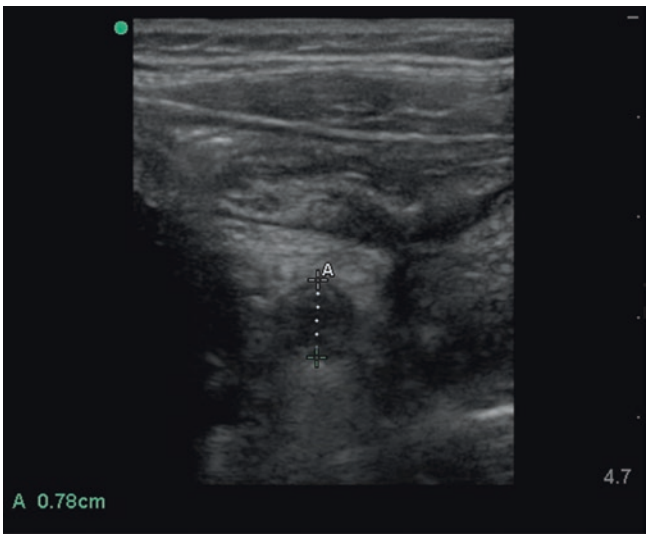

Fig. 27.10 An appendix suspicious of appendicitis will be non-compressible and will measure >6 mm in diameter under compression. Its wall thickness will be >3 mm

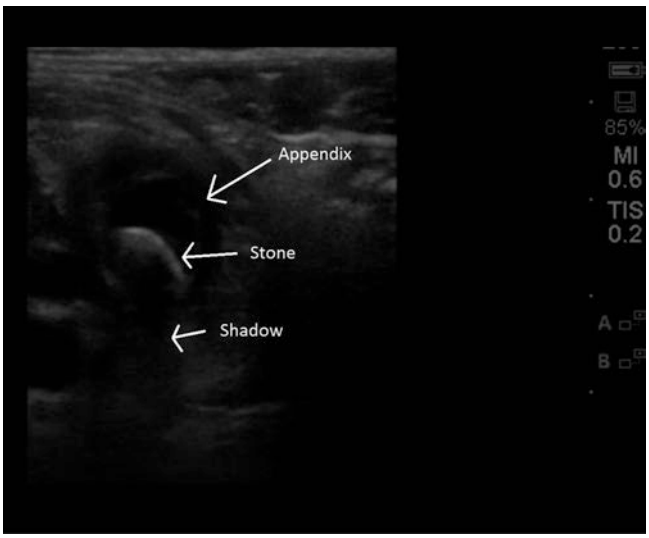

Fig. 27.12 The presence of an appendicolith appears as a hyperechoic focus with a posterior acoustic shadow

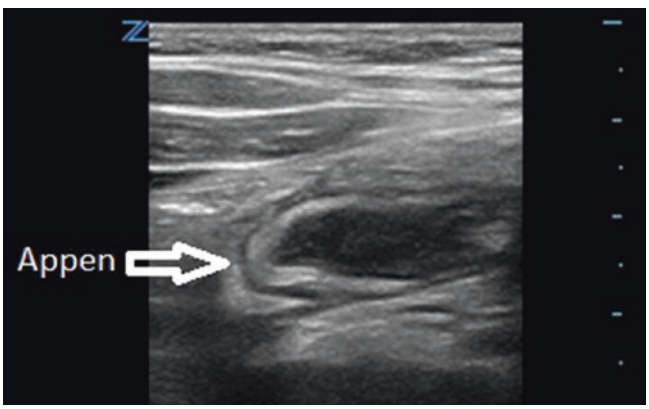

Fig. 27.13 Secondary signs of appendicitis include free fluid in the periappendiceal region and increased echogenicity of the periappendiceal fat. On the sagittal view, it will be seen as a blind-ending pouch. If the appendix is retrocecal it may be seen lateral to the psoas muscle

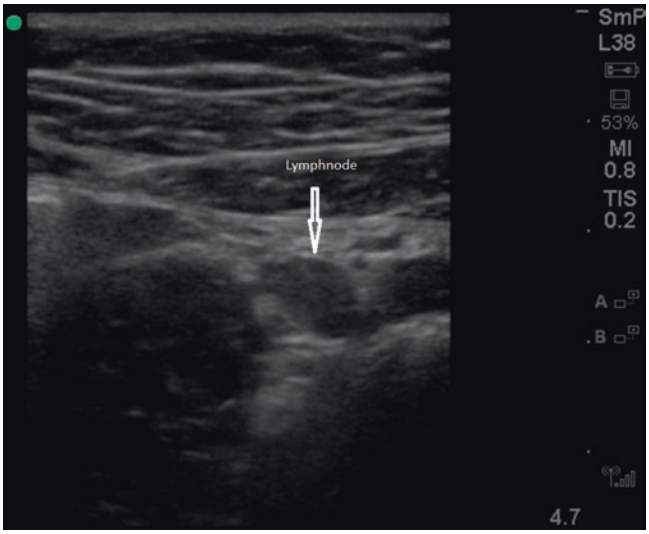

Fig. 27.14 Enlarged mesenteric lymph nodes can mimic appendicitis. The diagnosis of appendicitis may not be excluded even though mesenteric lymph nodes are present if the index of suspicion is high for appendicitis. A color Doppler may assist to distinguish between a vessel and an abdominal lymph node

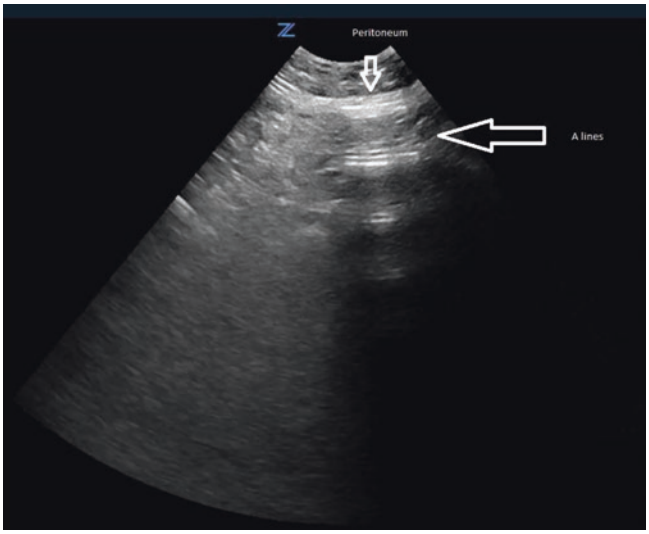

Fig. 27.16 Peritoneal "A lines" can be seen with large pockets of air such as in colonic perorations. Interpret with caution as stomach and dilated loops of bowel filled with air can give similar artifact. Look for bowel wall to help distinguish

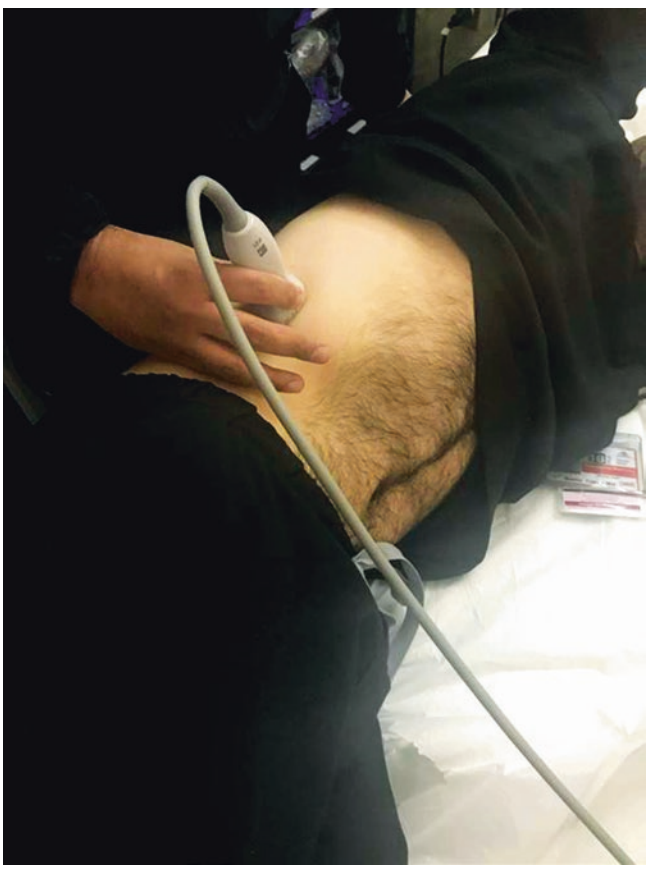

Fig. 27.15 Place the patient supine or in a left lateral decubitus position. Left lateral decubitus position allows the bowel to fall away from the liver

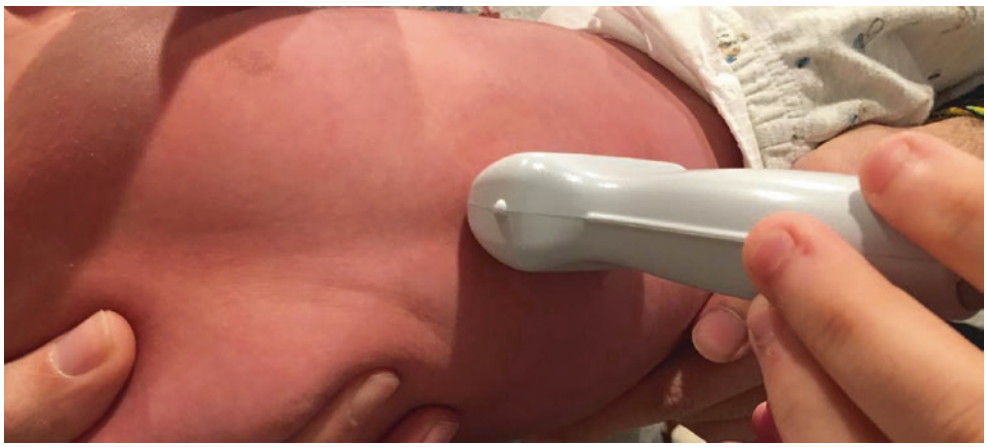

Fig. 27.17 The patient should be placed into a right lateral decubitus position (right shoulder down). A high frequency linear probe should be selected

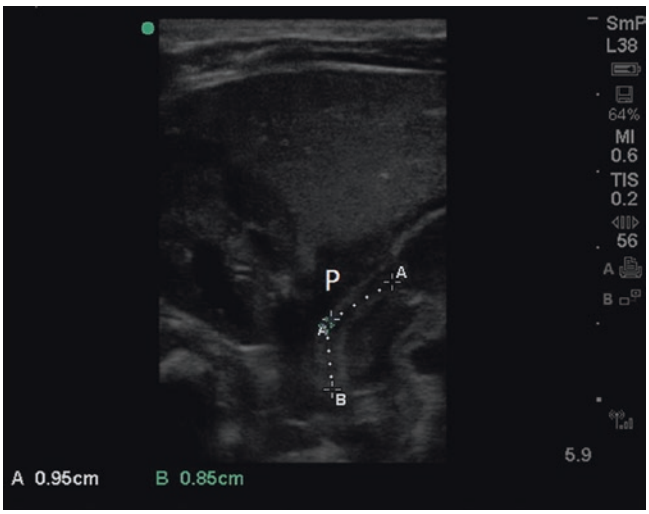

Fig. 27.18 From the anterior approach, the pylorus will be located between the gastric antrum and duodenum. Having the child drink before the examination will distend the stomach, making visualization of the pylorus easier. A measurement should be made at a perpendicular cross section of the pylorus in the long axis. Pyloric stenosis is suspected if one muscle wall of the pylorus has a thickness > 3 mm and a length > 14 mm

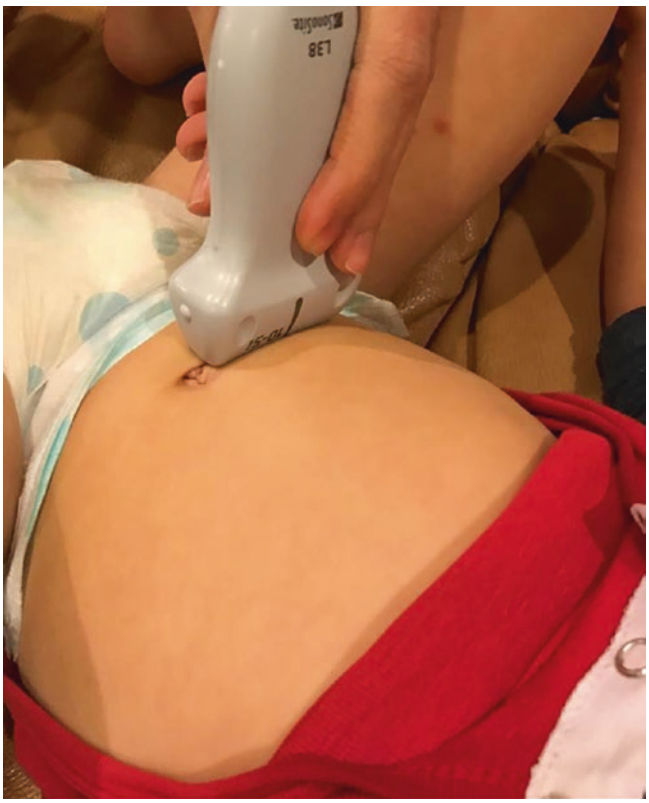

Fig. 27.19 The patient should be in a supine position. A high frequency linear probe is selected for this study

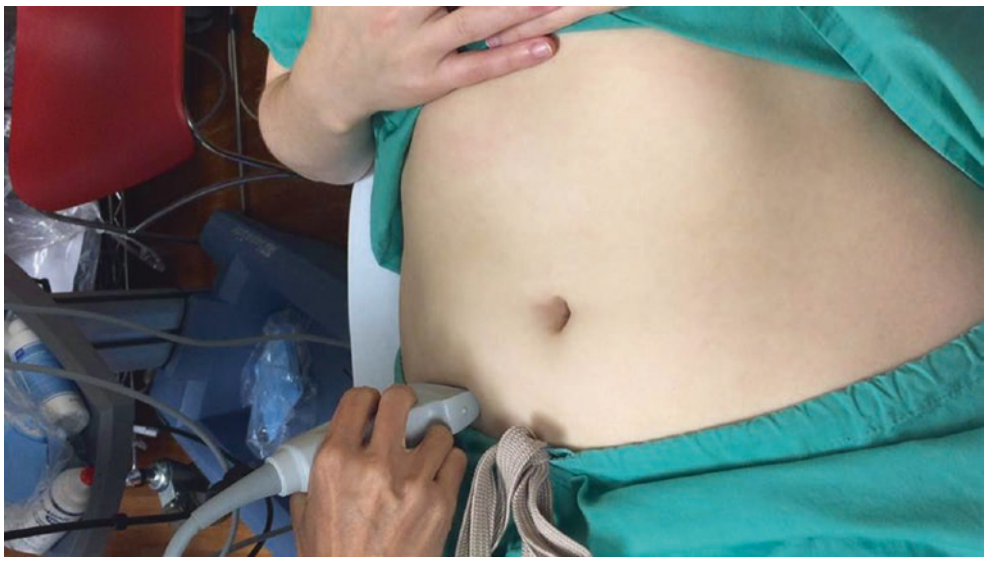

Fig. 27.20 Start in the right lower quadrant of the abdomen as most intussusceptions occur around the ileocecal region. Place the probe in transverse position with the probe marker toward the patient's right, then scan up toward the hepatic junction. Once there, turn the probe sagittal with the probe marker toward the patient's head, and scan across the abdomen toward the splenic flexure. At the splenic flexure, turn the probe transverse again with the probe marker to the patient's right, and scan down until you reach the sigmoid colon

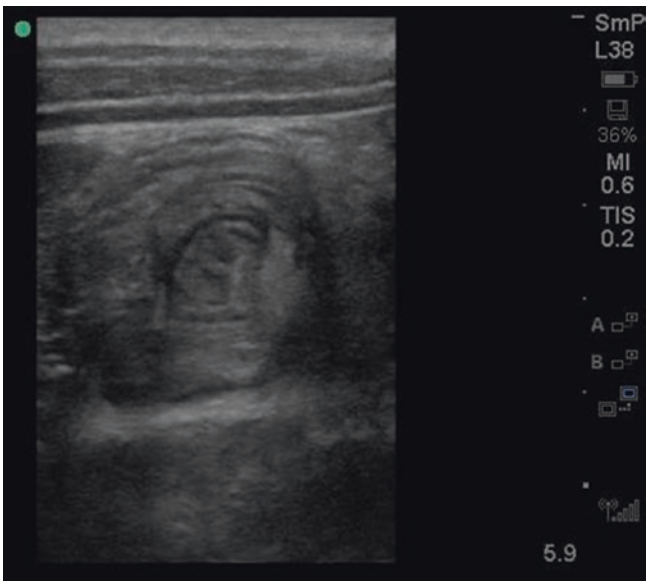

Fig. 27.21 A "target sign" is classically described. This occurs when a hyperdense center is surrounded by multiple layers of concentric hyperdense rings. The rings are composed of bowel that has folded onto itself as it telescopes into its receiving bowel. The size of this "target sign" should be significantly larger than those found in appendicitis

References

1. Greenberg J, Green JB. Over-testing: why more is not better. Am J Med. 2014;127(5):362–3.
2. Moynihan R, Doust J, Henry D. Preventing overdiagnosis: how to stop harming the healthy. BMJ. 2012;344:e3502.
3. Her Majesty's Stationery Office. Statutory instruments: the ionising radiation (medical exposure) regulations. 2000. No. 1059. http://www.legislation.gov.uk/uksi/2000/1059/pdfs/uksi_20001059_en.pdf. Accessed 17 Jun 2017.
4. Rice HE, Arbesman M, Martin DJ, Brown RL, Gollin G, Gilbert JC, et al. Does early ultrasonography affect management of pediatric appendicitis? A prospective analysis. J Pediatr Surg. 1999;34(5):754–8; discussion 758–9.
5. Blaivas M, Harwood RA, Lambert MJ. Decreasing length of stay with emergency ultrasound examination of the gall bladder. Acad Emerg Med. 1999;6:1020–3.
6. Elikashvili I, Tay ET, Tsung JW. The effect of point-of-care ultrasonography on emergency department length of stay and computed tomography utilization in children with suspected appendicitis. Acad Emerg Med. 2014;21:163–70.
7. Kanzaria HK, Probst MA, Ponce NA, Hsia RY. The association between advanced diagnostic imaging and ED length of stay. Am J Emerg Med. 2014;32(10):1253–8.
8. EU council. Health protection of individuals against the dangers of ionizing radiation in relation to medical exposure. EU directive 1997/43/Euratom. Off J Eur Comm. 1997;
9. Crady SK, Jones JS, Wyn T, Luttenton CR. Clinical validity of ultrasound in children with suspected appendicitis. Ann Emerg Med. 1993;22(7):1125–9.
10. Riera A, Hsiao AL, Langhan ML, Goodman TR, Chen L. Diagnosis of intussusception by physician novice sonographers in the emergency department. Ann Emerg Med. 2012;60(3):264–8.
11. Letton RW Jr. Pyloric stenosis. Pediatr Ann. 2001;30(12):745–50.

Kidneys

28

Stephen Alerhand

Bedside renal ultrasound (US) can be utilized to evaluate for nephrolithiasis, renal failure, urinary retention or decreased output, and hematuria (Figs. 28.1, 28.2, 28.3, 28.4, 28.5, 28.6, 28.7, 28.8, 28.9, 28.10, 28.11, and 28.12, Videos 28.1, 28.2, 28.3, 28.4, and 28.5). Although CT scan has classically been used to diagnose kidney stones, US has gained favor owing to its rapid application at the bedside, cheaper cost, and avoidance of ionizing radiation [1]. Larger kidney stones are more likely to be seen on US [2, 3], but more frequently it is the visualization of hydronephrosis as a secondary sign that can help point toward the diagnosis and guide management [4, 5].

Measurement of bladder diameter using US (see also Chap. 33) can reliably confirm urinary retention [6–8]. This finding can be helpful for those patients with benign prostatic hypertrophy or another obstructive process, concern for a neurogenic bladder, assessment of Foley catheter patency, and successful micturition in postoperative patients (Figs. 28.13, 28.14, and 28.15, Videos 28.6 and 28.7).

Electronic Supplementary Material The online version of this chapter (https://doi.org/10.1007/978-3-319-73855-0_28) contains supplementary material, which is available to authorized users.

S. Alerhand, M.D.
Department of Emergency Medicine, Icahn School of Medicine at Mount Sinai, New York, NY, USA

B. P. Nelson et al. (eds.), *Atlas of Handheld Ultrasound*, https://doi.org/10.1007/978-3-319-73855-0_28

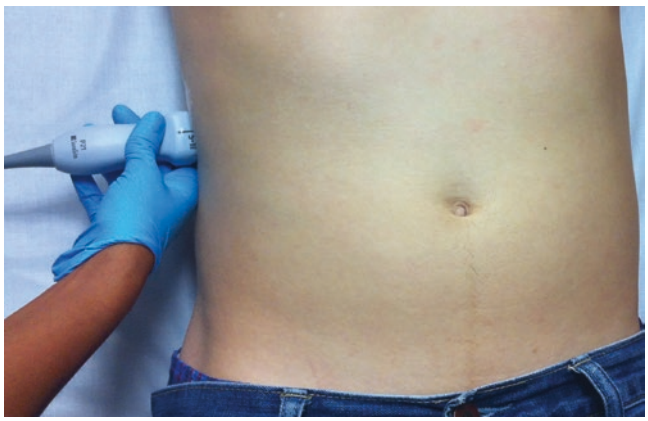

Fig. 28.1 Ultrasound probe position for visualizing the right kidney. To obtain sagittal views, point the probe marker toward the patient's head, and scan in the posterior axillary line at the level of the costal margin. Sweep both anterior-posterior and rostral-caudal to visualize the entire kidney. To obtain transverse views, point the probe marker toward the patient's posterior and scan in the posterior axillary line at the level of the costal margin. Sweep both rostral-caudal and anterior-posterior to visualize the entire kidney. (Image courtesy of Bret Nelson.)

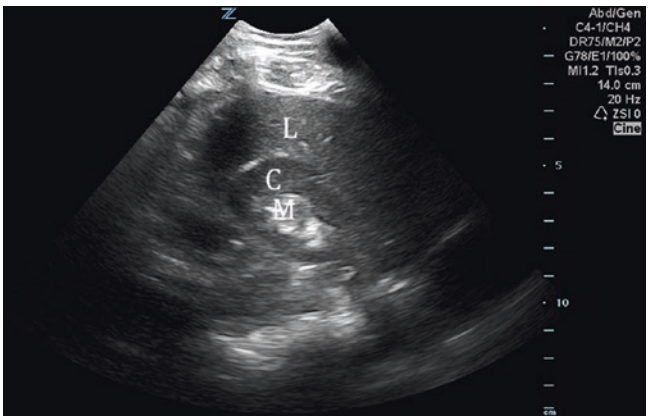

Fig. 28.3 Ultrasound image of the right kidney in the transverse plane. This view similarly demonstrates the cortex (C) and medulla (M) of the kidney. The liver (L) can be seen superior to the kidney. See Video 28.2. (Image courtesy of Stephen Alerhand.)

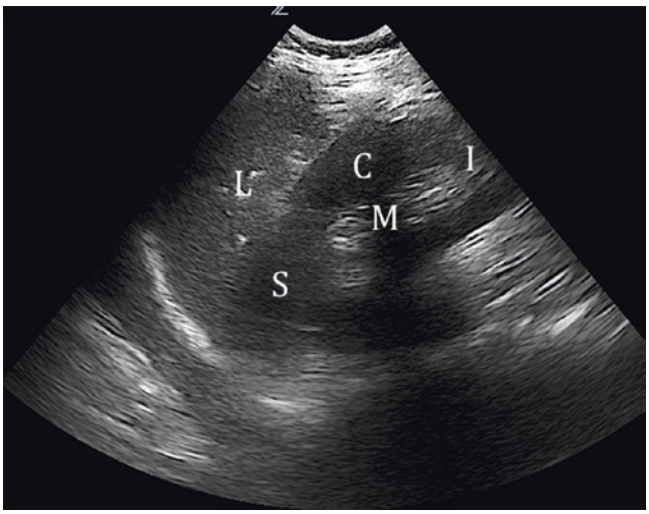

Fig. 28.2 Ultrasound image of the right kidney in the longitudinal plane. This view should demonstrate the superior (S) and inferior (I) poles, cortex (C), and medulla (M) of the kidney. The liver (L) can be seen superior to the kidney. See Video 28.1. (Image courtesy of Stephen Alerhand.)

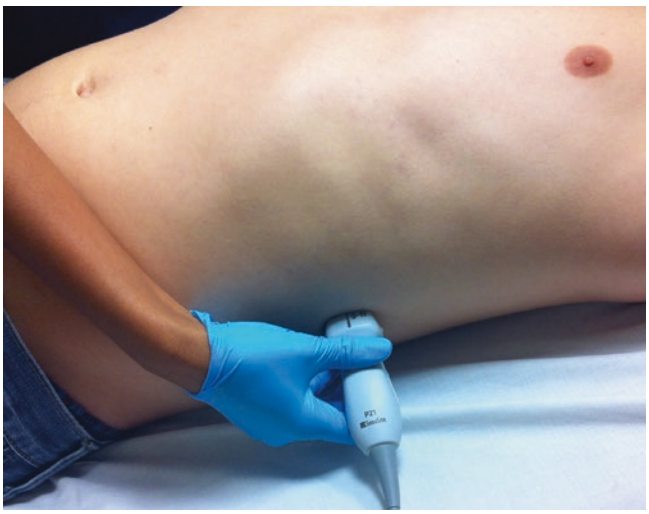

Fig. 28.4 Ultrasound probe position for visualizing the left kidney in the longitudinal plane. For longitudinal imaging, a similar process is repeated for the left kidney as for the right, keeping in mind that the left kidney is located more superior and posterior than the right. This view can best be obtained by placing the knuckles of the right hand on the patient stretcher and aiming the probe anteriorly toward the kidney. For transverse imaging, point the probe marker anteriorly and scan in the posterior axillary line at the level of the costal margin. Sweep both rostral-caudal and anterior-posterior to visualize the entire kidney. (Image courtesy of Bret Nelson.)

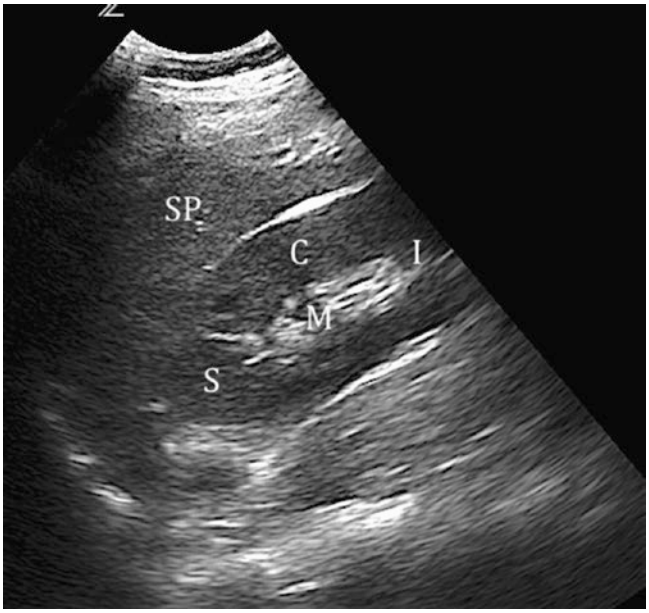

Fig. 28.5 Ultrasound image of the left kidney in the longitudinal plane. A longitudinal view of the kidney should demonstrate the superior (S) and inferior (I) poles, cortex (C), and medulla (M) of the kidney. The spleen (SP) can be seen superior to the kidney. See Video 28.3. (Image courtesy of Stephen Alerhand.)

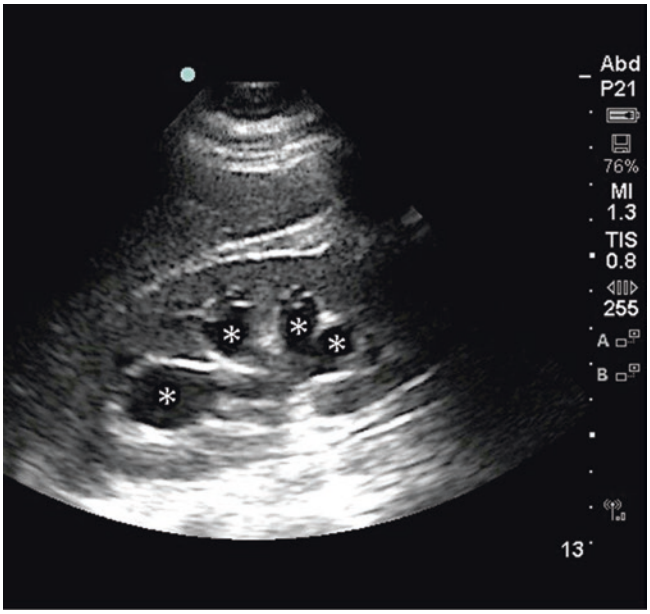

Fig. 28.7 Ultrasound image of right-sided hydronephrosis in the longitudinal plane. Multiple anechoic (black) structures represent the renal calyceal system (*asterisks*), which is dilated due to renal stone obstruction at the uretopelvic junction. Hydronephrosis can be categorized as mild (calyceal enlargement with preservation of renal papillae), moderate (calyceal rounding with obliteration of papillae, as in this image), or severe (calyceal ballooning with cortical thinning). See Video 28.5. (Image courtesy of Bret Nelson.)

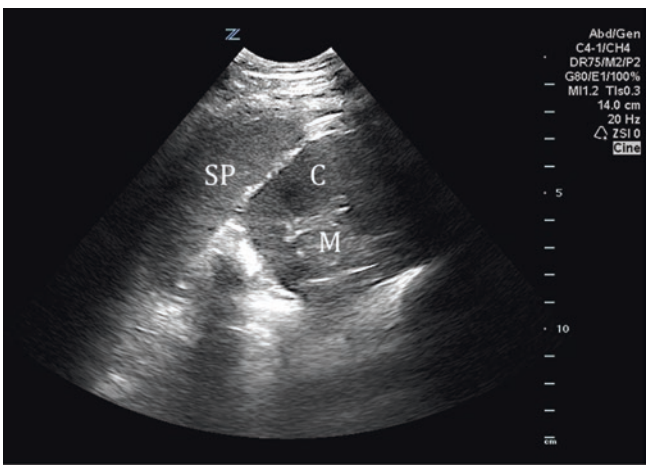

Fig. 28.6 Ultrasound image of the left kidney in the transverse plane. This view similarly demonstrates the cortex (C) and medulla (M) of the kidney. The spleen (SP) is once again visible superior to the kidney. See Video 28.4. (Image courtesy of Stephen Alerhand.)

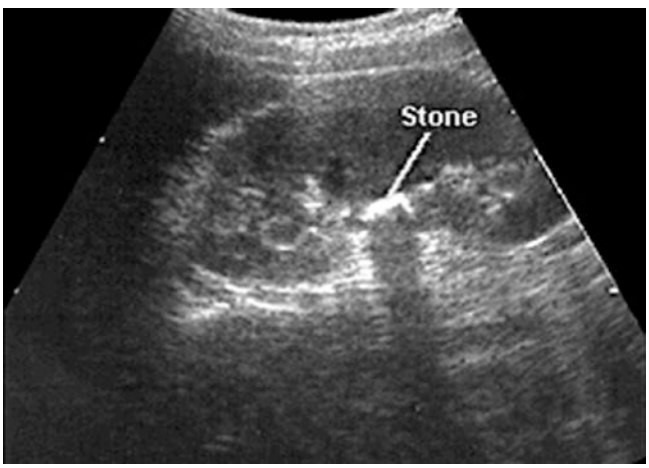

Fig. 28.8 Ultrasound image of a stone in the renal medulla. Though seen with less sensitivity than hydronephrosis, kidney stones can also be visualized in the collecting system. They appear as hyperechoic structures 1–15 mm in size, which cast a posterior shadow. (Image courtesy of Bret Nelson.)

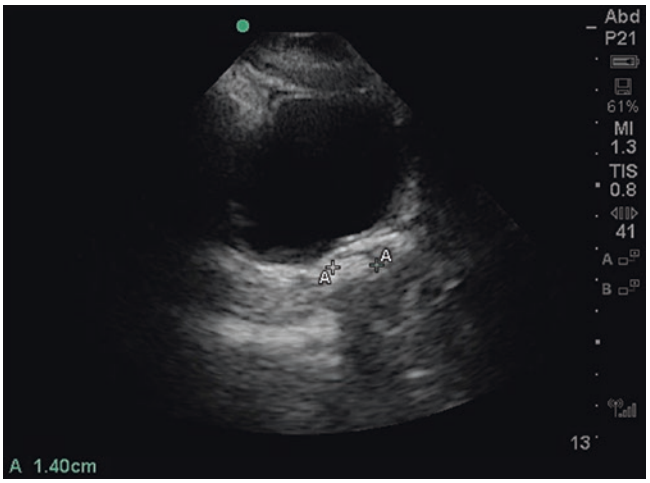

Fig. 28.9 Ultrasound image of a renal stone in the ureterovesicular junction (UVJ). This is the most common site of renal stone obstruction. (Image courtesy of Bret Nelson.)

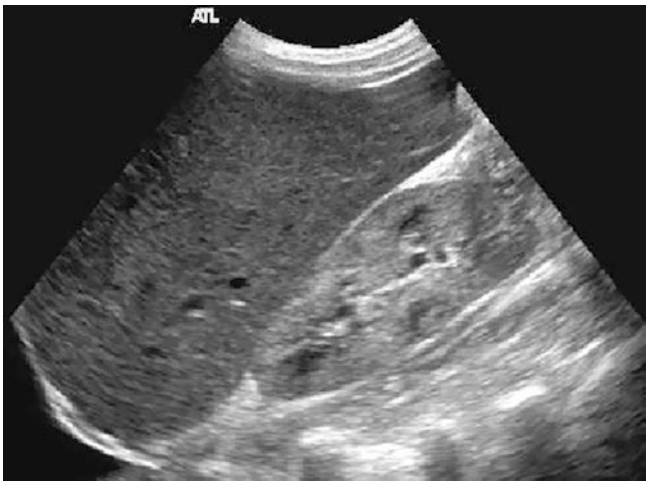

Fig. 28.11 Ultrasound image of acute renal failure. Kidneys in acute failure can appear enlarged and diffusely hyperechoic, with loss of differentiation between the cortex and medulla. This appearance is often referred to sonographically as "medical renal disease." (Image courtesy of Bret Nelson.)

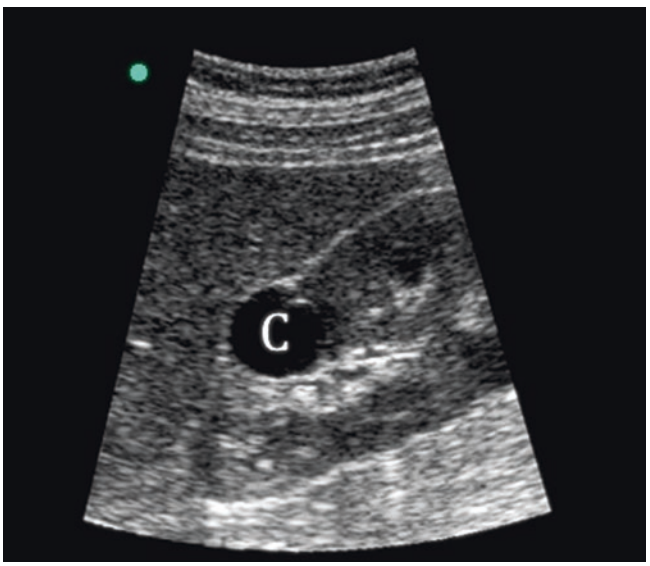

Fig. 28.10 Ultrasound image of a renal cyst (C) in the longitudinal plane. Simple cysts are smooth and oval-shaped, with a well-circumscribed border and posterior acoustic enhancement. Their center is anechoic and without septations. Cysts that do not fulfill these criteria are categorized as complex cysts. (Image courtesy of Bret Nelson.)

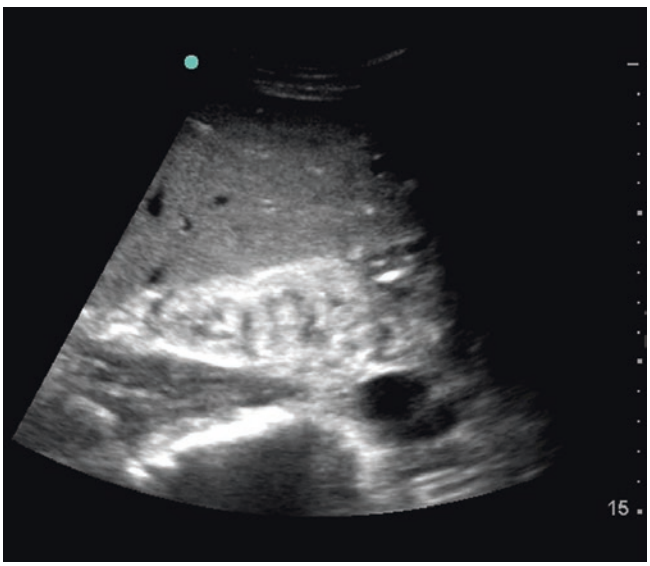

Fig. 28.12 Ultrasound image of chronic renal failure. Kidneys in chronic failure appear shrunken and demonstrate cortical thinning. (Image courtesy of Bret Nelson.)

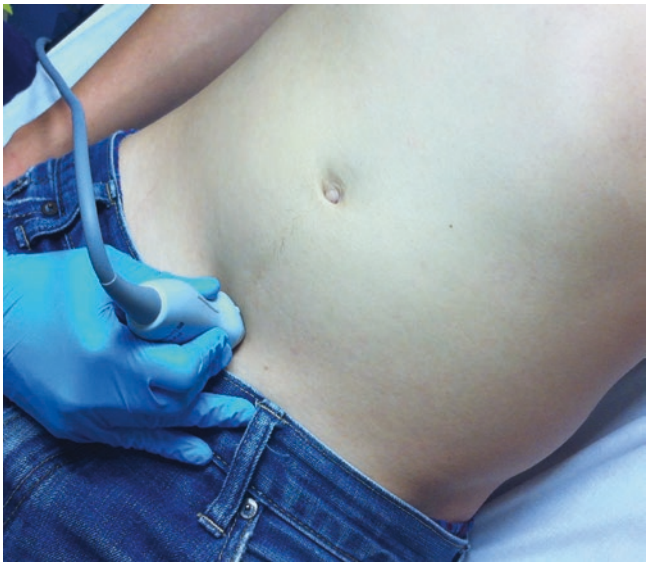

Fig. 28.13 Ultrasound position for visualizing the bladder. For longitudinal imaging, direct the probe marker superiorly and place the probe just above the level of the pubic symphysis, with the beam directed inferiorly, into the pelvis. Scanning in both the right-left and superior-inferior planes will allow visualization of the entire bladder. For transverse imaging, the probe marker is turned toward the patient's right. Scanning in the superior-inferior and right-left planes will allow visualization of the entire bladder. (Image courtesy of Bret Nelson.)

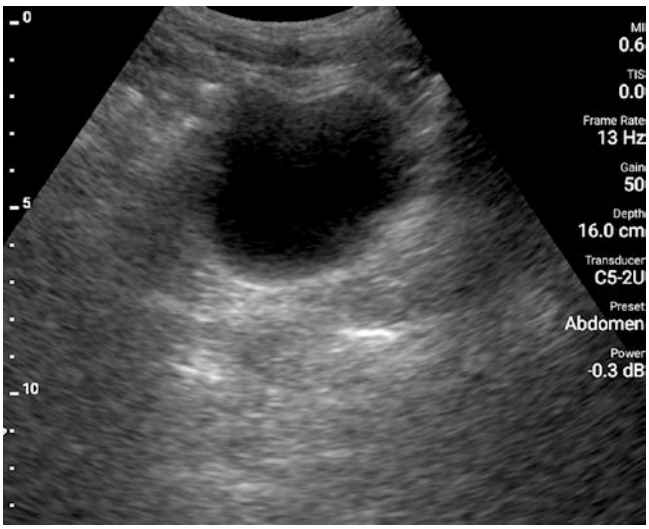

Fig. 28.14 Ultrasound image of bladder distention in the longitudinal plane. The dimensions of the anechoic fluid-filled bladder can be measured in order to calculate volume. See Video 28.6. (Image courtesy of Stephen Alerhand.)

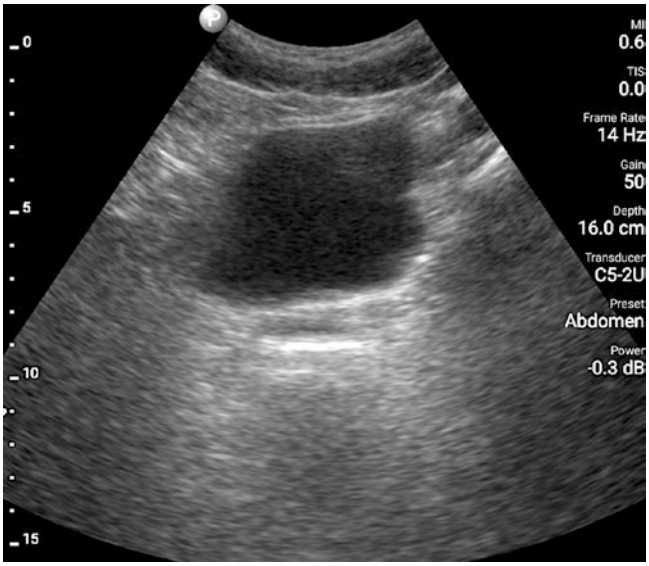

Fig. 28.15 Ultrasound image of bladder distention in the transverse plane. Once again, the dimensions of the anechoic fluid-filled bladder can be measured in order to calculate volume. See Video 28.7. (Image courtesy of Stephen Alerhand.)

References

1. Watkins S, Bowra J, Sharma P, Holdgate A, Giles A, Campbell L. Validation of emergency physician ultrasound in diagnosing hydronephrosis in ureteric colic. Emerg Med Australas. 2007;19:188–95.
2. Moak JH, Lyons MS, Lindsell CJ. Bedside renal ultrasound in the evaluation of suspected ureterolithiasis. Am J Emerg Med. 2012;30:218–21.
3. Riddell J, Case A, Wopat R, Beckham S, Lucas M, McClung CD, Swadron S. Sensitivity of emergency bedside ultrasound to detect hydronephrosis in patients with computed tomography-proven stones. West J Emerg Med. 2014;15:96–100.
4. Rosen CL, Brown DF, Sagarin MJ, Chang Y, McCabe CJ, Wolfe RE. Ultrasonography by emergency physicians in patients with suspected ureteral colic. J Emerg Med. 1998;16:865–70.
5. Goertz JK, Lotterman S. Can the degree of hydronephrosis on ultrasound predict kidney stone size? Am J Emerg Med. 2010;28:813–6.
6. Ding YY, Sahadevan S, Pang WS, Choo PW. Clinical utility of a portable ultrasound scanner in the measurement of residual urine volume. Singap Med J. 1996;37:365–8.
7. Daurat A, Choquet O, Bringuier S, Charbit J, Egan M, Capdevila X. Diagnosis of postoperative urinary retention using a simplified ultrasound bladder measurement. Anesth Analg. 2015;120:1033–8.
8. Coombes GM, Millard RJ. The accuracy of portable ultrasound scanning in the measurement of residual urine volume. J Urol. 1994;152:2083–5.

Urinary Bladder

29

Hiroshi Sekiguchi

Point-of-care urinary bladder imaging is often indicated in the setting of lower quadrant pain, hematuria, oligoanuria, or postoperative urinary retention. It is helpful to measure the size of the bladder or the degree of urinary retention, assess presence or absence of a significant mass, confirm the position of a bladder catheter, and guide suprapubic catheter placement.

A study demonstrated that the bladder volume can be estimated using this formula: W (width of the transverse view) × D1 (anteroposterior diameter of the transverse view) × D2 (superior-inferior diameter of the sagittal view) × 0.75 = volume (mL) (Figs. 29.1 and 29.2) [1]. Another study demonstrated that the largest transverse diameter of 9.7 cm or more can accurately predict a bladder volume ≥ 600 mL [2].

Detection and differentiation of some bladder pathologies are beyond the scope of the urinary point-of-care examination because an insufficiently or excessively filled bladder inhibits accurate assessment of bladder anatomy or pathological lesions [3, 4]. However, significant pathology such as a large mass in the bladder or a dysfunctional bladder catheter causing urinary retention can be identified with point-of-care ultrasound, which thus facilitates further testing and timely management (Figs. 29.3, 29.4, and 29.5).

H. Sekiguchi, M.D.
Division of Pulmonary and Critical Care Medicine, Mayo Clinic, Rochester, MN, USA
e-mail: sekiguchi.hiroshi@mayo.edu

B. P. Nelson et al. (eds.), *Atlas of Handheld Ultrasound*, https://doi.org/10.1007/978-3-319-73855-0_29

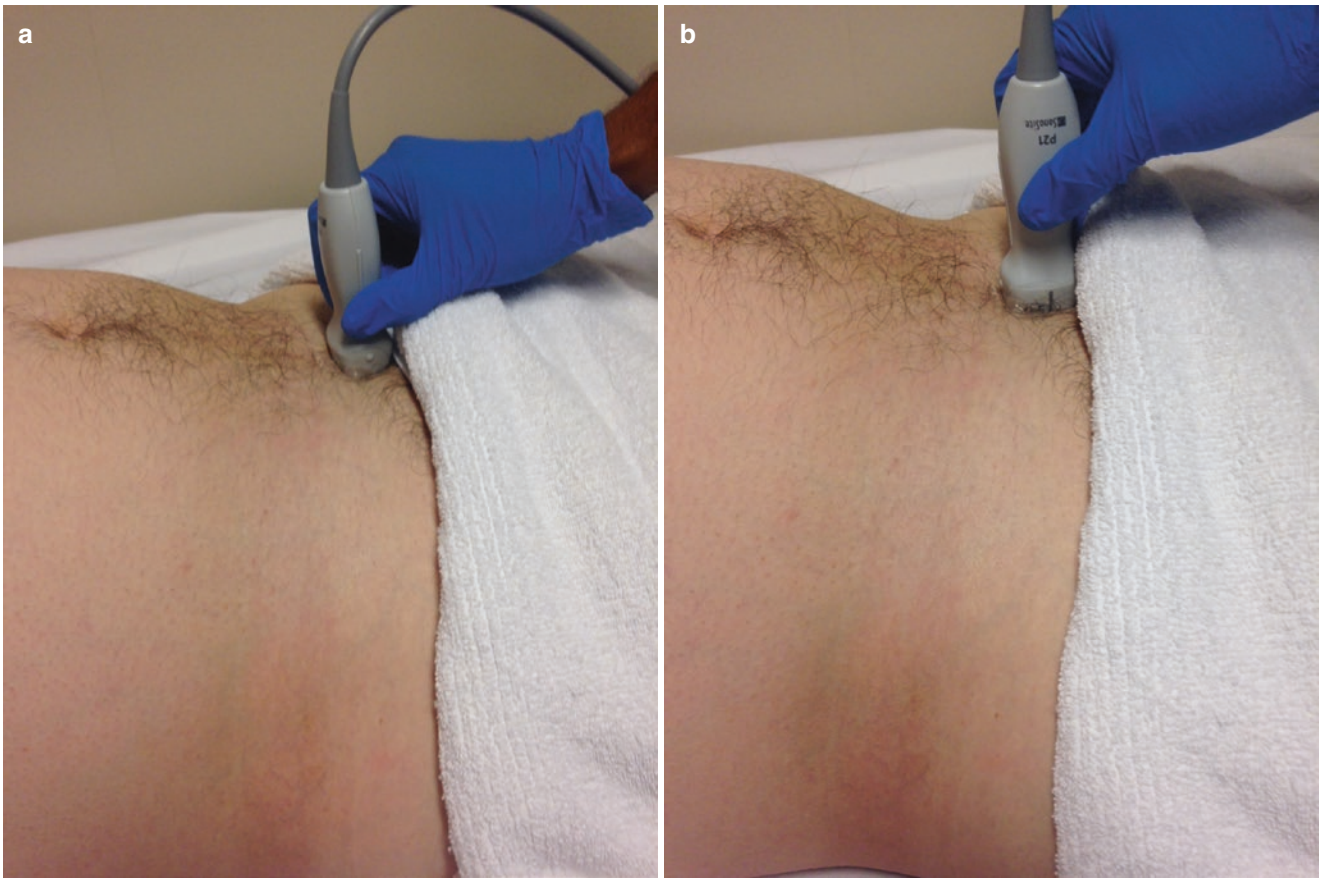

Fig. 29.1 Imaging of the normal urinary bladder. (**a**) Transverse view of the bladder: A curvilinear or phased array transducer is placed above the public symphysis, with its orientation marker pointing toward the patient's right side. (**b**) Sagittal view of the bladder: A curvilinear or phased array transducer is placed above the public symphysis, with its orientation marker pointing toward the patient's head

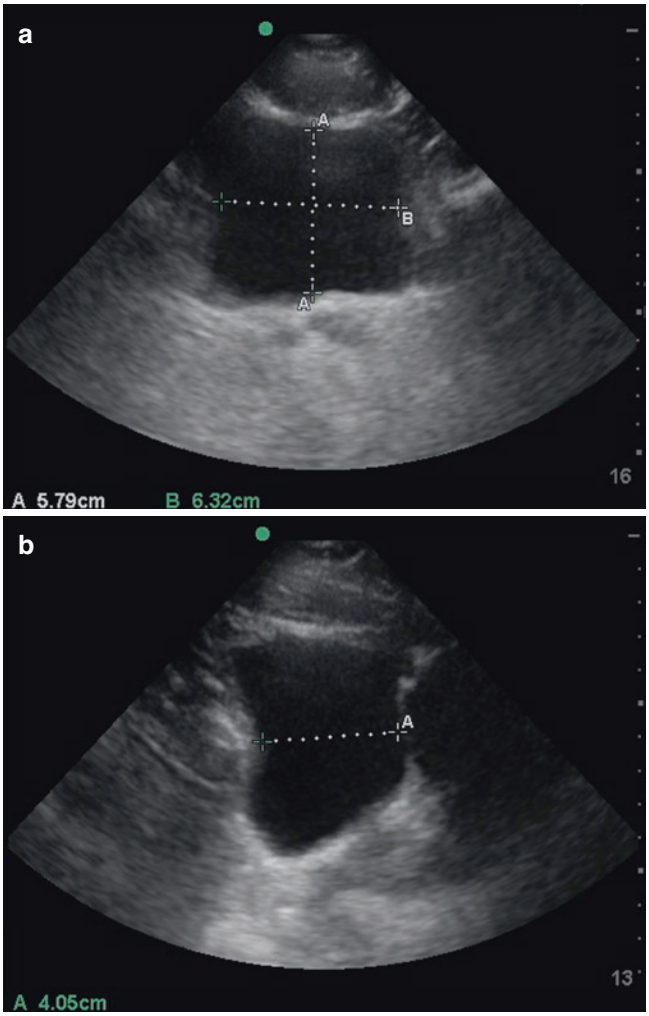

Fig. 29.2 Estimation of the urinary volume (6.32 × 5.79 × 4.05 × 0.7 5 = 111 mL). (**a**) Width (6.32 cm) and anteroposterior dimension (5.79 cm) of the transverse image is measured. (**b**) Superior-inferior dimension (4.05 cm) of the sagittal image is measured

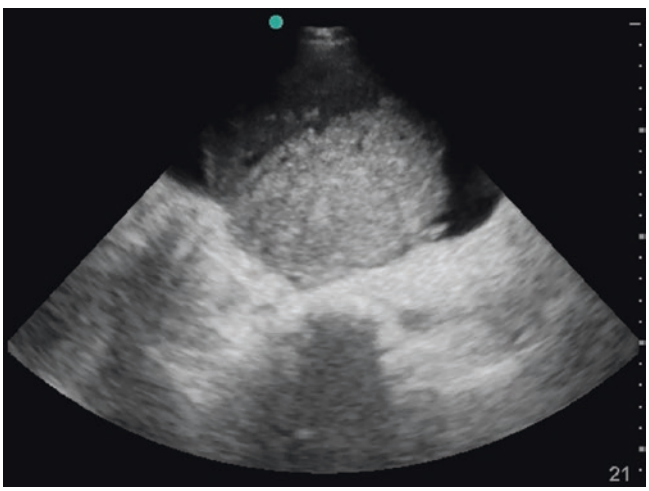

Fig. 29.3 Point-of-care ultrasound demonstrating a bladder tumor

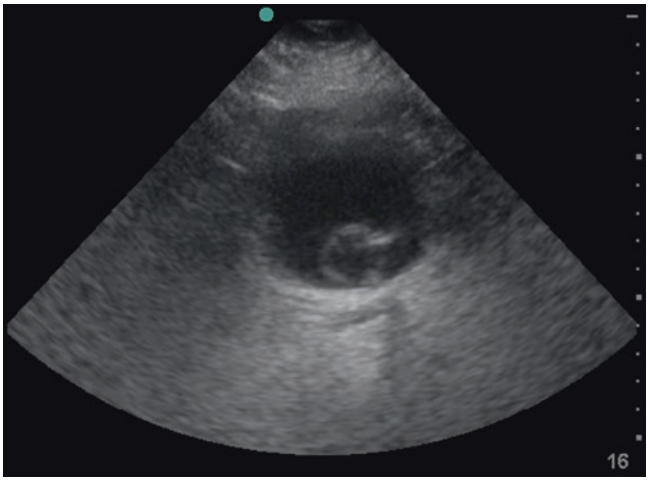

Fig. 29.4 Transverse view of the bladder, demonstrating anechoic-appearing urine surrounding a saline-filled catheter hub in a reportedly "anuric" patient. This finding suggests that the catheter is clogged or dysfunctional

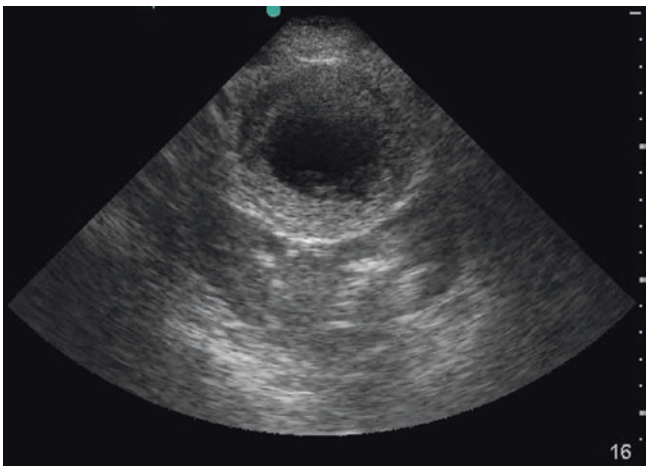

Fig. 29.5 Point-of-care ultrasound demonstrating a thickened bladder wall in a patient with cystitis

References

1. Chan H. Noninvasive bladder volume measurement. J Neurosci Nurs. 1993;25:309–12.
2. Daurat A, Choquet O, Bringuier S, Charbit J, Egan M, Capdevila X. Diagnosis of postoperative urinary retention using a simplified ultrasound bladder measurement. Anesth Analg. 2015;120:1033–8.
3. Itzchak Y, Singer D, Fischelovitch Y. Ultrasonographic assessment of bladder tumors. I. Tumor detection. J Urol. 1981;126:31–3.
4. Wieczorek AP, Wozniak MM, Tyloch JF. Errors in the ultrasound diagnosis of the kidneys, ureters and urinary bladder. J Ultrason. 2013;13:308–18.

Uterus

30

Carlo Canepa and Lauren Ferrara

The uterus is a pelvic organ that can be visualized with point-of-care ultrasound and can be helpful in patients with pelvic pain, vaginal bleeding, and newly diagnosed pregnancies. The primary goals of a focused uterus ultrasound are to assess for size, pathology, the location of an IUD, and in the case of pregnancy, an intra-uterine pregnancy. Pathology such as fibroids, cysts, free fluid, ectopic pregnancy, and empty gestational sac can be seen. The test characteristics for ruling out ectopic pregnancy using point-of-care ultrasound are excellent, with a sensitivity of 99.3% and negative predictive value approaching 100% [1]. Point-of-care ultrasound use has been shown to decrease evaluation time in patients being assessed for pregnancy complications [2]. Figures 30.1, 30.2, 30.3, 30.4, 30.5, 30.6, 30.7, 30.8, 30.9, and 30.10 and Videos 30.1, 30.2, 30.3, 30.4, 30.5, 30.6, 30.7, 30.8, and 30.9 provide examples of normal and pathological findings that may be found on transabdominal scanning.

Electronic Supplementary Material The online version of this chapter (https://doi.org/10.1007/978-3-319-73855-0_30) contains supplementary material, which is available to authorized users.

C. Canepa, M.D. (✉)
Department of Emergency Medicine, Harvard Medical School, Massachusetts General Hospital, Boston, MA, USA
e-mail: CCanepa@mgh.harvard.edu

L. Ferrara, M.D.
Icahn School of Medicine at Mount Sinai, New York, NY, USA
e-mail: lauren.ferrara@mssm.edu

B. P. Nelson et al. (eds.), *Atlas of Handheld Ultrasound*, https://doi.org/10.1007/978-3-319-73855-0_30

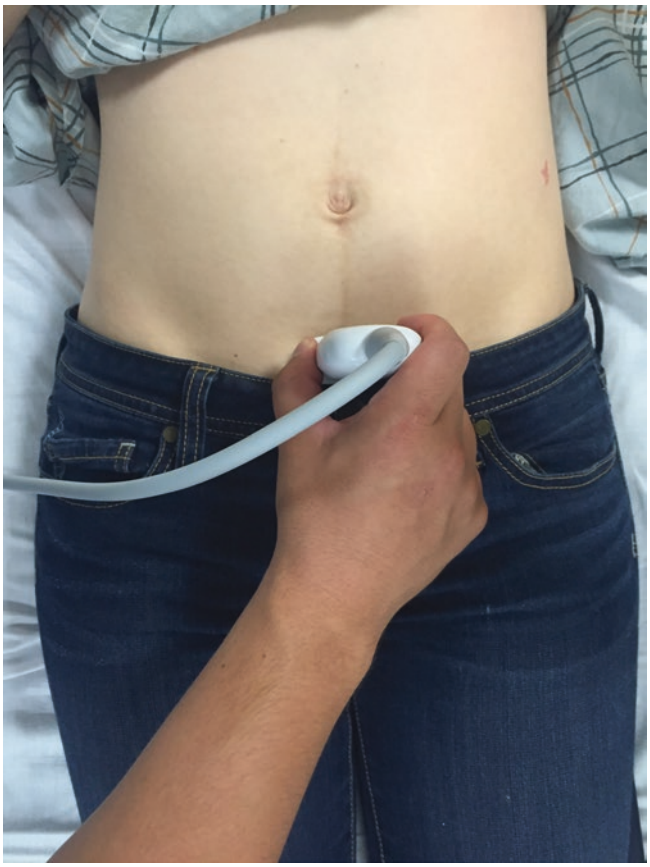

Fig. 30.1 A curvilinear or phased array probe should be used. Transverse views should be obtained with the probe marker facing the patient's right. Scan cranial-caudal in the supra-pubic area, just above the pubic symphysis. Image courtesy of Carlo Canepa

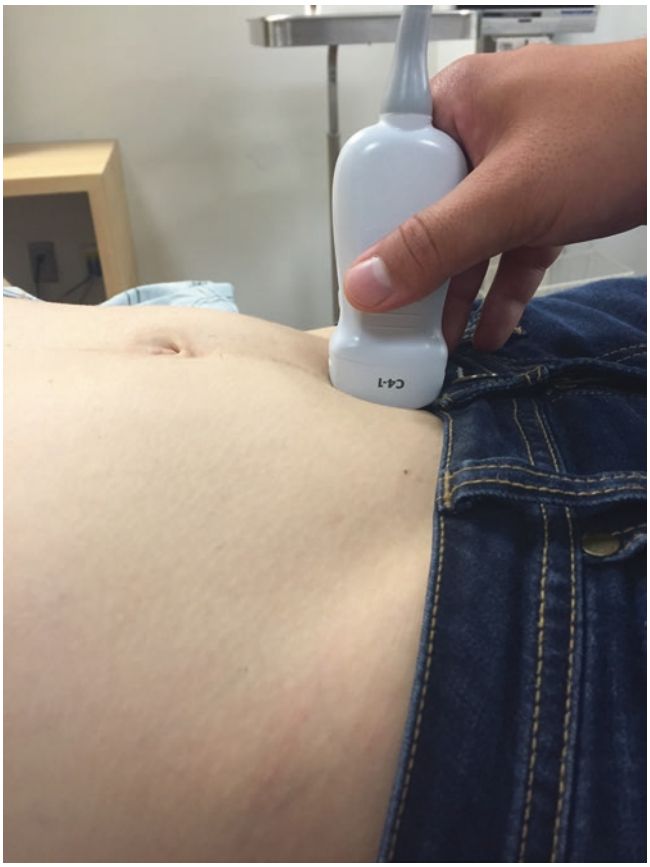

Fig. 30.2 Sagittal views should also be obtained with the probe marker facing the patient's head. Sweep right-left just above the pubic symphysis to visualize the entire uterus. Image courtesy of Carlo Canepa

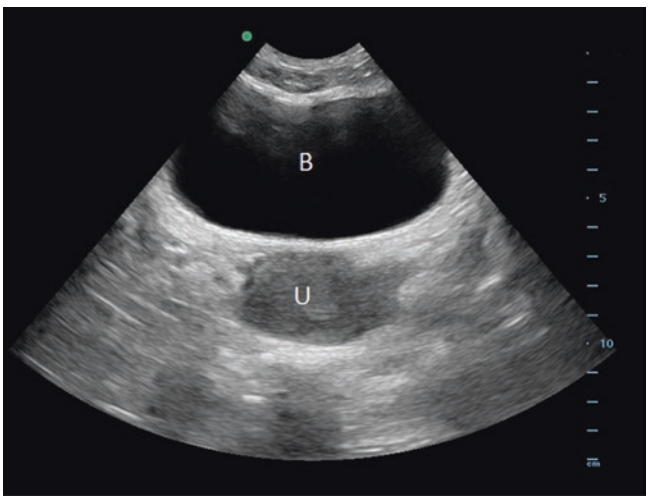

Fig. 30.3 In the transverse view, a non-pregnant uterus (U) will appear posterior to the bladder (B). You may have to aim the probe caudally to see a non-pregnant uterus. Image courtesy of Carlo Canepa

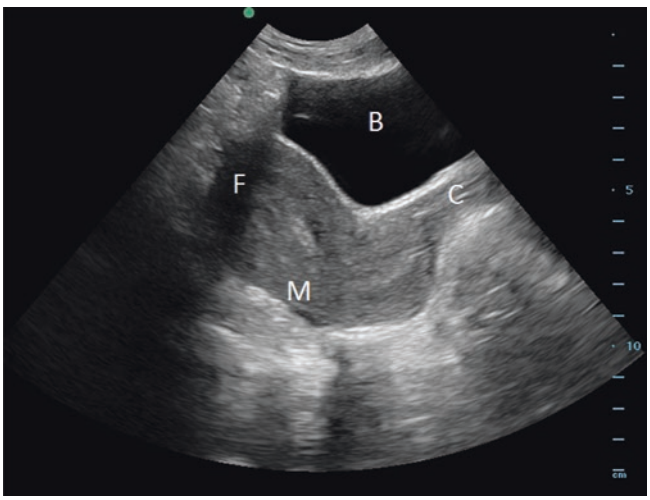

Fig. 30.4 A sagittal view of the non-pregnant uterus should demonstrate a fundus (F), myometrium (M), and cervix (C), posterior to the bladder (B). Image courtesy of Carlo Canepa

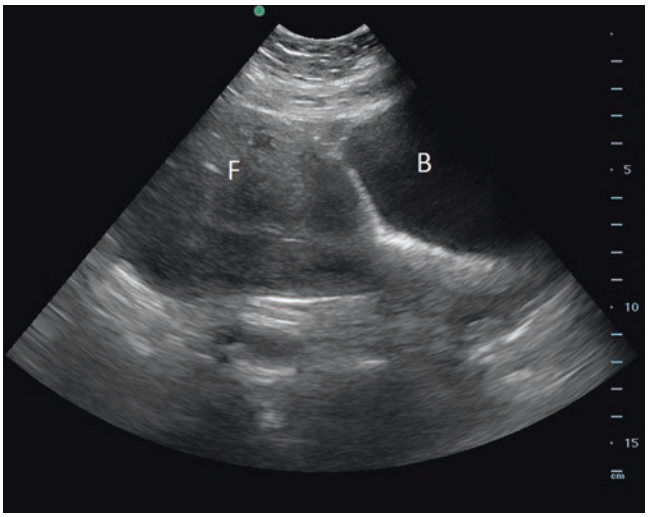

Fig. 30.5 An enlarged fibroid non-pregnant uterus is evident in this image. This uterus was so large that it rested superior to the bladder. Image courtesy of Carlo Canepa

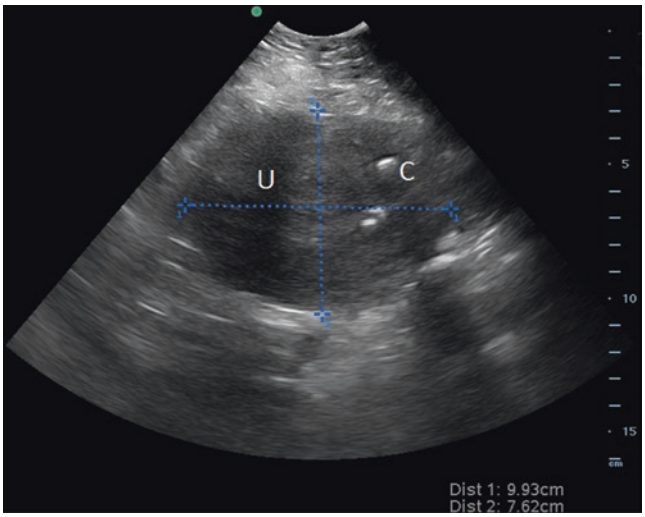

Fig. 30.6 This transverse view of a large uterus (U) with calcified fibroids (C). Image courtesy of Carlo Canepa

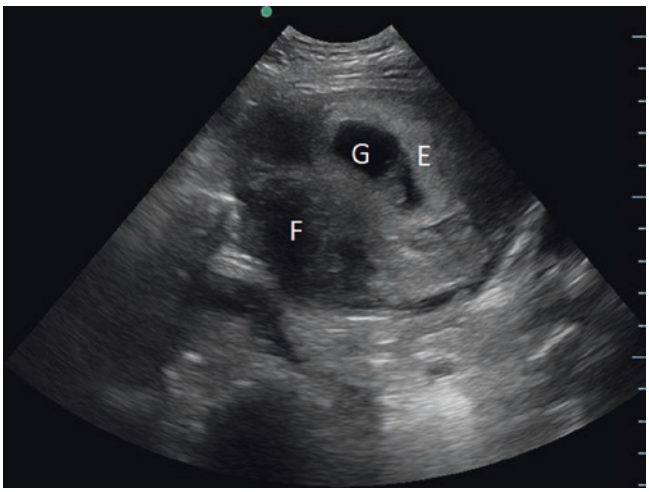

Fig. 30.7 This transverse view of a pregnant uterus demonstrates a gestational sac (G), endometrium (E), and a fibroid (F). Image courtesy of Carlo Canepa

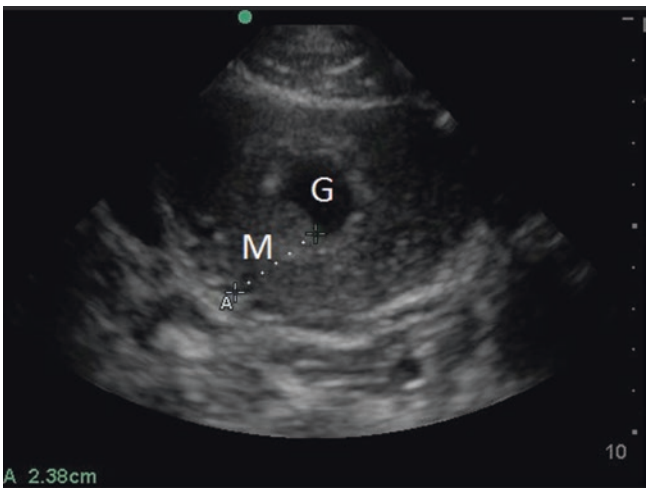

Fig. 30.8 A transverse view of a uterus with an empty gestational sac (G) and an endo-myometrial mantle measurement (M). Image courtesy of Carlo Canepa

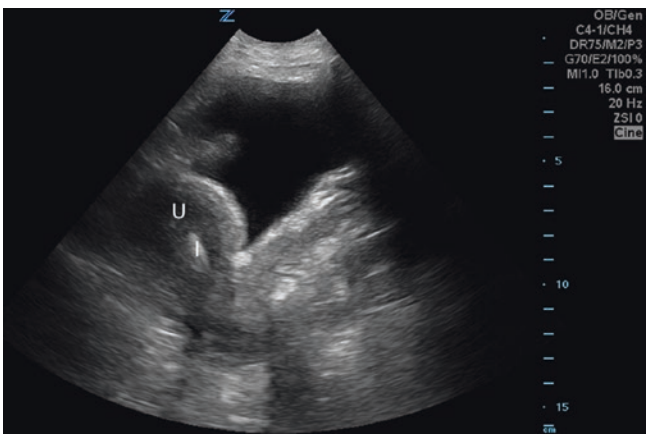

Fig. 30.9 An intra-uterine device (I) can be seen within the uterus (U). Image courtesy of Carlo Canepa

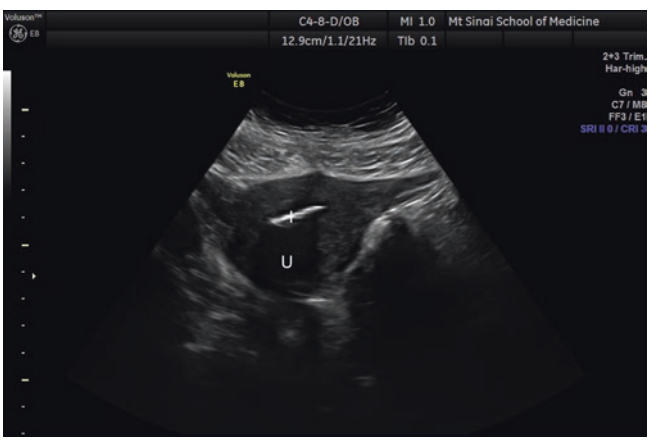

Fig. 30.10 Another intra-uterine device (I) within a uterus (U). Image courtesy of Lauren Ferrara

References

1. Stein JC, Wang R, Adler N, Boscardin J, Jacoby VL, Won G, et al. Emergency physician ultrasonography for evaluating patients at risk for ectopic pregnancy: a meta-analysis. Ann Emerg Med. 2010;56:674–83.
2. Blaivas M, Sierzenski P, Plecque D, Lambert M. Do emergency physicians save time when locating a live intrauterine pregnancy with bedside ultrasonography? Acad Emerg Med. 2000;7(9):988–93.

Ovary

31

Carlo Canepa and Lauren Ferrara

The ovaries can be visualized using a transabdominal or transvaginal approach. Although the latter is more invasive, it provides a more detailed assessment of anatomy. As of this writing, handheld ultrasound devices offer only transabdominal probes, so this chapter covers that approach. Ovarian imaging can be helpful in the female patient with pelvic pain or vaginal bleeding, and transabdominal ultrasound can often detect abnormalities such as polycystic ovaries or hyperstimulation syndrome [1, 2]. Ovarian pathology such as enlarged ovaries and ovarian cysts also can be seen incidentally in the setting of other examinations, such as Focused Assessment with Sonography for Trauma (FAST) exams or bowel scans (Figs. 31.1, 31.2, 31.3, 31.4, and 31.5; Videos 31.1 and 31.2).

Electronic Supplementary Material The online version of this chapter (https://doi.org/10.1007/978-3-319-73855-0_31) contains supplementary material, which is available to authorized users.

C. Canepa, M.D. (✉)
Department of Emergency Medicine, Harvard Medical School, Massachusetts General Hospital, Boston, MA, USA
e-mail: CCanepa@mgh.harvard.edu

L. Ferrara, M.D.
Icahn School of Medicine at Mount Sinai, New York, NY, USA
e-mail: lauren.ferrara@mssm.edu

B. P. Nelson et al. (eds.), *Atlas of Handheld Ultrasound*, https://doi.org/10.1007/978-3-319-73855-0_31

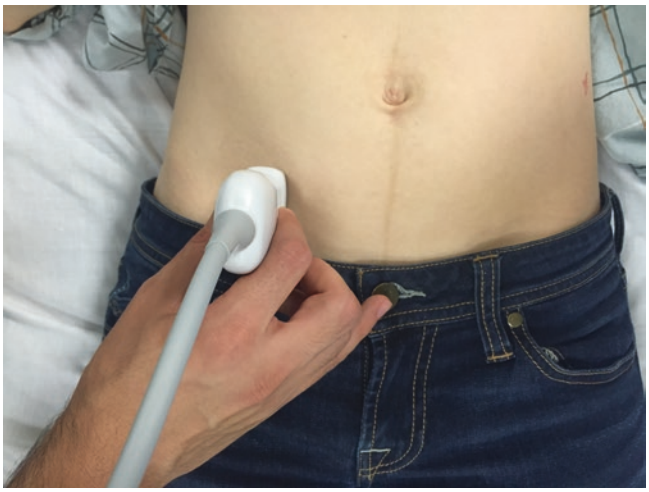

Fig. 31.1 A curvilinear or phased array probe should be used for ovarian imaging. To find the ovaries transabdominally, start with the probe in a transverse position midline in the suprapubic region. Aim the probe inferiorly and slide laterally to identify the iliac vessels. Next, aim the probe slightly superiorly to find the ovary

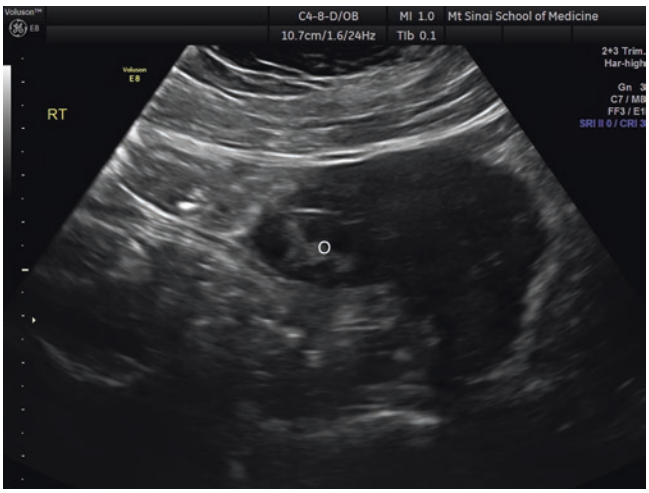

Fig. 31.4 A sagittal view of a normal ovary (O)

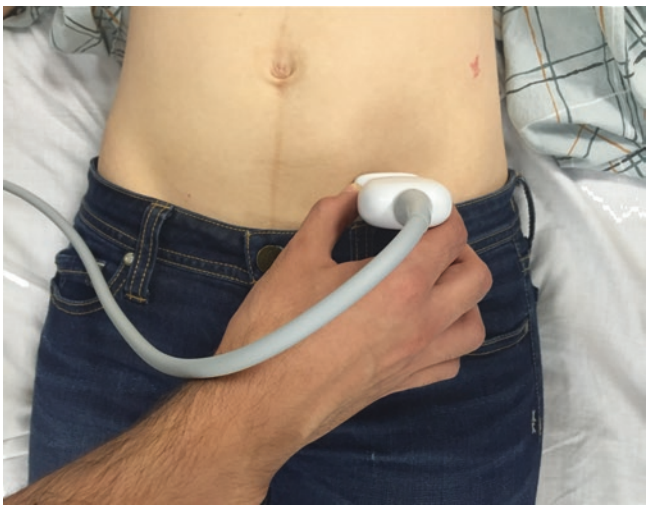

Fig. 31.2 The process should be repeated on the other side. Sagittal views should be obtained with the probe marker facing the patient's head, and transverse views with the probe marker facing the patient's right

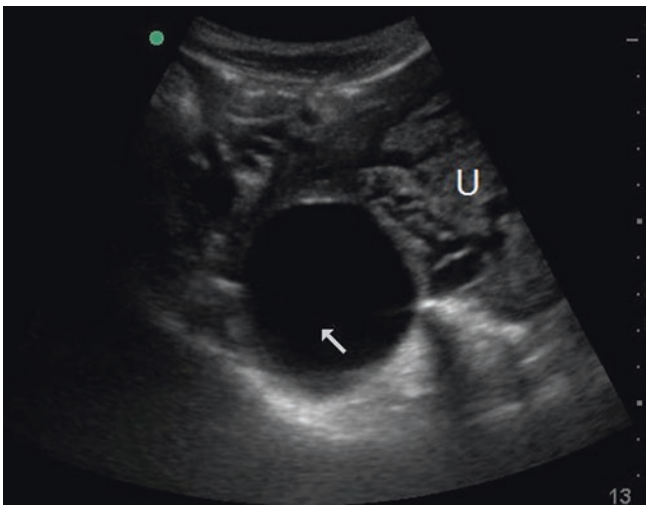

Fig. 31.5 This image demonstrates a large, simple right ovarian cyst (*arrow*) alongside the patient's uterus (U)

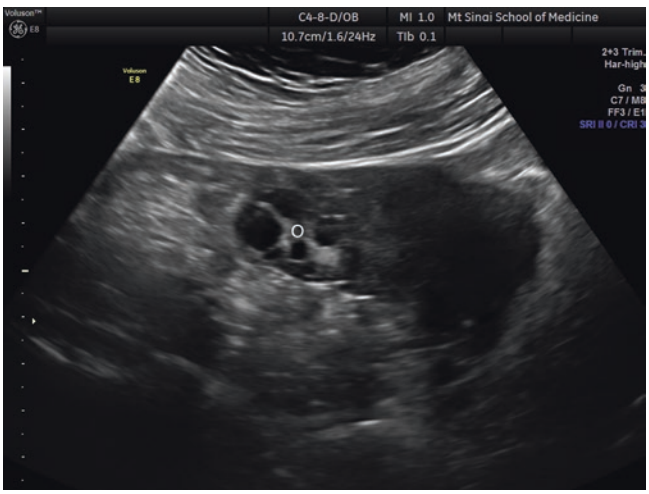

Fig. 31.3 A longitudinal view of the ovary (O) should show a structure resembling a chocolate chip cookie

References

1. Battaglia C, Mancini F, Percico N, Zaccaria V, de Aloysio D. Ultrasound evaluation of PCO, PCOS, and OHSS. Reprod Biomed Online. 2004;9:614–9.
2. Bellapu S, Guttman J. Use of point-of-care ultrasound for the diagnosis of ovarian hyperstimulation syndrome. J Emerg Med. 2017;52:e101–4.

Scrotum, Testes, and Paratesticular Structures

32

Daniel J. Schnobrich and Bruce R. Gilbert

Ultrasound is the optimal modality for imaging the scrotum, testicles, and paratesticular structures, and is an essential procedure when the traditional physical exam is inconclusive or incomplete [1]. Ultrasound is required in the evaluation of epididymitis, orchitis, torsion, hydrocele, varicocele, trauma, and other scrotal anomalies (Figs. 32.1, 32.2, 32.3, and 32.4).

Ultrasonographic findings of diffuse epididymal enlargement and decreased echogenicity are typically diagnostic of acute epididymitis (Fig. 32.5) [4]. When acute epididymitis is present, increased epididymal flow may be seen with the use of color Doppler ultrasound [5]. When acute orchitis is present, early ultrasonic findings may include focal or diffuse areas of hypoechoenicity, with increased testicular blood flow seen with Doppler ultrasound. Without treatment, infarction may subsequently occur, resulting in the loss of flow signal when Doppler is utilized [6]. Hydroceles are typically seen as anechoic fluid between the parietal and visceral layers of the tunica vaginalis, and may be either primary or secondary to another process.

Ultrasound may also be a useful tool in differentiating conditions which require surgery from those in which medical therapy is sufficient [7]. While the clinical exam and judgment are paramount in the diagnosis of testicular torsion (Fig. 32.6), ultrasound findings of a hypogenic testis, a lack of testicular blood flow, or a twisted spermatic cord may play a supportive role. In one study of 56 patients undergoing surgical exploration for an acute scrotum, none of 22 patients found to have testicular torsion operatively had a detectable Doppler signal; whereas 33 of the 34 without torsion did have a signal detected [8]. Ultrasonography may detect malignant masses even when they are clinically non-palpable (Fig. 32.7) [9]. Ultrasound is the optimal imaging method for evaluation of most types of scrotal trauma (Fig. 32.8) [10].

Testicular volume measurement by ultrasonography is highly accurate, exceeding that of a Prader orchidometer [11].

D. J. Schnobrich, M.D. (✉)
Department of Medicine, Division of General Internal Medicine, University of Minnesota, Minneapolis, MN, USA
e-mail: schn0364@umn.edu

B. R. Gilbert, M.D., Ph.D.
The Smith Institute for Urology, Zucker School of Medicine at Hofstra/Northwell, New Hyde Park, NY, USA

B. P. Nelson et al. (eds.), *Atlas of Handheld Ultrasound*, https://doi.org/10.1007/978-3-319-73855-0_32

This measurement is useful in the evaluation of male infertility; as testicular size measurement correlates with spermatogenesis [11, 12]. It may also be used to monitor pubertal status, and to assess the clinical significance of a varicocele [12]. When a complete examination including color Doppler ultrasound is performed, ultrasound is reliable in the diagnosis of testicular varicoceles (Fig. 32.9), and is likely less observer-dependent than the physical examination [13].

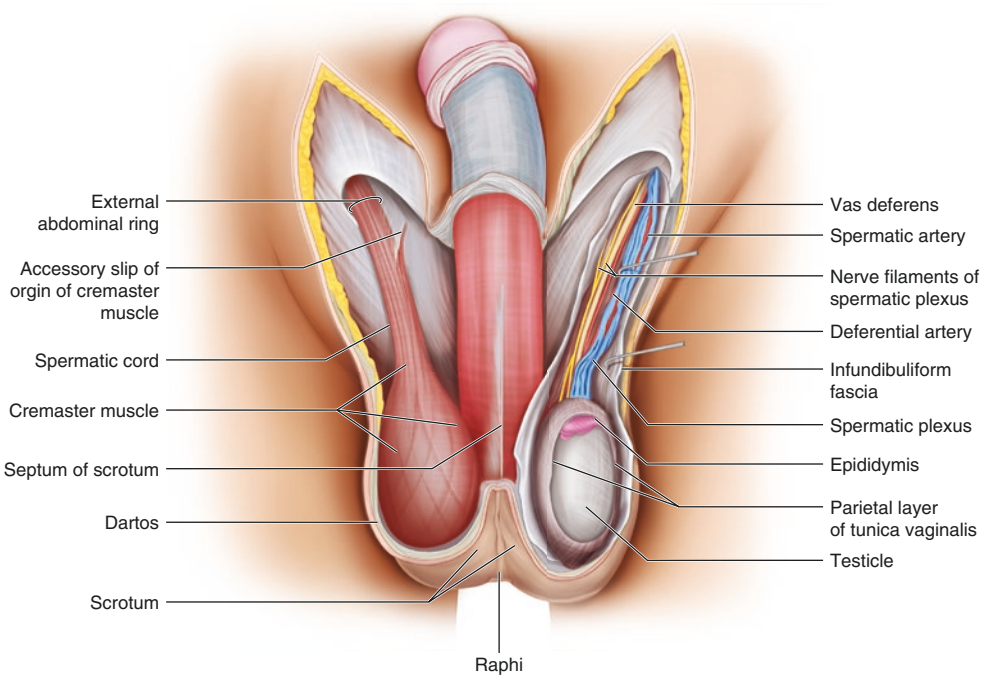

Fig. 32.1 Adult male anatomy: The normal adult testes are smooth and ovoid, 4–5 cm long (cranio-caudal), 3 cm wide, and 2–3 cm in the anterior-posterior dimension. The epididymis is typically 6–7 cm long, with the head measuring 10–12 mm in diameter and the body and tail measuring 2–5 mm in diameter. The head is triangular, and is typically posterolateral to the upper pole of the testis. (*From* Gray [2]; public domain)

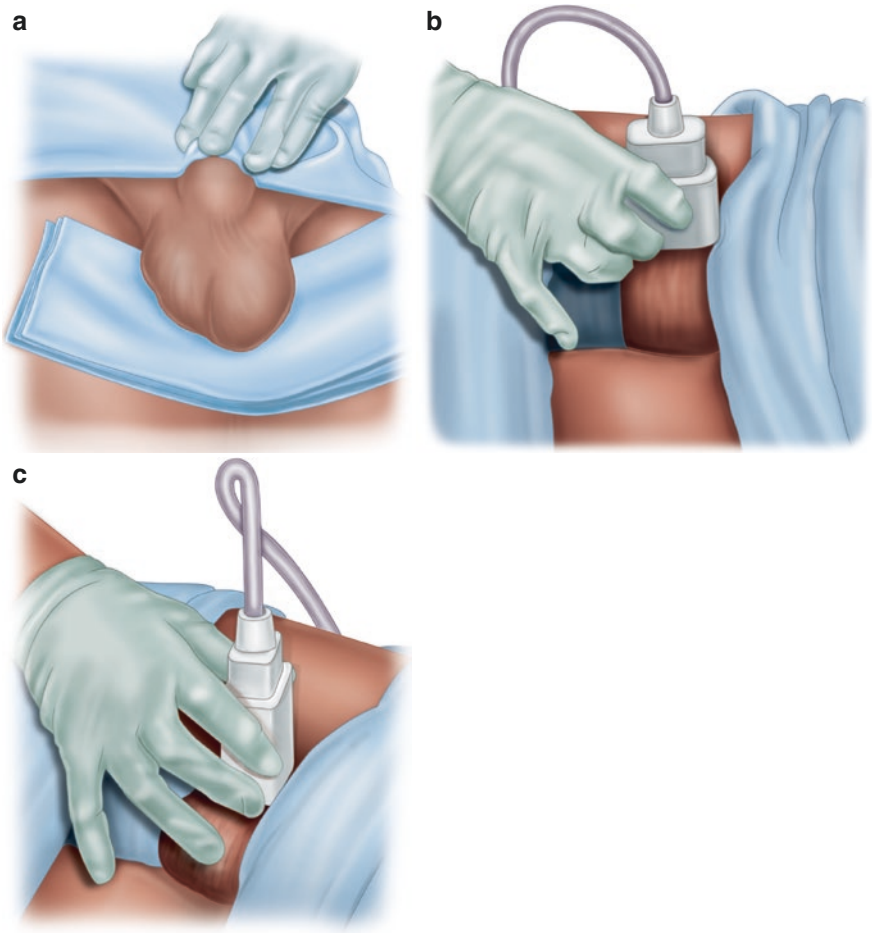

Fig. 32.2 (**a**) High-frequency linear array probe, ideally with a large footprint, should be used to view the testicles. The patient should lie supine with his scrotum supported. This could be by the patient's thighs or a towel. The phallus is placed on the pubis and covered for privacy. (**b**) The testicles are first evaluated longitudinally, with the probe marker pointed cranially. The fifth digit is placed on the thigh to steady the probe. A longitudinal survey is performed first, from medial to lateral. If the footprint is not long enough to visualize the entire testicle in one view, multiple scans should be performed. (**c**) The probe is then rotated 90°. A survey is performed by scanning from mid-testicle to the superior pole and then back to the inferior pole. (*From* Gilbert [3]; *with permission*)

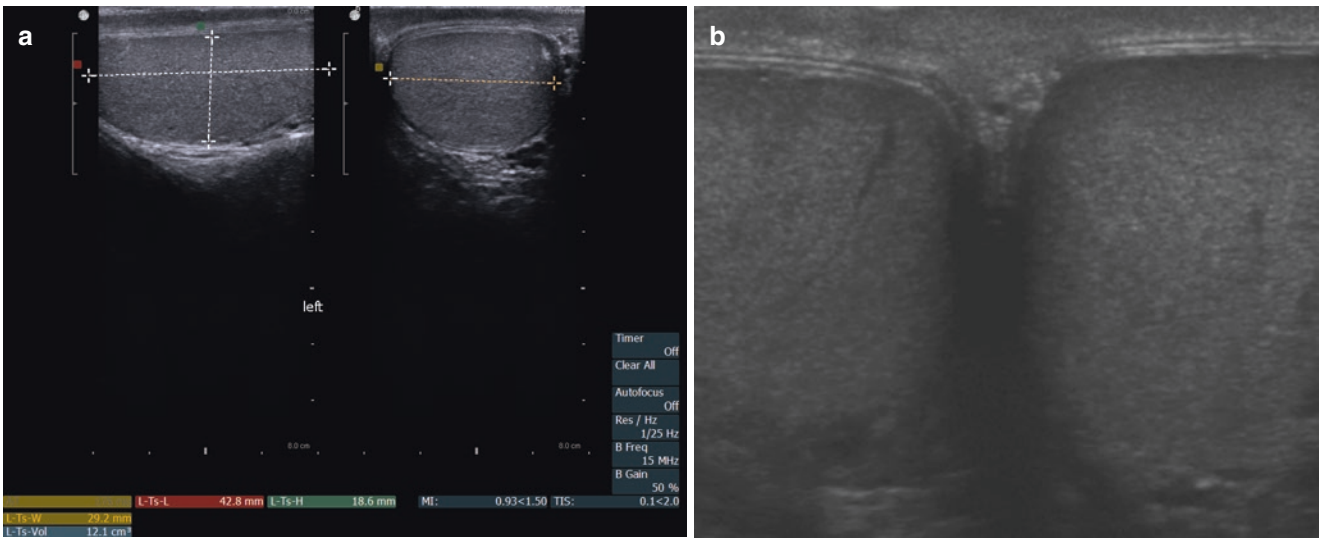

Fig. 32.3 (**a**) Grayscale ultrasound in longitudinal (left) and transverse planes (middle). The mid sagittal length, mid AP height (transverse or sagittal plane), and the mid transverse width are measured. Testicular volume is calculated, usually using the formula Length × Width × Height × 0.71. Lateral and medial longitudinal views as well as superior and inferior transverse views of each testis should be documented for completeness. (*Image courtesy of* Dr. Bruce Gilbert.) (**b**) A grayscale image with both testicles in a single image is taken to compare echogenicity and document the presence of two testes. (*From* Gilbert [3]; *with permission*)

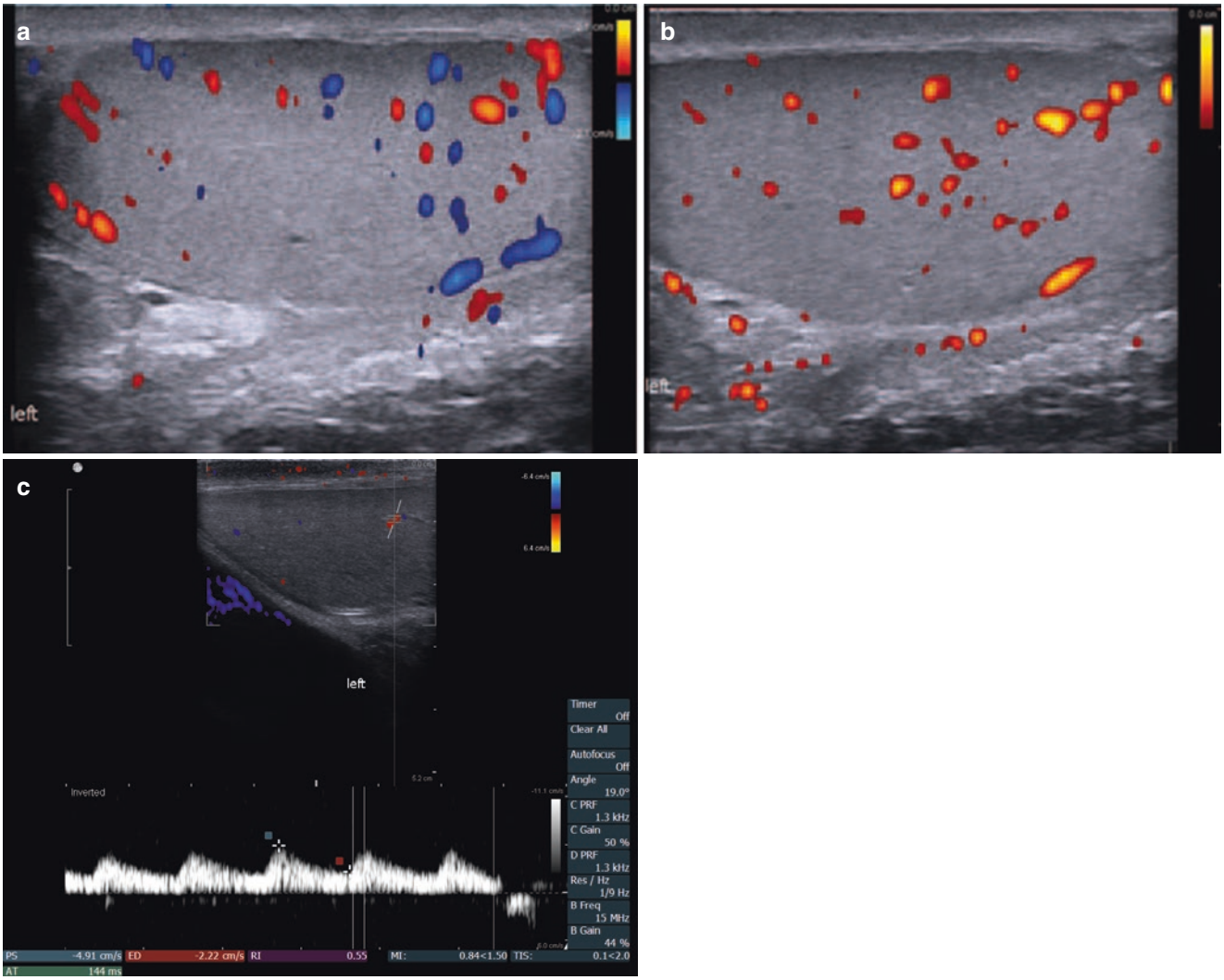

Fig. 32.4 (**a**) Testicular blood flow is best visualized using color Doppler. Color Doppler is shown in the image on the left as documented by the discontinuous color bar in the image. (*Image courtesy of* Dr. Bruce Gilbert.) (**b**) Power Doppler is used in the images on the right, which is more sensitive for flow but does not show directionality. Power Doppler is documented by the continuous color bar in the image (*From* Gilbert [3]; *with permission*). (**c**) Spectral Doppler shows a normal low-impedance pattern. (*Image courtesy of* Dr. Bruce Gilbert)

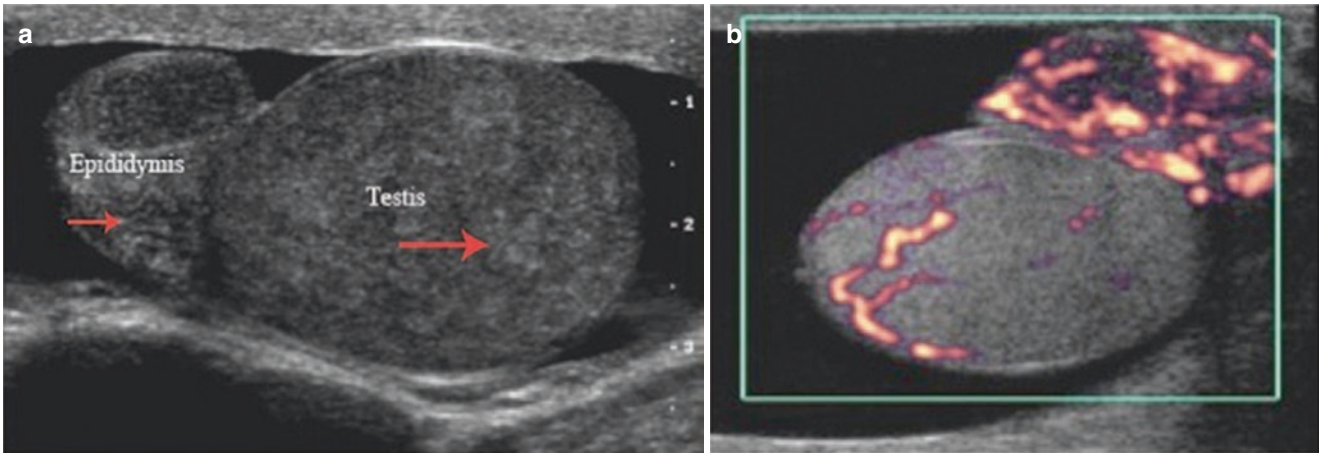

Fig. 32.5 (**a**) Epididymo-orchitis. Both the epididymis and testis are enlarged, with multiple hypoechoic patches on the testis. (**b**) Power Doppler shows increased vascular flow in the epididymis. (*From* Gilbert [3]; *with permission*)

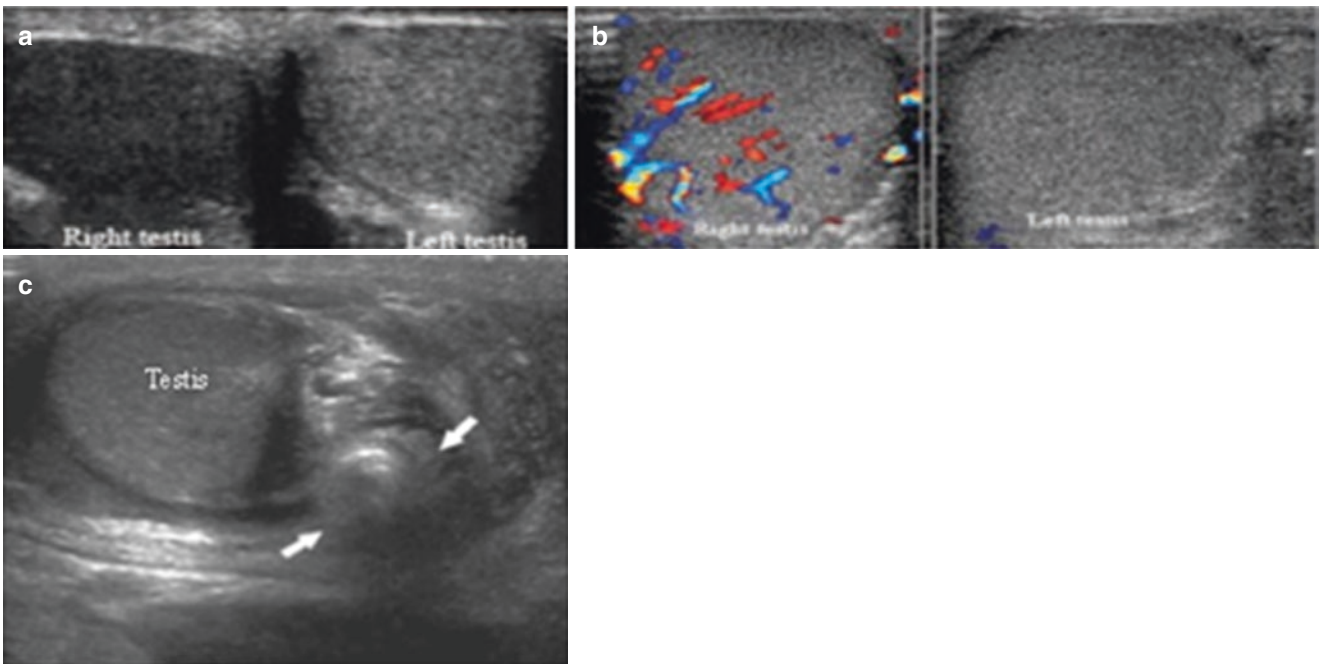

Fig. 32.6 (**a**) In torsion, the testis can be hypoechoic, as shown in the right testis (A) or devoid of blood flow as shown in the left testis using color Doppler (B). However, ultrasound evidence is not pathognomonic for torsion. The clinical exam is paramount. Only the surgeon, or the pathologist, can make the diagnosis. (**c**) The whirlpool sign is found when there is twisting of the spermatic cord. This is usually, but not always, associated with decreased or absent blood flow to the affected testicle. (*From* Gilbert [3]; *with permission*)

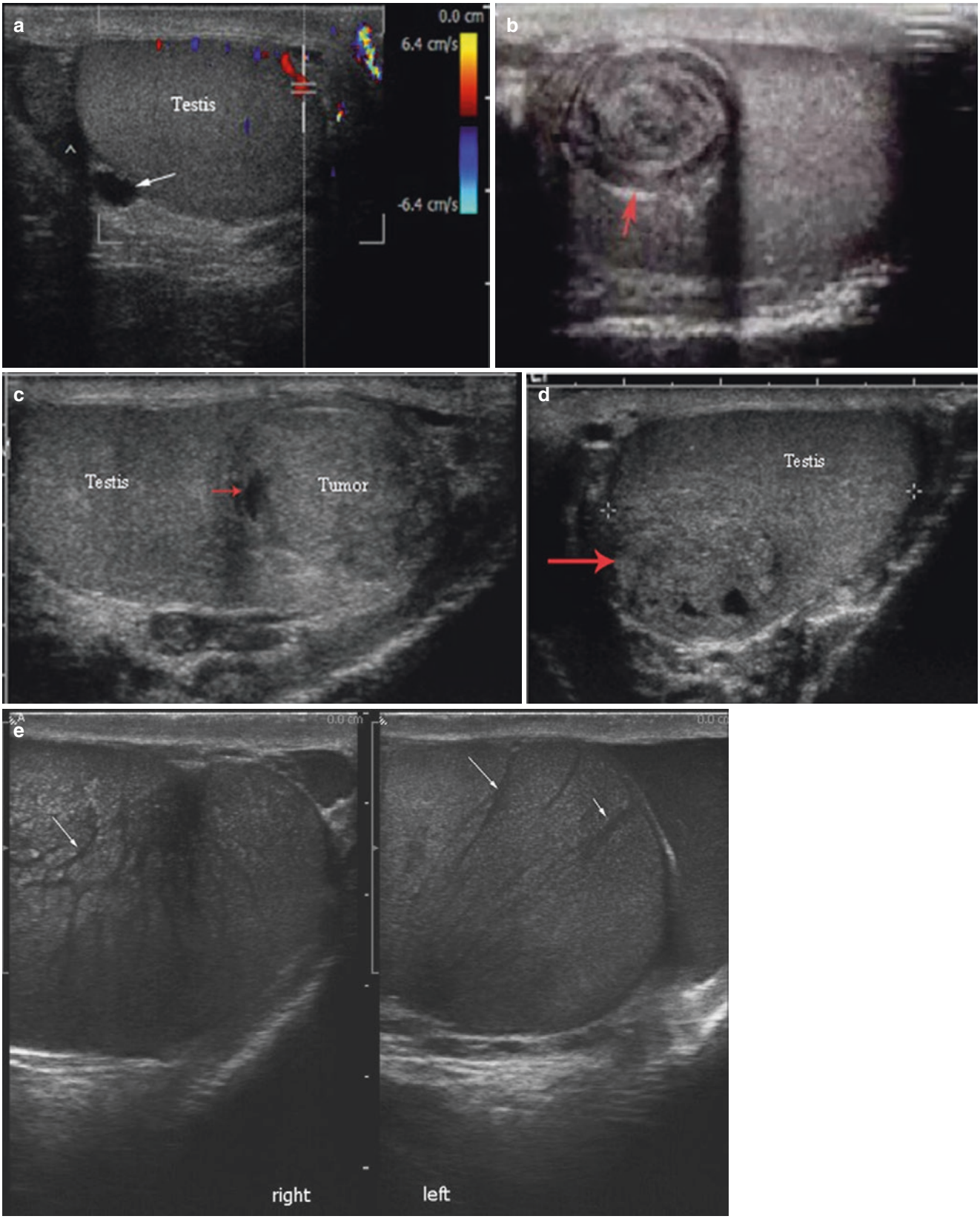

Fig. 32.7 (**a**) Many non-neoplastic and neoplastic testicular masses may be visualized with ultrasound. Simple testicular cysts are anechoic, and well-circumscribed. Tunica albugineal cysts are often found in the upper or lateral margins of the testes, and may be palpable. (**b**) An epidermoid cyst classically has an "onion ring" appearance due to alternating layers of hypoechogenicity and hyperechogenicity; and does not demonstrate flow when color Doppler is used. (**c**) Germ cell tumors account for approximately 95% of lesions, with the remainder being mostly sex cord stromal tumors, lymphomas, or metastasis. Seminomas (shown) are sonographically homogenous, well-defined, and hypoechoic, and may show increase blood flow with Color Doppler. (**d**) Non-seminomatous germ cell tumors (NSGCT) are characteristically irregular with a heterogeneous parenchyma. Color Doppler will show increased flow within the tumor (right). (**e**) Lymphomas may appear as diffusely enlarged testes. In this case, the right testis was 65 cm^3 and the left testis 69 cm^3. Increased vascularity may also be noted (not shown). (*From* Gilbert [3]; *with permission*)

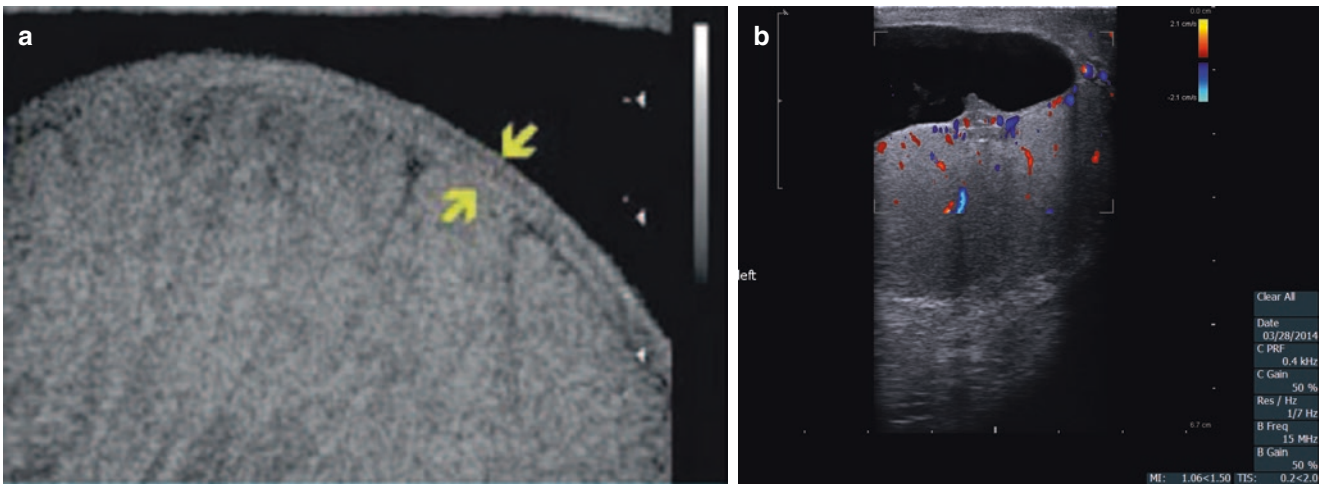

Fig. 32.8 (**a**) The tunica albuginea is a thin ring of fibrous tissue surrounding the testis, and appears hyperechoic on gray scale ultrasound. It is indicated by an arrow (*From* Gilbert [3]; *with permission*). (**b**) In this image, a discontinuity is seen in the tunica albuginea, which in the context of scrotal trauma is highly suggestive of scrotal rupture. (*From* Gilbert [3]; *with permission*)

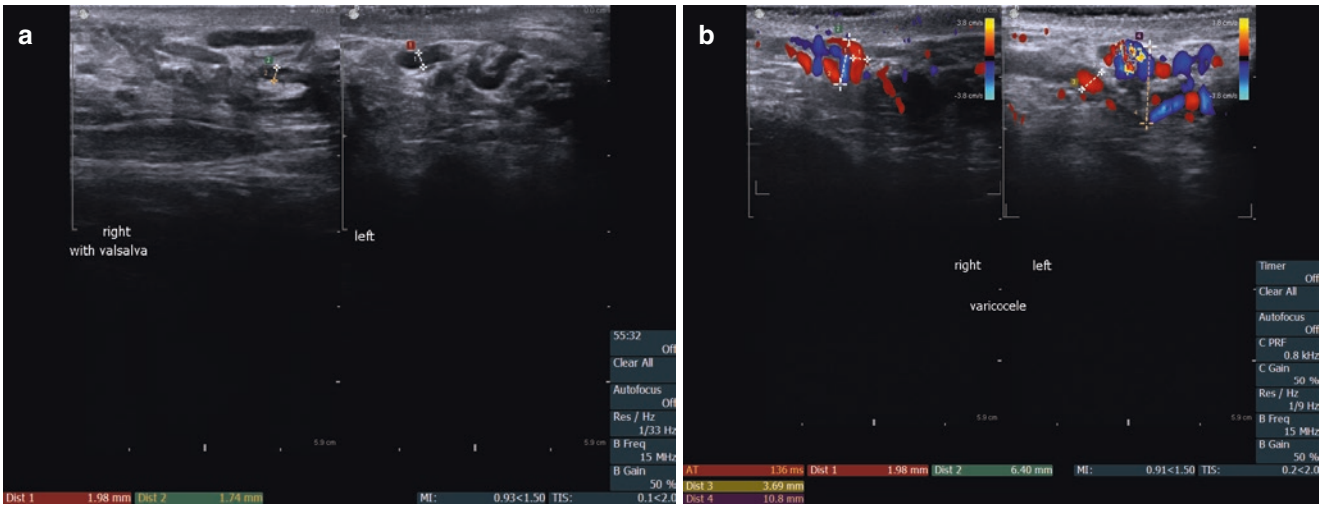

Fig. 32.9 (**a**) Varicoceles are a dilation of the testicular vein and pampiniform venous plexus within the spermatic cord, and may be a cause of reduced male fertility or occasionally scrotal pain. These veins may be visualized in grayscale as shown in this image. (**b**) Varicocele demonstrated with Valsalva with color Doppler above the testis. Measurements of both the width if the largest vein and complex are demonstrated. (*Image courtesy of* Dr. Bruce Gilbert)

References

1. Kuhn AL, Scortegagna E, Nowitzki KM, Kim YH. Ultrasonography of the scrotum in adults. Ultrasonography. 2016;35(3):180–97.
2. Gray H. Anatomy of the human body. 20th ed. Philadelphia: Lea and Febiger; 1918.
3. Gilbert BR. Ultrasound of the male genitalia. 1st ed. New York: Springer; 2015.
4. Rifkin MD, Kurtz AB, Goldberg BB. Epididymis examined by ultrasound. Correlation with pathology. Radiology. 1984;151(1):187–90.
5. Ralls PW, Jensen MC, Lee KP, Mayekawa DS, Johnson MB, Halls JM. Color Doppler sonography in acute epididymitis and orchitis. J Clin Ultrasound. 1990;18(5):383–6.
6. Cook JL, Dewbury K. The changes seen on high-resolution ultrasound in orchitis. Clin Radiol. 2000;55(1):13–8.
7. Blaivas M, Sierzenski P, Lambert M. Emergency evaluation of patients presenting with acute scrotum using bedside ultrasonography. Acad Emerg Med. 2001;8(1):90–3.
8. al Mufti RA, Ogedegbe AK, Lafferty K. The use of Doppler ultrasound in the clinical management of acute testicular pain. Br J Urol. 1995;76(5):625–7.
9. Comiter CV, Benson CJ, Capelouto CC, Kantoff P, Shulman L, Richie JP, et al. Nonpalpable intratesticular masses detected sonographically. J Urol. 1995;154(4):1367–9.
10. Deurdulian C, Mittelstaedt CA, Chong WK, Fielding JR. US of acute scrotal trauma: optimal technique, imaging findings, and management. Radiographics. 2007;27(2):357–9.
11. Sakamoto H, Saito K, Oohta M, Inoue K, Ogawa Y, Yoshida H. Testicular volume measurement: comparison of ultrasonography, orchidometry, and water displacement. Urology. 2007;69(1):152–7.
12. Arai T, Kitahara S, Horiuchi S, Sumi S, Yoshida K. Relationship of testicular volume to semen profiles and serum hormone concentrations in infertile Japanese males. Int J Fertil Womens Med. 1998;43(1):40–7.
13. Chiou RK, Anderson JC, Wobig RK, Rosinsky DE, Matamoros A Jr, Chen WS, et al. Color Doppler ultrasound criteria to diagnose varicoceles: correlation of a new scoring system with physical examination. Urology. 1997;50(6):953–6.

Prostate

33

Carlo Canepa and Eugene M. Fine

The prostate can be easy to visualize with point-of-care ultrasound. It is typically described as being walnut-sized (which tends to enlarge with aging) with a homogeneous echotexture located inferior to the bladder neck. A full bladder provides a very nice acoustic window and greatly facilitates visualization of the prostate. Transrectal ultrasound imaging of the prostate is best for improved resolution imaging. Prostate imaging can provide useful information for the evaluation of urinary retention, hematuria, cancer, urolithiasis, urinary tract infections, anuria, pelvic pain, and silent pathology [1–3]. The primary goal of a focused prostate ultrasound is to determine the size, shape, and assess for pathology such as obstructive uropathy and cancer. Advantages of using ultrasound in prostate imaging are like those of other organ assessments: decreased cost and risk compared to computed tomography or magnetic resonance imaging, not necessarily requiring contrast agents, painless, noninvasive, inexpensive, efficient, accurate, provides immediate information, and lacks ionizing radiation.

Figures 33.1, 33.2, 33.3, 33.4, 33.5, 33.6, 33.7, 33.8, 33.9, 33.10, and 33.11 and Video 33.1 provide examples of normal anatomy as well as a variety of commonly encountered prostate pathologies.

Electronic Supplementary Material The online version of this chapter (https://doi.org/10.1007/978-3-319-73855-0_33) contains supplementary material, which is available to authorized users.

C. Canepa, M.D. (✉)
Department of Emergency Medicine, Harvard Medical School, Massachusetts General Hospital, Boston, MA, USA
e-mail: CCanepa@mgh.harvard.edu

E. M. Fine, M.D.
Department of Urology, Icahn School of Medicine at Mount Sinai, New York, NY, USA

B. P. Nelson et al. (eds.), *Atlas of Handheld Ultrasound*, https://doi.org/10.1007/978-3-319-73855-0_33

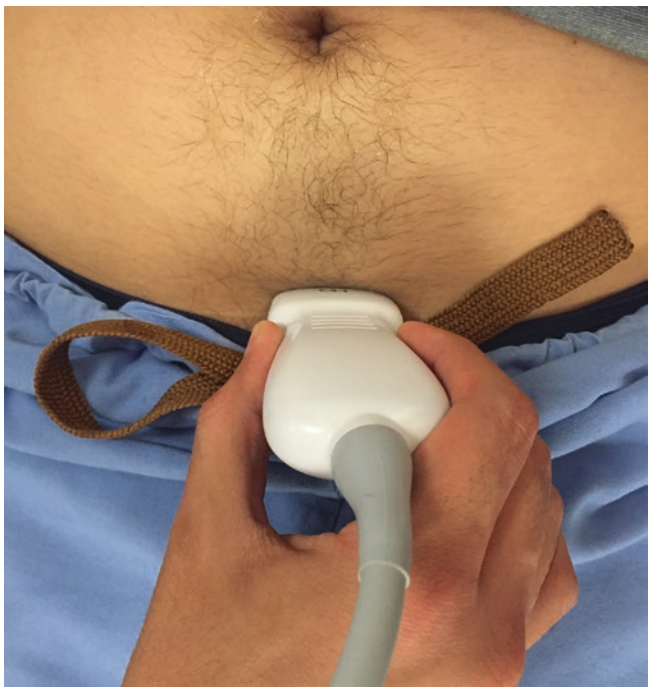

Fig. 33.1 A curvilinear or phased array probe should be used to penetrate deeply into the pelvis. Transverse views should be obtained with the probe marker facing the patient's right, and sagittal views with the probe marker facing the patient's head

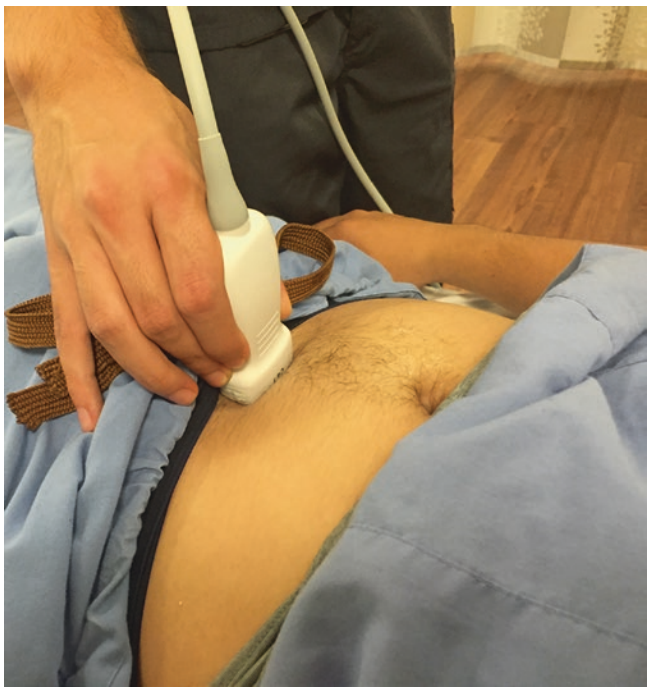

Fig. 33.2 Scan in the middle of the pelvis, just above the pubic symphysis. You should sweep cranial-caudal and left-right to find and visualize the entire prostate. You should use a full bladder as an acoustic window

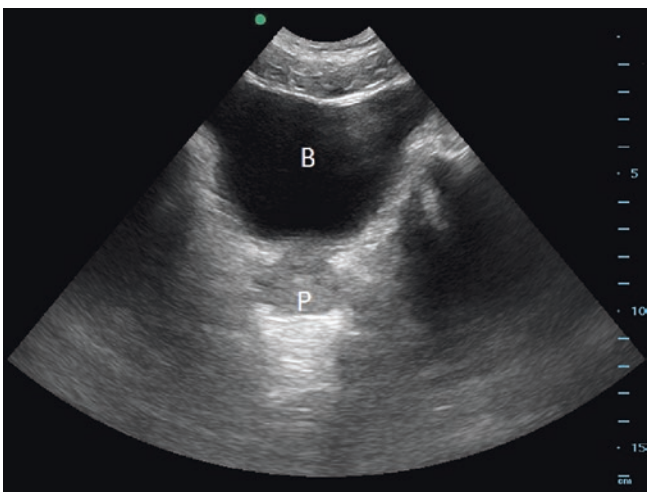

Fig. 33.3 A transverse view should demonstrate the prostate (P) posterior to the bladder (B). The bladder wall is smooth, not thickened. Urine within the bladder will appear hypo-echoic, or black

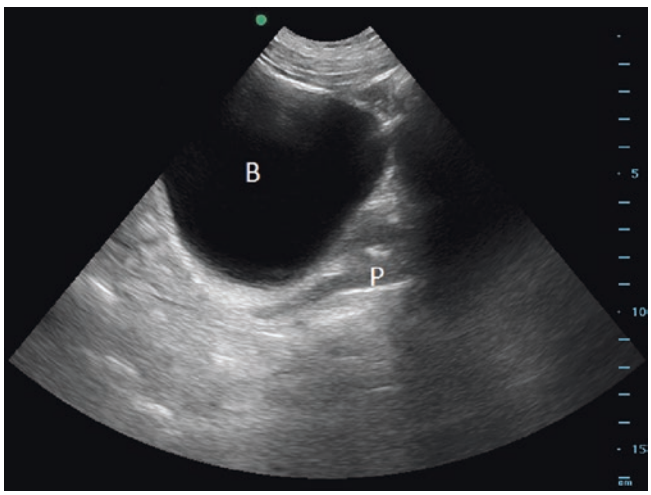

Fig. 33.4 A sagittal view should demonstrate the prostate (P) caudal to the bladder (B). The bladder is void of any pathology. A central prostate calculus (hyperechoic area) can be seen. One of the seminal vesicles, an elongated structure extending cephalad from the prostate, is also visualized

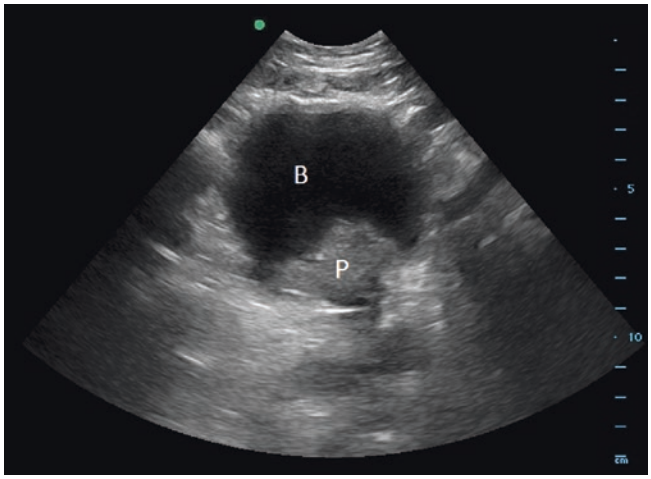

Fig. 33.5 This transverse view of the prostate (P) demonstrates benign prostatic hyperplasia (BPH) causing urinary retention of the bladder (B). This is a post-void residual after attempting to urinate

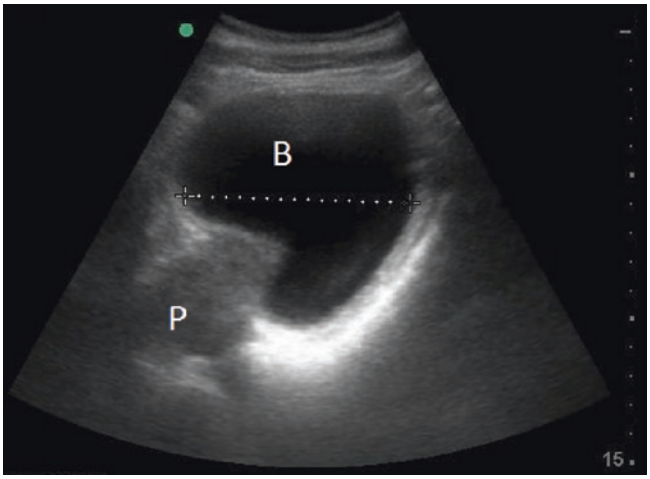

Fig. 33.7 Another sagittal view of a prostate (P) with benign prostatic hyperplasia (BPH) causing urinary retention of the bladder (B). The bladder volume, as well as the prostate, can be measured

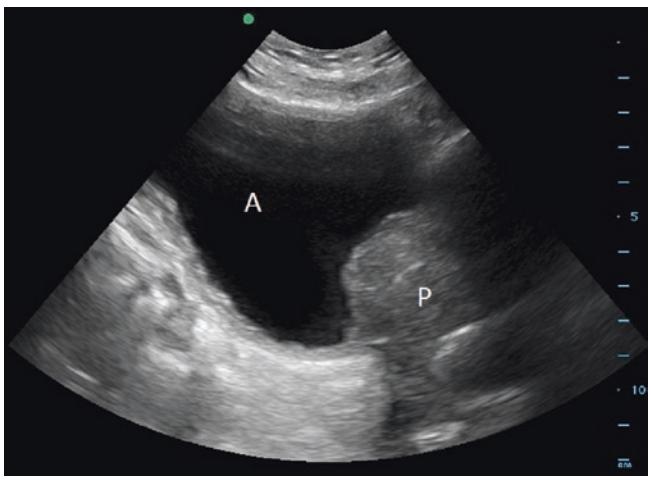

Fig. 33.6 This sagittal view of the prostate (P) demonstrates benign prostatic hyperplasia (BPH) causing urinary retention of the bladder (B). The bladder wall is visible and its dimensions and volume can be measured

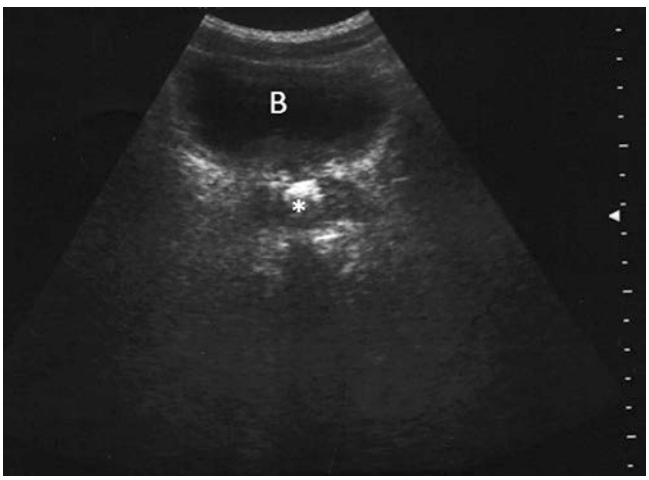

Fig. 33.8 This transverse view of the prostate posterior to the bladder (B) demonstrates a prostate stone (*asterisk*) that appears hyperechoic or echobright

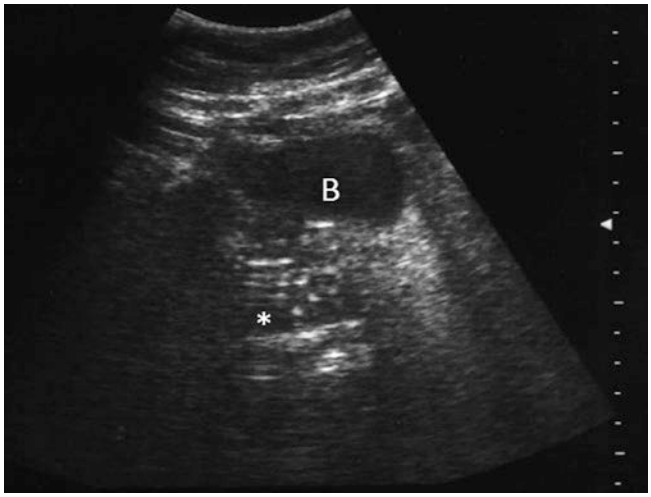

Fig. 33.9 This transverse view of the prostate posterior to the bladder (B) demonstrates radioactive titanium seeds, linear hyperechoic areas, used to treat prostate cancer (*asterisk*)

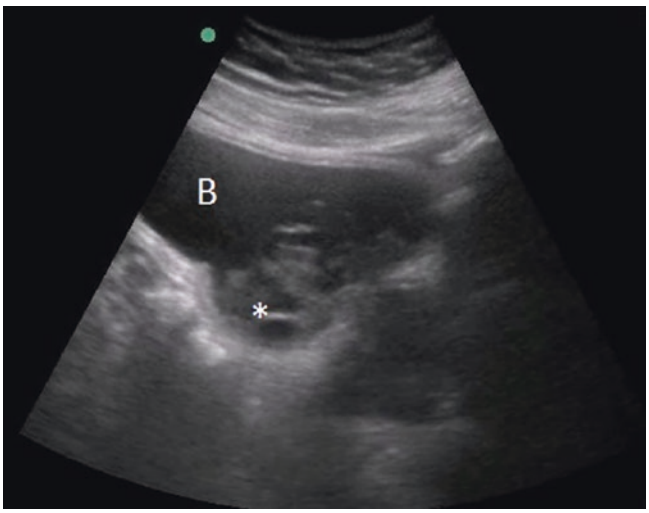

Fig. 33.10 This transverse view of the prostate posterior to the bladder (B) demonstrates adenocarcinoma of the prostate (*asterisk*), hypoechoic areas within an irregularly shaped prostate

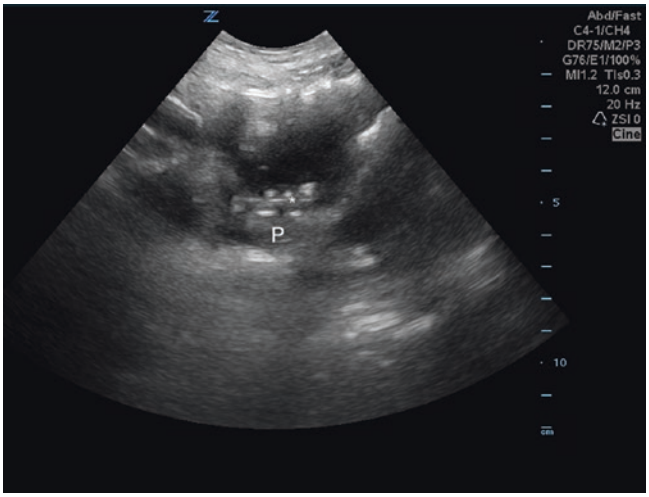

Fig. 33.11 The hyperechoic linear areas represent tiny radioactive titanium seeds (*) placed in the prostate (P) to treat cancer

References

1. Guideline developed in collaboration with the American College of Radiology; Society of Radiologists in Ultrasound. AIUM practice guideline for the performance of an ultrasound evaluation of the prostate (and surrounding structures). J Ultrasound Med. 2015;34(8):1–6.
2. Walz PH, Bertermann H. Ultrasound examination of bladder and prostate. Urol Int. 1990;45(4):217–30.
3. Tyloch JF, Wieczorek AP. The standards of an ultrasound examination of the prostate gland. Part 1. J Ultrason. 2016;16(67):378–90.

Evaluation of Shortness of Breath

34

David Tierney and Anjali Bhagra

Although thoracic ultrasound was thought to be impracticable for decades due to air interference, understanding of anatomy and artifacts has made it possible to gain a tremendous amount of clinical information from insonation of the chest. First described by European intensivists, thoracic ultrasound has become a powerful tool in the assessment of patients with undifferentiated shortness of breath or trauma. Although a microconvex array probe may be preferred, a variety of probe types (curvilinear, phased array, linear) can be used to examine the chest wall, pleural space and lung parenchyma [1]. Thoracic ultrasound has been used to assess for pneumothorax (with a 99% negative predictive value in ruling out this process) in the setting of trauma and medical illness [2, 3]. It is also accurate in diagnosing and following pulmonary edema, pneumonia, pleural effusion, and other pulmonary pathology [2, 4–6].

Although several symptom-based protocols have been described which incorporate lung sonography, perhaps the best known is the BLUE protocol, which systematically assesses patients for pneumothorax, pneumonia, pulmonary edema, and other etiologies of acute shortness of breath [7]. An adaptation of this approach, incorporating clinical history, bedside testing, and sonography, is detailed here (Fig. 34.1).

D. Tierney, M.D. (✉)
Department of Medical Education, Abbott Northwestern Hospital, Minneapolis, MN, USA
e-mail: david.tierney@allina.com

A. Bhagra, M.D.
Department of General Internal Medicine, Mayo Clinic, Rochester, MN, USA

B. P. Nelson et al. (eds.), *Atlas of Handheld Ultrasound*, https://doi.org/10.1007/978-3-319-73855-0_34

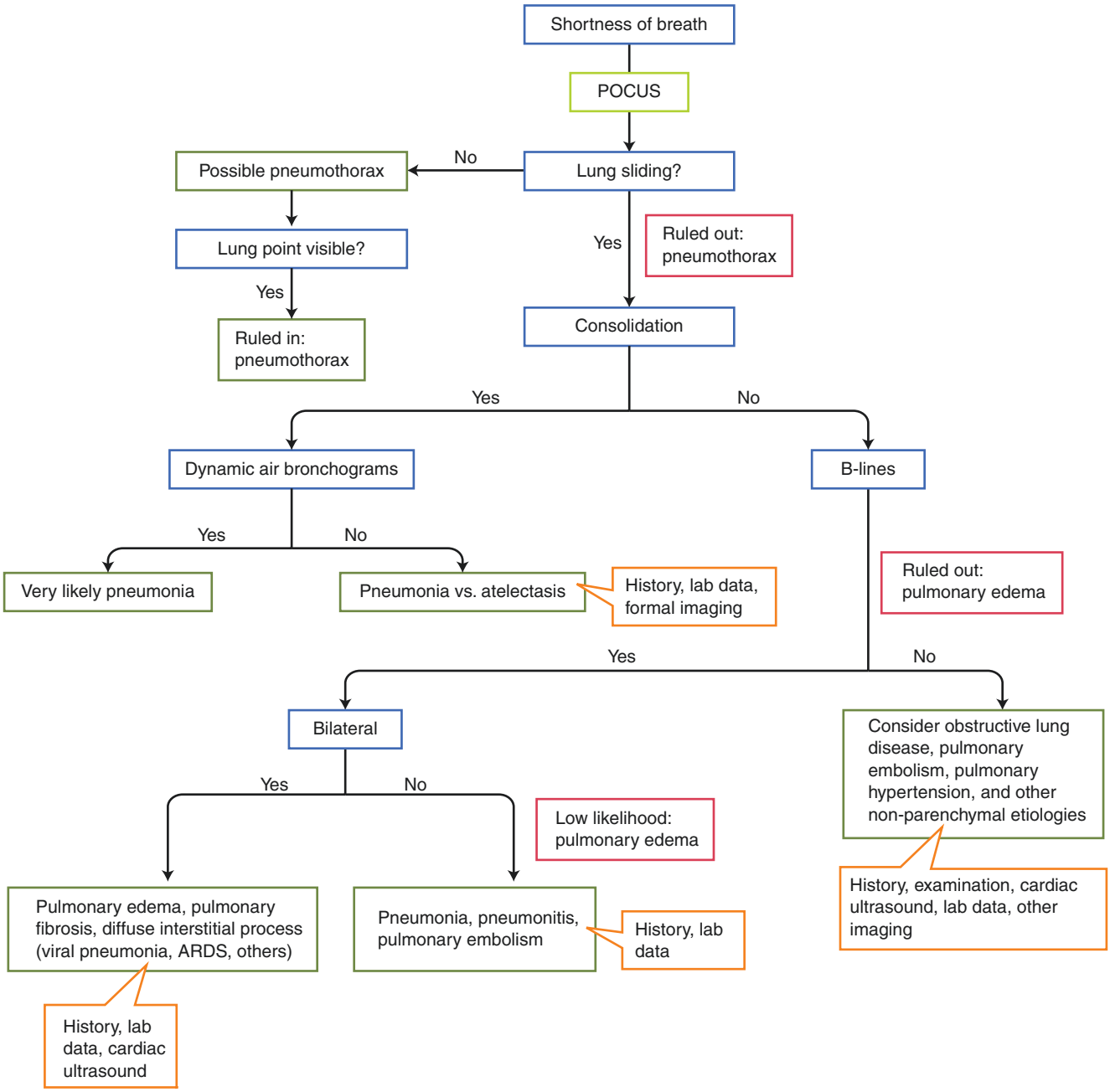

Fig. 34.1 Ultrasound-assisted differential diagnosis workflow in a patient with shortness of breath. ARDS—Acute respiratory distress syndrome; POCUS—Point-of-care ultrasound

References

1. Volpicelli G, Elbarbary M, Blaivas M, Lichtenstein DA, Mathis G, Kirkpatrick AW, et al. International evidenced-based recommendations for point-of-care lung ultrasound. Intensive Care Med. 2012;38:577–91.
2. Volpicelli G. Lung sonography. J Ultrasound Med. 2013;32(1):165–71.
3. Lichtenstein D, Mezière G, Biderman P, Gepner A. The "lung point": an ultrasound sign specific to pneumothorax. Intensive Care Med. 2000;26(10):1434–40.
4. Cortellaro F, Colombo S, Coen D, Duca PG. Lung ultrasound is an accurate diagnostic tool for the diagnosis of pneumonia in the emergency department. Emerg Med J. 2012;29:19–23.
5. Lichtenstein D, Mezière G, Seitz J. The dynamic air bronchogram. A lung ultrasound sign of alveolar consolidation ruling out atelectasis. Chest. 2009;135(6):1421–5.
6. Lichtenstein DA, Mezière GA, Lagoueyte JF, Biderman P, Goldstein I, Gepner A, et al. A-lines and B-lines: lung ultrasound as a bedside tool for predicting pulmonary artery occlusion pressure in the critically ill. Chest. 2009;136(4):1014–20.
7. Lichtenstein DA, Mezière GA. Relevance of lung ultrasound in the diagnosis of acute respiratory failure: the BLUE protocol. Chest. 2008;134:117–25.

Evaluation of Chest Pain

35

Sharon L. Mulvagh, Marko Balan, and Babar Haroon

Diseases of the heart, aorta, lungs, esophagus, stomach, mediastinum, pleura, and abdominal viscera may all cause chest discomfort. It is estimated that chest pain accounts for approximately six million visits to emergency departments (ED) in the United States annually [1]. Assessment of the patient presenting with non-traumatic chest pain requires immediate recognition and exclusion of potential life-threatening etiologies, with subsequent evaluation of other possible causes.

Life-threatening causes of chest pain include: acute coronary syndrome (acute myocardial infarction [MI] and unstable angina), aortic dissection, pulmonary embolism, inflammatory pericardial and/or myocardial diseases associated with cardiac tamponade and/or acute heart failure, tension pneumothorax, and mediastinitis (most often associated with esophageal rupture). POCUS can identify characteristic ultrasound features, as outlined in the algorithm, consistent with the diagnoses of acute coronary syndrome, aortic dissection, cardiac tamponade, pulmonary embolism, and tension pneumothorax. The information obtained can be utilized to optimize and expedite patient management by subsequent performance of the diagnostic testing and/or treatment as outlined in the algorithm (Fig. 35.1).

S. L. Mulvagh, M.D., F.R.C.P.C. (✉)
Department of Medicine, Division of Cardiology,
Dalhousie University, Halifax, NS, Canada
e-mail: Sharon.Mulvagh@nshealth.ca

M. Balan, M.D., F.R.C.P.C.
Department of Critical Care, Dalhousie University,
Halifax, NS, Canada

B. Haroon, M.D., F.R.C.P.C., Dip.(Clin Epi)
Department of Critical Care, Dalhousie University,
Halifax, NS, Canada

B. P. Nelson et al. (eds.), *Atlas of Handheld Ultrasound*, https://doi.org/10.1007/978-3-319-73855-0_35

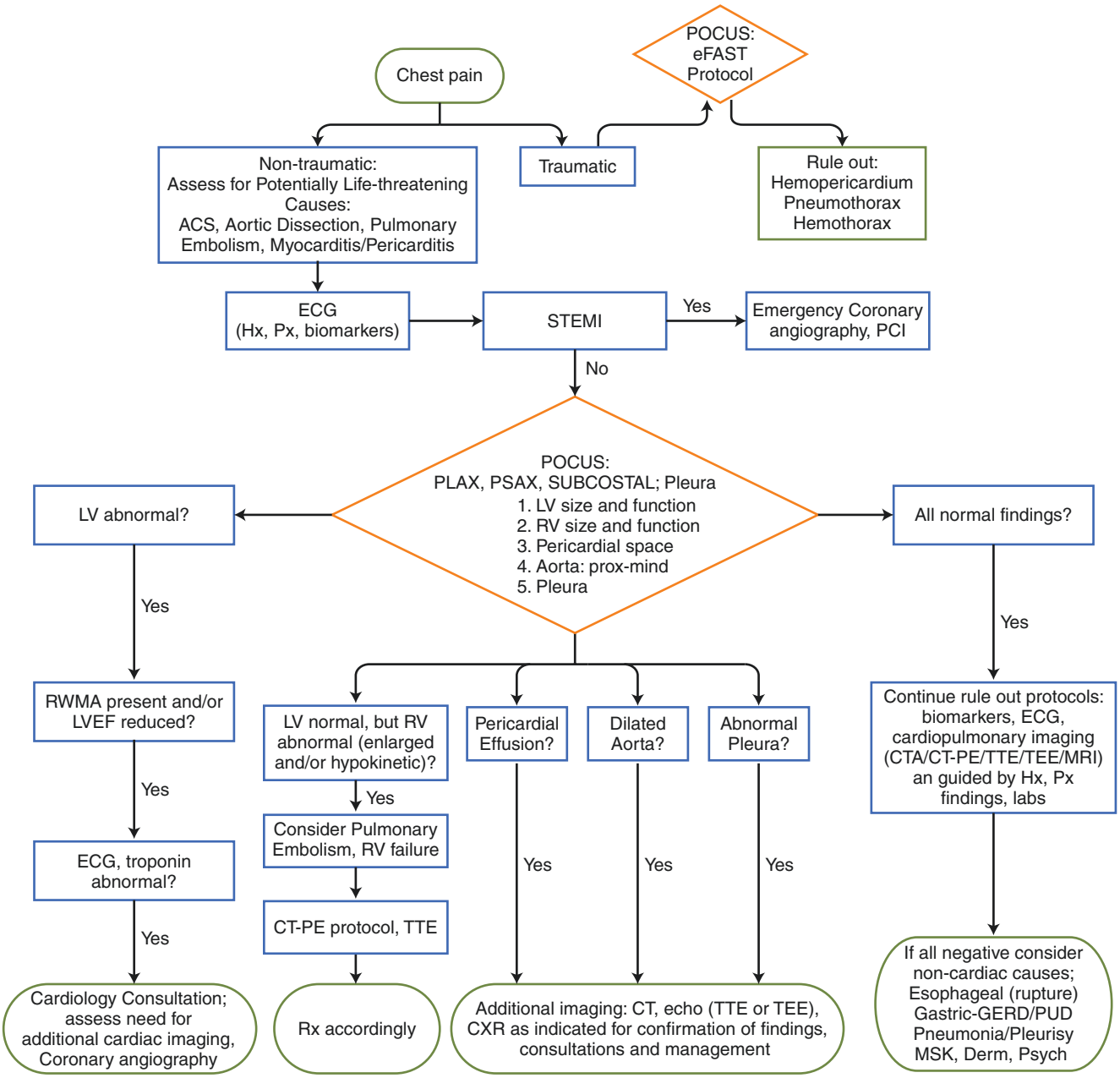

Fig. 35.1 Chest pain algorithm. *CT* computerized tomography, *CTA* computerized tomographic angiography, *CT-PE* computerized tomography-pulmonary embolism protocol, *Derm* dermatologic (shingles), *ECG* electrocardiogram, *eFAST protocol* extended focused assessment with sonography in trauma, *GERD* gastroesophageal reflux disease, *Hx* history, *MSK* musculoskeletal, *PCI* percutaneous coronary intervention, *PLAX* parasternal long-axis view, *POCUS* point of care ultrasound, *Prox-mid* proximal to mid level of the ascending aorta, *PSAX* parasternal short axis view, *Px* physical, *PUD* peptic ulcer disease, *Psych* psychiatric (panic attacks, anxiety), *LV* left ventricle, *LVEF* left ventricular ejection fraction, *RWMA* regional wall motion abnormalities, *RV* right ventricle, *Rx* treatment, *STEMI* ST elevation myocardial infarction, *TEE* transesophageal echocardiogram, *TTE* transthoracic echocardiogram

35.1 Acute Coronary Syndrome

Coronary artery disease is the leading cause of mortality in developed countries. However, less than 15–30% of patients who present to the ED with non-traumatic chest pain have an acute coronary syndrome [2, 3]. Thus it can sometimes be a challenging, but imperative, diagnosis to establish, as "time is muscle" and urgent treatment is necessary to minimize the resultant morbidity and mortality associated with coronary ischemia and myocardial infarction. The electrocardiogram is an essential test to diagnose an acute MI, specifically, an ST-elevation MI (STEMI), which signifies an impending transmural myocardial infarction requiring urgent revascularization to avoid extensive damage and scarring to the heart muscle. As such, "STEMI protocols" have been established, bypassing the routine stop in the ED, and proceeding directly to the cardiac catheterization laboratory where emergency coronary angiography and percutaneous revascularization are performed in order to optimize patient outcomes. However, POCUS may potentially be useful in the STEMI setting, to provide a rapid evaluation of LV function (LVEF and extent of RWMA), pericardial space, and/or aorta if clinically relevant information is urgently required.

35.2 Aortic Dissection

Aortic dissection occurs most often in hypertensive patients older than 60, and is far less common than acute coronary syndromes, with an incidence of approximately 3 in 100,000 patients per year. Aortic dissections may require emergent cardiovascular surgery or certain death could ensue.

35.3 Pulmonary Embolism

Pulmonary embolism (PE) occurs when a clot travels through the venous circulation and into the right heart, obstructing the pulmonary arteries, resulting in right ventricular dysfunction, pulmonary hypertension, impaired gas exchange, hemodynamic collapse and potential cardiac arrest most often due to PEA (pulseless electrical activity). PE is relatively common, occurring in approximately one in 1000 patients. Mortality and morbidity rates vary widely based upon comorbid conditions and the size of the embolus, and early diagnosis and treatment are imperative to reduce mortality for large hemodynamically unstable pulmonary emboli.

35.4 Cardiac Tamponade

Pericarditis and myocarditis can cause chest pain, which is usually described as pleuritic in nature, and can become life-threatening if associated with accumulation of pericardial fluid impairing cardiac filling, with resultant cardiac tamponade.

35.5 Tension Pneumothorax

Tension pneumothorax occurs when air accumulates in the pleural space causing compression and shift of the mediastinal structures. It can result following trauma or pulmonary/vascular procedures, but may also occur spontaneously in patients both with and without underlying lung disease (including COPD, cystic fibrosis, and asthma).

35.6 Mediastinitis

Mediastinitis is a relatively rare condition with a high mortality, which can be caused by esophageal perforation (spontaneous, procedural/post-operative, or traumatic) or infections.

35.7 Other Causes of Chest Pain

Common conditions that may cause chest pain, but are not usually considered to be immediately life-threatening include: Gastrointestinal problems, such as gastroesophageal reflux, or peptic ulcer disease; pulmonary/pleural causes, such as respiratory infections, including pneumonia, tracheitis, bronchitis, asthma exacerbations; musculoskeletal causes such as rib contusions and fractures, intercostal muscle strains, and costochondritis; psychiatric causes including panic attacks and anxiety; dermatologic causes such as herpes zoster.

35.8 Conclusion

POCUS can quickly augment the history and physical examination in the patient presenting with chest pain by providing useful information regarding both left and right ventricular size and function, including an estimate of left ventricular ejection fraction and regional wall motion abnormality assessment, determination of presence of pericardial fluid, and assessment of the proximal- to mid-ascending aorta. Generally, this information can be obtained from the parasternal and subcostal windows; those more experienced in

echocardiography will surely find additional cardiac function evaluations from the apical window, as well as color-flow Doppler examination (to assess for significant valvular regurgitation, e.g. aortic regurgitation can occur with aortic dissection) to be of value. Of course, abnormalities seen in the setting of acute chest pain cannot be determined to be acute versus chronic, unless comparison with a prior echocardiogram can be made, so it is critical for the clinician to be familiar with the patient's history, physical examination, and other clinical data (ECG, biomarkers) to accurately interpret findings of the POCUS examination.

The absence of findings on POCUS consistent with life-threatening causes of chest pain can be reassuring in the acute patient evaluation by a skilled clinician, but limitations must be recognized, and formal testing pursued if the clinical differential diagnosis suggests otherwise.

References

1. McCaig L, Burt C. National hospital ambulatory medical care survey: 2003 emergency department summary. In: Advance data from vital and health statistics. Centers for Disease Control and Prevention: Atlanta; 2005.
2. Launbjerg J, Fruergaard P, Hesse B, Jørgensen F, Elsborg L, Petri A. Long-term risk of death, cardiac events and recurrent chest pain in patients with acute chest pain of different origin. Cardiology. 1996;87:60–6.
3. Lindsell CJ, Anantharaman V, Diercks D, Han JH, Hoekstra JW, Hollander JE, et al. The internet tracking registry of acute coronary syndromes (i*trACS): a multicenter registry of patients with suspicion of acute coronary syndromes reported using the standardized reporting guidelines for emergency department chest pain studies. Ann Emerg Med. 2006;48:666–77.

Evaluation of Hypotension

36

Phillip Andrus and Kevin Hu

Identification of the etiology of hypotension is essential to early appropriate management of these critically ill patients. In these patients, point-of-care ultrasound (POCUS) makes diagnostic information rapidly available. One advantage of POCUS is that it is fast. It can be performed at the bedside as soon as shock or hypotension is identified. Hemodynamically unstable patients do not have to leave the clinical setting for diagnostic testing, allowing them to be monitored appropriately. Beyond its diagnostic utility, POCUS may be used dynamically to guide treatment such as fluid administration and to guide procedures like pericardiocentesis and central access.

Multiple protocols have been designed to guide clinicians using bedside sonography for patients with undifferentiated shock or hypotension [1–4]. By combining point-of-care ultrasound assessment of the heart, inferior vena cava (IVC), lungs, abdomen, and aorta, clinicians can quickly narrow their differential (Fig. 36.1). POCUS has been shown to improve diagnostic certainty and expedite management in these patients [5–9].

Probe placement and sequencing:

1. Heart (parasternal long and 4-chamber)
2. Inferior Vena Cava
3. Lungs
4. Abdomen
   (a) Right upper quadrant/Morrison's
   (b) Left upper quadrant
   (c) Bladder/pelvis
5. Aorta

P. Andrus, M.D. (✉) • K. Hu, M.D.
Department of Emergency Medicine, Icahn School of Medicine at Mount Sinai, New York, NY, USA

B. P. Nelson et al. (eds.), *Atlas of Handheld Ultrasound*, https://doi.org/10.1007/978-3-319-73855-0_36

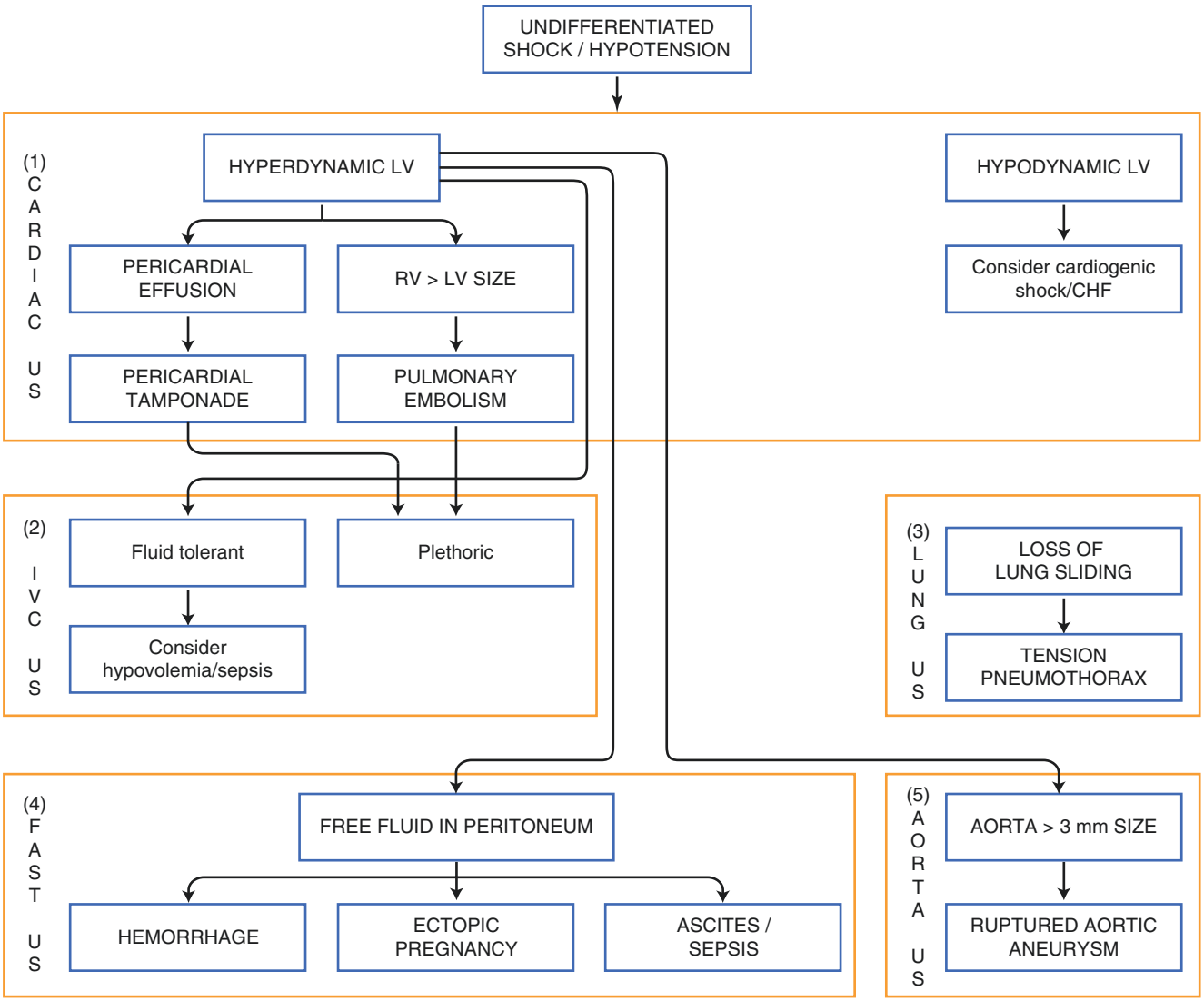

Fig. 36.1 Algorithm for undifferentiated shock/hypotension illustrating ultrasounds for (*1*) cardiac; (*2*) IVC; (*3*) lung; (*4*) FAST (Focused Assessment with Sonography in Trauma); and (*5*) aorta

References

1. Atkinson PR, McAuley DJ, Kendall RJ Abeyakoon O, Reid CG, Connolly J, et al. Abdominal and Cardiac Evaluation with Sonography in Shock (ACES): an approach by emergency physicians for the use of ultrasound in patients with undifferentiated hypotension. Emerg Med J. 2009;26(2):87–91.
2. Weingart SW, Duque DD, Nelson BN. The RUSH exam: rapid ultrasound for shock/hypotension. ACEP-EMED Home 2009. http://www.webcitation.org/5vyzOaPYU.
3. Perera P, Mailhot T, Riley D, Mandavia D. The RUSH exam: Rapid Ultrasound in SHock in the evaluation of the critically ill. Emerg Med Clin North Am. 2010;28(1):29–56, vii.
4. Rose JS, Bair AE, Mandavia D, Kinser DJ. The UHP ultrasound protocol: a novel ultrasound approach to the empiric evaluation of the undifferentiated hypotensive patient. Am J Emerg Med. 2001;19(4):299–302.
5. Shokoohi H, Boniface KS, Pourmand A, Liu YT, Davison DL, Hawkins KD, et al. Bedside ultrasound reduces diagnostic uncertainty and guides resuscitation in patients with undifferentiated hypotension. Crit Care Med. 2015;43(12):2562–9.
6. Milne J, Atkinson P, Lewis D, Fraser J, Diegelmann L, Olszynski P, et al. Sonography in Hypotension and Cardiac Arrest (SHoC): rates of abnormal findings in undifferentiated hypotension and during cardiac arrest as a basis for consensus on a hierarchical point of care ultrasound protocol. Cureus. 2016;8(4):e564.
7. Volpicelli G, Lamorte A, Tullio M, Cardinale L, Giraudo M, Stefanone V, et al. Point-of-care multiorgan ultrasonography for the evaluation of undifferentiated hypotension in the emergency department. Intensive Care Med. 2013;39(7):1290–8.
8. Jones AE, Tayal VS, Sullivan DM, Kline JA. Randomized, controlled trial of immediate versus delayed goal-directed ultrasound to identify the cause of nontraumatic hypotension in emergency department patients. Crit Care Med. 2004;32(8):1703–8.
9. Seif D, Perera P, Mailhot T, Riley D, Mandavia D. Bedside ultrasound in resuscitation and the rapid ultrasound in shock protocol. Crit Care Res Pract. 2012;2012:503254.

Evaluation of Fever

37

Gopal Narayanswami, Edgar Argulian, and Jagat Narula

Goal-directed point-of-care ultrasound (POCUS) is real-time, organ-focused ultrasonography performed by the clinician and it is arguably the most important contemporary extension of the physical examination for today's clinicians. Over the past decade, POCUS has become essential in the early diagnosis and management of a critically ill patient. Goal-directed ultrasound performed by physicians is focused on clinical problems and not limited to a single anatomical area [1]. While the general goals of sonography in the unstable patient are to evaluate cardiac function and assess intravascular volume, in a patient with fever, POCUS can also help to identify the cause of the patient's clinical condition. In addition, ultrasound guidance is essential in performing bedside procedures. The current chapter uses a case-based approach to illustrate the utility of ultrasound in making a rapid and acceptably accurate diagnosis for a patient with fever and sepsis (Figs. 37.1, 37.2, 37.3, 37.4, 37.5, 37.6, 37.7, 37.8, 37.9, 37.10, 37.11, 37.12, 37.13, 37.14, 37.15, 37.16, 37.17, 37.18, 37.19, and 37.20 and Videos 37.1, 37.2, 37.3, 37.4, 37.5, 37.6, 37.7a, 37.7b, 37.8, 37.9, 37.10, 37.11, 37.12, 37.13, 37.14, 37.15, 37.16, 37.17, 37.18, 37.19, and 37.20). Physicians caring for critical patients should strongly consider integrating focused ultrasound techniques into their routine clinical evaluation. The American College of Chest Physicians (ACCP) and the La Société de Réanimation de Langue Française (SRLF) selected a panel of experts to review the field of critical care ultrasound (CCUS) and to develop a consensus statement on competence in CCUS [3].

Electronic Supplementary Material The online version of this chapter (https://doi.org/10.1007/978-3-319-73855-0_37) contains supplementary material, which is available to authorized users.

G. Narayanswami, M.D. (✉)
Division of Pulmonary and Critical Care Unit, Mount Sinai St. Luke's Hospital, New York, NY, USA
e-mail: gopal.narayanswami@mountsinai.org

E. Argulian, M.D., M.P.H.
Mount Sinai St. Luke's Hospital, Icahn School of Medicine at Mount Sinai, New York, NY, USA

J. Narula, M.D., Ph.D.
Mount Sinai Hospital, Icahn School of Medicine at Mount Sinai, New York, NY, USA

B. P. Nelson et al. (eds.), *Atlas of Handheld Ultrasound*, https://doi.org/10.1007/978-3-319-73855-0_37

Fig. 37.1 Normal lung ultrasound findings. Lung ultrasound is easy to perform through several intercostal acoustic windows and can contribute to differential diagnosis in a critically ill patient. **A lines** are horizontal, regularly spaced hyperechoic lines that are repetition artefacts of the pleural line, and are what is seen in the normal lung. See also Video 37.1

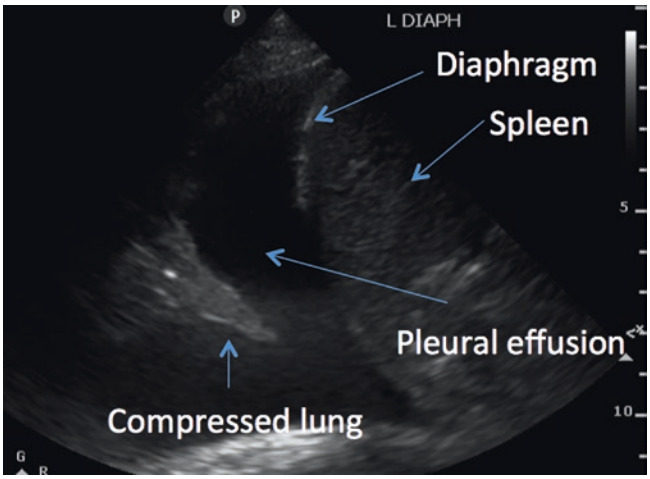

Fig. 37.3 Lung ultrasound for detection of pleural effusion. Pleural effusion can be rapidly diagnosed by using bedside lung ultrasound and small effusions can be localized for aspiration. Pleural effusion is best demonstrated in the dependent areas with the probe placed in the intercostal space with the indicator of the probe pointing cranially. The effusion appears as echo free or hypoechoic (i.e., dark) space and is delineated by the chest wall and the diaphragm. The fluid acts as an acoustic window and the underlying lung can also be visualized. In this case compressive atelectasis is seen. In compressive atelectasis, the underlying lung is not consolidated and therefore will change in shape with respiration demonstrating the "jellyfish sign." See also Video 37.3

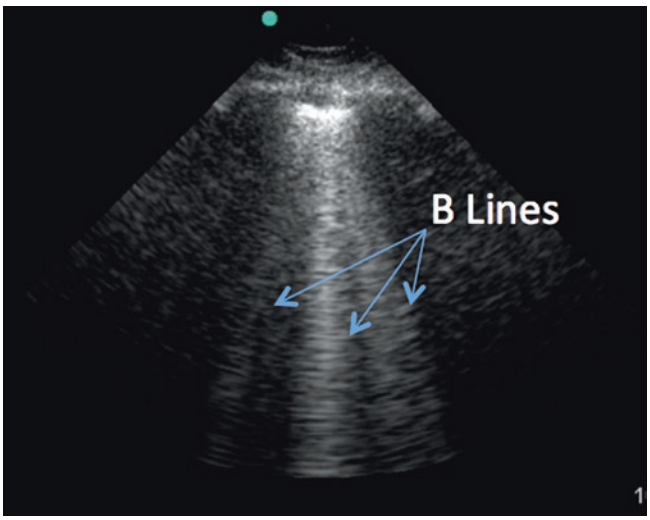

Fig. 37.2 Lung ultrasound in identifying extravascular lung water. **B lines** are vertical narrow based hyperechoic lines arising from the pleural line to the edge of the ultrasound screen. These are also known as "comet tail artifacts," and when several B lines are visible, the term "lung rockets" is used. The number and extent of B lines allow rapid and semi-quantitative estimation of extravascular lung water [2]. Multiple B lines in more than two lung zones suggest diffuse alveolar interstitial syndrome such as pulmonary edema or ARDS. See also Video 37.2

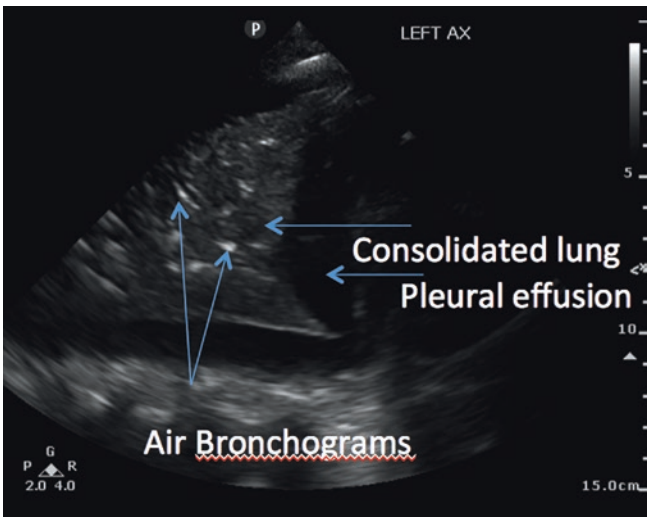

Fig. 37.4 Lung ultrasound for detection of pleural effusion. Pleural effusion is seen as an anechoic space. The underlying lung appears consolidated with areas of hyperechoic signal corresponding to air in the bronchi—the so-called ultrasound air bronchogram. This patient had pneumonia and sonographic-guided bedside aspiration revealed a simple parapneumonic effusion. See also Video 37.4

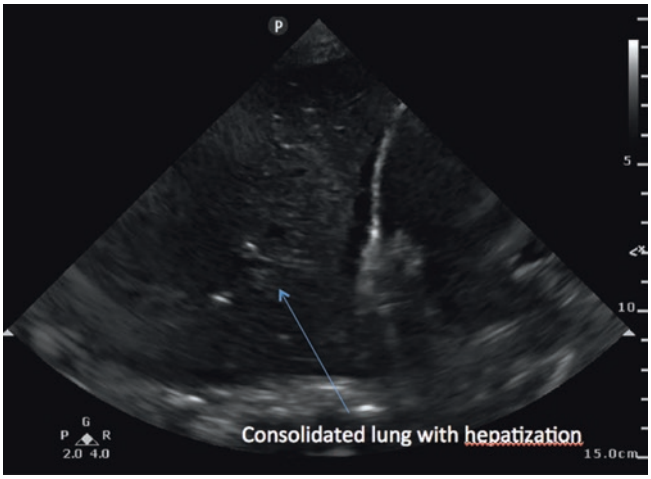

Fig. 37.5 Lung ultrasound in patients with pneumonia. In patients with pneumonia, bedside ultrasound can demonstrate dense consolidation of the lung tissue characterized as "sonographic hepatization" of the lung. The consolidated lung tissue should be differentiated from the liver or spleen by demarcating the thorax from the abdomen using the diaphragm as the landmark. See also Video 37.5

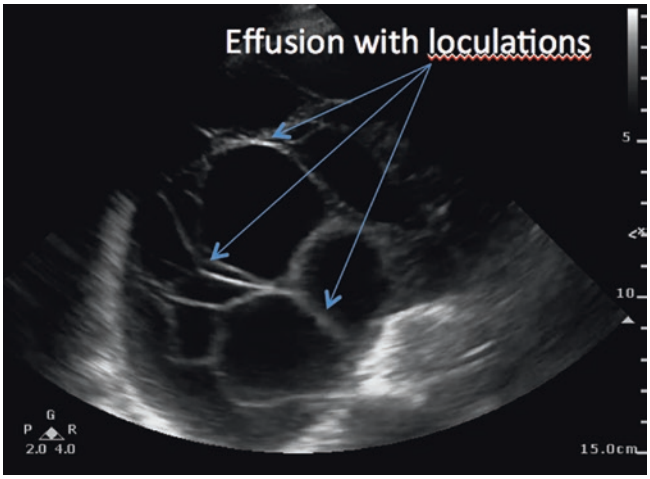

Fig. 37.6 Lung ultrasound for diagnosing loculated pleural effusions. This figure shows a parapneumonic effusion with multiple loculations necessitating a video-assisted thoracoscopic surgery (VATS) procedure. The loculations are easily identified by the multiple fibrin strands in the echo free effusion. See also Video 37.6

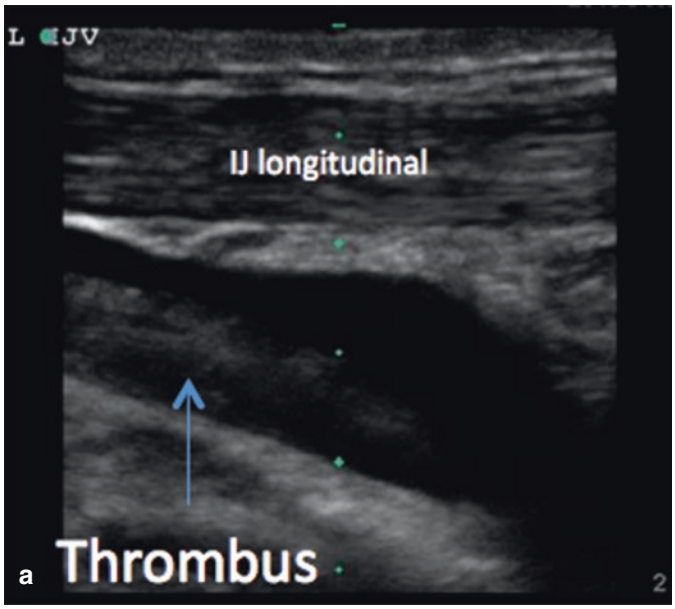

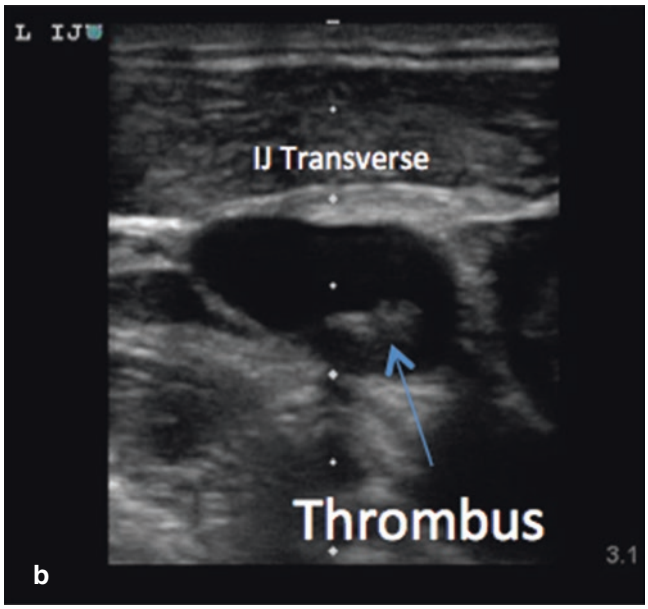

Fig. 37.7 (**a**) and (**b**)Venous ultrasound for detection of thrombosis. This figure shows left internal jugular vein thrombosis in a young male with pharyngitis and septic emboli to the lungs. The thrombus is identified as the echogenic material within the normally echo-free vessel and confirmed by non-compressibility of the vein. Thrombophlebitis of the jugular vein (Lemierre's syndrome) most commonly occurs due to the spread of the bacterial throat infection (e.g., Fusobacterium necrophorum) to the carotid sheath vessels and subsequently the bloodstream. See also Videos 37.7a and 37.7b

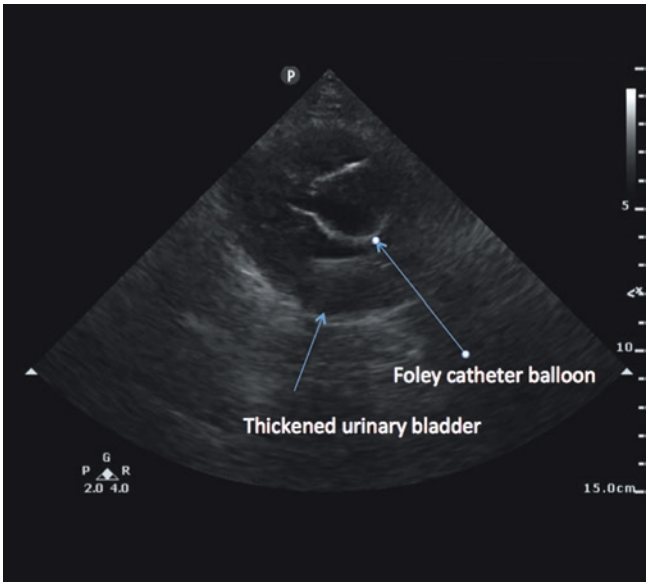

Fig. 37.8 Bedside ultrasound in a patient with urosepsis. A point-of-care ultrasound was performed in a 70-year-old male who was admitted with urosepsis and gram-negative bacteremia. The figure demonstrates the thickened urinary bladder with a Foley catheter in place which prompted a urology evaluation. See also Video 37.8

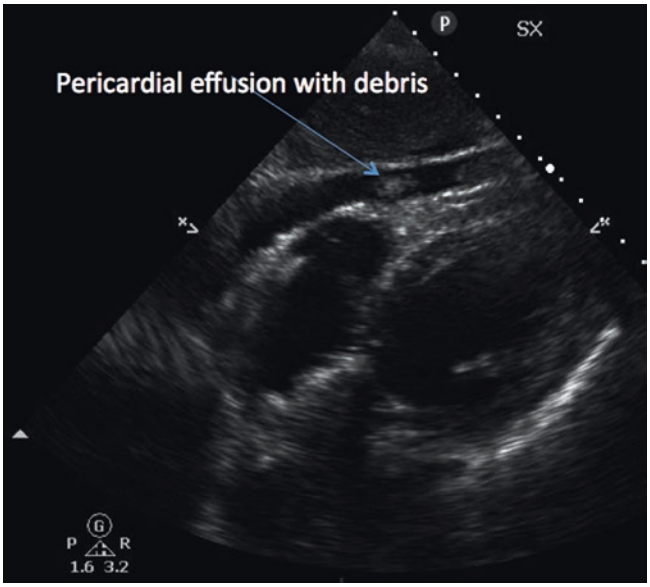

Fig. 37.10 Cardiac ultrasound for pericardial effusion. A point-of-care echocardiography shows a pericardial effusion (echo-free space surrounding the heart) with fibrinous debris in a middle age patient with end stage renal disease admitted with fever and chest pain. The patient was diagnosed with uremic pericarditis which resolved with dialysis. See also Video 37.10

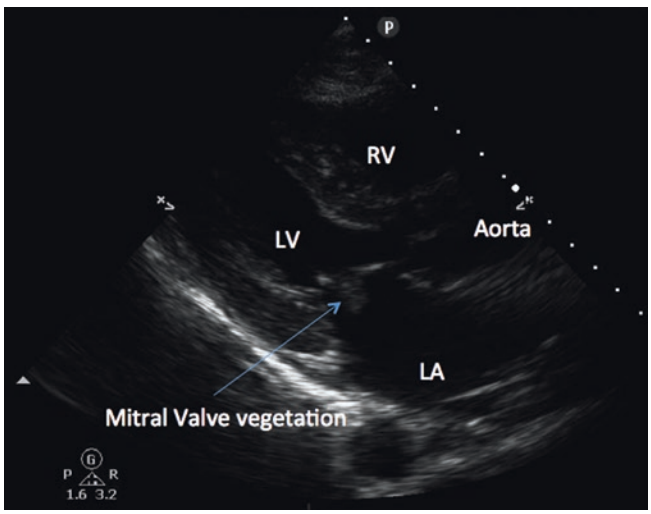

Fig. 37.9 Cardiac ultrasound in a patient with fever and pulmonary edema. Point-of-care echocardiography shows mobile mitral valve vegetation in a middle-aged male admitted for fever, dyspnea, and pulmonary edema. Severe mitral regurgitation was also seen by color Doppler (not shown). A vegetation is defined as a discrete echodensity with independent mobility typically attached to the valve leaflets. Transthoracic echocardiography has a limited sensitivity for detection of vegetations and should be followed by transesophageal echocardiography in patients with high suspicion for endocarditis. In patients with established endocarditis, transesophageal echocardiogram can delineate the extent of involvement and detect complications (such as valve perforation, abscess formation, etc.). See also Video 37.9

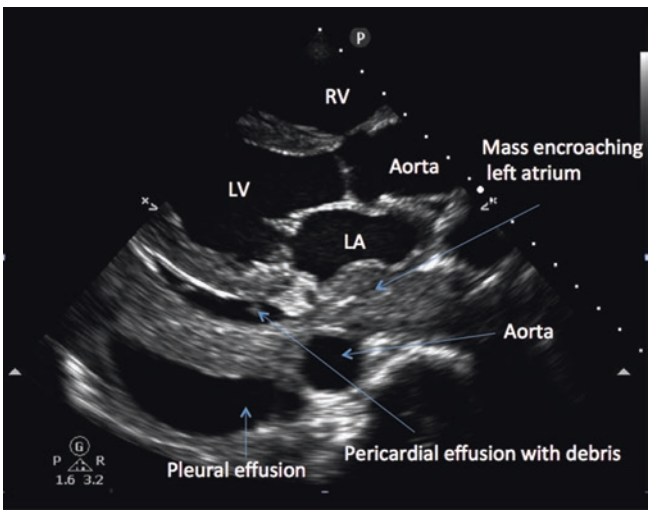

Fig. 37.11 Cardiac ultrasound in a patient with advanced cancer. A point-of-care ultrasound shows pericardial effusion with debris, pleural thickening, and left-sided pleural effusion in an elderly male with dyspnea. Pericardial effusion is seen in this parasternal long axis view as an echo-free space posterior to the heart but anterior to the descending aorta. Pleural effusion is seen as an echo-free space posterior to the aorta. A mass encroaching onto the left atrium is also seen. This patient was diagnosed with advanced widespread lung cancer. See also Video 37.11

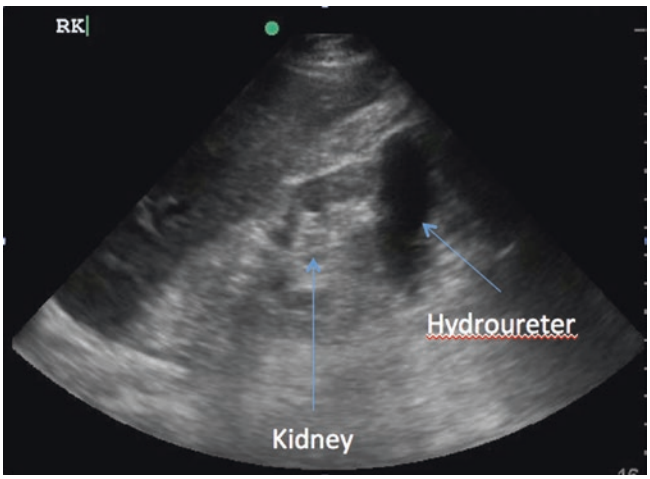

Fig. 37.12 Bedside ultrasound for suspected renal disease. Point-of-care sonography of the kidneys shows the hydroureter as hypoechoic (black) fluid-filled area next to the kidneys in this longitudinal image. This image was obtained in a young female with sepsis and flank pain. Subsequent CT scan confirmed an obstructing stone prompting urologic intervention. See also Video 37.12

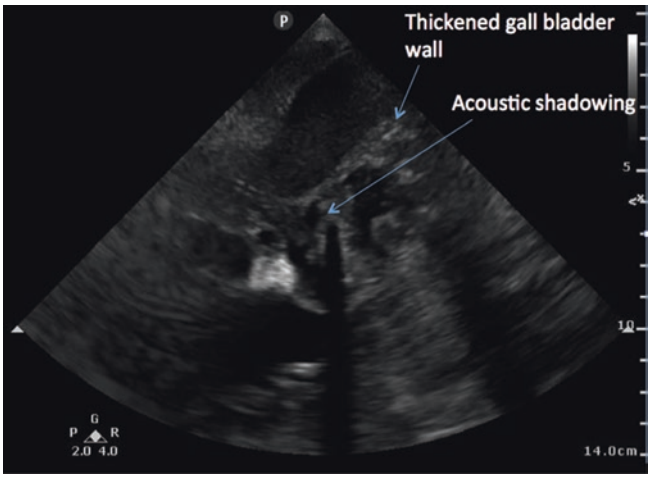

Fig. 37.14 Bedside ultrasound for suspected biliary disease. A point-of-care ultrasound shows a distended gallbladder with a thickened wall (>3 mm) and distal acoustic shadowing which usually represents a stone in the neck of the gallbladder or the cystic duct. This patient was admitted with septic shock and gram-negative bacteremia. The most sensitive ultrasound finding in acute cholecystitis is the presence of cholelithiasis in combination with the sonographic Murphy sign (tenderness in the right hypochondrium) while performing sonography. Both gallbladder wall thickening (>3 mm) and pericholecystic fluid are secondary findings. Other less specific findings include gallbladder distension and sludge (best appreciated with Video 37.14)

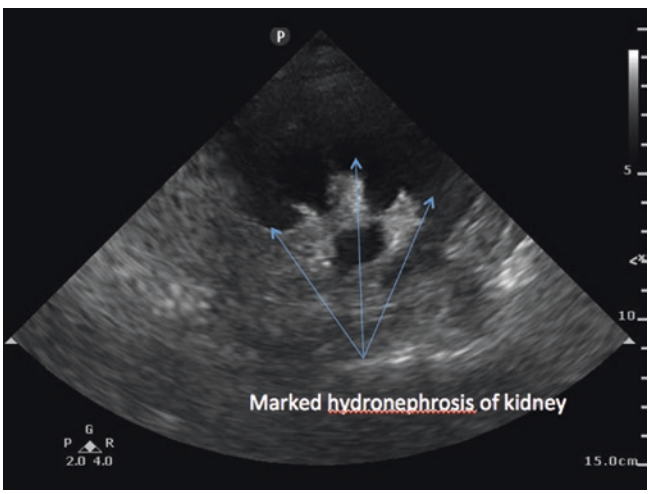

Fig. 37.13 Bedside ultrasound for suspected renal disease. The longitudinal ultrasound of a left kidney shows a large hypoechoic (black) area in the center of the kidney extending into the parenchyma consistent with hydronephrosis. A similar finding was seen on the on the right side in this middle-aged male admitted with septic shock, acute renal failure, and gram-negative bacteremia. Bilateral nephrostomies were required which yielded purulent urine. See also Video 37.13

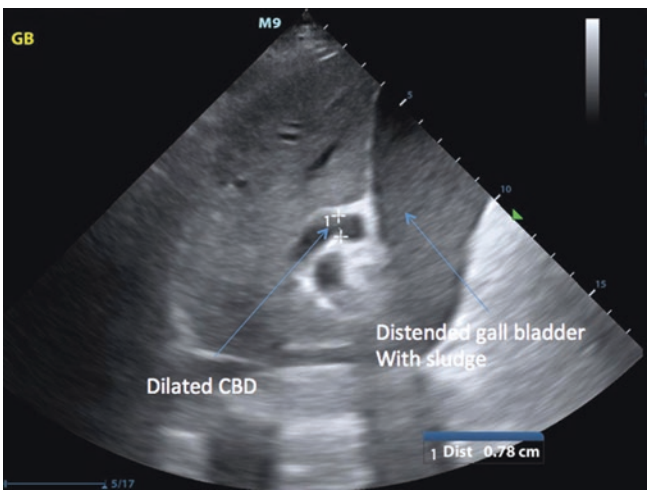

Fig. 37.15 Bedside ultrasound for suspected biliary disease. A distended gallbladder with extensive sludge is seen on this bedside ultrasound image. A distended common bile duct is also seen. See also Video 37.15

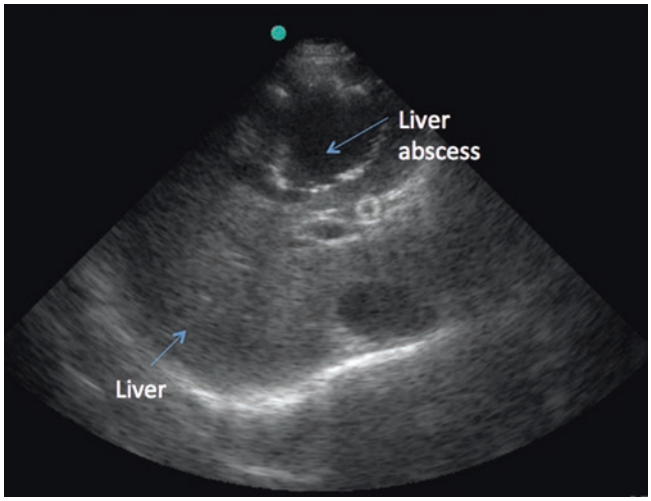

Fig. 37.16 Bedside ultrasound for liver disease. A point-of-care ultrasound shows a hypoechoic (black) lesion in the liver surrounded by a hyperechoic rim in a patient admitted with abdominal pain, right upper quadrant tenderness, malaise, and fever. The percutaneous drainage subsequently revealed polymicrobial pyogenic liver abscess. See also Video 37.16

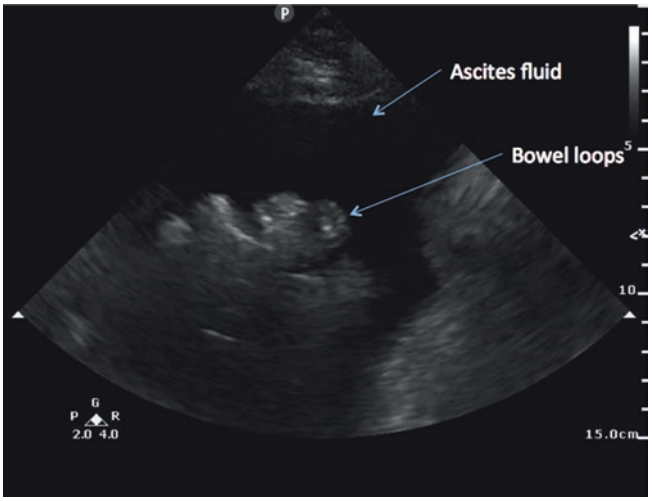

Fig. 37.18 Abdominal ultrasound in a patient with ascites. Ascitic fluid can be easily seen on bedside ultrasound as echo-free or hypoechoic (black) space in the abdominal cavity. Normal appearing bowel loops are also visualized. Ultrasound allows for safe sampling of the ascitic fluid for both diagnostic and therapeutic purposes. See also Video 37.18

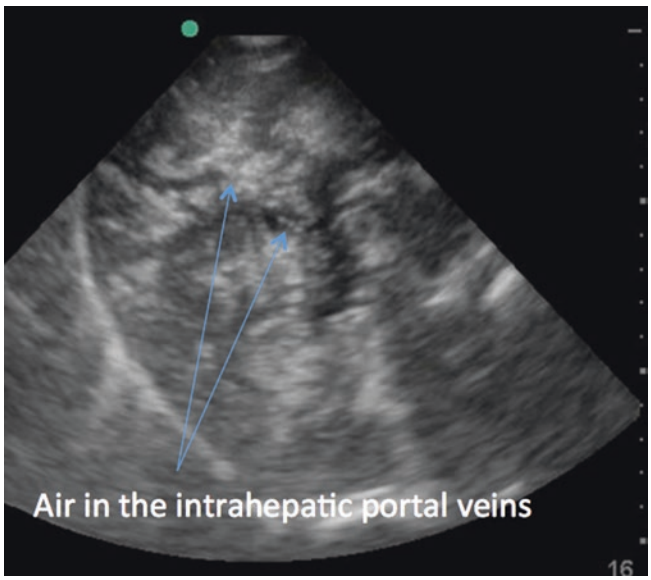

Fig. 37.17 Bedside ultrasound for liver disease. Point-of-care ultrasound examination reveals extensive air (hyperechoic white areas) in the portal venous circulation. This patient was admitted with profuse diarrhea and septic shock. He was subsequently diagnosed with severe C*lostridium difficle* colitis and pneumatosis intestinalis. See also Video 37.17, which shows the air bubbles in the portal circulation

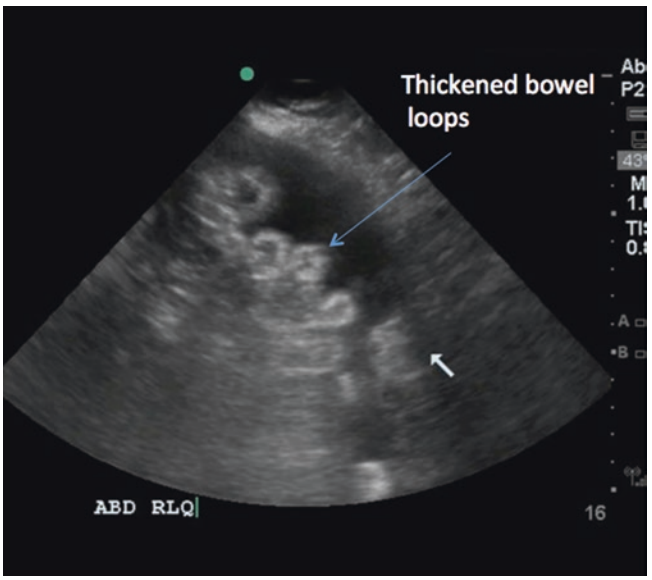

Fig. 37.19 Abdominal ultrasound in a patient with ascites. This image shows ascites with markedly thickened bowel loops due to gastroenteritis. Please compare to Fig. 37.17, in which normal appearing bowel loops are seen. See also Video 37.19

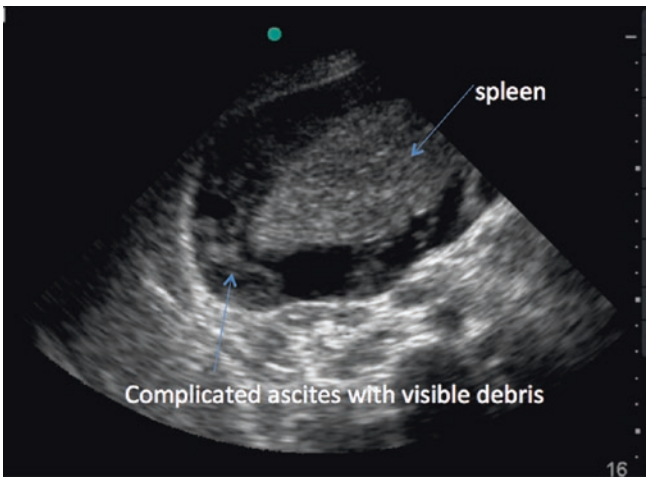

Fig. 37.20 Abdominal ultrasound in a patient with ascites. In this image, the ascites is complicated and thick echogenic fibrinous material is seen in the normally echo free ascitic fluid. See also Video 37.20, in which the debris is seen, appearing as flotsam

References

1. Perera P, Mailhot T, Riley D, Mandavia D. The RUSH exam: rapid ultrasound in SHock in the evaluation of the critically ill. Emerg Med Clin North Am. 2010;28(1):29–56.
2. Picano E, Pellikka PA. Ultrasound of extravascular lung water: a new standard for pulmonary congestion. Eur Heart J. 2016;37(27):2097–104.
3. Mayo PH, Beaulieu Y, Doelken P, Feller-Kopman D, Harrod C, Kaplan A, et al. American College of Chest Physicians/La Societé dé Réanimation de Langue Française statement on competence in critical care ultrasonography. Chest. 2009;135(4):1050–60.

Evaluation of Abdominal Pain

38

Marko Balan and Babar Haroon

38.1 Introduction

POCUS is an effective and efficient modality for bedside clinicians to safely and efficiently evaluate patients presenting with abdominal pain [1–5]. Figure 38.1 proposes a clinically integrated POCUS approach to patients with abdominal pain. Acutely traumatized or unstable patients should be rapidly examined for signs of bleeding or an abdominal aortic aneurysm (AAA). In stable patients, clinicians should use the history and physical exam to guide their POCUS evaluation. When using POCUS to evaluate patients with abdominal pain, the bedside clinician must consider the limitations that are dependent on clinician experience, patient characteristics, and disease factors.

M. Balan, M.D., F.R.C.P.C. (✉)
Department of Critical Care, Dalhousie University,
Halifax, NS, Canada
e-mail: marko.balan@dal.ca

B. Haroon, M.D., F.R.C.P.C., Dip.(Clin Epi)
Department of Critical Care, Dalhousie University,
Halifax, NS, Canada

B. P. Nelson et al. (eds.), *Atlas of Handheld Ultrasound*, https://doi.org/10.1007/978-3-319-73855-0_38

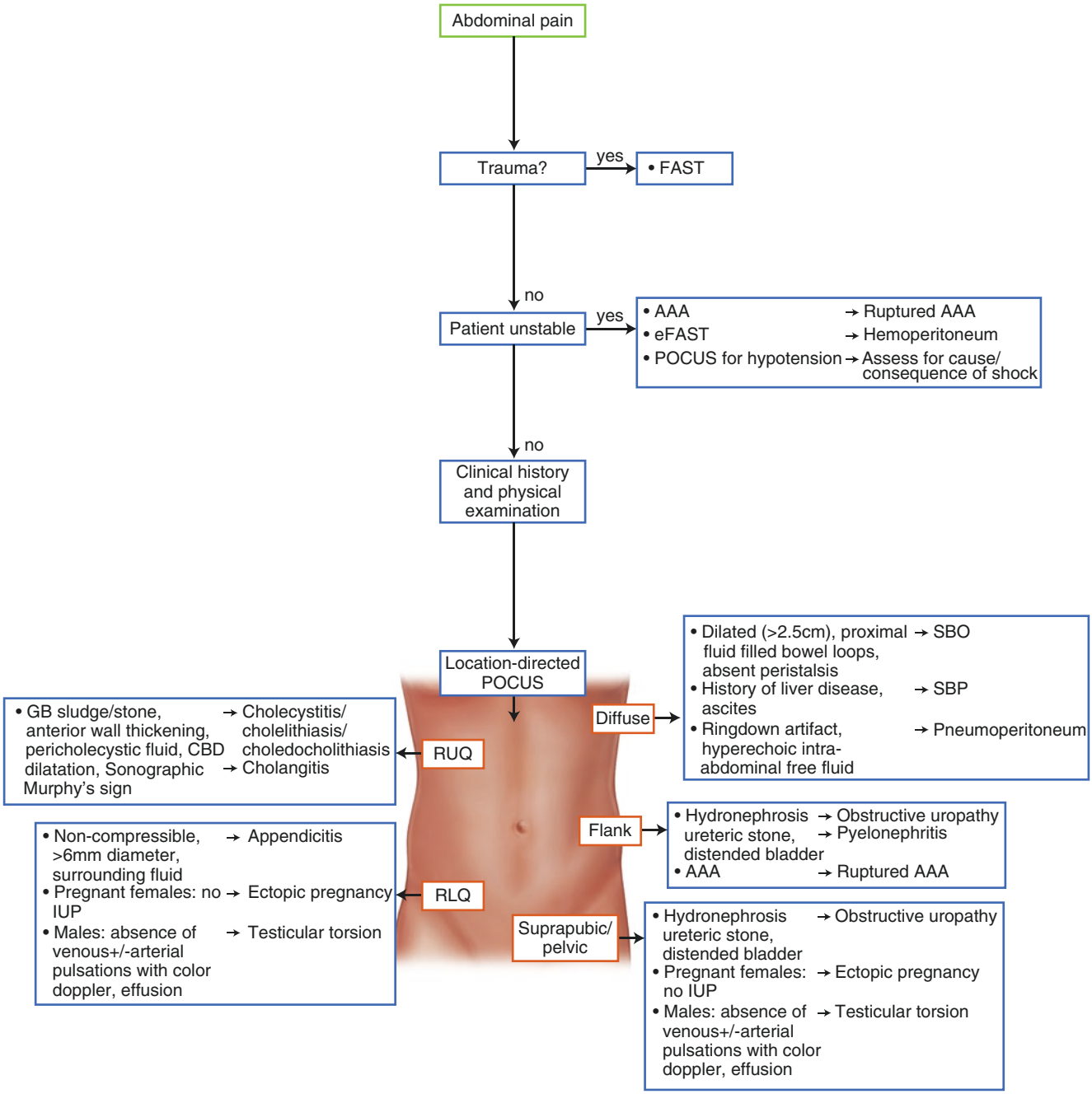

Fig. 38.1 Proposed POCUS Approach to Abdominal Pain. *AAA* abdominal aortic aneurysm, *CBD* common bile duct, *FAST* focused assessment with sonography in trauma, *GB* gallbladder, *IUP* intrauterine pregnancy, *IVC* inferior vena cava, *SBO* small bowel obstruction, *SBP* spontaneous bacterial peritonitis

38.2 POCUS Clinical Applications in Abdominal Pain

As outlined in the Abdomen section of this Atlas, there are several applications of POCUS that can aid the bedside clinician in accurately and more confidently evaluating patients with abdominal pathology [1–6]. For several years now, POCUS has been routinely used and studied in the evaluation of traumatized or unstable patients [7–10], with more recent application in a broader population of patients [1, 2, 4]. Specifically, POCUS can be used in the assessment of vascular [11], biliary [12], renal [13], intestinal [14, 15] and genito-urinary pathology [16]. POCUS guidance can also improve safety, efficiency and cost-effectiveness of bedside procedures [17].

38.3 Machine Set-Up

When evaluating most intra-abdominal structures, a low-frequency (curvilinear) probe should be used. Alternatively, a phased array probe can also be used particularly for convenience if it is already being used for other POCUS applications (i.e., cardiac). The abdominal pre-set should be selected for most POCUS applications when evaluating the abdomen.

38.4 POCUS Approach in Abdominal Pain

A proposed POCUS approach in evaluating patients with abdominal pain is shown in Fig. 38.1. Traumatized or unstable patients should be promptly examined for the presence of intra-abdominal free fluid which should be assumed to be hemoperitoneum until proven otherwise. This may lead to urgent surgical exploration in appropriately selected patients. In patients with vascular risk factors presenting with hypotension, the presence of an abdominal aortic aneurysm may suggest a possible aortic rupture.

In hemodynamically stable patients with abdominal pain, the POCUS examination should be guided by the presenting history, physical examination, and location of pain. In fact, for certain POCUS examinations (i.e., appendicitis, small bowel obstruction, cholecystitis) the clinician should ask the patient to point to the maximal location of pain and focus their examination on that region. As an extension of the physical examination, the bedside clinician should consider and evaluate for both likely and not-to-be-missed diagnoses relevant to the patient's presentation. Figure 38.1 lists suggested diagnoses based on the location of symptoms. See the Abdominal section for the specific approach to assess for these conditions. An alternative approach to the evaluation of abdominal pain with POCUS involves a systematic assessment of the abdominal organs [18], rather than an individualized approach guided by patient symptoms. Extra-abdominal causes of referred pain should also be considered by the thoughtful clinician, such as cardiac, respiratory, retroperitoneal, musculoskeletal and soft tissue.

38.5 Limitations

In order to effectively and safely use POCUS, it is critical for clinicians to understand both the applications and limitations of this tool. The bedside clinician incorporating POCUS must correctly acquire, interpret, and integrate the findings of their examinations. Inadequate, low-quality or misinterpreted scans limit the application of POCUS, delay accurate diagnoses or expose patients to unnecessary harm. Abdominal POCUS may be hindered by obesity, gas-filled bowel, patient discomfort, or difficult access to the location of important structures (i.e., retroperitoneal). Finally, the clinician should be aware that POCUS should not replace a formal comprehensive imaging test when clinically indicated.

References

1. Dickman E, Tessaro MO, Arroyo AC, Haines LE, Marshall JP. Clinician-performed abdominal sonography. Eur J Trauma Emerg Surg. 2015;41:481–92.
2. Hasani SA, Fathi M, Daadpey M, Zare MA, Tavakoli N, Abbasi S. Accuracy of bedside emergency physician performed ultrasound in diagnosing different causes of acute abdominal pain: a prospective study. Clin Imaging. 2015;39(3):476–9.
3. Lindelius A, Törngren S, Sondén A, Pettersson H, Adami J. Impact of surgeon-performed ultrasound on diagnosis of abdominal pain. Emerg Med J. 2008;25(8):486–91.
4. Kameda T, Taniguchi N. Overview of point-of-care abdominal ultrasound in emergency and critical care. J Intensive Care. 2016;4:53.
5. Rowland JL, Kuhn M, Bonnin RLL, Davey MJ, Langlois SLP. Accuracy of emergency department bedside ultrasonography. Emerg Med (Fremantle). 2001;13:305–13.
6. Bassler D, Snoey ER, Kim J. Goal-directed abdominal ultrasonography: impact on real-time decision making in the emergency department. J Emerg Med. 2003;24(4):375–8.
7. Wherrett LJ, Boulanger BR, McLellan BA, Brenneman FD, Rizoli SB, Culhane J, et al. Hypotension after blunt abdominal trauma: the role of emergent abdominal sonography in surgical triage. J Trauma. 1996;41(5):815–20.
8. Ma JO, Mateer JR, Ogata M, Kefer MP, Wittmann D, Aprahamian C. Prospective analysis of a rapid trauma ultrasound examination performed by emergency physicians. J Trauma. 1995;38(6):879–85.
9. Dolich MO, McKenney MG, Varela JE, Compton RP, McKenney KL, Cohn SM. 2,576 ultrasounds for blunt abdominal trauma. J Trauma. 2001;50(1):108–12.
10. Patel NY, Riherd JM. Focused assessment with sonography for trauma: methods, accuracy, and indications. Surg Clin North Am. 2011;91:195–207.
11. Tainter CR. Abdominal aorta. In: Soni NJ, Arntfield R, Kory P, editors. Point of care ultrasound. Philadelphia: Elsevier Saunders; 2015. p. 167–73.

12. Woo MY, Taylor M, Loubani O, Bowra J, Atkinson P. My patient has got abdominal pain: identifying biliary problems. Ultrasound. 2014;22(4):223–8.
13. Cox C, MacDonald S, Henneberry R, Atkinson P. My patient has abdominal pain and flank pain: identifying renal causes. Ultrasound. 2015;23(4):242–50.
14. Lam SH, Grippo A, Kerwin C, Konicki PJ, Goodwine D, Lambert MJ. Bedside ultrasonography as an adjunct to routine evaluation of acute appendicitis in the emergency department. West J Emerg Med. 2014;15(7):808–15.
15. Novak KL, Jacob D, Kaplan GG, Boyce E, Ghosh S, Ma I, et al. Point of care ultrasound accurately distinguishes inflammatory from non-inflammatory disease in patients presenting with abdominal pain and diarrhea. Can J Gastroenterol Hepatol. 2016;2016:4023065.
16. Allison SO, Lev-Toaff AS. Acute pelvic pain: what we have learned from the ER. Ultrasound Q. 2010;26(4):211–8.
17. Mercaldi CJ, Lanes SF. Ultrasound guidance decreases complications and improves the cost of care among patients undergoing thoracentesis and paracentesis. Chest. 2013;143(2):532–8.
18. Testa A, Lauritano EC, Giannuzzi R, Pignataro G, Casagranda I, Gentiloni Silveri NG. The role of emergency ultrasound in the diagnosis of acute non-traumatic epigastric pain. Intern Emerg Med. 2010;5:401–9.

Anuria Evaluation

39

Kevin M. Piro and Renee K. Dversdal

Classically, acute kidney injury (AKI) and anuria have been categorized in relationship to the location of the kidney injury: pre-renal, intrinsic, and post-renal. Anuria is defined as less than 100 mL urine per day [1]. True anuria carries a narrow differential that includes vascular lesions, total obstruction, severe acute tubular necrosis (ATN), and severe glomerulonephritis [1, 2]. While the patient's history and physical exam remain key to narrowing this differential, point-of-care ultrasound (POCUS) can act as an extension of the clinical examination to focus diagnostic workup (Fig. 39.1). POCUS can rapidly identify obstructive uropathy, and contribute to clinicians' understanding of underlying hemodynamic status and genitourinary anatomy without the added risk of nephrotoxic contrast that other imaging modalities carry [3].

Point-of-care ultrasound assessment should start by assessing for total bladder obstruction. The patient should first attempt to urinate and then the bladder should be evaluated by ultrasound (Fig. 39.2). The bladder should be measured to make a rudimentary assessment of bladder volume (Figs. 39.3, 39.4, and 39.5). Attention then should be turned to identifying both kidneys (Figs. 39.6, 39.7 and 39.8), looking for hydronephrosis or hydroureter (Figs. 39.9 and 39.10). Ultrasound is highly sensitive for urinary obstruction, thus the absence of hydronephrosis is clinically useful in ruling out obstruction in the evaluation of anuria [4]. Post-void residual of greater than 300 mL and/or bilateral hydronephrosis are suggestive of genitourinary obstruction. The clinician should then attempt to understand the patient's hemodynamics, which can be done by identifying and measuring the inferior vena cava (IVC) (Figs. 39.11, 39.12, and 39.13) and assessing left ventricular function from the parasternal long axis. An IVC that measures less than 2 cm and whose diameter collapses greater than 50% with respiration can suggest prerenal disease in the right clinical context. The IVC can be assessed globally with an "eyeball" assessment, or measured at both maximal and minimal diameters in a cine capturing at least one full respiratory cycle. Reduced LV function and a dilated IVC, non-collapsible IVC may suggest cardiorenal disease.

Electronic Supplementary Material The online version of this chapter (https://doi.org/10.1007/978-3-319-73855-0_39) contains supplementary material, which is available to authorized users.

K. M. Piro, M.D. (✉)
Division of Hospital Medicine, Oregon Health and Science University, Portland, OR, USA

Division of General Internal Medicine, Oregon Health and Science University, Portland, OR, USA
e-mail: piro@ohsu.edu

R. K. Dversdal, M.D.
Division of Hospital Medicine, Oregon Health and Science University, Portland, OR, USA

B. P. Nelson et al. (eds.), *Atlas of Handheld Ultrasound*, https://doi.org/10.1007/978-3-319-73855-0_39

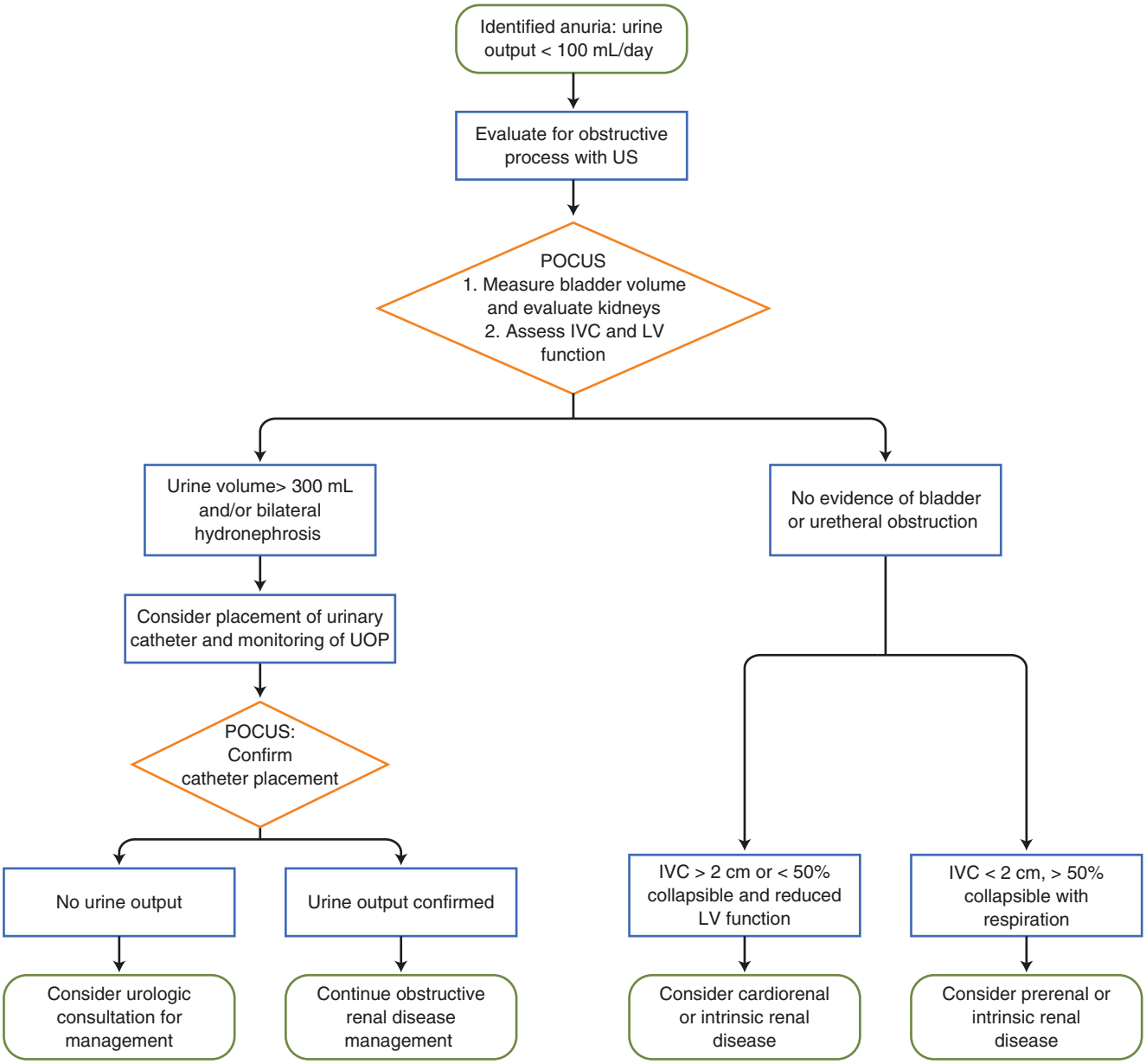

Fig. 39.1 Algorithm

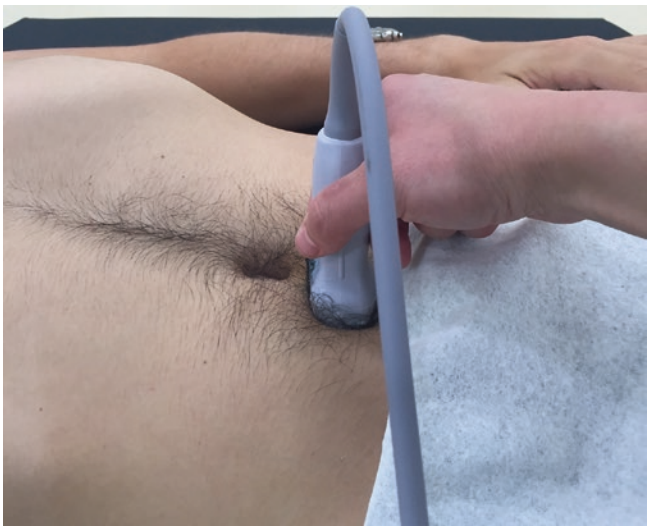

Fig. 39.2 Bladder image acquisition. The bladder should be viewed with the curvilinear (ideally) or phased array probe in both the transverse and sagittal planes. Locate the superior aspect of the symphysis pubis by palpation and place the probe cranial to this landmark. Fan through and identify both the superior and inferior margins of the bladder. Rotate the probe so that the probe marker is oriented cranially. Fan through the bladder and locate both lateral borders

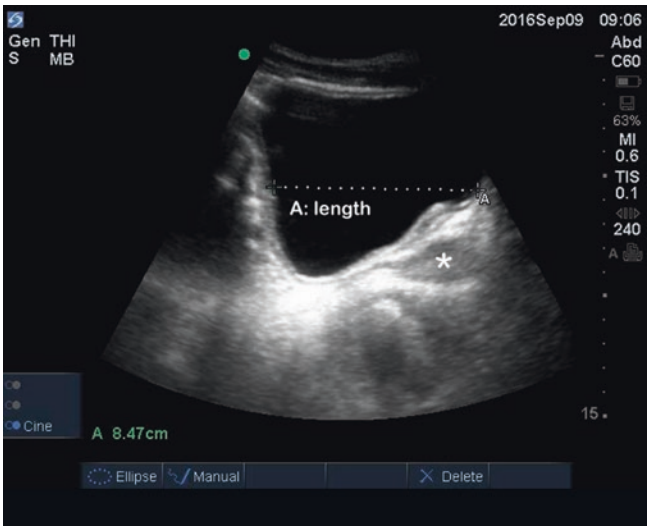

Fig. 39.4 Bladder in sagittal view. The probe should then be rotated clockwise so that the probe marker is facing cranially to obtain the sagittal view of the bladder. The diameter can then be measured as depicted. The prostate can be visualized (*) at the bladder outlet as shown. The bladder shown has roughly 480 mL (8.5 × 8.8 × 8.6 cm × 0.75) of anechoic urine in the bladder

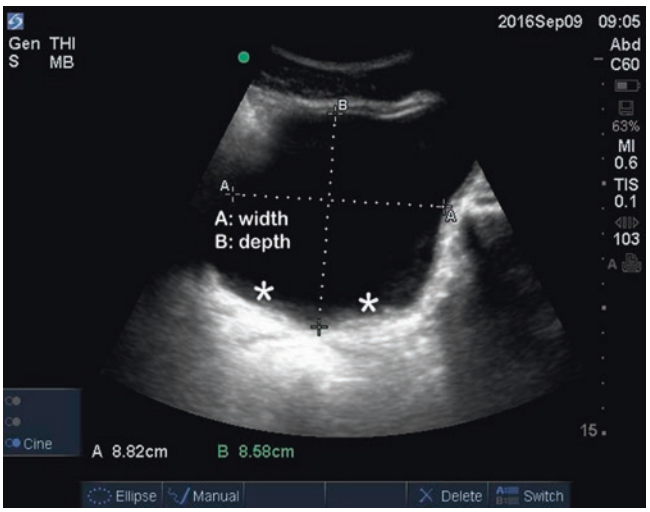

Fig. 39.3 Bladder in transverse view. The patient should attempt to void prior to scanning to help obtain a post-void residual volume. Bladder volume can be estimate by measuring the largest depth, width, and length (in cm) using the correction Depth × Width × Length × 0.7 5 = Bladder Volume. The depth and width of the bladder are measured in the transverse view of the bladder. This estimate has shown excellent correlation with catheterization volume measurement [5]. The trigone can be seen in the far field of this view (*)

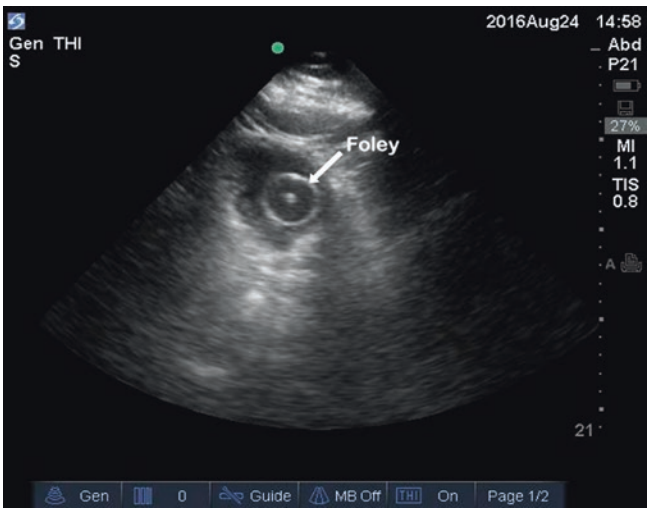

Fig. 39.5 Bladder with Foley catheter balloon in sagittal view. A Foley catheter has been placed in this picture, with the hyperechoic balloon appearing within the bladder. The bladder has been decompressed

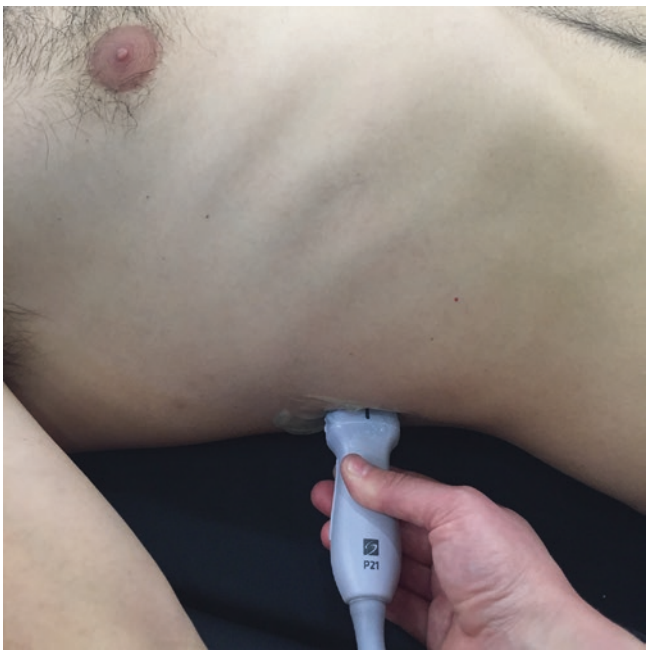

Fig. 39.6 Right kidney image acquisition. Using either a curvilinear or phased array probe with the probe marker oriented cranially, place the probe laterally and posteriorly at the level of the liver to use it as an acoustic window to visualize the kidney. Once the kidney is identified, the probe should be rotated to identify the true long axis of the kidney, then fan through posteriorly and anteriorly. Then rotate the probe 90° counterclockwise to identify the kidney in the short axis, and fan through the kidney cranially and caudally

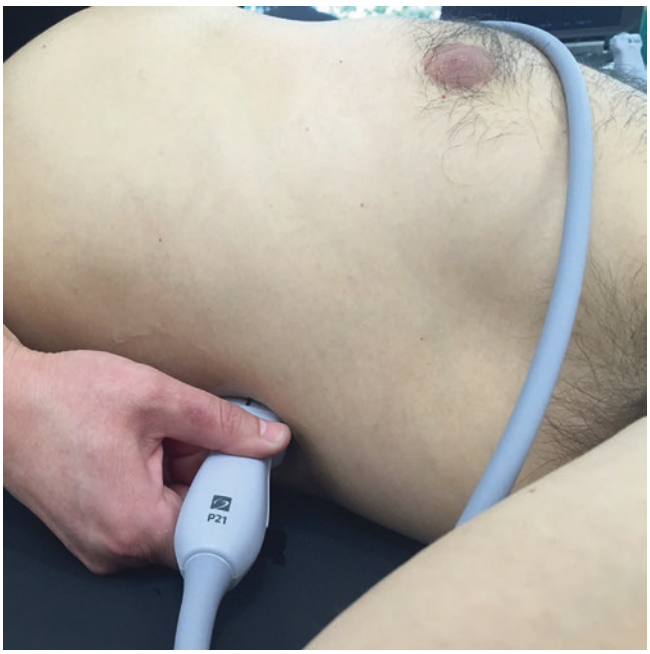

Fig. 39.7 Left kidney image acquisition. Repeat the same technique on the left kidney. The left kidney is located more posteriorly, which may necessitate placing the back of the hand holding the probe on the bed to visualize the kidney. Alternatively, the patient can be placed in the right lateral decubitus position to improve visualization. Additionally, asking the patient to inspire will displace the kidney inferiorly and may improve the operator's image

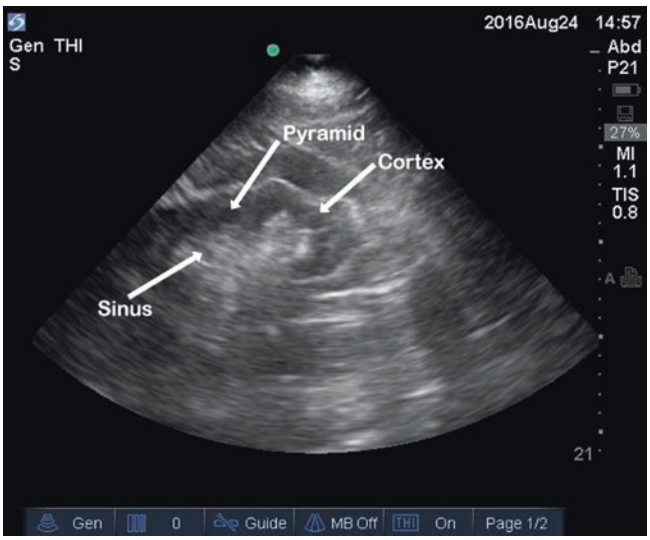

Fig. 39.8 Normal kidney long axis. A normal kidney in the long axis is shown here with the cortex, medullary pyramid, and renal sinus labeled. There is no evidence of hydronephrosis as there are no discrete pockets of anechoic fluid in the kidney (*see* Video 39.1)

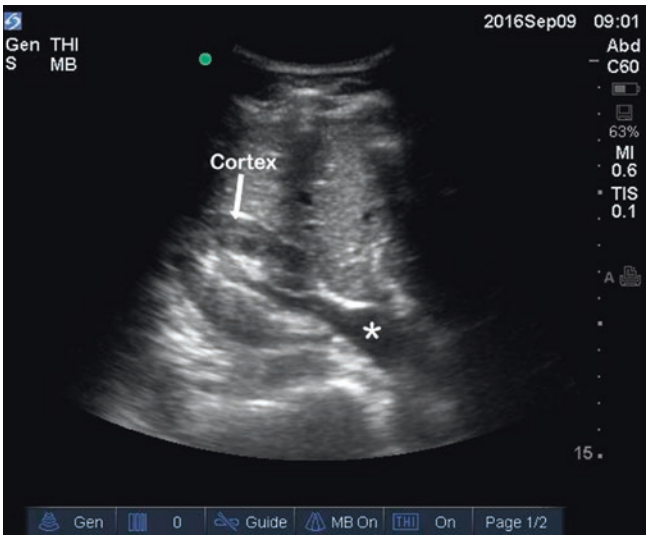

Fig. 39.9 Normal kidney short axis. A kidney is shown in the short axis with the ureter marked (*). The patient's ureter is dilated, but there is no hydronephrosis. In the short axis, the kidney should appear as a "C"

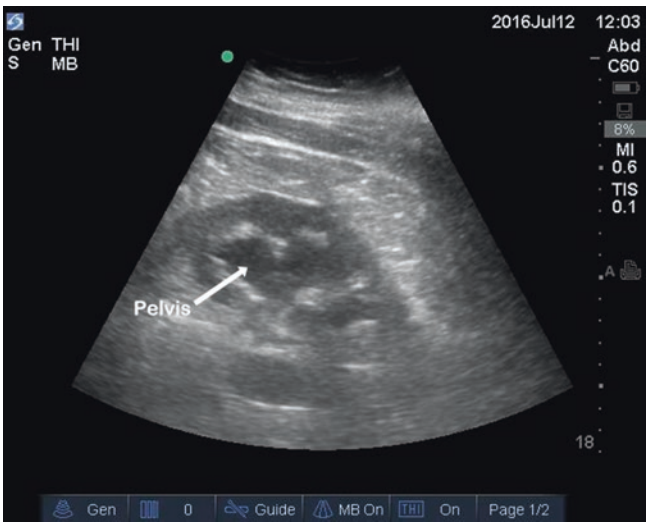

Fig. 39.10 Moderate hydronephrosis. Anechoic fluid collects within the pelvicalyceal system. Progressive distortion of the renal structures characterizes the degree of hydronephrosis. The degree is measured by dilation of the renal sinus (mild), then obscuration of the renal papillae and blunting of the pyramids (moderate), and finally to include cortical thinning (severe). Here, moderate hydronephrosis is seen with a dilated renal pelvis (*see* Video 39.2)

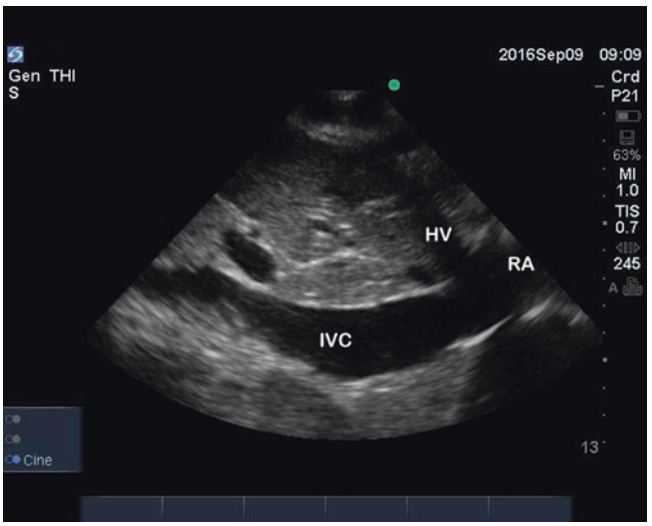

Fig. 39.12 Normal IVC. The ideal image of the IVC should show the hepatic veins (HV) emptying into the IVC and the IVC emptying into the RA to confirm that the IVC is the vessel being visualized. Tilting the probe may help the operator elongate the IVC and the operator should slightly rotate the probe to ensure the vessel is not improperly obliquely scanned

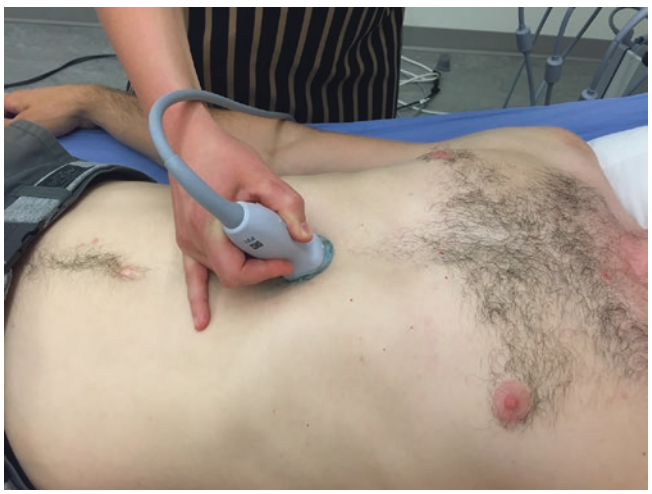

Fig. 39.11 IVC image acquisition. The IVC should be visualized from the substernal view using either a phased array or curvilinear probe. To optimize clinician time, this exam may be performed in tandem with the cardiac examination in the parasternal long axis using the cardiac mode. The probe marker should be located cranially and the right atrium should be visualized in most cranial aspects of the image. The IVC should be visualized emptying into the right atrium and the hepatic veins should be visualized emptying into the IVC. Fan through the IVC to ensure that you are visualizing it in its widest dimension (true long axis). The operator should be aware that the aorta is located opposite to the IVC (anatomic left) and is frequently mistaken for the IVC

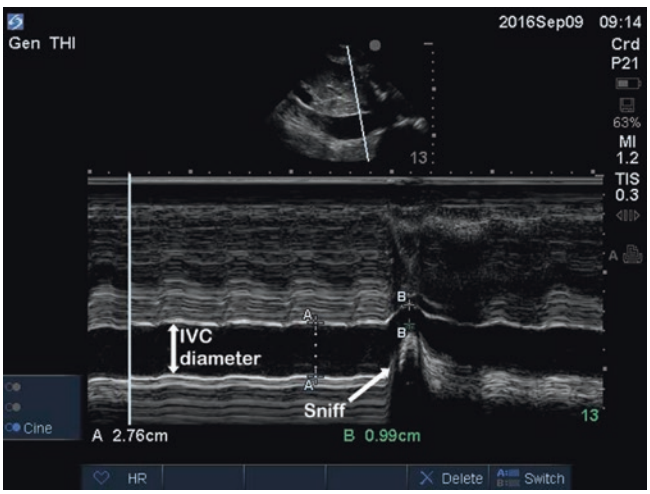

Fig. 39.13 IVC collapses with respiration shown here using M-mode. The IVC can be measured at both maximal and minimal diameters in a cine capturing at least one full respiratory cycle. The measurement should be taken just distal to the entrance of the hepatic veins into the IVC. If the IVC measures less than 2 cm at its maximal diameter and collapses by >50% with respiration (measured either during passive or active respiration), this could suggest clinical hypovolemia in the right context and could be consistent with prerenal disease

The clinician's history and physical examination can be augmented by POCUS to aid rapid diagnosis and save valuable time in the management of anuria.

References

1. Singri N, Ahya SN, Levin ML. Acute renal failure. JAMA. 2003;289:747–51.
2. Hilton R. Acute renal failure. BMJ. 2006;333:786–90.
3. Noble VE, Brown DFM. Renal ultrasound. Emerg Med Clin North Am. 2004;22:641–59.
4. Ellenbogen PH, Scheible FW, Talner LB, Leopold GR. Sensitivity of gray scale ultrasound in detecting urinary tract obstruction. Am J Roentgenol. 1978;130(4):731–3.
5. Chan H. Noninvasive bladder volume measurement. J Neurosci Nurs. 1993;25:309–12.

Evaluation of Leg Pain and Swelling

40

Christopher Gelabert

Point-of-care ultrasound for the assessment of leg pain and swelling is a rapid, high-yield assessment that can quickly lead to therapeutic interventions. Ultrasound of the lower extremity can be used to assess for deep venous thrombosis (DVT), lymphadenopathy, and visualization of subcutaneous edema for evaluation of cellulitis versus congestive heart failure (CHF). As most pathology in the lower extremity is relatively superficial, a high-frequency linear transducer is used for its superior linear resolution and flat footprint.

DVT is a disease process that affects 300,000–600,000 patients annually in the United States and carries with it an estimated 10–30% mortality within 30 days [1]. Ultrasound is the main diagnostic tool for the detection of DVT, although there are several different ultrasound protocols including two-point compression, whole leg compression, and duplex ultrasound examinations [2, 3]. While two-point compression uses the most common areas of thrombosis (proximal femoral vein and popliteal vein), a significant percentage of DVTs are missed with this technique [4]. Whole leg compression ultrasound involving serial compression from the common femoral vein to the calf veins has been found to be very accurate with a mean sensitivity and specificity of 0.64 (0.62, 0.65) and 0.98 (0.974, 0.983) [5]. Moreover, a single negative whole leg compression ultrasound has only a combined venous thromboembolism event rate of 0.57% (0.25%, 0.89%) at 3 months [6].

Frequently during lower extremity ultrasound for DVT, the clinician will find alternate diagnoses including cysts, masses, lymphadenopathy, phlebitis, hematoma, and cellulitis [7].

Figures 40.1, 40.2, 40.3, 40.4, 40.5, 40.6, 40.7, and 40.8 and Videos 40.1, 40.2, 40.3, 40.4, 40.5, 40.6, and 40.7 demonstrate technique, common pathology, and an algorithm for the assessment of leg swelling with point-of-care ultrasound.

Electronic Supplementary Material The online version of this chapter (https://doi.org/10.1007/978-3-319-73855-0_40) contains supplementary material, which is available to authorized users.

C. Gelabert, M.D.
Department of Emergency Medicine, UT Health San Antonio, San Antonio, TX, USA
e-mail: gelabert@uthscsa.edu

B. P. Nelson et al. (eds.), *Atlas of Handheld Ultrasound*,
https://doi.org/10.1007/978-3-319-73855-0_40

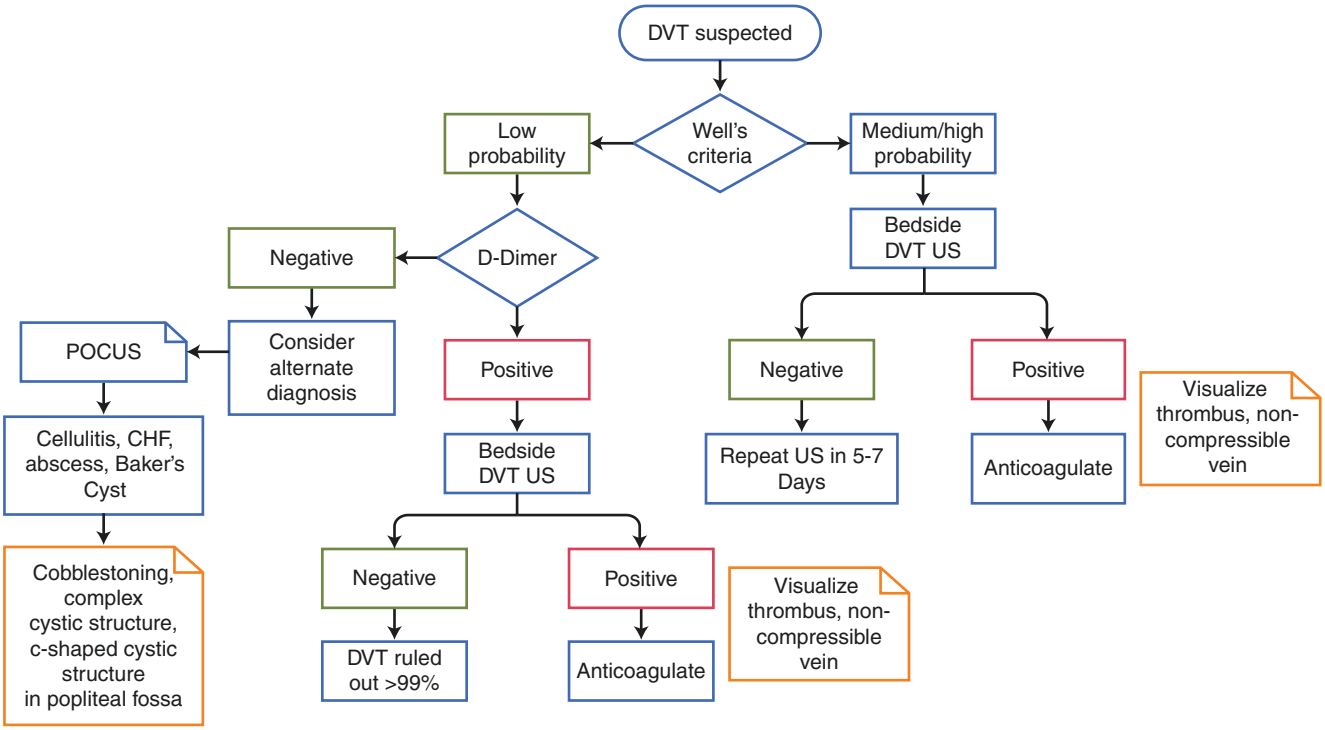

Fig. 40.1 Algorithm for diagnosis of DVT. This uses clinical-decision rules, laboratory tests, and point-of-care ultrasound in the diagnosis or exclusion of DVT

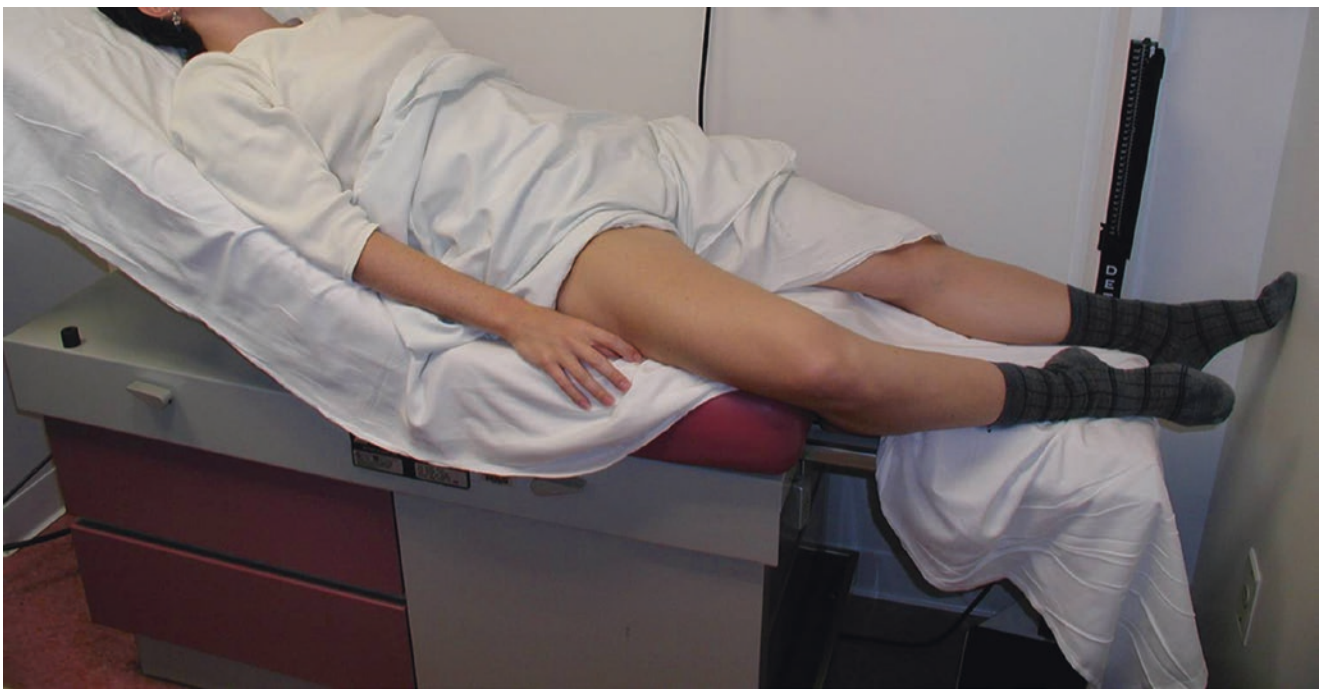

Fig. 40.2 Patient positioning for DVT ultrasound examination. Elevate the head of the bed 45° to facilitate blood pooling in the veins for improved visualization of the vasculature. The leg should be slightly flexed and held in external rotation to visualize all of the structures in the inguinal region. When visualizing the structures in the popliteal fossa, have the knee slightly bent. Image courtesy of Christopher Gelabert

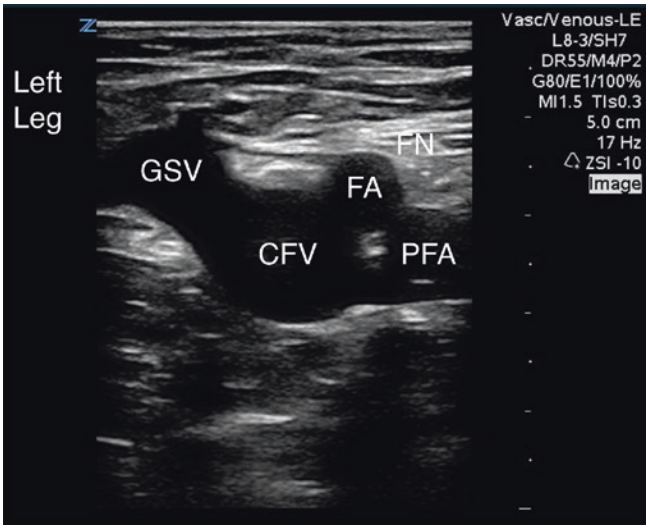

Fig. 40.3 Transverse view of the vasculature of the upper leg. Note the relationship of nerve, artery, and vein from lateral to medial. The greater saphenous vein (GSV) will terminate into the common femoral vein (CFV), and while the GSV is not considered a deep vein, its junction with the deep venous system is an area of turbulent flow and a common origin of thrombosis. The femoral artery (FA) will give off its first branch, the profunda femoris artery (PFA) at this level. The femoral nerve (FN) is a flat, thin, hyperechoic structure superficial and lateral to the FA. Courtesy of Christopher Gelabert

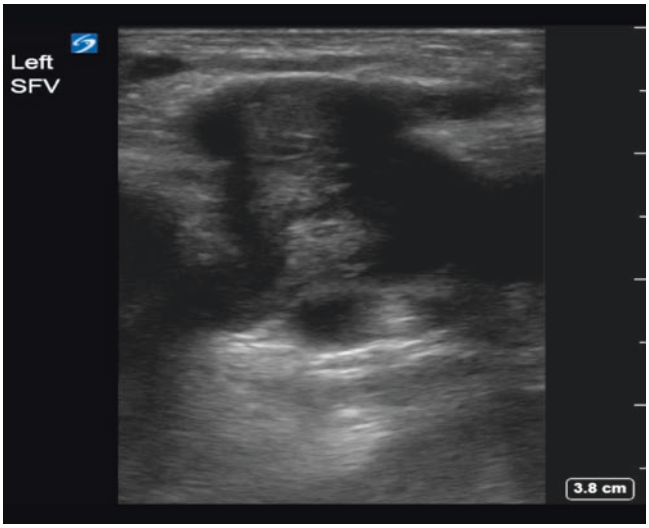

Fig. 40.5 This image demonstrates an echogenic thrombus in the lumen of the common femoral vein and greater saphenous vein. Courtesy of Christopher Gelabert

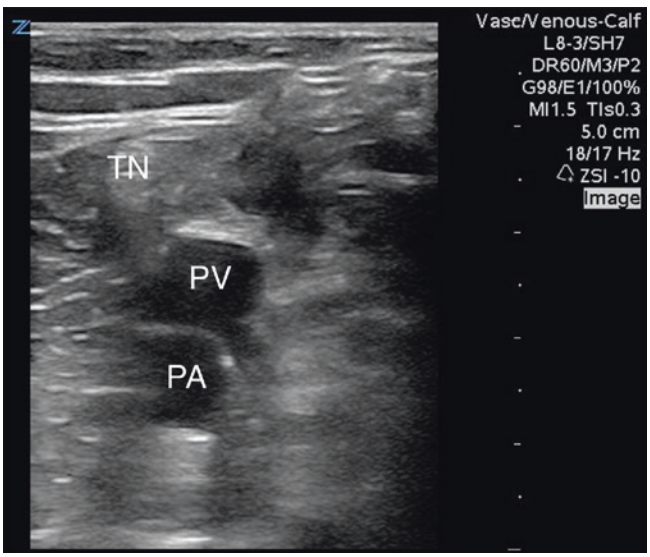

Fig. 40.4 This transverse view of the popliteal fossa demonstrates the popliteal vein (PV) superficial to the popliteal artery (PA). The tibial nerve (TN) is superficial to the vasculature. Courtesy of Chris Gelabert

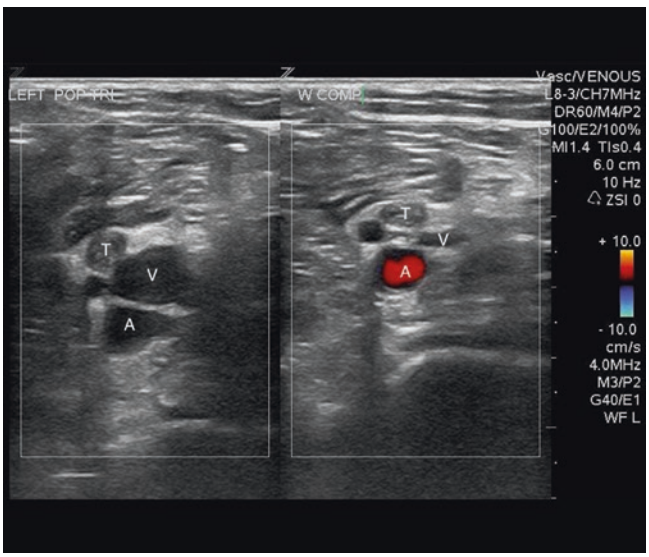

Fig. 40.6 This a split screen image of the popliteal fossa normally on the left, and with compression on the right with color doppler. A small thrombus (T) is evident one of the branches within the trifurcation of the popliteal vein (V). The artery (A) does not collapse. Courtesy of Christopher Gelabert

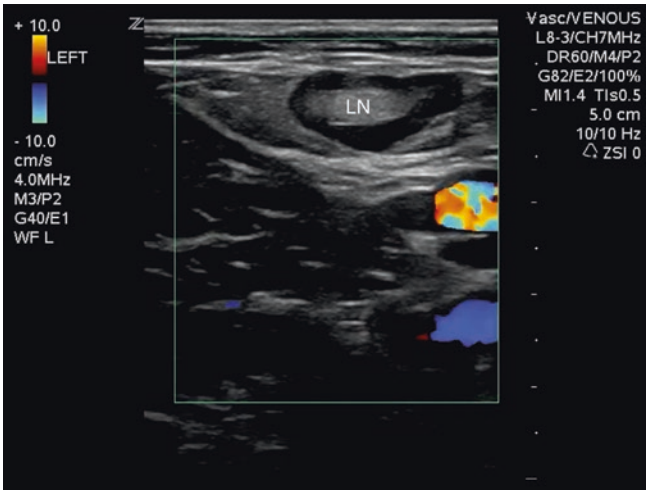

Fig. 40.7 Lymph node (LN) commonly seen while performing lower extremity ultrasound. Lymph nodes will be superficial to the vasculature and demonstrate a hyperechoic center and hypoechoic rim, typically described as a pseudokidney appearance. Courtesy of Christopher Gelabert

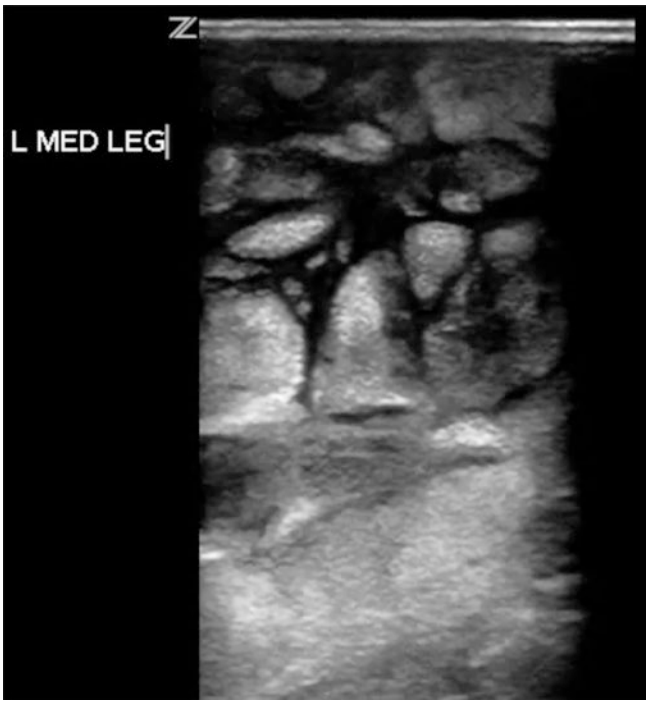

Fig. 40.8 When edema is present within the subcutaneous tissue, either from infection or congestive heart failure, it will surround lobules of adipose tissue, increasing the thickness of the skin layers, creating the classical cobblestone appearance. Courtesy of Christopher Gelabert

References

1. Beckman MG, Hooper WC, Critchley SE, Ortel TL. Venous thromboembolism: a public health concern. Am J Prev Med. 2010;38(4 Suppl):S495–501.
2. Scarvelis D, Wells PS. Diagnosis and treatment of deep-vein thrombosis. CMAJ. 2006;175(9):1087–92.
3. Gaitini D. Current approaches and controversial issues in the diagnosis of deep vein thrombosis via duplex doppler ultrasound. J Clin Ultrasound. 2006;34(6):289–97.
4. Fraser JD, Anderson DR. Deep venous thrombosis: recent advances and optimal investigation with US. Radiology. 1999;211(1):9–24.
5. Adhikari S, Zeger W. Non-thrombotic abnormalities on lower extremity venous duplex ultrasound examinations. West J Emerg Med. 2015;16(2):250–4.
6. Cogo A, Lensing AW, Prandoni P, Hirsh J. Distribution of thrombosis in patients with symptomatic deep vein thrombosis. Implications for simplifying the diagnostic process with compression ultrasound. Arch Intern Med. 1993;153(24):2777–80.
7. Johnson SA, Stevens SM, Woller SC, Lake E, Donadini M, Cheng J, et al. Risk of deep vein thrombosis following a single negative whole-leg compression ultrasound: a systematic review and meta-analysis. JAMA. 2010;303(5):438–45.

Index

B. P. Nelson et al. (eds.), *Atlas of Handheld Ultrasound*, https://doi.org/10.1007/978-3-319-73855-0